

Influence of Coal Dust on Premixed Turbulent Methane-Air Flames

Scott R. Rockwell

A Dissertation

Submitted to the Faculty

of

Worcester Polytechnic Institute

In partial fulfillment of the requirements for the

Degree of Doctor of Philosophy

in

Fire Protection Engineering

July 2012

APPROVED:

Professor Ali S. Rangwala, Advisor

Professor Kathy A. Notarianni, Head of Department

Professor Simon W. Evans

Professor Sanjeeva Balasuriya

Dr. Alfonso F. Ibarreta

Professor Forman A. Williams

Table of Contents

Table of Contents	2
List of figures	5
List of tables.....	6
Nomenclature	7
Acknowledgments.....	8
Abstract	9
1. Introduction.....	10
1.1 General overview	10
1.2 Hazard assessment used in dust industry	11
1.3 The explosion sphere	12
1.4 Prior related work	18
1.4.1 Laminar dust flame experiments.....	18
1.4.2 Turbulent dust flame experiments.....	30
1.4.3 Hybrid flame experiments	32
1.4.4 Modeling of dust flames.....	33
1.5 Goals and objectives of the current study	33
1.6 Organization of the thesis	35
References.....	35
2. Structure of a Dust Flame	40
2.1. Premixed or Non-Premixed?	40
2.2 Flame structure	41
3. Experimental Apparatus Construction and Procedure	49
3.1 Summary	49
3.2 Combustion chamber	49
3.3 Exhaust system.....	52
3.4 Burner test section	53
3.5 Burner nozzle design	55
3.6 Fuel control system	62
3.7 Optical system.....	65

3.8 Directions for using HFA.....	67
3.9 HFA data analysis	67
3.11 Experimental matrix.....	73
References.....	73
4. Results and Analysis	76
4.1 Laminar flames	76
4.2 Turbulent flames	80
4.2.1 Gas flames (validation study)	80
4.2.2 Turbulent combustion regimes	87
4.2.4 Effect of dust concentration on burning velocity.....	98
4.3 Correlation of turbulent burning velocity	100
References.....	103
5. Conclusions and recommendations.....	105
Appendix 2: HFA User's Manual	111
Recommended Personal Protective Equipment (PPE)	113
Turning on HFA:.....	114
Calibration:	119
Things to check:	121
Starting/Running test:	123
Collecting gas analysis data:	125
Turning off Experiment:	127
MATLAB Scripts.....	128
Using Hotwire Anemometer:	129
Appendix 3: Matlab scripts used in data analysis.....	132
Contents	132
A3.1 - Edge selection script	133
A3.2 - Edge data analysis script.....	136
A3.3 - Plotting figure 4.9	153
A3.4 - Plotting figure 4.13	157
A3.5 - Plotting figure 4.14	160

A3.6 - Plotting figure 4.15	165
A3.7 - Creating arrays of test data as a function of dust concentration (Burn_vel_func_dst_part_szev01)	170
A3.8 - Turbulent intensity calculation	190
A3.9 - Gas analysis data retrieval	193
A3.10 - plotAverage_noplot	194
Appendix 4: Error Bar values – standard deviation of velocity calculation	200
Appendix 5: Flame Images	201

List of figures:

- 1.1 Diagram of explosion sphere
- 1.2 Pressure vs time curve and change in pressure vs time curve from an explosion sphere
- 1.3 Diagram of explosion sphere with increasing turbulence as the flame propagates
- 2.1 Schematic illustration of the structure of a premixed dust – air flame
- 2.2 Schematic of flame structure in a dust-air flame
- 3.1 Hybrid Flame Analyzer (HFA) combustion chamber
- 3.2 HFA exhaust system diagram
- 3.3 Diagram of experimental section of Hybrid Flame Analyzer (HFA)
- 3.4 Images of burner nozzles
- 3.5 Diagram of turbulent burner nozzle
- 3.6 Turbulent burner parts
- 3.7 Image of premixed methane-oxygen pilot flame
- 3.8 Images of perforated plates
- 3.9 Calibration curve for hot wire anemometer
- 3.10 Turbulent intensity versus flow rate
- 3.11 Comparison of calculated turbulent intensity vs number of samples
- 3.12 Diagram of dust feeder block
- 3.13 Diagram of dust hopper used to calibrate dust feeder
- 3.14 Dust feeder calibration curves
- 3.15 Visual images of burner flames
- 3.16 Shadowgraph images of burner flames
- 3.17 Analysis method of turbulent images
- 3.18 Profiles of theoretical turbulent flame
- 3.19 Comparison of calculated burning velocity versus number of images used
- 4.1 Laminar Flame as a function of dust concentration
- 4.2 Comparison of laminar flames
- 4.3 Turbulent burning velocity of a methane-air flame vs. turbulent intensity
- 4.4 Flame images at various turbulent intensities
- 4.5 Comparison of this work with published data
- 4.6 Borghi diagram parameters
- 4.7 Characteristic parametric relationships of premixed turbulent combustion
- 4.8 Diagrams of turbulent flame structure
- 4.9 All data as a function of turbulent intensity
- 4.10 Error bars on data
- 4.11 Turbulent burning velocity vs. turbulent intensity
- 4.12 Influence of dust on the burning velocity of a gas flame
- 4.13 Images of turbulent flames at various dust concentrations
- 4.14 Nondimensionalized burning velocity as a function of dust concentration
- 4.15 Combined fitted curves of test data

List of tables:

- 1.1 Recent incidents of industrial dust or hybrid flame explosions
- 1.2 Main components for two typical explosion vessels
- 2.1 Fuel concentration scenarios in hybrid flames
- 3.1 Integral length scale calculations
- 3.2 Pittsburgh seam coal properties
- 3.3 Experimental matrix
- 4.1 Curve fitting parameters

Nomenclature:

A	pre-exponential factor	max	maximum value
A_T	cross sectional area of flame brush	o	ambient parameter
A_L	wrinkled laminar flame area	rms	root mean square
d	diameter of burner	st	dust
d_{st}	dust diameter		
Da	Damkohler number		
E	Activation energy		
h	height of flame cone		
k	thermal conductivity		
K_{st}	deflagration index		
l_0	integral length scale		
\dot{m}	mass flux		
MW	molecular weight		
n	number of moles Eq. 1.3		
n	number of samples Eq. 3.2		
P	pressure		
Q	Heat of combustion		
R	Radius of cone base		
Re_T	Turbulent Reynolds number		
S_L	laminar burning velocity		
S_T	turbulent burning velocity		
t	time		
u	velocity		
u'	velocity fluctuation		
\bar{u}	average velocity		
u'_{rms}	turbulent intensity		
V_o	volume		
x	displacement		

Greek:

α	half angle of flame cone (Eq. 3.5)
α	thermal diffusivity (Sec. 4.2.2)
δ_L	laminar flame thickness
ρ	density
$\rho_u(\tau)$	autocorrelation of velocity
λ_{st}	dust concentration
ϕ	equivalence ratio
Γ	time flame element interacts with eddy

Subscripts:

g	gas
---	-----

Acknowledgments:

The author would like to thank the National Science Foundation Graduate Research Fellowship program and the Koerner Fellowship program for funding this work. The author would also like to thank Dr. K. A. Joshi for his counsel, the faculty of the WPI FPE program for their guidance, and his parents for their support over the years.

Abstract

The hazard associated with dust deflagrations has increased over the last decade industries that manufacture, transport, process, or use combustible dusts. Identification of the controlling parameters of dust deflagration mechanisms is crucial to our understanding of the problem. The objective of this study is to develop an experimental platform, called the Hybrid Flame Analyzer (HFA), capable of measuring the laminar and turbulent burning velocity of gas, dust, and hybrid (gas and dust) air premixed flames as a function of properties specific to the reactants such as dust-particle size and concentration.

In this work the HFA is used to analyze a particle-gas-air premixed system composed of coal dust particles (75-90 μm and 106-120 μm) in a premixed CH_4 -air ($\phi_g = 0.8, 1.0$ and 1.2) flame. This work ultimately aims to improve the knowledge on fundamental aspects of dust flames which is essential for the development of mathematical models. This study is the first of its kind where multiple different parameters that govern flame propagation (initial particle radius, particle concentration, gas phase equivalence ratio, turbulent intensity, and integral length scale) are systematically analyzed in a spatially uniform cloud of volatile particles forming a stationary flame.

The experiments show that the turbulent burning velocity is more than two-times larger than the laminar counter-part for each and every case studied. It is observed that smaller particles and larger concentrations ($> 50 \text{ g/m}^3$) tend to enhance the turbulent burning velocity significantly compared to larger particle sizes and lower concentration ranges. The experimental data is used to develop a correlation similar to turbulent gas flames to facilitate modeling of the complex behavior.

1. Introduction

1.1 General overview

The hazards of dust combustion are often overlooked in industrial safety. In industries that manufacture, transport, process, or use combustible dusts, accidental dust deflagrations represent a real hazard to both personnel and equipment. Dust explosions cause injuries, fatalities, and significant financial cost. The insurance company FM Global reported that between 1983 and 2006 the cost of 166 manufacturing plant dust explosions were \$284 million [1]. The Ford motor Company Power house explosion in 1999 caused over \$1 billion in damage [2]. Table 1-1 lists a few of the most recent industrial explosions caused by dust and hybrid fuels.

Table 1.1 Recent incidents of industrial dust or hybrid flame explosions [2]

Industry Type	Fuel	Location	Date	Fatalities
Saw mill	Wood dust	Lakeland Mills sawmill in Prince George, Canada	2012	2
Saw mill	Wood dust	Babine Forest Products in Burns Lake, Canada	2012	2
Powder Manufacturer	Iron dust	Hoeganaes Corporation, TN USA	2011	5 (3 incidents)
Coal mine	Methane & coal dust	Upper Branch mine, West Virginia, USA	2010	29
Coal mine	Methane & coal dust	Pike River, New Zealand	2010	29
Sugar Manufacturer	Sugar dust	Imperial Sugar, Port Wentworth, GA	2008	13
Coal mine	Methane & coal dust	KY, USA	2006	5
Plastics Manufacturer	Plastic dust	North Carolina, USA	2003	8
Rubber recycling plant	Rubber dust	Rouse Polymerics International Inc., Vicksburg, MS	2002	5
Powerhouse	Coal dust	Ford Motor Company, Rouge Complex, Dearborn, MI	1999	6
Shell mold manufacturing	Phenol formaldehyde resin	Jahn Foundry, Springfield MA	1999	3

Over the last 20 years, advances in expanding chemical, metallurgical, and pharmaceutical industries have given birth to a steadily increasing number of new finely divided combustible materials [3, 4]. In a review by Abbasi and Abbasi [5], dust deflagrations caused a total of 125 casualties and 398 injuries between 1980 and 2003. These explosions were caused by a wide range of dust particles including grain, aluminum, coal, textile, rubber, tantalum, resin, and others. A recent report from the Occupational Safety & Health Administration (OSHA) [6] further investigating accidents involved with dust-related deflagrations has shown that the problem is still significant.

From a fundamental viewpoint dust combustion is studied for three main reasons: the risk of explosions and fire often caused by fugitive dust produced by industrial processes [3], propulsion, such as when aluminum dust is used as a stabilizer in rocket motors [7], and energy production, such as in oxy-coal combustors [8]. This work focuses on analyzing the risk of explosions caused by mixtures of combustible gasses and dusts (hybrid fuels). This type of explosion often occurs in coal mines which start with a methane air explosion and entrain coal dust as the flame propagates down the mine gallery (see table 1-1 for recent explosions involving this type of dust).

1.2 Hazard assessment used in dust industry

Palmer [9] describes a dust explosion (deflagration) in a facility as a series of explosions. The first primary explosion is relatively small. It ruptures the initial containment releasing a pressure wave followed by a relatively slow fire front. All subsequent explosions following the primary are referred to as secondary explosions. Secondary explosions can result in much higher pressures resulting in significantly greater damage to both personnel and property. Dust mine explosions often have a primary explosion fueled by a methane-air cloud and secondary

explosions fueled by mixtures of methane and coal dust. As discussed by Parnell [10], after the dust explosions in 2009, OSHA revised its Combustible Dust National Emphasis (NEP) program. The NEP looked into 64 industries with over 1000 inspections and found more than 4000 combustible dust related violations. This exhaustive report has led OSHA to consider new rules for facilities handling combustible dust.

A dust is any finely divided solid with a mean diameter less than 420 μm (National Fire Protection Association (NFPA) 68 standard [11]). A list of all relevant parameters quantifying the hazard associated with a particular type of dust, their classification and test methods is provided in Appendix 1. Of these, typically, three quantities [3]: the minimum ignition energy (MIE) [12], the minimum explosible concentration (MEC) [13], and the deflagration index (K_{st}) [14] are mainly used and incorporated in industrial standards. For example, dust hazards are ranked by the Occupational Safety and Health Administration (OSHA) using the dust deflagration index (K_{st}) [15] based on ASTM E 1226 [16]. The deflagration index is related to thermokinetic parameters governing both the flame propagation as well as pressure build up in deflagration and is measured using the explosion-sphere apparatus.

The MIE is the minimum spark energy required to ignite a fuel mixture. It is found experimentally using the Modified Hartmann Tube apparatus by creating a cloud of premixed fuel and sending a spark of known energy (1 kJ) through the mixture. The MEC represents the minimum amount of dust in terms of g/m^3 that can be ignited using an explosion sphere ASTM E 1226 [14], EN 13673 [17].

1.3 The explosion sphere

The explosion sphere (shown in Fig. 1.1) is an experimental device for measuring the deflagration index (K_{st}) discussed earlier. It is based on the early experimental work by Andrews

et al. [18], Abdel-Gayed and Bradley [19] and many subsequent publications by the Leeds group (cf. Bradley, [20]) where burning velocities of gas flames were measured by initiating a flame from a central spark and recording the spherical flame propagation in a closed vessel optically (via a quartz window) or by recording the pressure-time trace by placing a pressure transducer at the vessel walls as shown in Fig. 1.1. This set up was adopted for dust-air pre-mixtures as discussed below (a detailed history is given in Eckhoff [21]).

The standard dust explosion vessel is equipped with a vacuum, dust dispersion, ignition, and pressure sensor systems. The standard procedure begins by placing a measured quantity of a dust sample in a reservoir as shown in Fig. 1.1. Prior to ignition the dust air mixture is discharged into the vessel through a fast acting valve and a rebound nozzle. The dispersed dust cloud is ignited after a specified ignition delay time. The ignition source is typically two chemicals igniters, 5 kJ each, positioned near the center of the vessel. The main operating conditions for two typical explosion vessels are shown in Table 1.2. Measures for the energy content and the reactivity of the dust-air suspension are derived from the pressure-time history as shown in Fig. 1.2. Both the maximum pressure and deflagration index are determined from the same type of experiments in constant volume explosion vessels. Further details are described in standards: ISO 6184-1 [22], EN 14034-1 [23], EN 14034-2 [24], and ASTM E-1226 [14].

Table 1.2: Main operating conditions for two typical explosion vessels

Components	Operating Conditions	
	Standard 20 L vessel	36 L vessel
Reservoir volume	0.6 L	1 L
Initial pressure in vessel	-0.6 barg	-0.3 barg
Fast acting valve time	45 ms	50 ms
Pressure at time of ignition	0 barg	0 barg
Ignition delay time	60 ms	75 ms

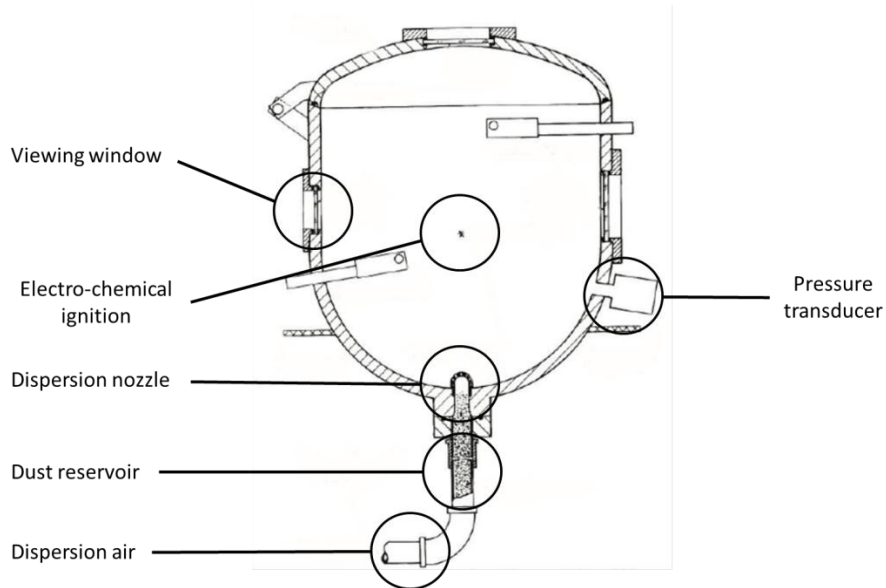


Figure 1.1: Diagram of explosion sphere (Image from ASTM E1515 [13])

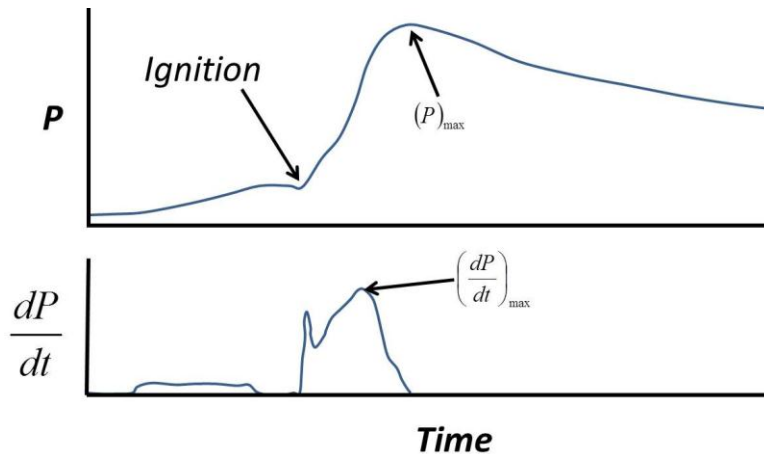


Figure 1.2: Pressure versus time curve and change in pressure versus time curve from an explosion sphere [13].

The deflagration index is determined by an explosion sphere apparatus based on the maximum rate of pressure rise and the volume of the explosion sphere [25] given by the cube root law:

$$K_{st} = \left(\frac{dP(t)}{dt} \right)_{\max} V_o^{1/3}, \quad (1.1)$$

where V_o is the volume of the explosion sphere and dP/dt is the change in pressure over time. It has been shown (Eckhoff [26]) that the deflagration index changes as the size of the explosion sphere changes. This makes the investigation of a dust flame rather difficult and also complicates the hazard classification as the quantity used to characterize the hazard is now dependent on the experimental apparatus. The problem arises mainly due to the increase in turbulent intensity caused by the expanding combustion products in a constant volume vessel.

Figure 1.3 shows an illustrative sketch of an expanding flame front at four different times inside of a typical explosion sphere. The graph shown in Fig. 1.3 shows the turbulent intensity at different time instants. Since the flame front is nonstationary, and accelerates as the flame grows in size, the turbulent intensity will also correspondingly increase as shown in Fig. 1.3. Location, t_1 indicates when the flame is initiating (usually using a chemical igniter or a spark). t_2 indicates the laminar flame propagating outward away from the ignition point. t_3 denotes onset of turbulence which wrinkles the flame. At t_4 the turbulent intensity (u'_{rms}) further increases as shown in the inset to Fig. 1.3.

If it is assumed that the dust particles are sufficiently small and well mixed to behave as premixed flames (and this can be argued as discussed in Chapter 2), the laminar burning velocity S_L or the velocity at which the flame front propagates normal to itself and relative to the flow into the unburnt mixture is very important. For a turbulent flow the turbulent burning velocity S_T , is equal to the *mean* normal velocity and depends on the turbulent intensity u' and the integral length scale l_o . Note that the turbulent burning velocity becomes an averaged quantity as per its

definition. Further, turbulence increases the mass consumption rate of the reactants, or reactant mixture, to values much greater than those that can be obtained with laminar flames. A greater mass consumption rate increases the chemical energy release rate and hence the “power” generated from a certain deflagration. Hence from a practical standpoint, it is important to develop laboratory experiments which can accurately characterize and re-create turbulence levels similar to those found in accidental explosions.

Currently, there is no methodology to incorporate or measure the turbulent burning velocity or the necessary parameters to quantify the turbulence (u' and l_o) using the current design of the explosion sphere. It thus becomes questionable to use the explosion sphere and relate the P vs. t curve to industrial explosions in a meaningful way. Dahoe et al. [27] show that no formal cube-root-law agreement could be found between a 20 L sphere and a 1000 L sphere explosion vessel (though there has been some success with normalization using an estimation of flame thickness by Dahoe [25]). This discrepancy limits the application of the cube root law in the design of deflagration venting and further shows the need to quantify the levels of turbulence and the corresponding effect on flame speed.

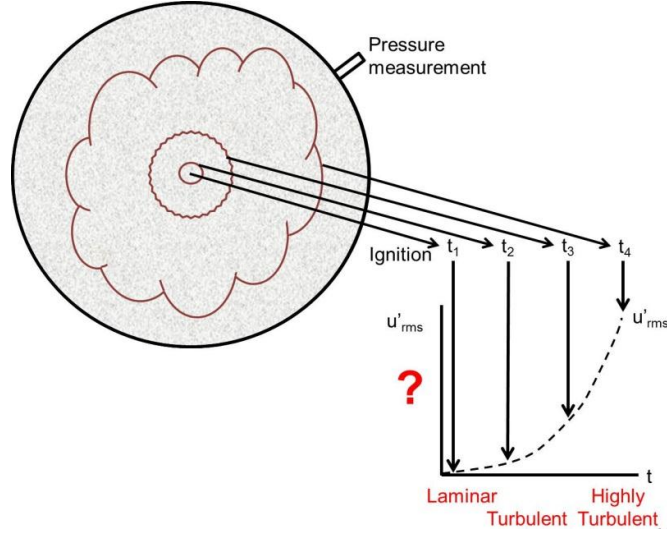


Figure 1.3: Diagram of explosion sphere with increasing turbulence as the flame propagates.

The deflagration index has also been used to estimate the laminar burning velocity for a given dust concentration and particle size using expressions such as [28]:

$$S_L = \frac{K_{st}}{4.84 \left(\frac{P_{max}}{P_o} - 1 \right) P_{max}}, \quad (1.2)$$

where 4.84 is an empirical constant, P_{max} is the maximum pressure, and P_o is the initial pressure. Similar expressions are also used in numerical CFD codes that are used to model dust explosions [29]. Modeling codes like FLACS [30] and similar modeling programs use an empirical correlation ($S_T = F(S_L, u'_{rms}, l_0)$) [20, 30], which correlates the turbulent burning velocity (S_T) as a function of the laminar burning velocity (S_L), turbulent intensity (u'_{rms}), and integral length scale (l_0). It should be noted that none of these are measured for dust-air mixtures. Additional parameters are needed to create a similar relationship for combustion including particles. The effect of dust particles on the turbulent burning velocity has not been thoroughly analyzed in the literature and is the focus of this work.

1.4 Prior related work

To understand the work already published on dust deflagrations, a literature review was conducted to find relevant information on dust flames, turbulent gas flames, experimental methods for studying burning velocity and, hybrid flame experiments. Excellent reviews of publications involving dust flames have been published by Robinson [31], Joshi [32] and Eckhoff [3]. Much of the work reported here is gathered using their reviews as a starting point.

1.4.1 Laminar dust flame experiments

1.4.1.1 Stationary flames

Cassel et al. [33] (1949) were one of the first to publish results using an experimental burner capable of making dust-air mixtures. The procedure consisted of blowing gas jets onto a layer of the pulverized material. This material was continuously agitated by magnetically vibrating an iron diaphragm which forms the bottom of the container. The particles were carried away by the gas current into a vertical pipe whose upper end is connected to a vertical glass tube which serves as the burner tube. The dust receptacle was a brass cylinder 15.24 cm diameter and 10.16 cm high. The pipe extends into the container to a distance of 226.06 cm from the diaphragm. Two gas jet orifices, on opposite sides, entering the receptacle 2.54 cm above the bottom were directed tangentially and turned downward at an angle of 45 deg. To obtain variations of the dust concentration at constant rate of flow, a valve-controlled bypass was provided between the top of the container and the outlet of the pipe so that the gas entraining the dust could be diminished while the rising cloud was diluted with practically dust-free gas. The apparatus could run tests over a period of 10 minutes without refueling. To ensure fully developed flow at the burner port, a length of 3 feet was used for the 2.54 cm glass tubes. The feeding mechanism was calibrated by weighing filtered samples from a constant volume of dust laden gas, aspirated from the emerging cloud.

Ghosh et al. [34] published results from two experiments for studying dust flames in 1957: one inside a furnace and one in open air. The apparatus used for studying pulverized coal flames inside a furnace consisted of a circulatory system for producing a coal dust suspension, and an electrically heated furnace within which combustion took place with the formation of a flame. The circulatory system consisted of a blower, the inlet and outlet of which were connected by a loop. Coal dust and air were circulated through this loop and the suspension produced was fed into the burner through an outlet tube attached vertically, axially to the elbow of the descending limb of the loop. A vibrator was placed against the descending limb of the apparatus in order to minimize settling of coal dust on the tube walls. The burner tube as a vertical water cooled copper tube 5mm ID, connected to an outlet tube of the circulatory systems by means of a short piece of rubber tubing. The tip of the burner tube projected one inch from the cooling jacket. When placed in the operating position, the tip was flushed with the ceiling of the furnace cavity. A mirror allowed observation of the flame from the bottom. The circulatory system was air-tight, therefore, the rate of flow suspension was obtained from the rate at which air was introduced into the system. The rate of coal flow was determined by removing the burner tube, collecting the coal flowing through the coal outlet of the loop for one minute, and weighing.

The apparatus used for studying flames in open air consisted of a blower for producing coal dust suspensions. Pulverized coal was kept in an inclined conical flask and was introduced into the blower by gently vibrating the flask. The coal concentration in the suspension could be varied by varying the speed of the blower and the rate of vibrating the flask. The coal concentration in the suspension was measured by aspirating a known volume of the suspension through a dust filter and weighing the coal collected.

Hattori [35] published results from a steady-state experimental method in 1957. Pulverized coal-air mixtures were discharged from a burner into free air, and ignited by an ignition source placed in the center of the burner. Flame propagated into the mixture and an inverted cone flame front was formed. Pulverized coal stored in hopper was fed continuously by a screw feeder driven by variable speed D.C. motor. Coal and air from the screw feeder were uniformly mixed in a cyclone mixer and led into the burner tube. The mixture passed through an annular space formed by the burner tube and ignition gas tube, and was discharged upward to open atmosphere. Acetylene (as ignition gas), was also discharged upward to open air through the ignition gas tube. Electromagnetic vibrators were attached to the hopper and the mixer lest the pulverized coal should adhere to the walls. When the acetylene was ignited a steady inverted cone flame was formed.

Burgoyne et al. [36] published results from a downward pointing steady state burner in 1958. The suspension for combustion was formed by jet impaction of a regular supply of solid by the carrier air, and was burnt on a downward pointing water cooled burner. The tendency of buoyancy to distort the flame was countered by an extraction system mounted below the burner. Two types of burner nozzles were used: a convergent nozzle with a throat/bore ratio of approximately $\frac{1}{4}$ and a short tube $2 \frac{1}{5}$ in long. Flames propagated only if a form of energy addition were maintained, and a convenient source was found to be an annular premixed coal gas-air flame, formed at the periphery of the coal-air stream. The concentration of the cloud was determined either before ignition or after extinction of the flame by collecting the issuing coal dust on a filter.

Palmer et al. and William et al. [37, 38] published results from a steady-state, laminar dust flame burner in 1962. Dispersion of the dust was achieved by means of a unit at the bottom of the

burner. In the dust dispersion unit was a hypodermic needle, through which the input gas stream passed at a pressure drop of about 20 psig. The exiting high velocity gases impinged on the dust bed, thus generating the dust dispersion. The dust reached the hypodermic needle through an opening cut in the base of the burner tube. A constant supply of dust was kept moving in to the dispersion chamber by the rotation of a brass container which enclosed the entire dispersion unit. In addition to the gas flowing through the hypodermic needle, another stream of gas flowed through a central dilution tube. This stream was used to decrease the proportion of the gas used to disperse the dust, thus allowing the concentration to vary. Regardless of the flow rate through the central tube, the pressure behind the hypodermic needle was normally maintained at 20 psig. The generated dust cloud rose vertically through the burner tube (2 cm. ID., 56 cm, length the top 22 cm of which could be heated electronically) which was tapped continuously by a 60 cycle electromagnet vibrator. Surrounding the upper 30 cm of the burner tube was a 5 cm ID aluminum jacket through which flowed the auxiliary nitrogen stream. From there, it flowed unrestricted to the top, where it was accelerated through a nozzle. In order to maintain a stable flame consistently it was necessary to use a flame-holding device: a brass ring with a conical cross section, where the apex of the cone was oriented downward toward the burner. The brass ring was customarily heated before igniting the flames.

Mason et al. [39] published results from a laminar, steady-state dust flame burner in 1967 where fluidizing air was supplied from a humidifying and metering system, via a Manostat and control valve. The resulting suspension flew up into the diverging section, where the flow was divided: part passed up the burner tube (10.9 mm bore) and the surplus was exhausted. The concentration of the suspension could be varied by adjusting the flow of fluidizing air, and the flow velocity up the burner tube could be varied independently by altering the exhaust flow. A flame trap was

fitted at the bottom of the burner tube. In the exhaust system the surplus air was filtered and measured, and then passed to a valve system. The pump was arranged so that all of the suspension formed in the fluidized bed could be exhausted or any desired fraction could be made to flow up the burner tube. The concentration of the suspension emerging from the burner could be measured by attaching to it a reducing nozzle with plastic tube leading to a weighed filter followed by a pump, control valves and bubble meter. The sampling time was at least one minute.

Bryant [40] built a steady-state burner apparatus in 1971. The various gases and solids were introduced into the narrow channel at the base of the burner where they were mixed and their flow streamlined as they passed upward through the conical volume and the coarse screen off which the flame was stabilized. The screen was required to prevent flashback. In some experiments the flame was surrounded by a blanket of oxygen. The powder-dispersing device was a modified S. S. White Model F abrasive cutting unit. The modifications consisted of the removal of the powder container and vibrating table from the original cabinet to a position immediately adjacent to the burner, manufacture of a gas-tight cap for the container, and the installation of remote controls for the vibrating table and carrier gas. The rates were determined by collecting and weighing. The oxygen and propane went directly into the base of the burner. The powder and gases were mixed in the burner and were expelled through the burner screen. Typical operating procedures consisted of establishing a propane-oxygen-nitrogen flame, introducing the powder by activating the vibrator, and finally reducing the propane, nitrogen, and oxygen flows until the desired flame conditions were obtained.

Strehlow et al. [41] published results from a steady state-burner in 1974. The basic objective of the burner design was to obtain two relatively large-area coaxial streams with flat laminar

velocity profiles, such that the central stream could be completely surrounded by hot products from the combustion of a gaseous fuel in the outer stream. The two innermost regions of the burner were fed by combustible streams. The inner rectangular test stream region can be fed a mixture of fuel air and suppressant consisting of up to five different gasses and two different solid powders, all independently metered. The coaxial annular region directly outside of the inner stream could be fed by a fuel-air mixture. This outer region provided an atmosphere containing products of combustion of a non-suppressed, premixed, laminar flame and therefore represented a continuous strong igniter for the inner test flow region. The flow area outside the ignition flame could contain only air and served to shield the outer edge of the flame from external disturbances. The burner was enclosed on all sides by 10 inch high windows to provide shielding from room disturbances and free edge mixing. Coal dust and one suppressant powder could be fed to the central stream by means of the feed disk scraper blade. The dust was kept suspended in the feed tube, in the diffuser, and as it passed through the bore tubes by means of a “white” noise acoustic energy field in the burner tube. Coal dust concentrations were determined at the burner head using a total capture technique by weighing the coal dust captured over a specified time.

Milne et al. [42] published results from a new experiment in 1977. Dry air from a cylinder entered at the bottom of a glass storage section and passed through a sintered-metal porous disk. This fluidizing air passed up through the column of coal dust. One portion flowed out through the exit tube and the rest exited through a filter and a flowing-meter at the top of the apparatus. An additional flow of gas, to assist transport of the coal-air along the tube and into the burner, was provided near the entrance of the intake tube. Best results were obtained when a stirrer was

added to continuously agitate the fluid bed of coal, when the outtake tube was periodically reamed out and when the pressure in the fluidizer was held constant with a pressure controller.

Bradley et al. [43] published results from an experiment in 1994 which used a graphite-entraining fluidized bed and burner to provide flat, laminar, adiabatic, methane-air flames, seeded with graphite. The stainless steel tube of the matrix burner was of 76 mm diameter, while the matrix at the end of it comprised of a disk of graphite-impregnated copper. This facilitated the drilling of approximately 2500 holes of 1mm diameter in it, with a distance between hole centers of 1.5mm. The burner tube moved vertically within a copper frame tube of 254 mm diameter. A smaller window enabled the flame to be observed and photographed. Methane-air mixtures were ignited by a retractable igniter and burned gasses were exhausted along the water cooled flame tube to atmosphere by a water-cooled rotary exhauster. A gate valve located in the exhaust line acted as a critical flow control and prevented back-transmission of pressure pulses to the flame. A large gate valve at the exhauster provided coarse control of the pressure. The dried air and methane mass flow rates were metered separately by orifices and mixed in a mixing chamber. Thereafter, the mixture divided into two streams, one of which passed through a fluidized bed to entrain the graphite. An important difference from previous work arose from the necessity to operate with a higher overall mass fraction of graphite in the final mixture. The gas and entrained particles passed into a top conical section and along a tube of 6 mm diameter to join the gas flow that had bypassed the bed, before entering the burner tube. The mass of graphite entrained was found by weighing at known time intervals. Linearity and constancy of calibration were maintained for up to one hour.

Goroshin et al. and Lee [44, 45] published results using an experimental setup comprised of a water-cooled, laminar, dust burner nozzle. The dust dispersion system included a syringe-type

dust feeder and a circular, annular, high-velocity gas jet sheet. The system had an ability to produce a uniform dust flow for a wide range of dust concentrations for duration of up to six minutes. A long, stainless steel tube of 70 cm length and inner diameter 25 mm was connected to the dispersion chamber through a small-angle conical diffuser. This provided laminarization of the initially turbulent dust flow as it exited the dust disperser. The dust flow exited the combustion tube through a small-angle conical nozzle. A water-cooled brass ring with a triangular cross section was used as a flame holder, located 1 cm above the nozzle exit. An auxiliary stream of N_2 , concentric to the dust stream, was used to maintain the cylindrical configuration of the dust cloud issuing from the burner. The flame shapes were recorded with a Canon single-lens reflex camera with a bellows macrophoto attachment at a scale of 3:1. A neutral filter with an optical density of about three had to be used to attenuate the flame radiation.

Andac et al. [46] published results from a counter flow experiment to study flame extinction from inert particles. The experimental configuration includes the use of two counter flowing jets exiting from two opposing burners. The particle seeder utilizes a piston which was attached beneath the bottom burner and fed the particles into the flow at a constant rate. Chemically inert aluminum oxide and nickel alloy particles were used. The particle mass delivery was determined by both the piston speed and the flow rate. The gas flow enters the top of the piston shaft through sixteen, 1 mm, diameter holes equally spaced around the shaft, which locally increase the gas velocity and improve the entrainment of particles into the flow. This design allowed for seeding under both normal and microgravity. However, it should be obvious that the particle pickup was strongly affected by gravitational forces. The particle seeder was calibrated by seeding the particles into the air flow for a specified time and measuring the mass collected.

Kolbe [47] published results from a new steady state dust burner in 2001. The typical experimental time span was approximately 5-6 minutes, from which a stable flame could be achieved for up to four minutes. The cylindrical steel hopper, in which the dust is contained, guided the piston, which pushed the dust sample upwards. The piston speed was controlled by means of an electro-mechanical actuator. Another cylindrical housing in which air is fed surrounded this contraction. As both dust and air traveled separately upward, they were mixed when the air is forced into a circumferential channel that encountered the upward moving dust pile and entrained it. By forcing the air jet through a thin slot, a very high rate of shear was created sufficient to provide the necessary turbulence to dislodge the dust particles. The mixture was laminarized by expanding the dust flow through a diffuser. A brass elbow fitting had the ability to decrease or increase the dust flow without affecting the dust-air dispersion or concentration. The ejector connected the main burner tube to a smaller bypass side tube. Following the location of the ejector were two sections of stainless steel tubing that made up the main burner tube. Resting on the brass connector was a glass tube that encompassed the second upper steel tube. Regular dry air was made to flow in this glass tube at relatively low flow rates, to provide an enveloping blanket or protective co-flow for the exiting dust air flow. This co-flow existed so that the dust-air mixture remained in a laminar, column-like form once it exited from the conical nozzle and recirculation eddies forming at the nozzle exit could be prevented. The dust flow finally exited the tube through a conical brass nozzle which could have varying contraction angles. The flame, directly stabilized on the nozzle, eliminating the uncertainty in flow rate that might occur from gas entrainment into the flame from the surrounding atmosphere beneath a cooling ring.

Gonzalez et al. [48] published results from an inverted burner to study the flame speed in a dust cloud, with a pilot-stabilized flame in 2006. Because of the large density of dust and the high particle loading of the cloud, they used a vertical, downward-facing flow. Dust stored in a hopper was fed continuously to the burner using a vibrator. A stable particle flow was obtained, regulating the opening exit in the hopper and the vibration frequency. Oxygen and air were fed in the upper part of the burner: each flow was measured and adjusted to get the desired concentration. The mixture passed through an annular space formed by the burner tube and the ignition gas pilot tube, and was discharged downward to the combustion chamber with an Acetylene and air pilot burner in the centre. The pilot's function was to initiate the reaction of the dust-air mixture and stabilize the flame.

1.4.1.2 Non-stationary flames

Palmer et al. [49] published results from a flame propagation apparatus using a long vertical tube in 1971 as described by Eckhoff [21]. The dust was introduced at the top of the tube by a screw feeder and dropped into a vibrating, 20 cm diameter and 15 cm high, dispersing cylinder hanging immediately underneath the screw exit. After having passed through the perforated bottom of the cylinder, the dispersed dust settled freely under gravity through the entire length of the tube, until finally being collected in a bin at the bottom end. Dust concentration and flame propagation could not be measured in the same test, but had to be determined in separate tests at nominally identical dust cloud generation conditions, i.e. rotating speed of the feeding screw conveyor and vibration mode of the dust disperser. The dust concentration was measured gravimetrically. A manually operated sliding tray was inserted into the tube like a gate valve. By simultaneously closing the tube at the top by a conventional sliding gate valve, the volume of dust cloud between the top valve and the tray was trapped. Immediately before performing an

explosion test the dust feed was stopped and the bottom end of the tube closed by a gate valve located just below the ignition zone. The ignition source was a propane flame, generated by injecting a small pocket of propane-air mixture into the bottom region of the explosion tube and igniting by means of an electric spark located at the tube axis. By means of this apparatus, a flame traveled vertically upwards, away from the ignition source, and could be determined as a function of the average dust concentration.

Proust [4, 50] used a vertical square tube 10 by 10 cm, with a length of 1.5 m. Another apparatus with larger dimensions was also used by Proust et al. [51]: 3 m long tube, the cross section of the duct was square (0.2 m x 0.2m) and, over 2 m. The tube was made of glass in order to obtain good conditions for visualization. The suspension was generated through the elutriation of dust particles above a fluidized bed. Ignition of the mixture was achieved using an electrically heated tungsten wire. The flame propagates from the open end of the tube (at the bottom) up to the closed end (at the top). Ionization probes were used to determine the flame location; thermocouples were used to measure the maximum flame temperature and collimated photodiodes to record the light emitted by the flame front. Two kinds of photographic records were performed: self-emitted light and laser tomographic records. Dust concentrations were determined by measuring the decrease of mass of the elutriator and by metering the air flow rate. The laser tomographic system was used to control the homogeneity of the suspension.

Goroshin et al. [52] published results from an experiment which consisted of two parts: a dust feeder and a disperser. The dust was fed via a syringe-type device which had an internal diameter of 2.5 cm and a maximum piston stroke of 20 cm. The rate at which the dust was supplied to the flow (and hence the dust concentration in the suspension) was controlled by varying the piston speed with the help of a special electromechanical system. The range of the piston speed was

0.5-3 cm/min. The dust was dispersed at the base of a conical chamber through the impact of a high velocity cylindrical jet issuing from an adjustable circular slot. A Pyrex flame tube (5 cm i.d. and 120 cm length) where combustion experiments were performed was connected to the dispersion chamber through an 8" conical diffuser. The diffuser provided expansion and laminarization of the dust flow which is initially turbulent in the dust disperser.

Han et al. [53, 54] published results from a combustion system for laminar flame propagation in dust-air mixtures. The main part of the system consisted of a vertical duct, 1800 mm height with 150x150 mm square cross-section, a shutter, an ignition device, a dust cloud generator and an airflow feeder with pressure controller. The dimensions of the combustion duct were chosen to reduce the amount of lateral heat losses from the flame to the duct walls similar to Proust et al. [51]. Dust suspensions were generated through elutriation of dust particles above a fluidized bed. Aspects of flame propagation were observed through a glass 1800 mm high in the front of the vertical duct. Using the slide-type windows of quartz glass on the side of the duct, it was possible to make a laser light sheet from the side wall of the duct and change the observation area of flame propagation. A pair of electrodes for spark ignitions was placed 150 mm above the lower end of the duct. The dust particles were layered on a fine porous plate at the bottom of the duct. Air at appropriate rates was introduced through the porous plate which acted as a flow rectifier to disperse the dust particles when the upper end of the duct was open. When the duct was entirely filled with a dust cloud, a time controlling system interrupted the air flow and removed the fluidized bed from the bottom of the duct. To reduce the influence of the initial turbulence of flow in the duct, the ignition time was delayed by 0.3–0.5 s before ignition. The flame will propagate upwards in a quasi-quiescent medium. Dust concentration was determined by measuring the decrease of mass of dust in the movable system (fluidized bed). The process of

flame propagation was recorded by several video cameras. An ion probe and thermocouple with schlieren optical system were used to examine the structure of the combustion zone and the temperature distribution simultaneously.

Dobashi et al. [55] published results from an experiment to burn stearic acid particles in 2006. Stearic acid was heated to become liquid and sprayed through a two-phase nozzle. The sprays of liquefied stearic acid quickly solidified into suspended combustible particles. The concentration and particle size distribution were controlled by supply pressures of liquid and air to the nozzle. Ignition was started after some duration from the end of the spraying in order to sufficiently suppress the flow turbulence induced by spraying. After ignition by an electric spark, a flame propagated outward from the ignition point. In this set-up, the flame propagation in an open field could be observed. The propagating flame was recorded by a CCD video camera.

1.4.2 Turbulent dust flame experiments

1.4.2.1 Stationary flames

Turbulent gas flames have been reviewed by Bradley et al. [56], Williams [57], Pope [58], Borghi et al. [59], Chomiak [60], and Ballal [61]. Some turbulent burner design ideas from Kobayashi et al. [62]. Smallwood et al. [63], and Filatyev [64] have been incorporated in the current design discussed in section 3.

1.4.2.2 Non-stationary flames

Hertzberg et al. [65] published results from a 7.8-liter flammability chamber, a modified and larger version of the "standard" 1.2-liter Hartmann apparatus. This instrument included a dust probe, pressure transducer, oxygen sensor, dust cup, and ignition point. The top plate of the chamber was fitted with a sapphire window assembly, through which the infrared radiance of the explosion could be measured. The normal procedure was to spread a measured mass of dust

uniformly around the disperser cone. The top plate was then bolted and the chamber partially evacuated to about 0.2 atm. The air-dispersion tank was pressurized to 5 atm. This 0.2 sec air impulse dispersed the dust, mixed with it, and raised the chamber pressure to 1.0 atm. After another 0.1 sec delay to allow for more uniform dispersion, the ignition source was energized. If the mixture was flammable, the developing pressure and infrared spectral radiance were monitored. When flame propagation was complete and after the combustion products cooled, the residual oxygen content was measured and dust or gas samples could be taken for analysis.

Li et al. [66] published results from a long tube to study dust combustion called the Flame Acceleration Tube (FAT) which was a 70-m-long, 30-cm-diameter tube. The FAT was instrumented with static pressure transducers, dynamic pressure transducers, and photodiodes at eight stations along the tube. A four-wavelength optical pyrometer was mounted near the end of the tube. The initiator consisted of two parts: a 2.44-m-long and 5.08-cm-diameter detonation tube separated from the FAT by a Mylar diaphragm, which was filled with a flammable mixture, followed by a 3-m-long section of the FAT in which dust was dispersed by loading it into a V channel fitted with air injection holes. A specially designed cart, equipped with a 6-L dust pan, an auger, two motors and a fan, was used to travel inside the FAT to deposit a dust layer with a predetermined thickness and width on the bottom of the FAT.

In 2001 Sun et al. [67] published results using an experimental setup in which a flame could propagate in an open field without any influence from the chamber wall. This experiment was comprised of an air supplying part, a controller part, a combustion chamber, an ignition part, a laser light source, a temperature measurement setup and a high-speed video camera with a microscopic optical system. The combustion chamber (76 mm inside diameter) was provided with an air nozzle, a sample dish, a pair of ignition electrodes, and a movable tube. Before the

movable tube started to move down, the iron dust was dispersed by air into the combustion chamber. Just after the movable tube had moved down to its bottom position, the suspended iron dust was ignited by an electric spark. A flame then started to propagate throughout the iron particle cloud.

Ju et al. and Chen et al. [68, 69] published results from a constant pressure flash fire burner. The system consists of an atomizing nozzle, cylindrical ducts and electric heaters. To minimize the influence of air flow on cloud behavior, a piece of aluminum plate was placed closely around the nozzle. In the experiments, the fuel in a reservoir was heated to become liquid just above its melting point and sprayed by the nozzle. The liquid droplets turned into solid particles during their rise along to the test section. The distribution of particles diameters was controlled by changing the pressure of the feeding air and fuel. To avoid influences of turbulence caused by fuel spraying on the combustion phenomena, the ignition time was delayed by 0.5 s after the end of fuel spraying. The particle cloud was ignited at its centre by an electric spark. Just before the particle cloud ignited, the middle part of the duct was moved down. Thus the combustion of the particle cloud could be kept free from the influence of the wall.

1.4.3 Hybrid flame experiments

Hybrid flames have been studied by a number of researchers (Chen et al. [70], Amyotte et al. [71], Bradley et al. [72], Ju et al. [73], Andac et al. [74]). Relevant to this work, Benedetto et al. [75] and Liu et al. [76] both studied hybrid mixtures of coal dust-methane-air hybrid flames. Liu showed that the hybrid mixture had a lower flammability limit than coal dust flames meaning that hybrid mixtures were more hazardous than a gas or dust alone. Benedetto et al. [75] showed that the turbulence generated by the expanding products of combustion needs to be quantified in order to determine the correct turbulent burning velocity. These two studies injected coal

dust/methane clouds into a combustion chamber, ignited the clouds using electronic igniters, and analyzed the clouds using either visual or Schlieren measurements recorded on a high speed camera. While they noted the importance of turbulent intensity, Benedetto et al. [75] and Liu et al. [76] were not able to quantify it. Laminar hybrid flames of methane-coal and air were successfully studied by Xie et al. [77, 78] using a Bunsen burner style burner nozzle, similar to the one used for laminar flames in this study.

1.4.4 Modeling of dust flames

The earliest work on dust-air premixed flames was reported by Nusselt [79] in 1924 who investigated coal mine explosions and focused on incorporating particle radiation in the classical gaseous premixed flame model developed by Mallard and Le Chatelier [80] in 1883. Effects of conduction, devolatilization, gas-phase reaction and diffusion were subsequently added by several researchers with a comprehensive review by Eckhoff [26] in 2003. Noteworthy in this group of literature is the work by Seshadri et al. [81], as it is the first study that incorporated both gas and condensed-phase kinetics, and thereby systematically analyzed the influence of volatilization on dust flame dynamics. Recent work by Bidabadi and Rahbari [82] extended the theory to include the effects of inter-particle conduction as well. A detailed literature is available in Smoot and Horton [83], Krazinski et al. [84], and Slezak et al. [85].

1.5 Goals and objectives of the current study

Initiation and propagation of dust deflagrations are extremely complex phenomena due to the interaction between solid particles and the gaseous flame front. In comparison with premixed gas deflagration, a dust-oxidizer deflagration depends on the rate of evolution of volatiles, the mixing of these volatiles with the oxidizer surrounding the particles, coupling of the particles and gas phase oxidation as well as radiative energy exchange between the flame and its surroundings.

Though engineering tools such as the DESC code produced by Gexcon have been created, due to the complications discussed above, a comprehensive mathematical theory to predict deflagration mechanisms of dust clouds is at present beyond reach. Although vast amount of testing, both small scale (20 liter explosion vessel) and large scale tests have been done over the last 50 years, most theories that connect the data to models are heavily empirical and the problem has never been analyzed from a fundamental viewpoint.

Identification of the controlling parameters of dust deflagration mechanisms is crucial to our understanding of the problem. As a first step, a scientific experimental platform is needed to understand the physical and chemical processes that control the behavior of dust flames in both laminar and turbulent flow fields. The objective of this study is to develop such an experimental platform capable of measuring the laminar and turbulent burning velocity of a dust-air premixed flame as a function of properties specific to the reactants such as dust-particle size and concentration.

The experimental set up is then used to analyze the a particle-gas-air premixed system composed of micron sized coal dust particles (75 – 90 and 106 – 120 μm) in a premixed CH_4 -air ($\phi = 0.8, 1.0$ and 1.2) flame. This work will ultimately improve the knowledge on fundamental aspects of dust flames which is essential for the development of mathematical models. This study is the first of its kind where different parameters that govern flame propagation in a spatially uniform cloud of volatile particles are systematically analyzed. These parameters include initial particle radius, number density or concentration, turbulent intensity and length scale. The major improvement of the experiment used in this work beyond the experiments described in the work above is the ability to control and quantify the turbulent intensity and integral length scale in the burner which, as discussed, play a major role in the turbulent burning velocity.

1.6 Organization of the thesis

The thesis is organized into five chapters as follows:

Chapter 1, provides a broader background to the topic of dust deflagrations as well as a literature review related to the topic.

Chapter 2, analyzes the structure of a dust flame. This chapter forms the body of a paper that is currently under review in the Fire Safety Journal (submitted in Dec 2011).

Chapter 3 is a detailed discussion of the experimental set up capable of analyzing a turbulent dust flame

Chapter 4 is a discussion of the experimentally observed behavior of a turbulent hybrid flame

Chapter 5 summarizes the conclusions of this study

A total of five appendices A1 to A5 are provided at the end of the document as supplementary material.

References:

1. Hoekstra, G., *Knowledge of wood-dust explosions not widespread in B.C. industry*. 2012, Vancouver Sun.
2. Frank., W.L. and M.L. Holcomb, *Housekeeping Solutions*.
3. Eckhoff, R.K., *Dust Explosions in the Process Industries, Third Edition*. Third ed. 2003, Boston: Gulf Professional Publishing.
4. Proust, C., *A Few Fundamental Aspects About Ignition and Flame Propagation in Dust Clouds*. Journal of Loss Prevention in the Process Industries, 2006. **19**: p. 104-120.
5. Abbasi, T. and S.A. Abbasi, *Dust explosions-cases, causes, consequences, and control*. Journal of Hazardous Materials, 2007. **140**: p. 44-77.
6. *Occupational Safety and health Administration (OSHA), Combustible dust expert forum - meeting summary report*. 2011.
7. Galfetti, L., L.T. De Luca, F. Severini, L. Meda, G. Marra, M. Marchetti, M. Regi, and S. Bellucci, *Nanoparticles for Solid Rocket Propulsion*. Journal of Physics: Condensed Matter, 2006. **18**: p. 33.
8. Buhre, B.J.P., L.K. Elliott, C.D. Sheng, R.P. Gupta, and T.F. Wall, *Oxi-fuel Combustion Technology for Coal Fired Power Generation*. Progress in Energy and Combustion Science, 2005. **31**(4): p. 283-307.
9. Palmer, K.N., *Dust Explosions and Fires*. 1973, London, United Kingdom: Chapman and Hall Ltd.
10. C. B. Parnell, J., R.O. McGee, F.J. Vanderlick, and A. Contreras, *A Critical Evaluation of Combustible Dust Test Methods*, in *Beyond Regulatory Compliance: Making Safety Second Nature*. 2011: Texas A&M University, College Station, Texas.
11. *NFPA 68 Standard on Explosion Protection by Deflagration Venting*. 2007, National Fire Protection Association.
12. ASTM-E2019, *Standard Test Method for Minimum Ignition Energy of Dust Cloud in Air*. 2010.

13. ASTM-E1515, *Standard Test Method for Minimum Explosible Concentration of Combustible Dusts*. 2010.
14. ASTM-E1226 *Standard Test Method for pressure and rate of pressure rise for combustible dusts*. 2010, American Society for Testing and Materials (ASTM).
15. OSHA, *Hazard Communication Guidance for Combustible Dusts*. 2009.
16. ASTM-E-1354, *E 1354 Standard Test Method for Heat and Visible Smoke Release Rates for Materials and Products Using an Oxygen Consumption Calorimeter*. 2009.
17. EN 13673-1: *Determination of the maximum explosion pressure and the maximum rate of pressure rise of gases and vapours. Determination of the maximum explosion pressure*. 2003.
18. Andrews, G.E., D. Bradley, and S.B. Lwakabamba, *Turbulence and Turbulent Flame Propagation - A Critical Appraisal*. *Combust. Flame*, 1975. **24**: p. 285-304.
19. Abdel-Gayed, R.G. and D. Bradley, *Dependence of turbulent burning velocity on turbulent reynolds number and ratio of laminar burning velocity to R.M.S. turbulent velocity*. *Proc. Combust. Inst.*, 1977. **16**: p. 1725-1735.
20. Bradley, B., *How Fast Can We Burn*. *Proc. Combust. Inst.*, 1992. **24**: p. 247-262.
21. Eckhoff, R.K., *Explosion Hazards in the Process Industries*. 2005, Houston, TX.
22. ISO 6184-1 *Explosion Protection Systems - Part 1: Determination of explosion indices of combustible dusts in air. International Organization for Standardization (ISO)*. 1985.
23. EN 14034-1 *Determination of explosion characteristics of dust clouds - Part 1: Determination of the maximum explosion pressure Pmax of dust clouds*. 2004, European Committee for Standardization (CEN): Brussels.
24. EN 14034-2 *Determination of explosion characteristics of dust clouds - part 2: Determination of the maximum rate of explosion pressure rise of dust clouds*. 2006, European Committee for Standardization (CEN): Brussels.
25. Dahoe, A.E., J.F. Zevenbergen, P.J.T. Verheijen, S.M. Lemkowitz, and B. Scarlett (1996) *Dust Explosions in Spherical Vessels: Prediction of the Pressure Evolution and Determination of the Burning Velocity and Flame Thickness*. **Volume**,
26. Eckhoff, R.K., *Dust Explosions in the Process Industries*. 2003, Boston: Gulf Professional Publishing.
27. Dahoe, A.E., R.S. Cant, and B. scarlett, *On the Decay of Turbulence in the 20-Liter Explosion Sphere*. *Flow, Turbulence and Combustion*, 2001. **67**: p. 159-184.
28. Cashdollar, K.L., *Overview of Dust Explosibility Characteristics*. *Journal of Loss Prevention in the Process Industries*, 2000. **13**: p. 183-199.
29. Skjold, T., *Review of the DESC project*. *Journal of the Loss Prevention in the Process Industries*, 2007. **20**: p. 291-302.
30. Arntzen, B.J., H.C. Salvesen, H.F. Nordhaug, I.E. Storvik, and O.R. Hansen, *CFD Modelling of Oil Mist and Dust Explosion Experiments*.
31. Robinson, G.F., *Pollutant Formation in Turbulent Flames*, in *Field of Mechanical Engineering & Astronautical Sciences*. 1974, Northwestern University: Evanston, Illinois.
32. Joshi, N.D., *Gravitational Effects on Particle Cloud Flames*, in *Mechanical Engineering*. 1984, State University of New York at Stony Brook: New York.
33. Cassel, H.M., A.K.D. Gupta, and S. Guruswamy, *Factors Affecting Flame Propagation Through Dust Clouds*. *Third Symposium on Combustion, Flame and Explosion Phenomena*, 1949: p. 185-190.
34. Ghosh, B., D. Basu, and N.K. Roy. *Studies of Pulverized Coal Flames*. in *Proc. Combust. Inst.* 1957.

35. Hattori, H. *Flame Propagation in pulverized coal-air mixtures*. in *Proc. Combust. Inst.* 1957.
36. Burgoyne, J.H. and V.D. Long, *Some Measurements of the Burning Velocity of Coal-in-air Suspensions*, in *Conference on Science in the use of coal*. 1958.
37. Palmer, H.B., D.J. Seery, and W.F. Marshall, *A study of the burning velocity of laminar coal dust flames*. 1962.
38. William F. Marshall, J., *The Effect of Concentration and Particle Size on the Burning Velocity of Laminar Coal Dust Flames*, in *Department of Fuel Technology*. 1964, Pennsylvania State University.
39. Mason, W.E. and M.J.G. Wilson, *Laminar Flames of Lycopodium Dust in Air*. *Combustion and Flame*, 1967. **11**(3): p. 195-200.
40. Bryant, J.T., *The Combustion of Premixed Laminar Graphite Dust Flames at Atmospheric Pressure*. *Combustion Science and Technology*, 1971. **2**: p. 389-399.
41. Strehlow, R.A., L.D. Savage, and S.C. Sorenson, *Coal Dust Combustion and Suppression*, in *AIAA/SAE 10th Propulsion Conference*. 1974: San Diego, CA.
42. Milne, T.A. and J.E. Beachey, *The Microstructure of Pulverized Coal-Air Flames I: Stabilization of Small Bunsen Burner and direct sampling techniques*. *Combustion Science and Technology*, 1977. **16**: p. 123-138.
43. Bradley, D., Z. Chen, S. El-Sherif, S.E.-D. Habik, and G. John, *Structure of Laminar Premixed Carbon-Methane-Air Flames and Ultrafine Coal Combustion*. *Combustion and Flame*, 1994. **96**: p. 80-96.
44. Goroshin, S., I. Fomenko, and J.H.S. Lee. *Burning Velocities in Fuel-Rich Aluminum Dust Clouds*. in *Proc. Combust. Inst.* 1996: The Combustion Institute.
45. Lee, J., *Burning velocity measurements in aluminum-air suspensions using bunsen-type dust flames*. 2001.
46. Andac, M.G., F.N. Egolfopoulos, C.S. Cambell, and R. Lauvergne, *Effects of inert dust clouds on the extinction of strained, laminar flames at normal- and micro-gravity*. *Proc. Combust. Inst.*, 2000. **28**: p. 2921-2929.
47. Kolbe, M., *Laminar Burning Velocity Measurements of Stabilized Aluminum Dust Flames*, in *Mechanical Engineering*. 2001, Concordia University Montreal: Quebec, Canada.
48. Gonzalez, O., J.F. Richards, and J.D.D. Rivera, *Measurement of Flame Speed in Copper Concentrate Clouds*. *Journal of the Chilean Chemical Society*, 2006. **51**(2): p. 869-874.
49. Palmer, K.N. and P.S. Tonkin, *Coal Dust Explosions in a Large-Scale Vertical Tube Apparatus*. *Combustion and Flame*, 1971. **17**: p. 159-170.
50. Proust, C., *Flame Propagation and Combustion in some dust-air mixures*. *Journal of Loss Prevention in the Process Industries*, 2006. **19**: p. 89-100.
51. Proust, C. and B. Veysiere, *Fundamental Properties of Flames Propagating in Starch Dust-Air Mixtures*. *Combustion Science and Technology*, 1988. **62**(4): p. 149-172.
52. Goroshin, S., M. Bidabadi, and J.H.S. Lee, *Quenching Distance of Laminar Flame in Aluminum Dust Clouds*. *Combustion and Flame*, 1996. **105**: p. 147-160.
53. Han, O.-S., M. Yashima, T. Matsuda, H. Matsui, A. Miyake, and T. Ogawa, *Behavior of flames propagating through lycopodium dust clouds in a vertical duct*. *Journal of Loss Prevention in the Process Industries*, 2000. **13**: p. 449-457.
54. Han, O.S., M. Yashima, T. Matsuda, H. Matsui, A. Miyake, and T. Ogawa, *A study of flame propagation mechanisms in lycopodium dust clouds based on dust particles' behavior*. *Journal of Loss Prevention in the Process Industries*, 2001. **14**(3): p. 153-160.

55. Dobashi, R. and K. Senda, *Detailed analysis of flame propagation during dust explosions by UV band observations*. Journal of Loss Prevention in the Process Industries, 2006. **19**: p. 149-153.
56. Bradley, D., M.Z. Haq, R.A. Hicks, T. Kitagawa, M. Lawes, C.G.W. Sheppard, and R. Woolley, *Turbulent Burning Velocity, Burning Gas Distribution, and Associated Flame Surface Definition*. Combustion and Flame, 2003. **133**: p. 415-430.
57. Williams, F.A., *An Approach to Turbulent Flame Theory*. Journal of Fluid Mechanics, 1970. **40**(2): p. 401-421.
58. Pope, S.B., *Monte Carlo Calculations of Premixed Turbulent Flames*. The Combustion Institute, 1981. **18**: p. 1001-1010.
59. Borghi, R. and D. Dutoya, *On the Scales of the Fluctuations in Turbulent Combustion*. 17th Symp.(Int.) on Combustion, 1979(1): p. 235-244.
60. Chomiak, J., *Basic Considerations in the Turbulent Flame Propagation in Premixed Gases*. Prog. Energy Combustion Science, 1979. **5**: p. 207-221.
61. Ballal, D.R. and A.H. Lefebvre, *The Structure and Propagation of Turbulent Flames*. Proc. R. Soc. Lond. A., 1975. **334**: p. 217-234.
62. Kobayashi, H., T. Tamura, K. Maruta, T. Niioka, and F.A. Williams, *Burning Velocity of Turbulent Premixed flames in a high Pressure Environment*. Proc. Combust. Inst., 1996. **26**: p. 389-396.
63. Smallwood, G.J., O.L. Gulder, D.R. Snelling, B.M. Deschamps, and I. Gokalp, *Characterization of Flame Front Surfaces in Turbulent Premixed Methane / Air Combustion*. Combustion and Flame, 1995. **101**: p. 461-470.
64. Filatyev, S.A., J.F. Driscoll, C.D. Carter, and J.m. Donbar, *The Study of the Turbulent Burning Velocity by Imaging the Wrinkled Flame Surface*, in *40th Aerospace Sciences Meeting & Exhibit*. 2002: Reno, NV.
65. Hertzberg, M., K.L. Cashdollar, and C.P. Lazzara. *The Limits of Flammability of Pulverized Coals and other dusts*. in *Proc. combust. Inst.* 1981: The combustion Institute.
66. Li, Y., C.W. Kauffman, and M. Sichel, *An Experimental Study of Deflagration to Detonation Transition Supported by Dust Layers*. Combustion and Flame, 1995. **100**: p. 505-515.
67. Sun, J., R. Dobashi, and T. Hirano, *Temperature profile across the combustion zone propagating through an iron particle cloud*. Journal of Loss Prevention in the Process Industries, 2001. **14**: p. 463-467.
68. Ju, W., R. Dobashi, and T. Hirano, *Dependence of flammability limits of a combustible particle cloud on particle diameter distribution*. Journal of Loss Prevention in the Process Industries, 1998. **11**: p. 177-185.
69. Chen, J.-L., R. Dobashi, and T. Hirano, *Mechanisms of flame propagation through combustible particle clouds*. Journal of Loss Prevention in the Process Industries, 1996. **9**(3): p. 225-229.
70. Chen, D.L., J.H. Sun, Q.S. Wang, and Y. Liu, *Combustion Behaviors and Flame Structure of Methane/Coal Dust Hybrid in a Vertical Rectangle Chamber*. Combust. Sci. and Tech., 2008. **180**: p. 1518-1528.
71. Amyotte, P.R., K.J. Mintz, M.J. Pegg, Y.-H. Sun, and K.I. Wilkie, *Laboratory Investigation of the Dust Explosibility Characteristics of Three Nova Scotia Coals*. Journal of Loss Prevention in the Process Industries, 1991. **4**(2): p. 102-109.

72. Bradley, D., G. Dixon-Lewis, and S.E.-D. Habik, *Lean Flammability Limits and Laminar Burning Velocities of CH₄-Air-Graphite Mixtures and Fine Coal Dusts*. Combustion and Flame, 1989. **77**: p. 41-50.
73. Ju, Y. and C.K. Law, *Dynamics and Extinction of Non-Adiabatic Particle-Laden Premixed Flames*. Proc. Combust Inst, 2000. **28**: p. 2913-2920.
74. Andac, M.G., F.N. Egolfopoulos, and C.S. Campbell, *Effects of Combustible Dust Clouds on the Extinction Behavior of Strained, Laminar Premixed Flames in Normal Gravity*. Proc. Combust Inst, 2002. **29**: p. 1487-1493.
75. Benedetto, A.D., A. Garcia-Agreda, O. Dufaud, I. Khalili, R. sanchirico, N. Cuervo, L. Perrin, and P. Russo, *Flame Propagation of Dust and Gas-Air Mixtures in a Tube*, in MCS 7, *The Comb. Institute.it*. 2011: Chia Laguna, Cagliari, Sardinia, Italy.
76. Liu, Y., J. Sun, and D. Chen, *Flame Propagation in Hybrid Mixture of Coal Dust and Methane*. Journal of Loss Prevention in the Process Industries, 2007. **20**: p. 691-697.
77. Xie, Y., *Study of Interaction of Entrained Coal Dust Particles in Lean Methane - Air Premixed Flames*, in *Fire Protection Engineering*. 2011, Worcester Polytechnic Institute: Worcester, MA.
78. Xie, Y., V. Raghavan, and A.S. Rangwala, *Study of interaction of entrained coal dust particles in lean methane-air premixed flames*. Combust. Flame, 2012. **159**: p. 2449-2456.
79. Nusselt, W., *Die Verbrennung und die Vergasung der Kohle auf dem Rost*. 1924. **68**: p. 124.
80. Mallard, E. and H.L.I. Chatelier, *Recherches Experimentales et Theoretiques sur la Combustion des Melanges Gazeux Explosifs*. Annals des Mines, 1883. **4**.
81. Seshadri, K., A.L. Berlad, and V. Tangirla, *The Structure of Premixed Particle-Cloud Flames*. Combustion and Flame, 1992. **89**: p. 333-342.
82. Bidabadi, M. and A. Rahbari, *Modeling Combustion of Lycopodium Particles by Considering the Temperature Difference between the Gas and the Particles*. Combustion, Explosion, and Shock Waves, 2009. **45**(3): p. 278-285.
83. Smoot, D. and M.D. Horton, *Propagation of Laminar Pulverized Coal-Air Flames*. Prog. Energy Combustion Science, 1977. **3**: p. 235-258.
84. Krazinski J.L., Buckius R. O., and K. H., *Coal Dust Flames: A Review and Development of a Model for Flame Propagation*. Progress in energy and Combustion Science, 1979. **5**: p. 31-71.
85. Slezak, S.E., R.O. Buckius, and H. Krier, *A modle of Flame Propagation in Righ Mixtures of Coal Dust in Air*. Combustion and Flame, 1985. **59**: p. 251-265.

2. Structure of a Dust Flame

2.1. Premixed or Non-Premixed?

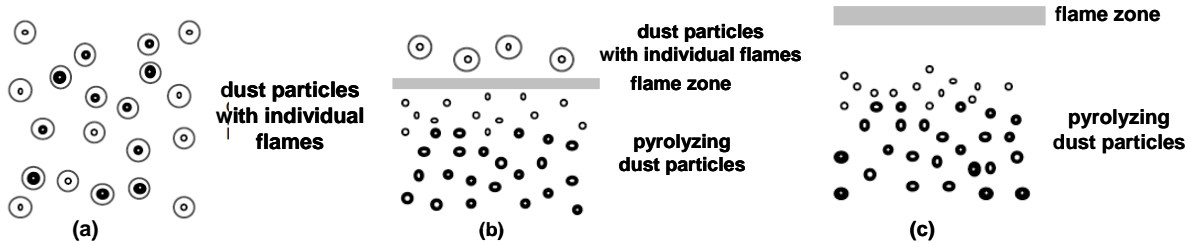


Figure 2.1: Types of dust flames (a) non continuous flames around individual particles (b) continuous gas flame with individual particles continuing to burn after flame zone (c) continuous gas flame front

Unlike a premixed gas flame, a mixture of dust and oxidizer involves a multiphase flow which causes difficulty in both experiments and modeling [1-5]. Since gas combustion is a process involving only one phase (homogeneous combustion), the reactants are represented by their smallest entities (i.e. molecules) [6]. When the fuel and oxidant are thoroughly mixed, they are separated only by molecular distances. Premixed combustion is therefore guaranteed down to very small scales. By contrast, dust explosions and dust flames involve the combustion of a dust-air suspension. A dust cloud, which is uniform when viewed at a macro-scale (e.g. cloud radius), may not be considered premixed at a small scale (e.g. inter-particle distance). This caused researchers to make a distinction between two types of dust flames [7]: the Nusselt flame and the volatile flame. In the Nusselt flame, strictly heterogeneous combustion occurs at the surface of the particles, sustained by the diffusion of oxygen towards the particles' surface. Therefore, a Nusselt flame, which on a macroscopic scale may seem like premixed combustion, consists of an ensemble of local diffusion flames as shown in Fig. 2.1a. In the case of the volatile flame, vapors, volatiles and/or pyrolysis gases are produced by the particles prior to or during

combustion. When mixed with air, these gases and vapors burn as a premixed gas. Depending on the nature of the solid, three distinct mechanisms have been proposed for the combustions of particles in volatile flames [8]:

1. Devolatilization and burning of volatiles followed by combustion of a solid residue as shown in Fig 2.1b.
2. Melting followed by evaporation and subsequently vapor phase burning as shown in Fig. 2.1c (e.g. sulphur, plastics).
3. Evaporation through a solid oxide shell followed by combustion of the vapor outside the shell (e.g. metals like magnesium and aluminum) 2.1 a, b or c

When a flame propagates through clouds of coal dust and many organic powders, additional complexities arise. These occur because after the homogeneous combustion of the liberated volatiles has occurred, combustion of the remaining solid char may take place in the tail of the flame. The volatile flame is thus coupled to a Nusselt flame.

2.2 Flame structure

Fundamentally, flame propagation in dust flames requires three sequential processes: heating and devolatilization of the particles, mixing of the volatiles, and ultimately combustion of the mixture [9]. The last step can involve gas-phase combustion of the volatiles released by the condensed fuel or surface reactions or a combination of both and is the most complicated. The three processes are illustrated in Fig. 2.2 where five potential scenarios based on equivalence ratios ϕ_u and ϕ_g are presented. The variable ϕ_u represents the equivalence ratio based on the total condense phase fuel in the ambient zone, whereas, ϕ_g represents the equivalence ratio based on the volatilized gas vapor evolved at the end of the preheat zone. Equivalence ratio can be calculated using [10]

$$\phi = \frac{\frac{n_{fuel} MW_{fuel}}{n_{air} MW_{air}}}{\left(\frac{n_{fuel} MW_{fuel}}{n_{air} MW_{air}} \right)_{stoichiometric}} \quad (2.1)$$

where n is the number of moles and MW is the molecular weight.

There are five scenarios because scenario B can have ϕ_u greater or less than 1. In Fig. 2.2, label “A” denotes the condition where $\phi_u < 1$ and $\phi_g < 1$. Label “B” denotes the condition where ϕ_u can be greater or less than 1 but ϕ_g is less than one. Label “C” denotes the condition where both ϕ_u and ϕ_g are greater than 1. In conditions C_I the particles completely vaporize in the preheat zone, while in condition C_{II} the particles do not completely vaporize in the preheat zone. The color gradients shown indicate the mass fraction of fuel vapor present with a darker color representing higher mass fraction.

The inset labeled “D” shows a close-up of the ambient zone where the random distribution of both particle separation and size in a potential dust-air flame is highlighted.

The inset labeled “E” shows a close-up of the preheat zone. During this process the differences in particle size will play a significant role as smaller particles get heated up faster and vaporize almost completely, while larger particles continue to be in the condensed phase as they move into the reaction and convection zones. The inset labeled “F” shows a close-up view of a single vaporizing particle. The inset labeled “G” shows the surface of a particle in the preheat zone where the fuel changes phase from solid to gas and premixes with the oxidizer to establish a

flame front. At this stage, it is possible that the burning is localized on the surface alone; however, this condition is not analyzed in the current study. It should be noted that the change in phase slows down the burning velocity significantly as compared to a gas flame. Further, as shown in “G”, the heat transfer fluxes related to in-depth conduction (\dot{q}_{cond}'') and radiation ($\dot{q}_{rad,in}''$, $\dot{q}_{rad,out}''$) also play a significant role. The inset “G” also shows the vaporization rate (\dot{w}_v'''), which is determined by an energy balance of the net heat transfer divided by heat of gasification. These additional parameters influence the burning dynamics of particle air flames as discussed further in Fig. 2.2, which shows a sketch of the flame structure for the five types of equivalence ratios combinations considered.

The profiles of mass fraction of condense-phase fuel (Y_s), mass fraction of vaporized fuel (Y_{FC}), the vaporization rate (\dot{w}_v'''), the reaction rate (\dot{w}_R'''), and the temperature (T), across ambient, preheat, reaction and convection zones, are shown in Fig. 2.3. Case “A” represents the conditions where $\phi_g \leq 1$ and all of the condense phase fuel is vaporized as shown in Fig. 2.1 (A). When $\phi_g \leq 1$, fuel is the limiting reactant and is completely consumed in the reaction zone. Vaporization predominantly takes place in the preheat zone, with the mass fraction of the condense phase particles (Y_s) dropping to zero and the mass fraction of the fuel vapor (Y_F) reaching a maximum in the preheat zone. The temperature increases through the preheat zone, attains the maximum value in the reaction zone, and remains constant in the convection zone, where losses can be neglected.

Case “B” represents the conditions of $\phi_g \leq 1$ and particles continue to burn even in the convection zone, resulting in $T_b > T_f$. The inset labeled “H” in Fig. 2.2 shows the convection zone in case “B”, where the fuel particles continue to burn in the presence of excess oxygen. The presence of

these particles is mainly due to their larger sizes and/or slow vaporization rate. It is important to note that this case results in increase of the temperature in the convection zone.

Case C_I represents a condition where $\phi_g \geq 1$. All the condensed-phase particles are vaporized in the preheat zone as shown in Fig. 2.3 (C_I). However, in this case, only part of the gas phase fuel is burned in the flame zone, due to the fuel-richness of the mixture, and there is fuel vapor left over in the convection zone. Oxygen is the limiting reactant in this case. It should be also noted that the temperature remains constant in the convection zone.

Case C_{II} represents the conditions where $\phi_g \geq 1$ and the condensed-phase fuel is not completely vaporized in the preheat zone as shown in Fig. 2.2 (C_{II}). Similar to case C_I, oxygen is the limiting reactant for this case also. However, as the condensed fuel continues to vaporize, the mass fraction of the fuel vapor increases and the temperature in the convection zone decreases. The inset labeled “I” in Fig. 2.2 shows a close up of the convection zone, which occurs in case C_{II} where fuel particles continue to vaporize but do not burn due to oxygen limitation. This continued vaporization increases the fuel vapor mass fraction and decreases the convection zone temperature.

Figures 2.2 and 2.3 summarize the dust problem and shows the significant diversity in situations which can occur in a flame containing condense phase fuel. Not only can the fuel change, but for a given fuel the flame can behave differently given the amount of vaporization which takes place. These figures show the increased complexity of the dust air problem and give a clear impression on the need to study this behavior.

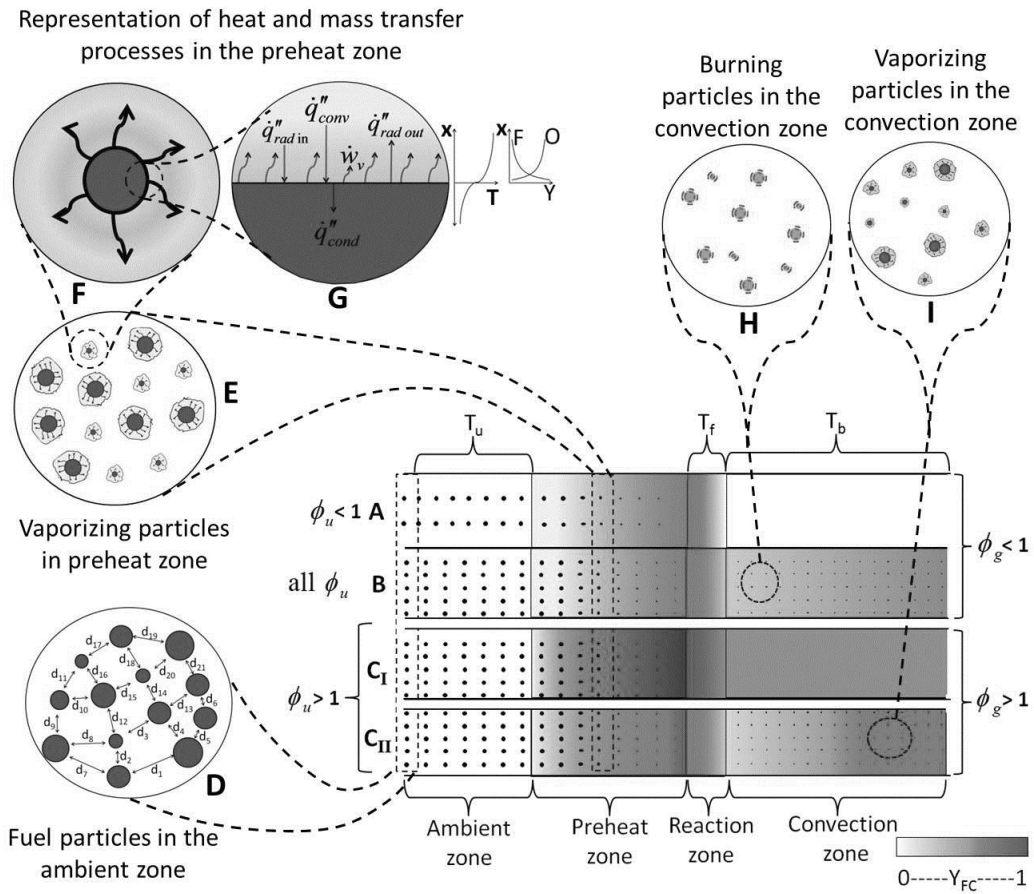


Figure 2.2: Schematic illustration of the structure of a premixed dust – air flame.

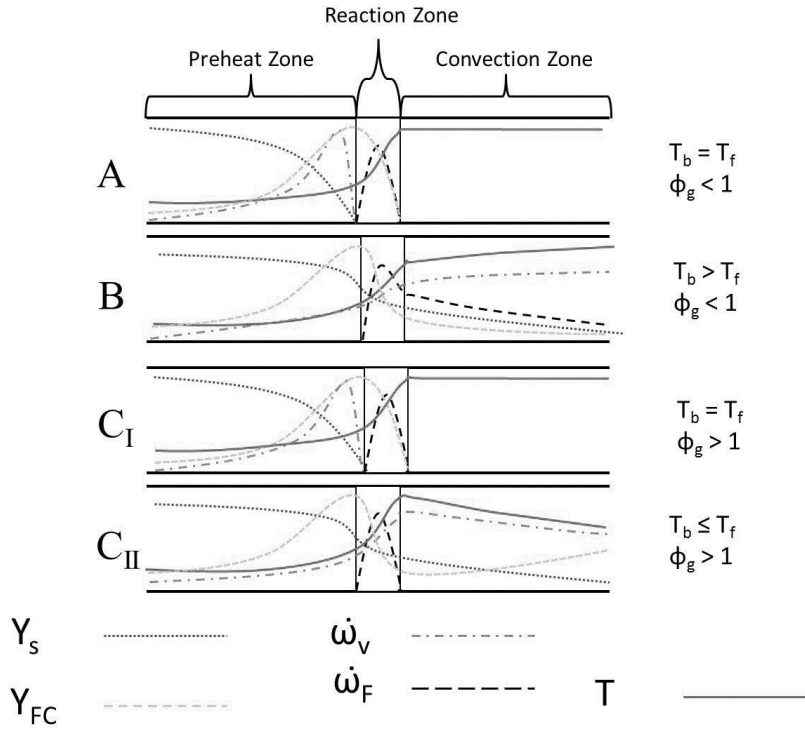


Figure 2.3: Schematic of flame structure in a dust-air flame.

To study the dust flame problem, a hybrid flame is the optimum tool because it allows the creation of all 5 scenarios by varying the gas phase and condense phase equivalence ratios. These scenarios are succinctly described in table 2.1.

Table 2.1: Fuel concentration scenarios in hybrid flames.

	Ambient zone	Preheat zone	Convection zone
1	The condense phase and gas phase have a lean condition	The dust completely vaporizes in the preheat zone	There is excess oxygen
2	The condense phase and gas phase have lean conditions	The dust does not completely vaporize in the preheat zone	There is continuous burning of the particles behind the reaction zone
3	The condense phase has a rich condition but the gas phase has a lean condition	The dust does not completely vaporize in the preheat zone	There is continued burning of the dust particles behind the reaction zone
4	The condense phase has a rich condition and the gas phase in the preheat zone is rich.	The dust does not completely vaporize in the preheat zone	There is continued vaporization behind the flame
5	The condense phase has a rich condition and the gas phase has a rich condition	The dust completely vaporizes in the preheat zone.	There is excess fuel behind the flame.

References

1. Proust, C., *Flame Propagation and Combustion in some dust-air mixures*. Journal of Loss Prevention in the Process Industries, 2006. **19**: p. 89-100.
2. Eckhoff, R.K., *Dust Explosions in the Process Industries, Third Edition*. Third ed. 2003, Boston: Gulf Professional Publishing.
3. Huang, Y., G.A. Risha, V. Yang, and R.A. Yetter, *Combustion of Bimodal Nano/Micro-Sized Aluminum Particle Dust in Air*. Proceedings of the Combustion Institute, 2007. **31**: p. 2001-2009.
4. Sun, J., R. Dobashi, and T. Hirano, *Structure of Flames Propagating through Aluminum Particles Cloud and Combustion Process of Particles*. Journal of Loss Prevention in the Process Industries, 2006. **19**: p. 769-773.
5. Horton, M.D., F.P. Goodson, and L.D. Smoot, *Characteristics of Flat, Laminar coal-Dust Flames*. Combust. Flame, 1977. **28**: p. 187-195.
6. Dahoe, A., *Dust Explosions: a Study of Flame Propagation*, in *Applied Sciences*. 2000, Delft University of Technology. p. 298.
7. Eckhoff, R.K., *Dust Explosions in the Process Industries*. 2003, Boston: Gulf Professional Publishing.
8. Bardon, M.F. and D.E. Fletcher, *Dust Explosions*. Science Progress (Oxford), 1983. **68**: p. 459-473.
9. Hertzberg, M., K.L. Cashdollar, and C.P. Lazzara. *The Limits of Flammability of Pulverized Coals and other dusts*. in *Proc. combust. Inst.* 1981: The combustion Institute.

10. Turns, S.R., *An Introduction to Combustion: Concepts and Applications*. 2000, New York: McGraw Hill.

3. Experimental Apparatus Construction and Procedure

3.1 Summary

The primary objective of this study is to develop an experimental platform to accurately measure the turbulent burning velocity of a hybrid flame with the capability of systematic variation of the parameters which influence the problem such as particle size, dust type, turbulent intensity, integral length scale, dust concentration, and gas phase equivalence ratio. To accomplish these goals a new instrument called a Hybrid Flame Analyzer (HFA) was designed, instrumented, and constructed during this study. This instrument can control the laminar burning velocity (S_L), turbulent intensity (u'_{rms}), and length scale (l_0) along with the particle size (d_{st}) and concentration (λ_{st}) of condense phase fuel to provide a measure of the burning velocity of gas, dust, or hybrid flames. The HFA is divided into several sections: combustion chamber, exhaust system, burner nozzles, dust feeder, and optical setup which are explained in this chapter.

3.2 Combustion chamber

The HFA's combustion chamber is used to contain the dust and ash generated and minimizes ambient air disturbances. Figures 3.1a-b shows the details of the combustion chamber. The external frame (a) is made out of 3.81 cm (1.5") angle aluminum 0.3175 cm (1/8") thick. The external dimensions of the frame are 44 cm (17.25") tall and 17.8 cm (7") wide. The frame is held together using #8-32 bolts with Loctite to prevent the nuts from coming loose over time. The edges of the frame were sealed using a high temperature RTV gasket maker (Permatex). Two of the walls were made of plate glass (b) 25.4 cm (10") tall, 20.32 cm (8") wide, and 0.238 cm (3/32") thick. Rubber gasket 0.159 cm (1/16") thick is used between the glass and the aluminum to prevent leaks and help prevent the glass from cracking. The glass was held onto the aluminum frame by eight tabs, two on each side.

The combustion chamber is divided into two sections, the main section with the burner and a small section at the bottom (c) 7.62 cm (3") high where the makeup air is injected and allowed to disperse. The air enters the combustion chamber through hundreds of 0.159 cm (1/16") holes drilled into a 28 gauge steel plate which separates the section (d) similar to the experiment used in Bradley et al. [1]. The makeup air is controlled using a flowmeter. During tests, 30 lpm of air is injected into the combustion chamber by a 0.635 cm (1/4") Swagelok female tube adapter (e). The air is distributed through a 1.27 cm (1/2") copper tube (not shown) with 1 inch wide slits cut into the side to help distribute the air in the lower section. Water for cooling the burner is injected and removed through two 0.635 cm 1/4" Swagelok female tube adapters (f). The fuel for the burner pilot flame is injected into the combustion chamber through another 0.635 cm (1/4") Swagelok female tube adapter (g). The third side of the combustion chamber is made of a plate of 28 gauge galvanized steel plate (i). The water cooling fittings (f), pilot fuel gas (i), a biconvex lens (h), and the spark igniter (j) are connected through this steel plate and sealed with high temperature RTV gasket maker. The optics system uses two bi-convex lenses (h), which are attached to the combustion chamber. The spark igniter (j) is mounted on a 30.48 cm (12") aluminum rod surrounded by a rubber housing. This housing allows the igniter to be moved inside of the combustion chamber allowing it to ignite the pilot and then be moved out of the way. The 4th side of the combustion chamber is a door (l) to access the inside of the combustion chamber. This door is composed of 0.3175cm (1/8") thick aluminum frame with a 25.4 (10") by 20.32 cm (8") by 0.238 cm (3/32") plate glass allowing to see inside the combustion chamber. The door was attached to the main aluminum frame using a one-piece door hinge. EPDM rubber weather sealing, 0.794 cm (5/16") and 1.51 cm (19/32") wide, is used to seal the door. Pressure

clamps (not shown) are used to hold the door closed during testing. The top of the combustion chamber contains a fume hood (m) to remove combustion products.

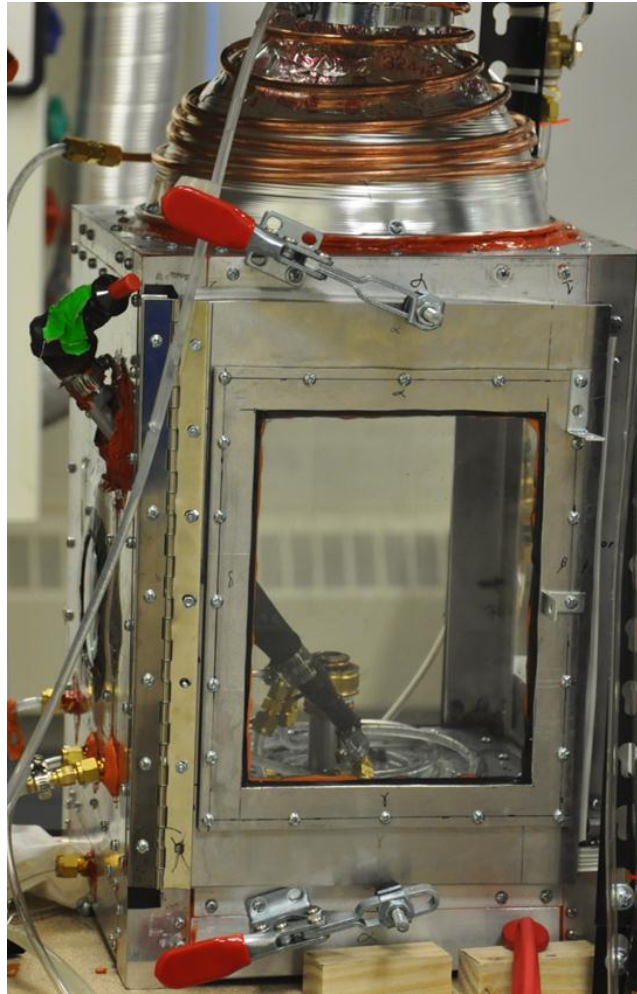


Figure 3.1a: Picture of combustion chamber

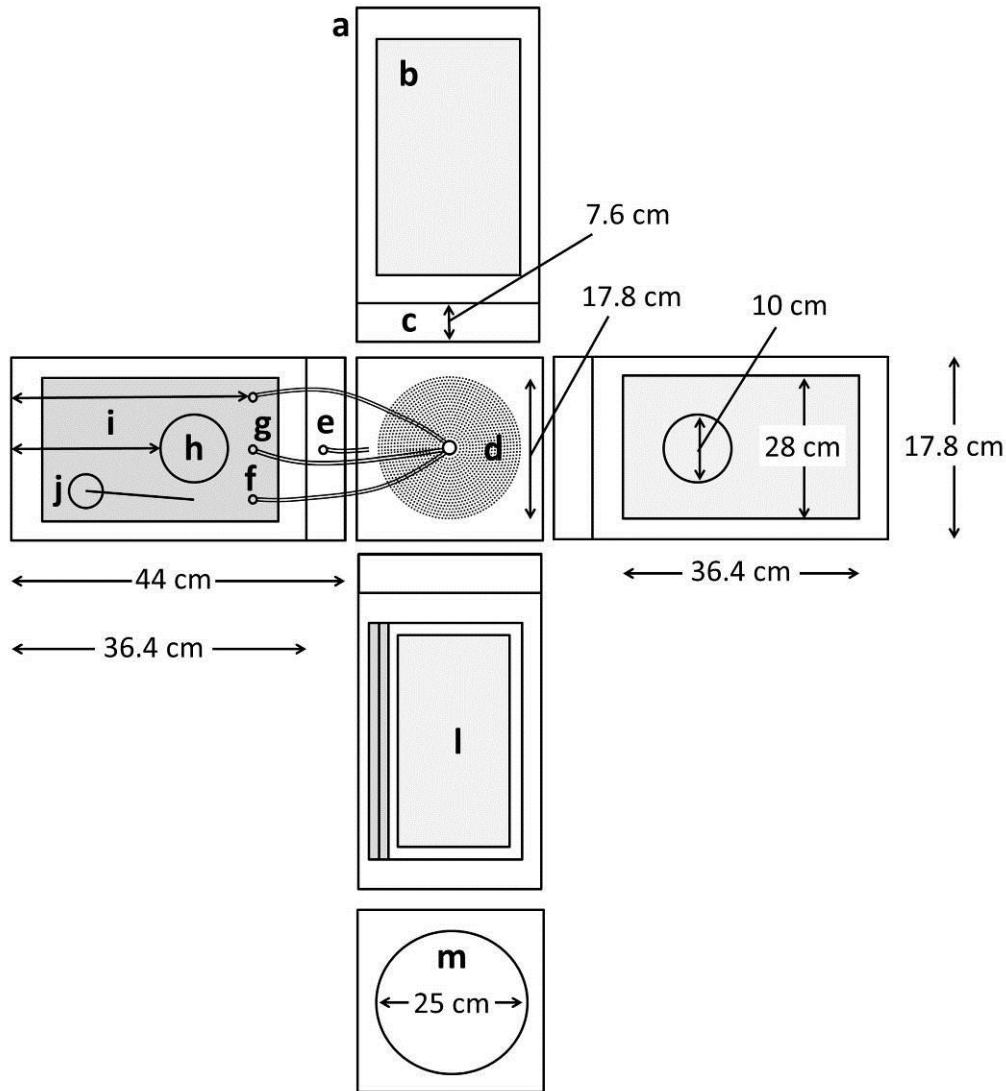


Figure 3.1b: Hybrid Flame Analyzer (HFA) combustion chamber (exploded view)

3.3 Exhaust system

The HFA's exhaust system is shown in Fig. 3.2. Combustion products are removed from the combustion chamber through a water cooled fume hood. The water cooled tubing (not shown) consists of 0.635 cm (1/4") OD copper tubing wrapped around the aluminum hood. Water flows at a rate of 10 lpm. The combustion products are pulled into exhaust tubing by a centrifugal pump. To help cool the exhaust products and prevent any pressure differential in the combustion chamber, excess air is pulled into the exhaust ducting through a makeup air system. The makeup

air ducting contains an s-bend to prevent hot combustion products from escaping into the laboratory. The cooled combustion products are exhausted out of the lab through more 10.16 cm (4") diameter tubing. The flow through the exhaust system is $0.0178 \text{ m}^3/\text{s}$ (1068 lpm).

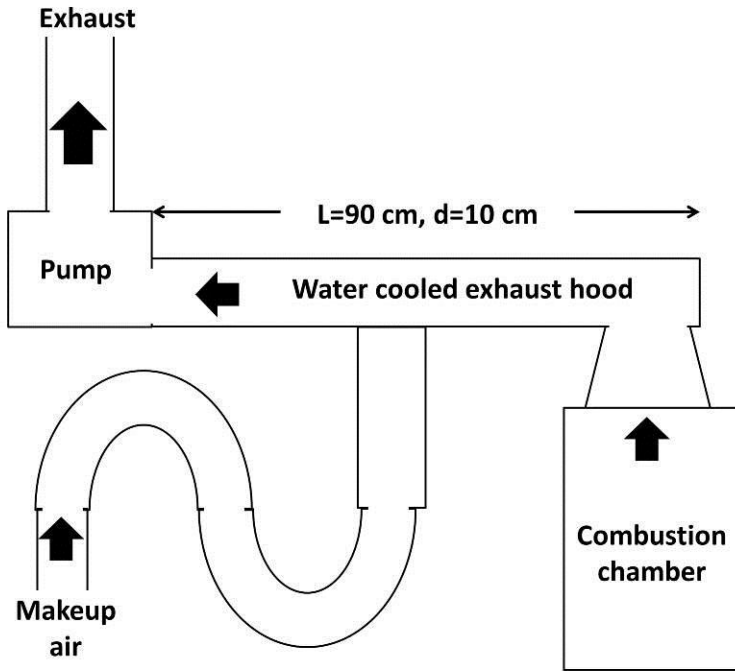


Figure 3.2: HFA exhaust system diagram

3.4 Burner test section

To determine the best way to study hybrid flames, a literature search for published methods of experimental burning velocity measurements of flames was conducted. Based on this study (full details are given in the literature review in Cha. 1) and the critical reviews by Andrews et al. [2] and Lewis and Elbe [3] the anchored Bunsen burner experimental design used in this work was chosen. This style of experiment is the simplest to use and analyze, and allows a turbulent flame which can be studied for an extended period of time facilitating easier instrumentation and measurement accuracy. This is important because turbulent flames are inherently not steady state; therefore, average quantities determined about the flame should come from many

measurements taken over time. This requires the flame to be anchored at the burner exit for several minutes.

Figure 3.3 shows a diagram of the hybrid flame analyzer's test section. The side view and top view of the combustion chamber are shown: the outline of combustion chamber (a), the point source of light (b) uses a bulb from a projector (480 watt). A steel plate with a pin hole in the center is used to create the point source. This point source of light is placed at the focal point of a bi-convex lens (b) with a 100 mm diameter and a 200 mm focal length. This creates a 100 mm diameter test section of parallel light (d) inside the combustion chamber. The parallel light passes through the flame (l) and through a second identical bi-convex lens which reduces the diameter of the image. This reduction makes the image small enough to fit on the sensor of a digital single reflective lens camera with a 1-1 macro lens (f) with the focus set to infinity. To reduce the intensity of the coal dust emissions, a short pass filter (e) with a cutoff of 550 nm is placed in front of the camera lens, similar to the experiment by Goroshin et al. [4]. The flame (l) is fueled from a methane source (h), an air source (i), and a dust hopper (j). The dust is injected into the fuel-air mixture using the injector block (k) as described in detail in Fig. 3.11. Known turbulent intensities are created using a set of perforated plates as described below. Makeup air is injected into the combustion chamber through the ¼" fitting (o) and distributed in the subsection of the combustion chamber (g). Combustion products are removed from the water-cooled (n) 12 cm diameter exhaust duct. A removable spark igniter (s) is used to ignite the pilot flame, similar to the experiment used by Bradley et al. [1].

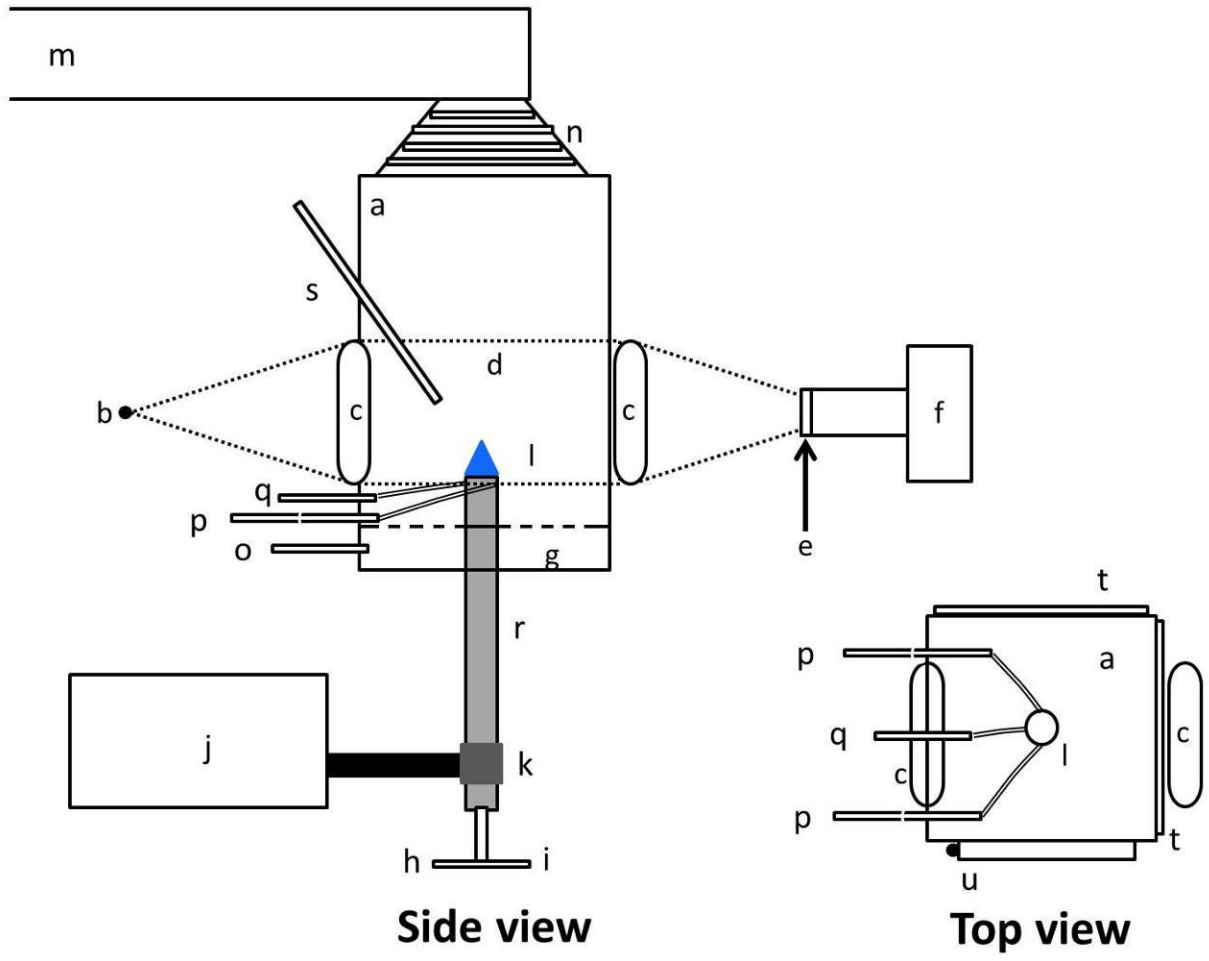


Figure 3.3: Diagram of experimental section of Hybrid Flame Analyzer (HFA)

3.5 Burner nozzle design

At the top of the vertical feeder tube two different water cooled nozzles, with internal diameters of 14.5 mm, are attached to the top of the feeder tube as shown in Fig. 3.4. The first nozzle (a) is a straight tube used for creating laminar flames. Laminar flames are generated using a combined air-methane flow rate of 10 lpm. The second nozzle (b) uses a set of perforated plates to generate turbulence and has a methane-oxygen annular pilot to anchor the flame.

The details of construction of the turbulent burner nozzle are illustrated in Figs. 3.5 and 3.6. The turbulent flame (a) fueled by the dust air mixture (j) is anchored to the burner nozzle using a

methane oxygen pilot flame (b). The nozzle tip is water cooled using 1/8" copper tubing (c). The pilot flame fuel air mixture (e) is injected through pilot fuel housing (d) with a 0.635 cm (1/4") Swagelok tube to MNPT fitting (not shown). The stainless steel housing (g) with an internal diameter (l) of 14.5 mm was cooled using 0.318cm (1/8") copper tubing (f) similar to Bradley et al. [1] 1994, and Kobayashi et al. [5]. Turbulence is generated by nylon perforated plates (h) mounted 10-30 mm from the nozzle exit (k) (shown in Fig. 3.8). The pilot flame housing (shown in a close-up view) is made up of three sequential copper tubes. The inner tube (g) has the same inner diameter as the stainless steel tube (g) and is 0.036 cm (0.014") thick. The 2nd tube (o) is an insert which both creates the uniform high speed flow around the radius of the burner and maintains the constant spacing of the third tube (q), attached to the pilot fuel housing. This insert (o) is 0.071 cm (0.028") thick and has 8 vertical slots cut into the inside (p) 0.127 cm (0.050") deep. The top of the insert was machined on a lathe to create a double notch at the top. The deeper notch (n) allows gas to distribute around the circumference of the tube evenly and is approximately 0.254 cm (0.100") deep. The second notch (m) creates an anchored methane-oxygen flame and is approximately 0.127 cm (0.050") deep.

Figure 3.6 shows pictures of the individual components in the turbulent burner nozzle. (a) shows a side view of the main burner tube without the pilot flame assembly or water cooling (b) shows the fitting which allows the pilot fuel gas to be added and evenly distributed around the circumference. (c) shows the spacing insert which keeps the spacing of the pilot gap constant around the circumference and increases the velocity of the oxygen-methane mixture. Figure 3.8 shows an image of the perforated plates used in this work. Five perforated plates were created having a variety of hole diameters: 4mm (a), 3mm (b), 2mm (c), 1mm (d), and 0.6mm (e). These round perforated plates are similar to the ones used by Khramtsov[6]. The perforated plates are

mounted in identical nylon tubes (f) which have a threaded hole for the adjusting pin. The 1 mm perforated plate has a blockage ratio (area of holes/total area) of 50%. The perforated plate design is similar to work by Kobayashi et al. [5] and Liu et al. [7].

The annular pilot, shown in Fig. 3.7, is similar to the one used by Kobayashi et al. [5]. It is necessary to hold the flame due to the high flow rates used to generate turbulent intensity and is fueled by methane and oxygen mixture ($\phi=1$). This mixture was used because of the higher burning velocity which (compared to air) prevents the turbulence in the main burner flow from disturbing the pilot. Both burner nozzles have water cooling (10 liters per hour controlled by a flowmeter) made out of copper tubing wound around the burner diameter with thermal grease (Arctic Silver Ceramique Thermal Compound) to increase conductive heat transfer.

The main burner flow is measured using a hot wire anemometer (Dantec Dynamic 9055P011), sampling at a rate of 100 kHz. The platinum-plated tungsten wire sensor has a diameter of 5 microns and is 1.25 mm long. The hot wire anemometer was calibrated using the average bulk flow velocity through the burner based on the mass flow controller. The calibration curve follows a power law relationship as shown in Fig. 3.9.

Turbulent flow can be described using [8]

$$u = \bar{u} + u' , \quad (3.1)$$

where u is the flow velocity, \bar{u} is the average flow velocity, and u' is the fluctuating component of the flow velocity. The turbulent intensity is defined as the root mean square (RMS) of the turbulent fluctuation in the u' [8] and can be calculated using

$$u'_{rms} = \sqrt{\frac{(u'_1)^2 + (u'_2)^2 + \dots + (u'_n)^2}{n}} . \quad (3.2)$$

The velocity measurements in the experiments described below are done in cold flow without a flame similar to Kobayashi et al. [5]. Pope [9] discussed how the flame could have an effect on the turbulent velocity field due to the large temperature rise of the flame, but with few exceptions, these effects have not been studied. However, Chomiak [10] found that a wrinkled, continuous laminar flame does not generate additional turbulence and actually reduces the overall intensity of the turbulent velocity fluctuations. Many studies in the literature have used the cold flow measurement of turbulence to characterize the turbulence experienced by a flame. This procedure is followed in this work as well.

The impact of turbulent intensity and length scale on premixed combustion has been studied by Borghi [11]. Turbulence and the decay in turbulent intensity in experimental setups are discussed by Liu [12] and Roach [13]. The use of perforated plates, as discussed below, has been shown to be a reliable way to produce predictable turbulence intensities. In the HFA, the turbulence intensity is controlled with the flow rate through the burner and the distance of the perforated plate from the burner exit. Combined air-methane flow rates of up to 4 m/s are used to generate a range of turbulent intensities up to 0.532 m/s. Figure 3.10 shows the turbulent intensity generated as a function of perforated plate location and flow velocity. Positions 1, 3, and 6 (as shown in Fig 3.6a, as the notches in the side of the slit, the first notch is covered by water cooling tubing and is not used) are located 10, 15, and 30 mm below the nozzle exit, respectively. The red dots in Fig. 3.10 indicate the perforated plate location and flow velocity range used in the current study. This set of conditions was chosen because it matched the turbulent intensities used by Kobayashi et al. [5] and further, when the 1mm perforated plate was raised to position 3, the flame flashed back inside of the burner. Due to time constraints, all of

the possible perforated plate and flow rate combinations were not tried with a flame to determine which combinations had a stable condition.

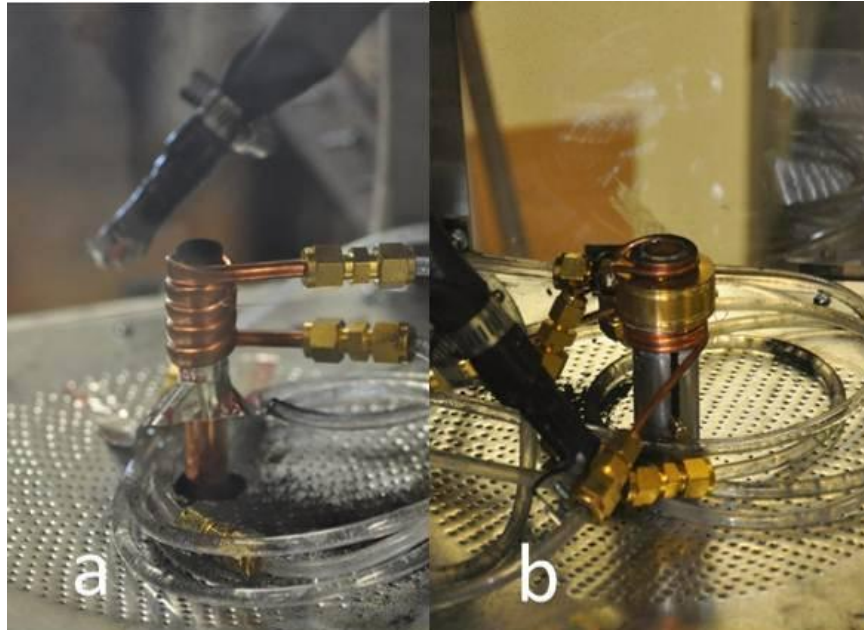


Figure 3.4: Images of burner nozzles (a) laminar burner (b) turbulent burner

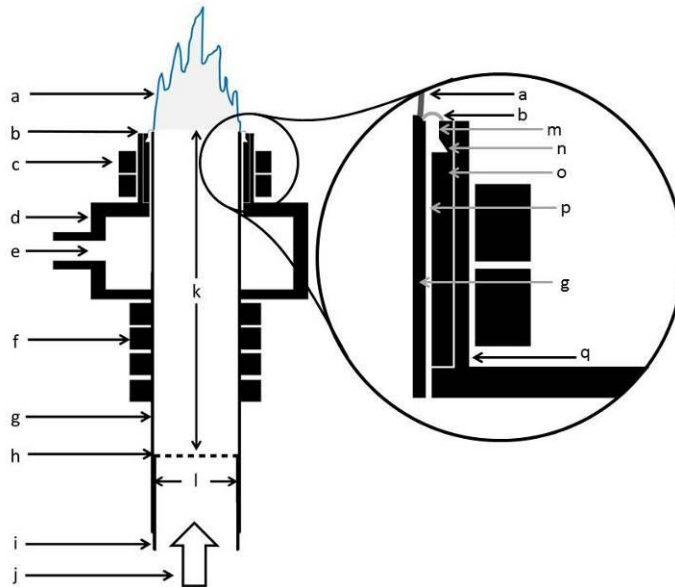


Figure 3.5: Diagram of turbulent burner nozzle

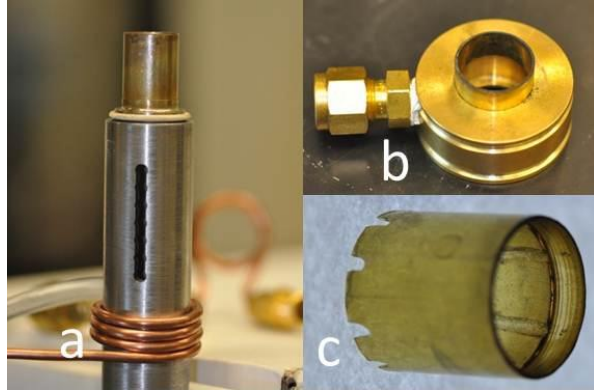


Figure 3.6: Turbulent burner parts (a) side view of turbulent burner without pilot gas fitting (b) pilot flame gas fitting (c) pilot flame spacing insert



Figure 3.7: Image of premixed methane-oxygen pilot flame

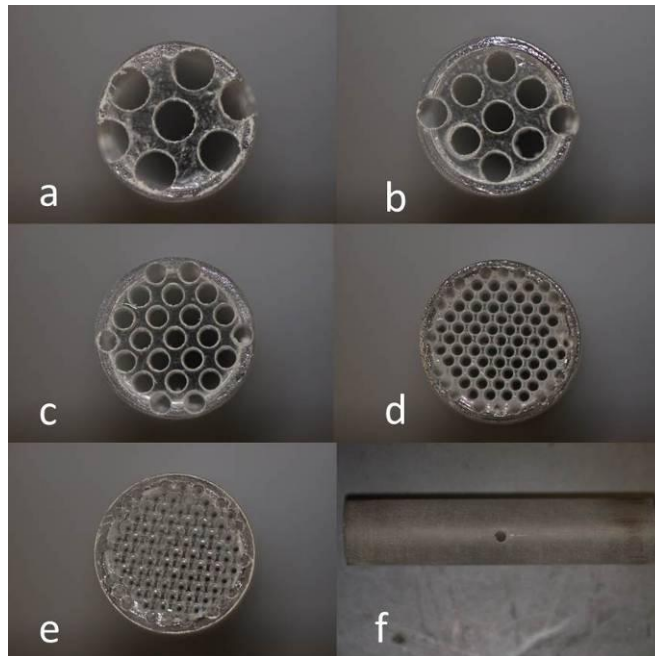


Figure 3.8: Images of perforated plates

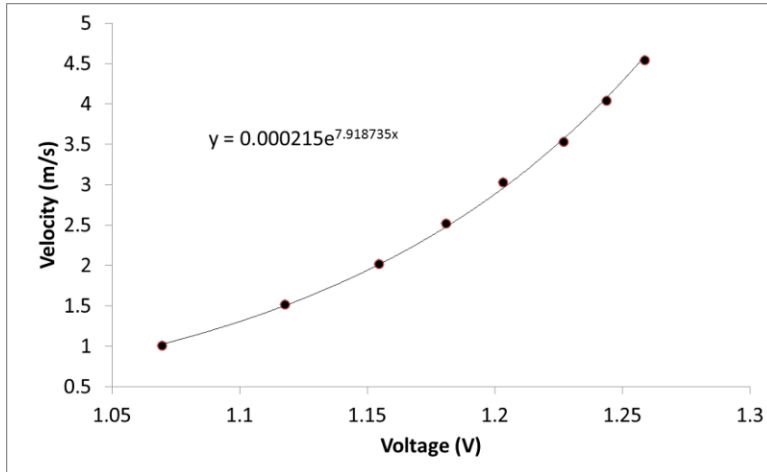


Figure 3.9: Calibration curve for hot wire anemometer

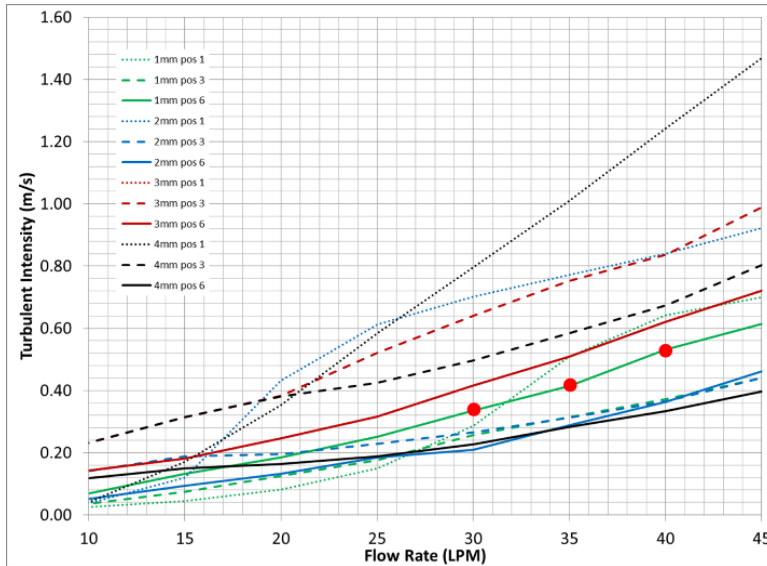


Figure 3.10: Turbulent intensity versus flow rate

The integral length scale l_0 of the turbulence can be calculated using [14]

$$l_0 = \bar{u} \int_0^{\infty} \rho_u(\tau) d\tau, \quad (3.3)$$

where \bar{u} is the average flow velocity and $\rho_u(\tau)$ is the autocorrelation of the velocity fluctuation

u' .

Table 3.1 shows the flow rate, flow velocity, turbulent intensity, integral length scale, and Re (using the nozzle diameter as the characteristic diameter) values for tests performed in this work using a 1 mm perforated plate for the turbulent flow regime.

Table 3.1 Integral length scale calculations

Flow regime	Flow rate (lpm)	Flow velocity (m/s)	u'_{rms} (m/s)	% u'_{rms}	l_0 (mm)	Re
Turbulent	30	3.03	0.185	6.1	1.6	2802
	35	3.53	0.335	9.5	1.4	3264
	40	4.04	0.532	13.2	1.1	3736
Laminar	10	1.00	0.024	0.024	2.07	926

Figure 3.11 shows a calculation of the turbulent intensity versus the number of samples used. Due to the consistent nature of the result 100,000 samples were used in the results shown.

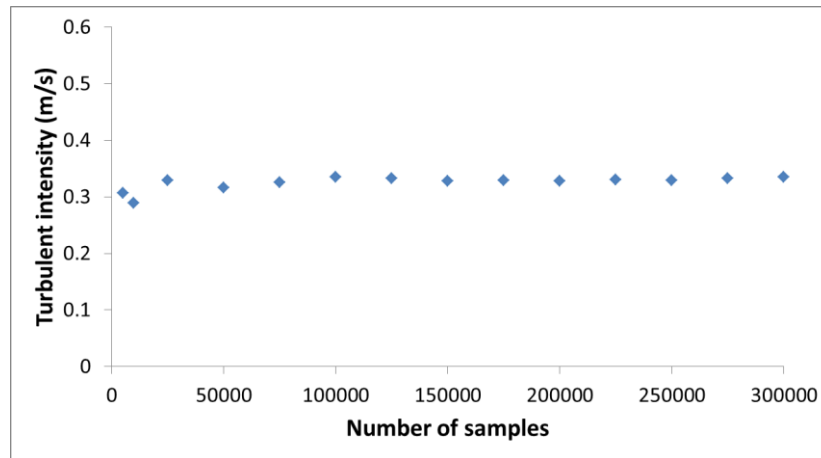


Figure 3.11: Comparison of calculated turbulent intensity versus number of samples used in the calculation

3.6 Fuel control system

The gas phase fuel equivalence ratio and flow rate is controlled using a pair of mass flow controllers (50 lpm full scale for air and 10 lpm full scale for methane with uncertainties of 1% of full scale). The gas phase equivalence ratio ranged from 0.8 - 1.2. Dust particle feed rate is controlled using a volumetric screw feeder, which is calibrated for different dusts and particle

sizes, similar to the setup used by Hattori et al. [15]. The dust is mixed with the CH₄-air in the bottom of the 50 cm vertical feeder tube (ID=14.5 mm).

Figure 3.12 shows a diagram of the dust injector block used to add coal dust (Pittsburgh seam, c.f. table 3.2 for property data) into the premixed fuel mixture before it travels to the nozzle exit. Dust is held in an agitated hopper (a) and fed into the burner feed system using a 0.635 cm (1/4") helix (b) housed inside of a stainless steel tube (c). The dust (e) is fed into a wooden block (h) with a thin slit 0.159 cm (1/16") wide (i). The methane air mixture (d) coming up through 1.27 cm (1/2") copper tubing (g) creates a shear flow in the thin slit (i) entraining dust similar to the experiment used by Kolbe et al. [16]. This prevents clumping of the dust and helps provide continuous injecting of the dust into the fuel stream. The combined dust-gas (f) mixture exits the block through a 1.27 cm (1/2") copper tube (g).

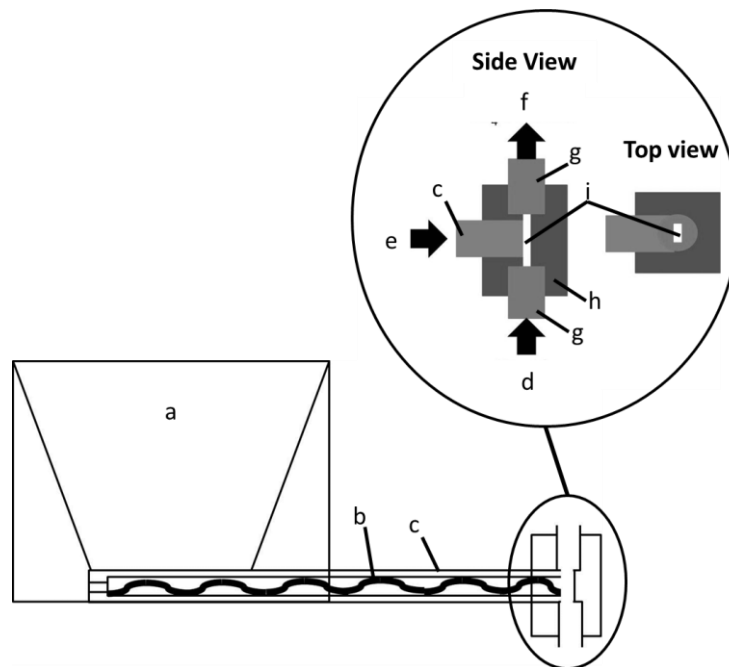


Figure 3.12: Diagram of dust feeder block

The dust feeder is calibrated by collecting the dust coming out of the nozzle over the range of settings for each dust used. For each calibration point the dust feeder is operated for one minute.

The dust is collected in a filtered dust hopper which allows gas to escape but collects the dust particles, as shown in Fig. 3.13 similar to Cassel et al. [17] and Gosh et al. [18], the dust air mixture flows up through (c), the dust is collected in the open area (d) and the air passes through a dust filter (e). The filter is held on by a rubber gasket (g) and 4 bolts (f). The output is weighed on a scale producing a linear line which is fitted to an equation as shown in Fig. 3.14. These regression equations are used to provide the settings required for the desired dust concentration in terms of g/m^3 for each test. The coal dust is sieved to different sizes using *Retsch* AS300 Sieve Shaker. It is important to maintain the purity while sieving different materials, therefore, whenever a different material is sieved, all sieving steel pans are cleaned by a *Retsch* 12" ultrasonic cleaner.

Table 3.2 Pittsburgh seam coal properties [19, 20]

E	65.4 kJ/mol
A	6.6×10^4 1/s
k	0.1 W/(m K)
ρ	492 kg/m^3
Q	3.04×10^9 J/kg

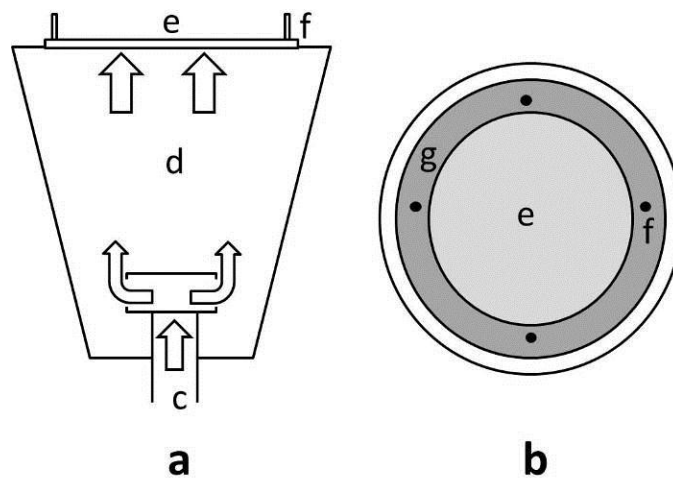


Figure 3.13: Diagram of dust hopper used to calibrate dust feeder (a) side view of dust catch (b) top view of dust catch

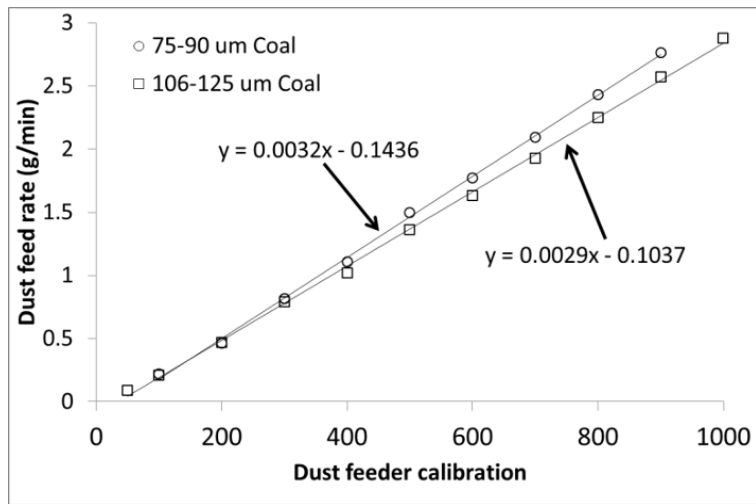


Figure 3.14: Dust feeder calibration curves (feed rate versus feeder setting from 1-1000)

3.7 Optical system

The HFA uses a shadowgraph to determine the flame edge of the premixed portion of the hybrid flame. Shadowgraphs have been used by a number of researchers to study the burning velocity of gas flames including Sherrat et al. [21], Garner et al. [22], Anderson et al. [23, 24], and Whol et al. [25]. Figure 3.15 shows an example of visual images taken of (a) a methane-air flame and (b) a hybrid flame including coal dust. It is clear that the premixed flame edge cannot be determined from visual images. Figure 3.16 shows shadowgraph images of (a) a methane air only flame, and (b) a hybrid flame including coal dust. The flame edges are clear in both of these cases; though in (b) contrast is reduced due to emissions from the coal. This effect is further discussed in Chapter 4.

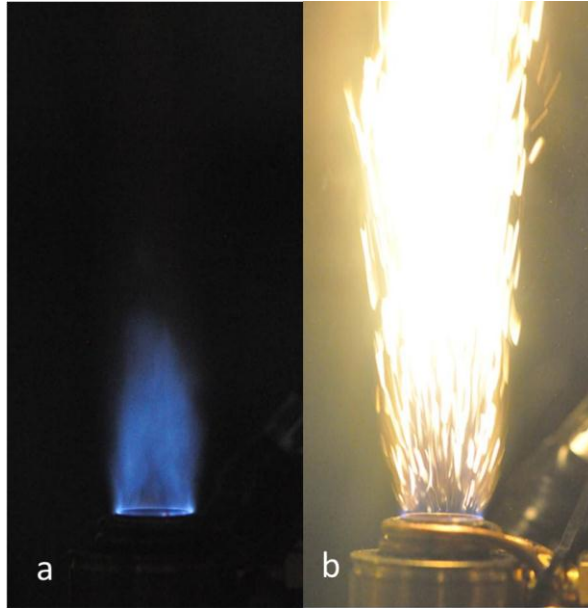


Figure 3.15: Visual images of burner flames (a) methane air only ($\phi = 0.8$, $u'_{\text{rms}} = 0.532 \text{ m/s}$) (b) hybrid flame including coal dust ($\lambda_{\text{st}} = 50 \text{ g/m}^3$, $d_{\text{st}} = 106\text{-}125 \text{ }\mu\text{m}$)

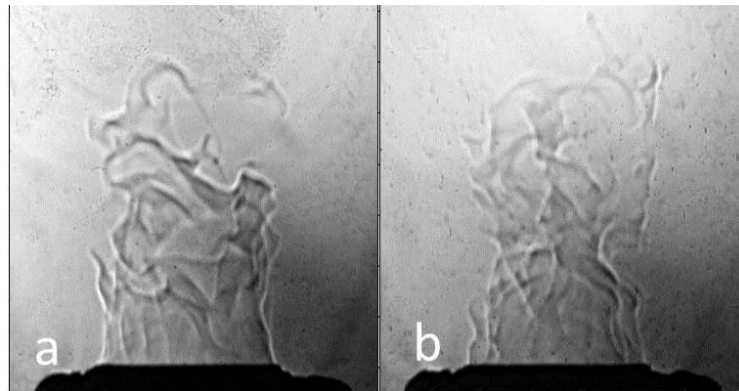


Figure 3.16: Shadowgraph images of burner flame (a) methane air only (b) hybrid flame including coal dust ($\lambda_{\text{st}} = 50 \text{ g/m}^3$, $d_{\text{st}} = 75\text{-}90 \text{ }\mu\text{m}$)

The shadowgraph shown in Fig. 3.16 uses the fan cooled bulb (480 W) from a projector covered by a steel plate with a pin hole in the center to make a point source of light. This is placed at the focal length of the biconvex lens mounted in the side of the combustion chamber. This creates a column of parallel light which passes through the flame and into an identical bi-convex lens. This second lens condenses the image so that the test section can be captured on a camera lens. The image is captured on a Canon EOS 5D digital camera attached with a macro lens with the focus set to infinity. Images are recorded at an average rate of 3 frames per second using a

shutter speed of 1/8000 seconds, fstop of 2.8 (reported), and ISO of 800. A remote shutter release is used to prevent any camera movement due to handling of the camera. A short wave optical filter is used on the front of the macro lens with a cutoff of 550 nm to reduce the effect of the bright orange/yellow emissions of the burning dust particles. The camera is mounted on a 20 kg block of concrete to prevent movement during testing.

3.8 Directions for using HFA

A user's manual for operating the HFA is shown in App. 2. Instructional videos were also created on how to run tests using the hybrid flame analyzer and using individual components which can be found at www.firesciencetools.com in the Hybrid Flame Analyzer section. These videos include:

1. Hybrid Flame Analyzer startup sequence
2. Hybrid Flame Analyzer shutdown sequence
3. Running laminar flame tests
4. Electrical system for Hybrid Flame Analyzer
5. Exhaust system for Hybrid Flame Analyzer
6. Fuel control system for Hybrid Flame Analyzer
7. Water cooling system for Hybrid Flame Analyzer
8. Building Annular/Ring Pilot Flame for Turbulent Burner - Hybrid Flame Analyzer
9. Simple shadowgraph design description - Hybrid Flame Analyzer
10. Gas analysis for combustion system - Hybrid Flame Analyzer
11. How to use mass flow controllers - Hybrid Flame Analyzer
12. Changing perforated plate in Hybrid Flame Analyzer
13. Calibrating volumetric dust feeder - Hybrid Flame Analyzer
14. Setting up hot wire anemometer for Hybrid Flame Analyzer
15. Checking hotwire anemometer voltage for Hybrid Flame Analyzer

The MATLAB scripts used in the analysis of images and data acquisition are shown in Appendix 3.

3.9 HFA data analysis

Abdel-Gayed [26] provides an excellent review of methods that have been used to measure turbulent burning velocities. There are three main methods used to determine the turbulent

burning velocity with a stabilized vertical Bunsen burner type of flame. The first is by determining an average flame angle used by Ballal et al. [27, 28], Karlovitz et al. [29, 30], Richmond et al. [31], and Kobayashi et al. [5] among others. The second method is called the “inner area” method and was used by Damkohler [32], Khramtsov [6], Petrov et al. [33], Williams et al. [34], and Zotin et al. [35, 36]. The “total area” method, which involves using the area of a right angle cone fitted to the flame shape, is used by Bollinger et al. [37], and Grover et al. [38]. The calculation of the turbulent burning velocity in this work is similar to Grover et al. [38] who averaged the measured flame height for 22 images to determine the burning velocity of a turbulent flame. The area method uses

$$S_T = \bar{u} \sin \alpha, \quad (3.5)$$

to calculate the burning velocity where \bar{u} is the mean flow velocity and α is the half angle of the right cone with a height equal to the mean flame height. This method uses a number of simplifying assumptions as discussed by Lewis et al. [3]:

1. The burning velocity is constant over the whole cone surface.
2. The boundary between unburned and burned gases approximates a mathematical surface, with the temperature changing abruptly from the initial to the final on passing through it.
3. The flow lines retain their direction and velocity from the orifice right up to the cone surface.

Figure 3.17 shows a diagram of the process used to get the average flame height in this work. (a) shows a sample shadowgraph image collected ($\phi = 0.8, u'_{rms} = 0.185, \lambda_{st} = 0$). Using a MATLAB program (shown in App.) the image is cropped, the blue channel is extracted, the intensity of the image is increased, and the edge of the flame is selected by manually clicking along the edge, shown as a blue line in (b). The pixel locations are converted to a distance with 1

pixel being equal to 0.04315 mm. The location of the selected points is stored as part of a matrix (c). This process is repeated 25 times and using another MATLAB program (shown in App.) the location of the flame edges are combined as shown in (d) and averaged as shown in (e). The average shown in (e) is done by averaging the height location of the curves moving across the horizontal axis between the two average anchoring points at the edges of the burner nozzle. A linear line is shown connecting the cutoff point to the base location but is not employed in the analysis method used. The resulting curve is smoothed using a point averaging method and the maximum height of the fitted curve is used to calculate the half angle as:

$$\alpha = \tan^{-1}\left(\frac{0.5d}{h}\right), \quad (3.6)$$

where d is the internal diameter of the nozzle exit and h is the mean flame height. Using this procedure, the calculated burning velocities for turbulent methane-air flames match reasonably well with published data as shown in the next section.

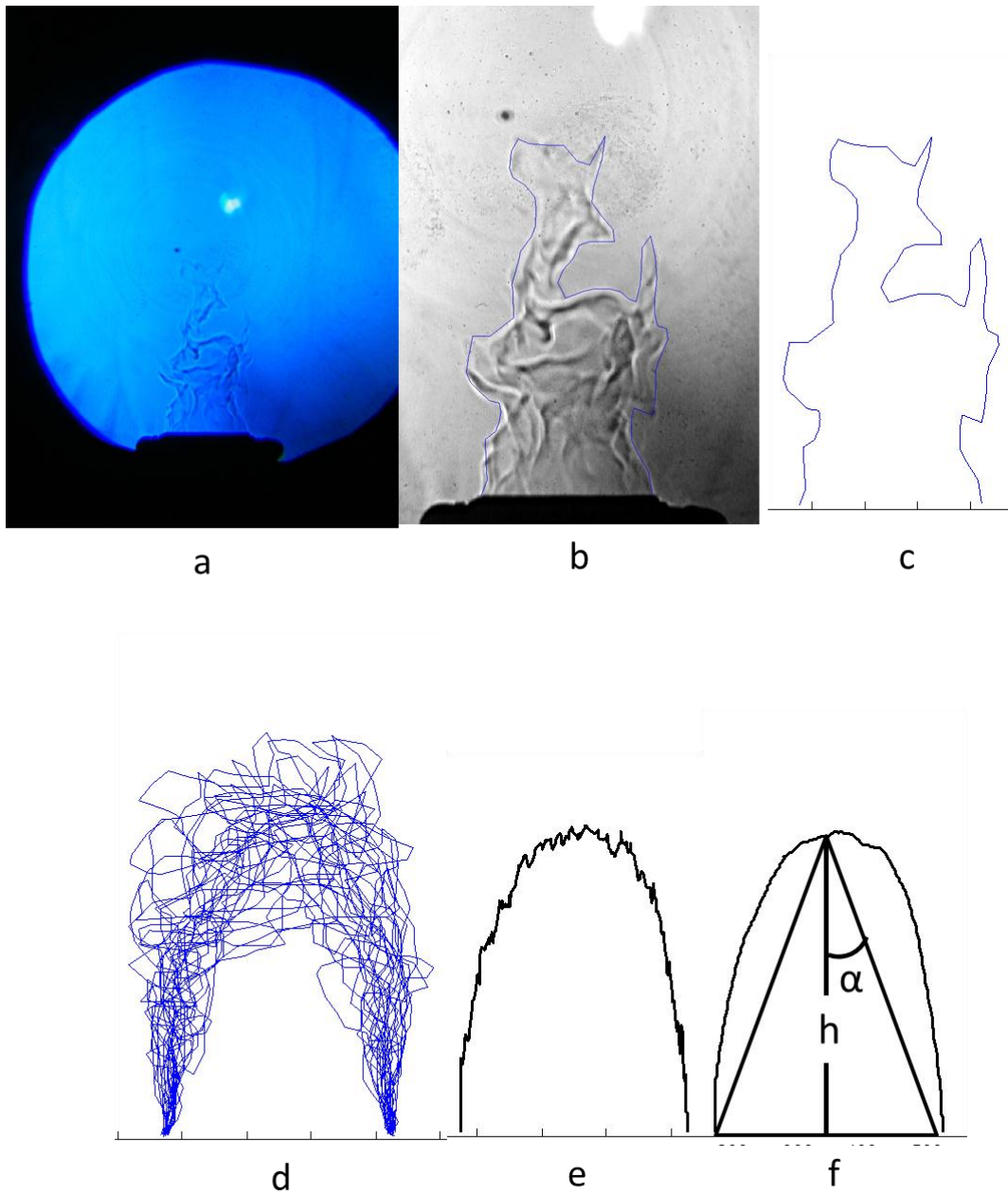


Figure 3.17: Analysis method of turbulent images

The method shown above was used due to the difficulty in determining a quantitative total flame surface area (as opposed to the “total area” method). Figure 3.18 shows top and side profiles for a theoretical turbulent flame. As shown, to completely quantify the surface area of a turbulent flame, instantaneous measurements of the side view (a) and top view profiles (b) at each height along the flame (this could require 100’s or 1000’s of slices, similar to the way an MRI is done)

are required. While some work has been done to make 3D images of turbulent flames using high speed cameras [39] this was not possible due to the need to use the shadowgraph with the addition of the dust particles.

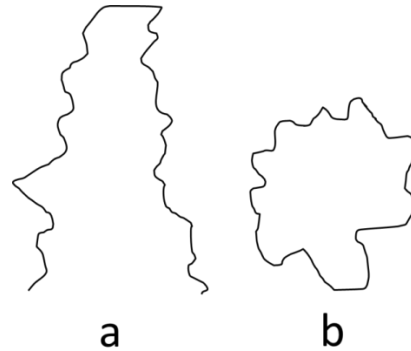


Figure 3.18: Profiles of theoretical turbulent flame (a) side view (b) top view at a specific height

To determine the number of images required for determining the burning velocity, a parametric study was done as shown in Fig. 3.19 comparing the calculated burning velocity versus the number of images used. It is shown that the asymptotic velocity calculation is reached at 10-15 images. To add a factor of safety, 25 images are sampled for each test to determine the average turbulent burning velocity.

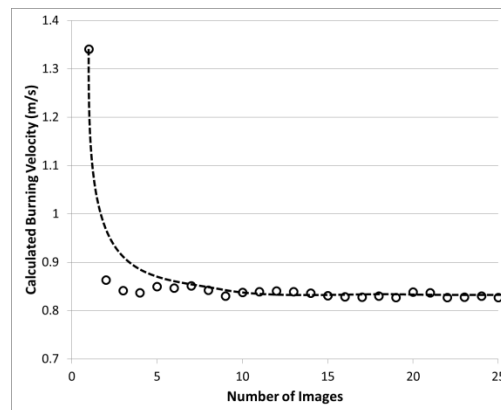


Figure 3.19: Comparison of calculated burning velocity versus number of images used

3.10 Uncertainty

Each individual component adds a certain amount of uncertainty to the work. The mass flow controllers have an uncertainty of 1% of full scale (0.5 lpm for air and 0.05 lpm for methane). The dust feeder adds an amount of uncertainty to the flow. The instantaneous fluctuations in the feed rate were not able to be quantified during the current work. This could lead to uncertainty in the measurement. However, due to the long duration of sampling time, the potential effect is minimalized. An uneven distribution of dust inside of the dust tube would also lead to uncertainty in the measurement. Qualitative measurements of the uniformity of the dust concentration were not able to be carried out. Makeup air was controlled using a rotometer with an uncertainty of 5% of full scale. This could lead to slight variations in the ambient flow speed inside the combustion chamber. The high speed shadowgraph images were taken with a shutter speed of 125 microseconds. The flame can move some amount during this exposure time depending on the level of turbulent intensity. The flame edges were selected manually using a MATLAB program. The uncertainty associated with selecting the images by hand is not quantified in the current work. Since the uncertainty of the experiment could not be quantitatively measured error bars are calculated as the standard deviation of the burning velocity as calculated from the maximum heights of the individual flame edges. This provides a region of 95% confidence in the calculated result as shown in Chapter 4.

3.11 Experimental matrix

Table 3.3 Experimental matrix

total flow rate (lpm)	10				30				35				40											
u'_{rms} (m/s)	0				0.185				0.335				0.532											
75 -95 um Coal																								
ϕ	Air	CH ₄	Dust Conc				Air	CH ₄	Dust Conc				Air	CH ₄	Dust Conc									
			g/m ³						g/m ³						g/m ³									
	(LPM)	0	25	50	75	(LPM)	0	25	50	75	(LPM)	0	25	50	75	(LPM)	0	25	50	75				
0.8	9.23	0.775	0	123	201	279	27.68	2.325	0	279	514	748	32.29	2.712	0	318	592	865	36.90	3.100	0	357	670	982
1	9.05	0.950	0	123	201	279	27.15	2.851	0	279	514	748	31.67	3.326	0	318	592	865	36.20	3.801	0	357	670	982
1.2	8.88	1.119	0	123	201		26.64	3.357	0	279	514	748	31.08	3.917	0	318	592	865	35.52	4.476	0	357	670	982
106-125 um Coal																								
	Air	CH ₄	Dust Conc				Air	CH ₄	Dust Conc				Air	CH ₄	Dust Conc									
			g/m ³						g/m ³						g/m ³									
	(LPM)	0	25	50	75	(LPM)	0	25	50	75	(LPM)	0	25	50	75	(LPM)	0	25	50	75				
0.8	9.23	0.775	0	123	208	293	27.68	2.325	0	293	548	803	32.29	2.712	0	336	633	930	36.90	3.100	0	378	718	
1	9.05	0.950	0	123	208	293	27.15	2.851	0	293	548	803	31.67	3.326	0	336	633	930	36.20	3.801	0	378	718	
1.2	8.88	1.119	0	123	208	293	26.64	3.357	0	293	548	803	31.08	3.917	0	336	633	930	35.52	4.476	0	378	718	

Table 3.3 shows the test matrix of experiments conducted in this study. A total of 92 tests were performed. The numbers highlighted in grey are the dust feeder settings for the prescribed dust concentration based on the feeder calibration curve and represent individual tests. The particle size of the coal was determined using a sieve shaker. The fuel dust is Pittsburgh seam coal, bituminous, with approximately 30% volatiles.

References

1. Bradley, D., Z. Chen, S. El-Sherif, S.E.-D. Habik, and G. John, *Structure of Laminar Premixed Carbon-Methane-Air Flames and Ultrafine Coal Combustion*. Combustion and Flame, 1994. **96**: p. 80-96.
2. Andrews, G.E., D. Bradley, and S.B. Lwakabamba, *Turbulence and Turbulent Flame Propagation - A Critical Appraisal*. Combust. Flame, 1975. **24**: p. 285-304.
3. Lewis, B. and G.V. Elbe, *Stability and Structure of Burner Flames*. Journal of Chemical Physics, 1943. **11**: p. 75-97.

4. Goroshin, S., I. Fomenko, and J.H.S. Lee. *Burning Velocities in Fuel-Rich Aluminum Dust Clouds*. in *Proc. Combust. Inst.* 1996: The Combustion Institute.
5. Kobayashi, H., T. Tamura, K. Maruta, T. Niioka, and F.A. Williams, *Burning Velocity of Turbulent Premixed flames in a high Pressure Environment*. *Proc. Combust. Inst.*, 1996. **26**: p. 389-396.
6. Khramtsov, V.A., *Investigation of pressure effect on the parameters of turbulence and on turbulent burning*. *Proc. Combust. Inst.*, 1959. **7**: p. 609-620.
7. Liu, Y. and B. Lenze, *The influence of turbulence on the burning velocity of premixed CH₄-H₂ flames with different laminar burning velocities*. *Proc. Combust Inst*, 1988. **22**: p. 747-754.
8. Turns, S.R., *An Introduction to Combustion: Concepts and Applications*. 2000, New York: McGraw Hill.
9. Pope, S.B., *Turbulent Premixed Flames*. *Ann. Rev. Fluid Mech.*, 1987. **19**: p. 237-270.
10. Chomiak, J., *Basic Considerations in the Turbulent Flame Propagation in Premixed Gases*. *Prog. Energy Combustion Science*, 1979. **5**: p. 207-221.
11. Borghi, R. and D. Dutoya, *On the Scales of the Fluctuations in Turbulent Combustion*. 17th Symp.(Int.) on Combustion, 1979(1): p. 235-244.
12. Liu, R., D.S.-K. Ting, and G.W. Rankin, *On the Generation of Turbulence with a Perforated Plate*. *Experimental Thermal and Fluid Science*, 2004. **28**: p. 307-316.
13. Roach, P.E., *The Generation of Nearly Isotropic Turbulence by Means of Grids*. *Heat and Fluid Flow*, 1987. **8**(2): p. 82-92.
14. Bruun, H.H., *Hot-Wire Anemometry: Principles and Signal Analysis*. 1995: p. pg. 64.
15. Hattori, H. *Flame Propagation in pulverized coal-air mixtures*. in *Proc. Combust. Inst.* 1957.
16. Kolbe, M., *Laminar Burning Velocity Measurements of Stabilized Aluminum Dust Flames*, in *Mechanical Engineering*. 2001, Concordia University Montreal: Quebec, Canada.
17. Cassel, H.M., A.K.D. Gupta, and S. Guruswamy, *Factors Affecting Flame Propagation Through Dust Clouds*. Third Symposium on Combustion, Flame and Explosion Phenomena, 1949: p. 185-190.
18. Ghosh, B., D. Basu, and N.K. Roy. *Studies of Pulverized Coal Flames*. in *Proc. Combust. Inst.* 1957.
19. Kobayashi, H., J.B. Howard, and A.F. Sarofim, *Coal devolatilization at high temperatures*. *Proc. Combust. Inst.*, 1977. **16**: p. 411-415.
20. Reddy, P., P.R. Amyotte, and M.J. Pegg, *Effect of inerts on layer ignition temperature of coal dust*. *Combust. Flame*, 1988. **114**: p. 41-53.
21. Sherrat, S. and J.W. Linnett, *The determination of flame speeds in gaseous mixtures*. *Trans. Faraday Soc.*, 1948. **44**: p. 596-608.
22. Garner, F.H., R. Long, and G.R. Ashforth, *Determination of burning velocities in benzene-air mixtures*. *Fuel*, 1949. **28**(12): p. 272-276.
23. Anderson, J.W. and R.S. Fein, *Measurements of normal burning velocities and flame temperatures of Bunsen flames*. *J. Chem. Phys.*, 1949. **17**: p. 1268-1273.
24. Anderson, J.W. and R.S. Fein, *Measurment of normal burning velocities of propant/air flames from shadow photographs*. *J. Chem. Phys.*, 1950. **19**: p. 441-443.
25. Whol, K., N.P. Kapp, and C. Gazley, *The stability of open flames*. *Proc. Combust. Inst.*, 1949. **3**: p. 3-20.

26. Abdel-Gayed, R.G., D. Bradley, and M. Lawes, *Turbulent Burning Velocities: A General Correlation in Terms of Straining Rates*. Proceedings of the Royal Society of London. Series A, Mathematical and Physical Sciences, 1987. **414**(1847): p. 389-413.
27. Ballal, D.R. and A.H. Lefebvre, *The Structure and Propagation of Turbulent Flames*. Proc. R. Soc. Lond. A., 1975. **334**: p. 217-234.
28. Ballal, D.R., *The influence of laminar burning velocity on the structure and propagation of turbulent flames*. Proc. R. Soc. Lond. A., 1979. **367**: p. 485-502.
29. Karlovitz, B., D.W. Denniston, and F.E. Wells, *Investigation of turbulent flames*. Journal of Chemical Physics, 1951. **19**(5): p. 541-547.
30. Karlovitz, B. 1954, AGARD: London: Butterworths. p. 247-262.
31. Richmond, J.K., J.M. Singer, E.B. Cook, J.R. Grumer, and D.S.J. Burgess, Proc. Combust. Inst., 1957. **6**: p. 301-311.
32. Damkohler, G., 1940.
33. Petrov, E.A. and A.V. Talantov, 1959.
34. Williams, C.G., H.C. Hottel, and A.C. Scurlock, Proc. Combust. Inst., 1949. **3**: p. 21-40.
35. Zotin, V.K. and A.V. Talantov, Izv. vyssh. ucheb. Zaved., Aviat. Teknol, 1966a. **1**: p. 115-122.
36. Zotin, V.K. and A.V. Talantov, Izv. vyssh. ucheb. Zaved., Aviat. Teknol, 1966b. **3**: p. 98-103.
37. Bollinger, L.M. and D.T. Williams. 1949.
38. Grover, J.H., E.n. Fales, and A.C. Scurlock, Proc. Combust. Inst., 1963. **9**: p. 21-35.
39. Ishino, Y., K. Takeuchi, s. Shiga, and N. Ohiwa, *Measurement of Instantaneous 3D-Distribution of Local Burning Velocity on a Trubulent Premixed Flame by Non-Scanning 3D-CT Reconstruction*, in Proc. Combust. Inst. 2009.
40. Fells, I. and H.G. Rutherford, *Burning velocity of methane-air flames*. Combustion and Flame, 1969. **13**: p. 130.
41. Halpern, C. 1958, Res. Natl. Bur. Std. p. 535.
42. Lee, J., *Burning velocity measurements in aluminum-air suspensions using bunsen-type dust flames*. 2001.
43. Rallis, C.J. and A.M. Garforth, *The Determination of Laminar Burning Velocity*. Prog. Energy Combustion Science, 1980. **6**: p. 303-329.

4. Results and Analysis

Chapter 4 discusses the experimental results for laminar and turbulent flames using the hybrid flame analyzer (HFA) discussed in Chapter 3.

4.1 Laminar flames

Figure 4.1(a-f) shows the laminar burning velocity ($S_{L,st}$) as a function of dust concentration for the three gas-phase equivalence ratios ($\phi_g = 0.8, 1.0, 1.2$) and two dust particle sizes ($d_{st} = 75-90 \mu\text{m}, 106-125 \mu\text{m}$). The subscript “L” denotes laminar, while “st” denotes the presence of dust. (st represents staub in the German language for dust). The naming convention is consistent with that adapted by NFPA 68 and 69.

For the 75-90 μm particle range and equivalence ratio $\phi_g = 0.8$ and 1.2 (Figs. 4.1a and 4.1e) it is observed that the burning velocity is reduced (when compared to the gas-only value) as the dust concentration is increased from 0 to 75 g/m^3 . The effect is small, less than 10% but more than the experimental uncertainty. A similar experimental trend was also observed recently by Xie et al. [1]. The effects of the dust particles on the burning velocity are likely to originate from three competing sources, the energy absorption by the dust particles (a decreasing effect), the increase in local equivalence ratio due to fuel vapor released from the particles (increasing in fuel lean but decreasing effect in fuel rich), and the effect of the particles on the local fluid mechanics of the flame sheet (c.f. Fig. 4.2, which could increase or decrease $S_{L,st}$). In the current case, the laminar burning velocity shows a general decreasing trend mainly due to the heat absorption by the particles, which overcomes the effect of change of effective equivalence ratio due to pyrolysis of the coal particles. In the stoichiometric case ($\phi_g = 1.0$) there is almost no effect as the dust particle concentration is increased (the maximum variation is only $\sim 6.5\%$). This is because the effective equivalence ratios in these cases reach slightly rich limit where the burning velocity

becomes maximum, and this compensates for the decrease flame temperature due to heat absorption by the dust particles.

At higher particle size range of 106 - 125 microns, the laminar burning velocity is almost constant with a variation of approximately $\pm 4.5\%$ around the mean value over all the dust concentrations. For the lean case ($\phi_g = 0.8$), at a particle loading of 25 g/m^3 the measured burning velocity is increased but at the two higher particle loadings (50 and 75 g/m^3) the burning velocity is decreased. This also occurs in the fuel rich case ($\phi_g = 1.2$), and in the stoichiometric case ($\phi_g = 1.0$) the 50 g/m^3 case is slightly increased but the 25 and 75 g/m^3 cases are slightly decreased. These fluctuations are within the uncertainty of the measurement. The trend for the larger sized particles may be due to the combined effect of heat absorption by the particles compensated by the increase in the effective equivalence ratio due to increased pyrolysis resulting from increased surface area of the particles at a similar gas velocity.

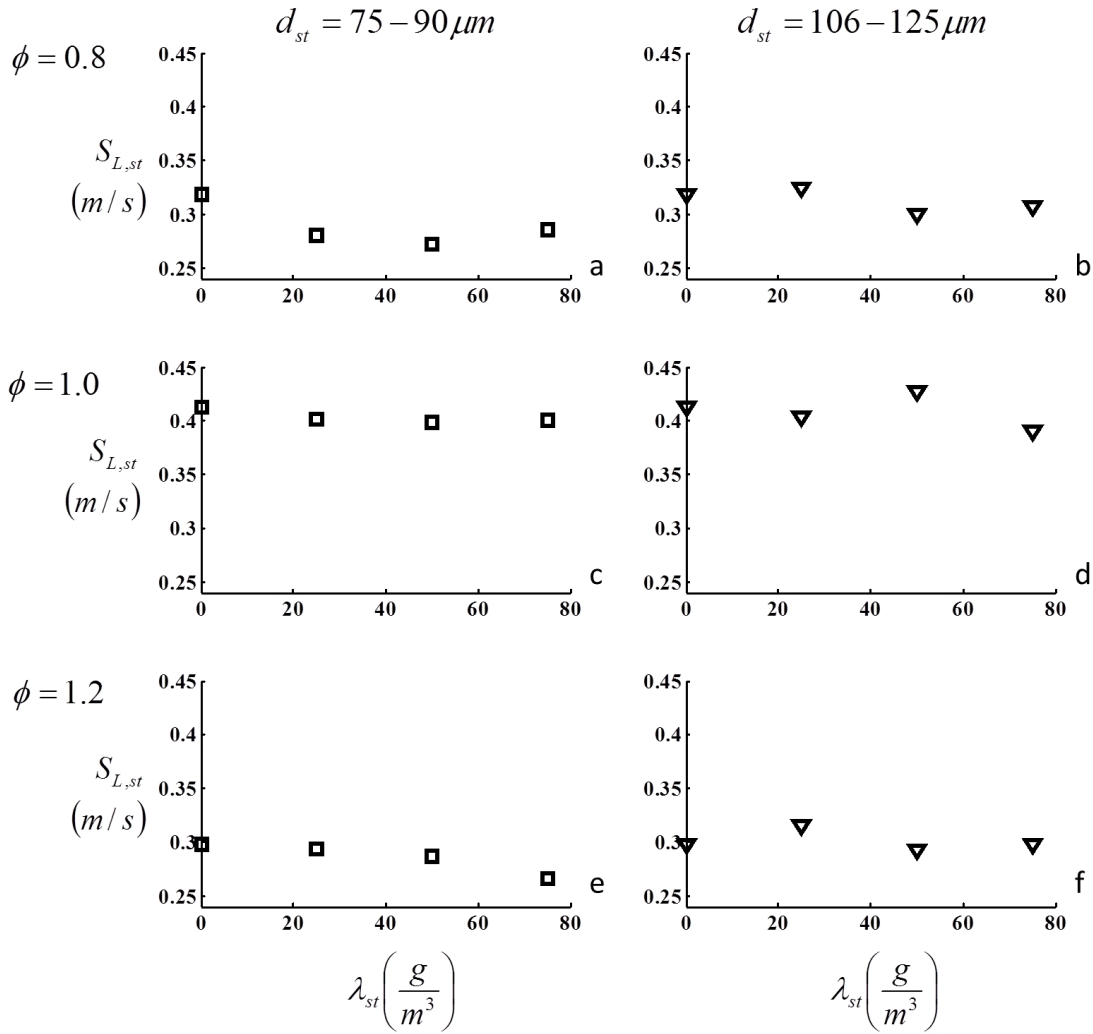
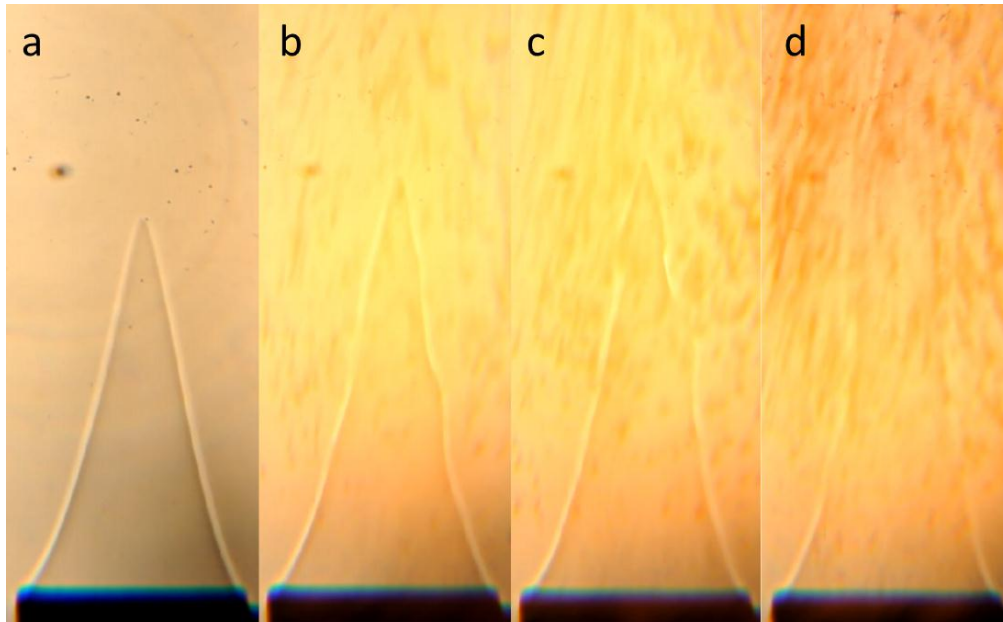


Figure 4.1: Laminar flame as a function of dust concentration

Figure 4.2 shows a comparison of a sample set of laminar flames $\phi=1.2$ (a) gas only (b) $\lambda_{st} = 50 \text{ g/m}^3$ (c) $\lambda_{st} = 100 \text{ g/m}^3$ (d) $\lambda_{st} = 200 \text{ g/m}^3$. These shadowgraph images are from video recordings using a Nikon d90 fitted with a macro lens and can be used for a qualitative understanding of the influence of particle concentration on the nature of the flame sheet. The lines in the shadowgraph represent the premixed gas phase reaction zone. The influence of the particles on the smoothness of the flame sheet is evident in comparing Fig. 4.2 (a) and (b)

representing a gas only and a gas-flame with dust particle ($d_{st}=75-90 \mu\text{m}$, $\lambda_{st}=50 \text{ g/m}^3$). As shown in Fig. 4.2, the particles cause slight bending of the flame sheet but do not create turbulent structures as observed with turbulent flames discussed later. In Fig. 4.2 (c) small sections of the premixed gas flame (closer to the apex) begins to extinguish. In Fig. 4.2 (d) the entire top of the premixed flame is extinguished. This extinguishment phenomenon may occur because the dust particles are absorbing energy as they heat up. Also, as the dust concentration increases, the production of volatile gases in the preheat zone will increase which may raise the local equivalence ratio above the upper flammability limit for the gas mixture. This phenomenon is exacerbated by the lengthening of the residence time of a particle in the preheat zone as the burning velocity is reduced.

The observed reduction in contrast of the flame tip observed in Fig. 4.2 may also be due to light saturation in the optical set up or decrease in relative temperature change. As shown in Fig. 4.2, the contrast of the flame in the shadowgraph is reduced as the dust concentration is increased. The increase in dust causes an increase in the light emissions from the coal dust passing through the optics and collected on the camera sensor, thereby saturating it in regions with high emissivity. In the gas only flame the ambient gas temperature outside the premixed flame is significantly lower than the flame temperature. In a hybrid mixture the preheated coal dust continues to burn after leaving the premixed gas flame front causing relative difference between the premixed flame temperature and the surrounding gas to be lower. This effect reduces the intensity of the shadow created by the region on either side of the reaction zone.



**Figure 4.2 Comparison of laminar flames ($\phi = 1.2$, $d_{st} = 75-90 \mu\text{m}$)
 (a) gas only (b) $\lambda_{st} = 50 \text{ g/m}^3$ (c) $\lambda_{st} = 100 \text{ g/m}^3$ (d) $\lambda_{st} = 200 \text{ g/m}^3$.
 Original videos are available for viewing at www.firesciencetools.com**

4.2 Turbulent flames

4.2.1 Gas flames (validation study)

To validate the experimental apparatus and procedure the turbulent methane-air flame data is compared with data from published work by Kobayashi et al. [2] as shown in Fig. 4.3. Fig. 4.3 shows the turbulent burning velocity $S_{T,g}$ of a methane-air ($\phi = 1.0$) flame as a function of turbulent intensity (u'_{rms}). Turbulence is generated using a perforated plate (1mm hole diameter, blockage ratio of 50%) placed 30 mm below the exit of the nozzle similar to that used by Kobayashi et al. [2]. Error bars, representing the uncertainty in the measurement are one standard deviation of the burning velocity calculated from the individual flame heights (from 25 images). These bars represent a 95% confidence level that the burning velocity exists within the range (in the laminar case the error bars do not exceed the size of the data marker).

Reasonably good agreement is observed between the two experimental methods. Similar to Kobayashi et al.'s data, the burning velocity increases as turbulent intensity increases and eventually begins to level off when higher levels of turbulent intensity are reached. It is also interesting to note that Kobayashi et al. used the angle method (c. f. Fig. 3 on pg. 391 of [2]) to extract the turbulent burning velocity from schlieren images of turbulent flames whereas in this study an alternative method similar to Grover et al. [3] is used as discussed in Chapter 3 and provides similar results.

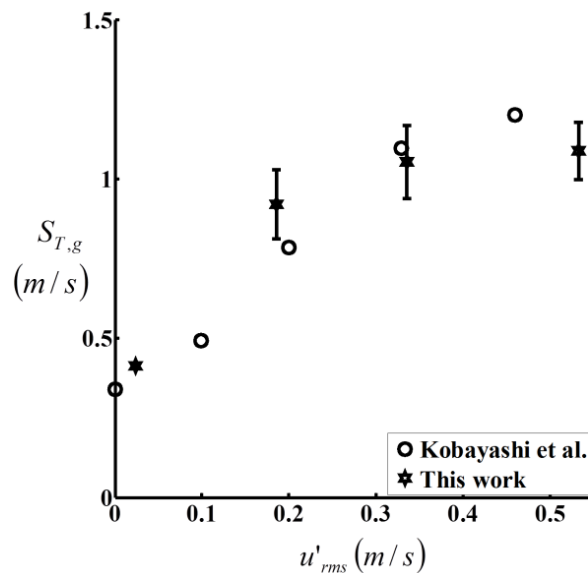


Figure 4.3: Turbulent burning velocity of a methane-air flame ($\phi = 1.0$) vs. turbulent intensity.

Figure 4.4 (a-d) shows a comparison of the shadowgraph results for the laminar and turbulent gas-only flames. Figure 4.4(a) shows the smooth and clearly defined edge of a laminar flame. Figures 4.4 (b-d) showing turbulent flames with increasing turbulent intensity clearly show the wrinkled combustion zone. Further, flame wrinkling is observed to increase as the turbulent intensity is increased. The increased wrinkling causes an increase in the reaction zone area which

means that the flame structure can consume the fuel-air mixture at a faster rate. This results in an increase in the value of the burning velocity as shown in Fig. 4.3.

Damkohler [5] was one of the first to propose a theory that covered a range of wrinkled and severely wrinkled flames which is discussed next. It should be noted that although a laminar burning velocity (S_L) is a physiochemical and chemical kinetic property of the unburned mixture, a turbulent burning velocity (S_T) is in reality a mass consumption rate per unit area divided by the unburned gas mixture density. Thus S_T must depend on the properties of the turbulent field in which it exists.

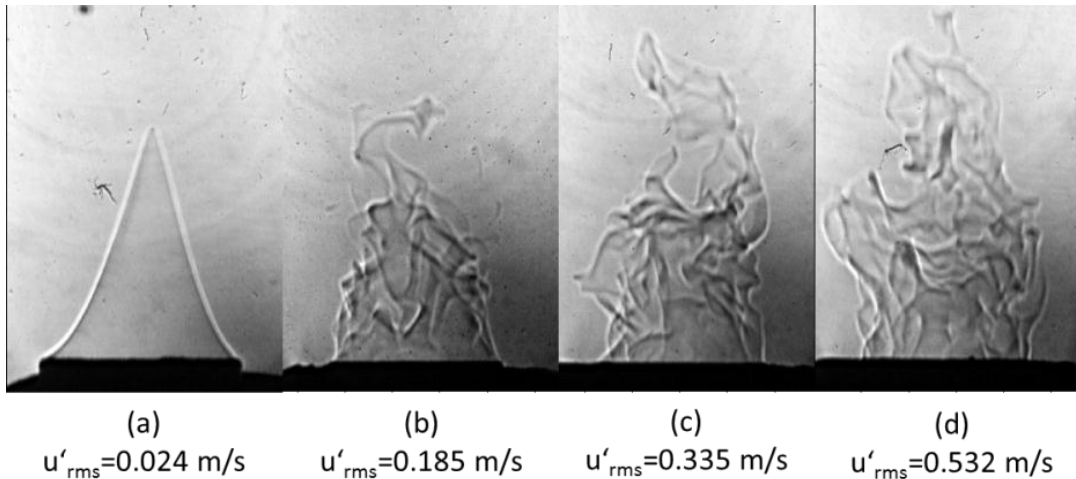


Figure 4.4 Flame images at various turbulent intensities (CH_4 -air) (gas only) $\phi_g = 1$

To further analyze the problem a theoretical treatment similar to Dahoe [4] is utilized on the current experimental data. In the case of large scale, low intensity turbulence, the instantaneous flame front will be wrinkled while the transport properties remain the same. The wrinkles increase the flame front area per unit cross section of the turbulent flame brush which results in a higher propagation velocity without a change in the instantaneous local flame structure itself. The instantaneous flame surfaces in such a turbulent flame are known as laminar flamelets. With this picture in mind, Damkohler [5] and Schelkin [6] derived the earliest models for the turbulent

burning velocity. Both researchers equated the mass flux, \dot{m} , through the cross sectional area of the flame brush, A_T , to the mass flow of the unburnt mixture through the wrinkled laminar flame area, A_L :

$$\dot{m} = \rho_u A_T S_T = \rho_u A_L S_L, \quad (4.1)$$

$$\frac{S_T}{S_L} = \frac{A_L}{A_T}, \quad (4.2)$$

Damkohler [5] proposed that the ratio of the area of the wrinkled laminar flame and the cross section of the turbulent flame brush could be approximated by

$$\frac{A_L}{A_T} = \frac{S_L + u'_{rms}}{S_L} = 1 + \frac{u'_{rms}}{S_L} \quad (4.3)$$

and substitution of this expression in Eq. 4.2 leads to

$$\boxed{\frac{S_T}{S_L} = 1 + \frac{u'_{rms}}{S_L}} \quad (4.4)$$

In the limit $u'_{rms} \gg S_L$, Eq. 4.4 implies that the turbulent burning velocity becomes independent of the laminar burning velocity and the chemistry has no effect on the propagation velocity. This is known as the Damkohler hypothesis.

Schelkin [6] proposed another approximation for the surface of the wrinkled laminar flame by reasoning that turbulence creates conical bulges in a laminar flame and that the increased flame surface is proportional to the average cone area divided by the average cone base. If the radius of the cone base and the cone height are, respectively denoted by R and h , then the surface area of the cone base and the cone mantle are equal to πR^2 and $\pi R(R^2 + h^2)^{1/2}$. Thus, when a circular

element of a planar laminar flame is bulged into a cone, the surface area increases by a factor $(R^2+h^2)^{1/2}/R$. Schelkin [6] assumed that the diameter of the cone base is proportional to the average length scale of the turbulence, $R \propto 1/2l_t$, and that the apothem scales as $h \propto u'_{rms} l_t / S_L$. He considered the apothem to be proportional to the average fluctuating velocity u'_{rms} and the time during which an element of the flame interacts with an eddy l_t / S_L . These assumptions lead to

$$\boxed{\frac{S_T}{S_L} = \frac{\sqrt{R^2 + h^2}}{R} = \sqrt{1 + \left(\frac{2u'_{rms}}{S_L}\right)^2}} \quad (4.5)$$

If $u'_{rms} \gg S_{uL}$, the first term under the root sign is made negligible by the second term and the turbulent burning velocity becomes independent of the laminar burning velocity. This is in accordance with Damkohler's hypothesis.

Karlovitz et al. [7] derived several expressions for the effect of large scale turbulence ($l_t > \delta_L$) on the turbulent burning velocity from the assumption that an additional velocity produced by the turbulent diffusion, S^t , has to be added to the laminar burning velocity:

$$S_T = S_L + S^t \quad (4.6)$$

The additional velocity was taken into account by dividing the root-mean-square displacement due to the turbulence by the average time interval during which a flame element interacts with an eddy, $\Gamma = l_t / S_{uL}$:

$$S^t = \frac{\left(\overline{x'^2}\right)^{1/2}}{\Gamma} \quad (4.7)$$

If the turbulent flow field is characterized by the root-mean-square of the instantaneous velocity fluctuations and the autocorrelation coefficient,

$$u'_{rms} = \left(\overline{u'^2}\right)^{\frac{1}{2}} \text{ and } \rho(\tau) = \frac{\overline{u'(t)u'(t+\tau)}}{u'^2(t)}, \quad (4.8)$$

the length scale, time scale, and variance of the displacement are related through the following relationships [8]:

$$l_t = u'_{rms} \int_0^\infty \rho(\tau) d\tau, \quad \tau_l = \int_0^\infty \rho(\tau) d\tau, \quad (4.9)$$

$$\text{and } \frac{d\overline{x'^2}}{dt} = 2\overline{u'^2} \int_0^\infty \rho(\tau) d\tau. \quad (4.10)$$

In the case of weak turbulence, that is $u'_{rms} \ll S_L$ the root-mean-square displacement within the interaction time between a flame element and a turbulent eddy becomes (by integrating Eq. 4.10)

$$\left(\overline{x'^2}\right)^{\frac{1}{2}} = u'_{rms} \Gamma \quad (4.11)$$

and therefore

$$S^t = \frac{\left(\overline{x'^2}\right)^{\frac{1}{2}}}{\Gamma} = \frac{u'_{rms} \Gamma}{\Gamma} = u'_{rms}. \quad (4.12)$$

For strong turbulence the integral on the right side of the Eq. 4.10 assumes a definitive value which is equal to the time scale of the turbulence, therefore

$$\left(\overline{x'^2}\right)^{\frac{1}{2}} = \sqrt{2l_t u'_{rms} \Gamma}, \quad (4.13)$$

and

$$S^t = \frac{\left(\overline{x'^2}\right)^{\frac{1}{2}}}{\Gamma} = \frac{\sqrt{2l_t u'_{rms} \Gamma}}{l_t / S_L} = \sqrt{2S_L u'_{rms}}. \quad (4.14)$$

Combining this with Eq. 4.6 and dividing by S_L yields:

$$\boxed{\frac{S_T}{S_L} = 1 + \sqrt{2} \left(\frac{u'_{rms}}{S_L} \right)^{\frac{1}{2}}} \quad (4.15)$$

In the case of intermediate turbulence, the root mean-square displacement depends on the shape of the correlation function. If the shape of the correlation function is approximated by a parabola,

$$\rho(\tau) = 1 - \frac{1}{2} \frac{\tau^2}{\tau_m^2}, \quad (4.16)$$

The integral on the right hand side of Eq. 4.10 may be solved for the variance of the displacement, consequently

$$S' = \sqrt{\frac{5}{12}} u'_{rms}, \quad (4.17)$$

and

$$\frac{S_T}{S_L} = 1 + \sqrt{\frac{5}{12}} \frac{u'_{rms}}{S_L} \quad (4.18)$$

Small scale turbulence is believed to contain insufficient kinetic energy to distort a laminar flame, but in view of Eqs. 4.6 and 4.7 it is reasonable to expect that the turbulent burning velocity behaves in accordance with Eq. 4.4.

According to Karlovitz's analysis, the turbulent burning velocity should at first increase linearly but then more slowly as turbulence intensity increases (this is similar to what is observed experimentally in Fig. 4.3). In order to find a correlation for the effect of any particular type of turbulent motion on the turbulent burning velocity researchers have adopted a generalization of equations 4.4, 4.5, 4.15, and 4.18:

$$\frac{S_T}{S_L} = 1 + C \left(\frac{u'_{rms}}{S_L} \right)^n, \quad (4.19)$$

where n is known as the bending exponent and C is a parameter that contains the influence of the scale of turbulence.

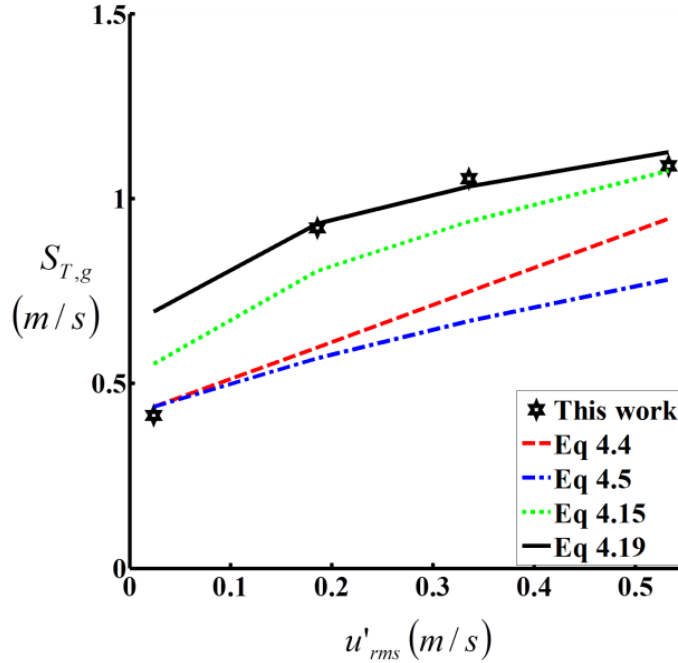


Figure 4.5: Correlation of experimental results $\phi_g = 1$

Equations 4.4, 4.5, 4.15, and 4.19 are shown along with the current experimental data in Fig. 4.5. It is observed that Damkohler's Eq. 4.4, Schleklin's Eq. 4.5, and Eq. 4.15 under predict the experimental data. The best fit is obtained by using Eq. 4.19 using values of $C=1.6$ and $n=0.3$ (similar to those used by Dahoe [4] for propane air flames).

4.2.2 Turbulent combustion regimes

Figure 4.4 showing the flame images epitomizes how the reaction zone of a flame can be affected by a turbulent field. To understand the effect a suitable starting point is the consideration of the quantities that determine the fluid characteristics of the system. The structure of the

turbulent velocity field may be presented in terms of two parameters – the scale and the intensity of the turbulence. The intensity is the square root of the turbulent kinetic energy which essentially gives a root-mean-square velocity fluctuation u'_{rms} . Based on the three length scales used in turbulence [9]: (1) the integral length scale l_0 which characterizes the large eddies, or the length beyond which various fluid-mechanical quantities become essentially uncorrelated; (2) the Taylor microscale λ , which is obtained from the rate of strain; and (3) the Kolmogorov microscale l_k , which typifies the smallest dissipative eddies. These length scales and the intensity can be combined to form 3 Reynolds numbers: $R_l = u'_{rms} l_0 / \nu$, $R_\lambda = u'_{rms} \lambda / \nu$, and $R_k = u'_{rms} l_k / \nu$, with an inter-relationship that can be derived [9] as $R_l \sim R_\lambda^2 \sim R_k^4$. Similarly, the length scale associated with laminar flame structures in reacting flows is the characteristic thickness of a premixed flame δ_L (calculated here using $\delta_L = 2\alpha / S_L$ where α is the thermal diffusivity of air [10] estimated at 650 K). Comparison of an appropriate chemical length with a fluid dynamic length provides a nondimensional parameter that has a bearing on the relative rate of reaction. Nondimensional numbers of this type are called Damkohler numbers and given the symbol Da . For large Da the chemistry is fast (reaction time is short) and reaction sheets of various wrinkled types may occur. For small Da , the chemistry is slow (compared to the fluid mechanics) and well-stirred flames may occur.

Diagrams defining the regimes of premixed turbulent combustion in terms of the nondimensional groups discussed above have been proposed by several researchers (cf. Peters [11], Turns[10]).

To determine the regime in which the current experiments exist two such diagrams are examined. One adapted from Turns [10] is a plot of the Da -number $\left(\frac{l_0}{\delta_L}\right)\left(\frac{S_L}{u'_{rms}}\right)$ vs. the turbulent Reynolds number $\left(\frac{u'_{rms} l_0}{\nu}\right)$ based on the integral length scale commonly referred to as

the Borghi diagram; and another adapted from Peters [11] is a plot of $\frac{u'_{rms}}{S_L}$ vs. $\frac{l_o}{\delta_L}$ commonly referred to as the modified Borghi diagram. Figure 4.5 (a) shows the functional relationship between Da and Re_T and Fig. 4.6 (b) shows the relationship between $\frac{u'_{rms}}{S_L}$ and $\frac{l_o}{\delta_L}$ characterizing the fluid mechanics of the current experimental setup.

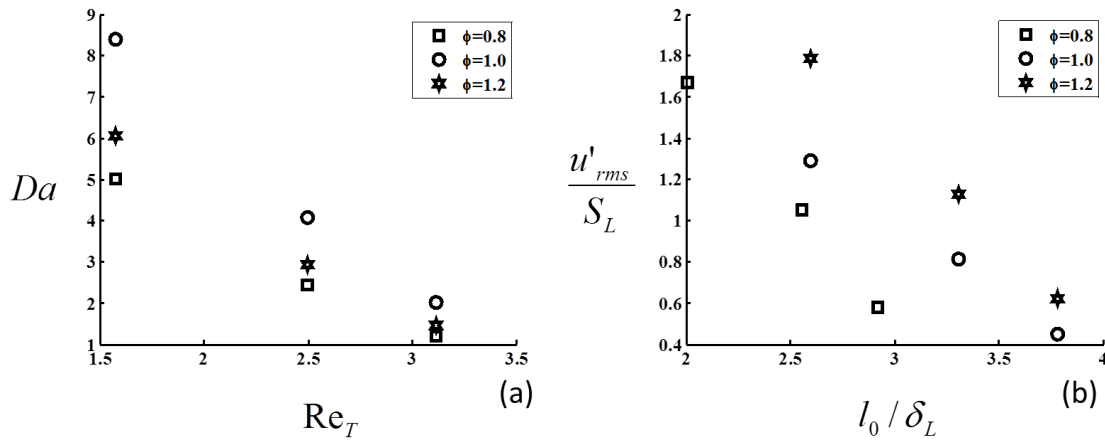


Figure 4.5: (a) Parameters (Da vs. Re_T) (b) Parameters for Borghi diagram

Figures 4.6(a) and (b) depict the characteristic parametric relationships of premixed turbulent combustion. The Da -number for the experiments used in this work ranged from 1.1 to 8.5, while the turbulence Reynolds number, (Re_T) ranged from 1.6 to 3.1. This range is shown in Fig. 4.6(b) as a red rectangle. For the current set of experiments, this range is hard to analyze due to the large ranges on the X and Y axis. The regime of the current experiments is once again within the rectangular region shaded red and shown in Fig. 4.6(b). This range includes the distributed, corrugated, and wrinkled reaction zone.

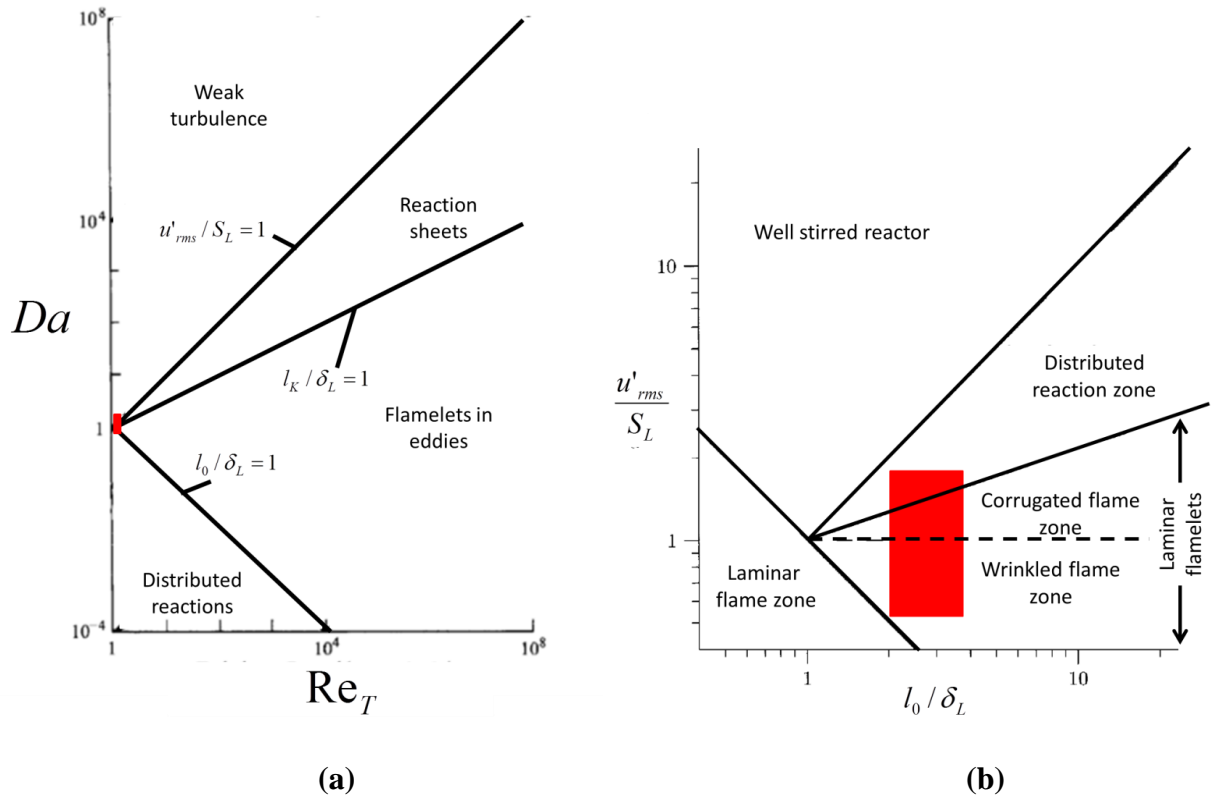


Figure 4.6: Characteristic parametric relationships of premixed turbulent combustion (a) diagram recreated from Turns [10] (b) modified Borghi diagram recreated from Dahoe [4] (also shown in Peters [11]). Region of testing in this work is shown by area shaded in red.

An illustrative sketch of the turbulent flame structure in these regimes is shown in Fig. 4.7(a-c) [4]. For the relatively low levels of turbulence created in this work the testing mostly existed in the laminar-flamelet regime where the macro structure is not rapid enough to destroy the laminar flame structure to such a degree that the laminar burning velocity becomes an irrelevant parameter and the chemistry is so fast that every change in the flame shape due to the large eddies is being reflected in the turbulent burning rate as the flame propagates normal to itself. This flamelet regime is divided into the wrinkled and corrugated sub sections (Fig. 4.8 a and b). If the turbulent intensity is less than the laminar burning velocity (and assuming that the turbulent intensity is the rotation speed of the largest eddies) then the eddies cannot fold the

flame. The turbulence only wrinkles the flame front and the turbulent burning velocity is largely determined by the laminar flame propagation.

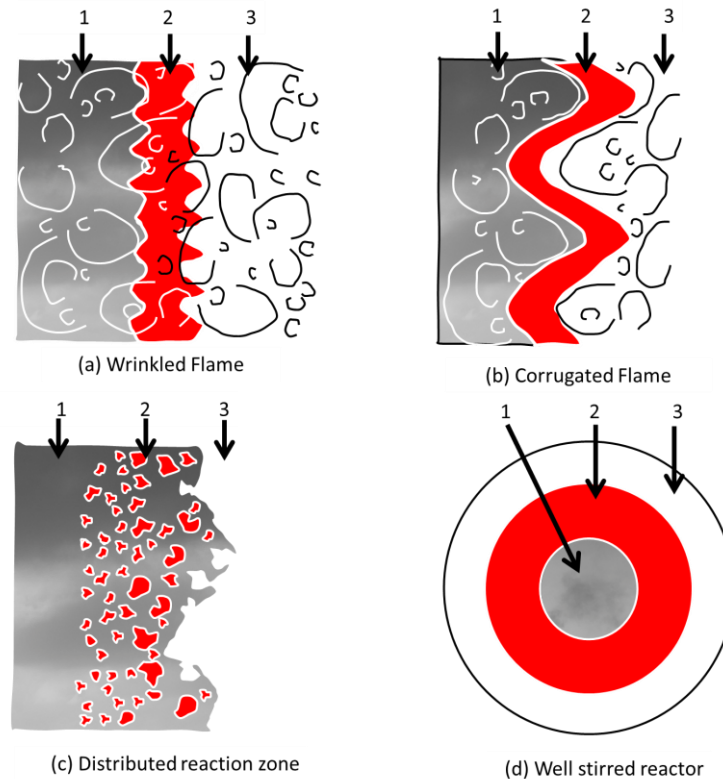


Figure 4.7: Diagrams of turbulent flame structure (1) burned mixture (2) reaction zone (3) unburned mixture [4]

In the corrugated flame regime the flame front will be pushed around and folded by the largest eddies. The smallest eddies which are just capable of affecting the flame are those with a rotational velocity (assumed to be the turbulent intensity) equal to the laminar burning velocity.

In the distributed reaction zone regime the macro eddies fold the flame front to form bulges of a size in the order of the integral length scale. If these bulges extend into the unburned mixture then the local laminar burning velocity becomes less than that of an unstretched flame. At the small bulges the radius of curvature is so small that the effect of quenching due to curvature is large enough to cause local extinction. The flame is cut into pieces by the small eddies and these

pieces are scattered across the flame zone by the larger eddies. As a consequence there is no well defined flame structure, and the flame front consists of a collection of pockets of unburnt and burnt mixture. Therefore the results of using the shadowgraph to examine the flame edge is less reliable in this range.

It should be understood that the discussion so far pertains to turbulent gas-flames alone. Additional parameters will arise for turbulent dust flames owing to the coupling between the condensed phase and gas phase. Micron sized particles influence the turbulent flow structure by (Crowe et al. [12]): (1) displacement of the flow field by flow around a dispersed phase element; (2) generation of wakes behind particles; (3) dissipation of turbulence transfer of turbulence energy to the motion of the dispersed phase; (4) modification of velocity gradients in the carrier flow field and corresponding change in turbulence generation; (5) introduction of additional length scales which may influence the turbulence dissipation; and (6) disturbance of flow due to particle-particle interaction.

Considering fluid mechanics alone (no combustion), additional length scales may also need to be considered. Some obvious examples are the diameter of the particles and the average inter-particle spacing. The wakes produced by particles yield a length scale on the order of the particle size. If the particle size is smaller than the Kolmogorov scale, the particle diameter is probably not a significant length scale affecting the dissipation. If the concentration particles introduced into a flow yields an average interparticle spacing smaller than the inherent dissipation length scale, the particles may interfere with existing eddies breaking them up so that the new dissipation length scale is proportional to the average interparticle spacing rather than the geometry such as the size of the perforated hole size.

Gore and Crowe [13] have shown that a critical parameter that offers a demarcation of particle size which causes the turbulent intensity to either decrease or increase with the addition of particles in the flow is given by the ratio d_{st}/l_o , where, d_{st} is the particle diameter and l_o is the integral length scale. The corresponding change in turbulent intensity is shown in Fig. 4.8 [13]. As observed in Fig. 4.8 when the ratio of d_{st}/l_o is above ~ 0.07 , the presence of particles increases the turbulent intensity. In the current experiments, for the 75-90 μm range, d_{st}/l_o varies between 0.06 - 0.08, while for the 106 – 125 μm range, d_{st}/l_o varies between 0.07 – 0.11. Thus, it can be concluded that if only fluid dynamics (no combustion) effects are considered, the particles will tend to increase the turbulent intensity. Further, Crowe [14] has shown that the increase in turbulent intensity becomes more pronounced as concentration of particles is increased (cf. Fig. 3 in [14]).

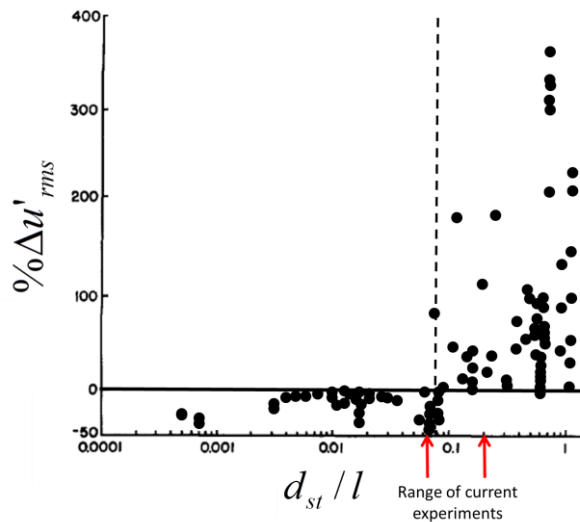


Figure 4.8: Change in turbulent intensity as a function of length scale ratio [13]

4.2.3 Effect of turbulence on burning velocity of a hybrid (dust-CH₄-air) flame

Figures 4.9 (a-f) show relationships of the experimentally measured turbulent burning velocity for the different equivalence ratio and particle size ranges tested (d_{st} , and λ_{st} represent the particle size range, and particle concentration respectively). The Y-axis is nondimensionalized by the laminar burning of the corresponding dust flame ($S_{L,st}$), while the X-axis is nondimensionalized using the laminar burning velocity of the gas flame ($S_{L,g}$) at corresponding equivalence ratio. In the following figures $S_{L,st}$ is used to normalize the turbulent velocity data, to prevent the increase in uncertainty caused by the division of two experimentally measured points the laminar data was fit to linear lines and these functions were used to calculate the value used for the normalization.

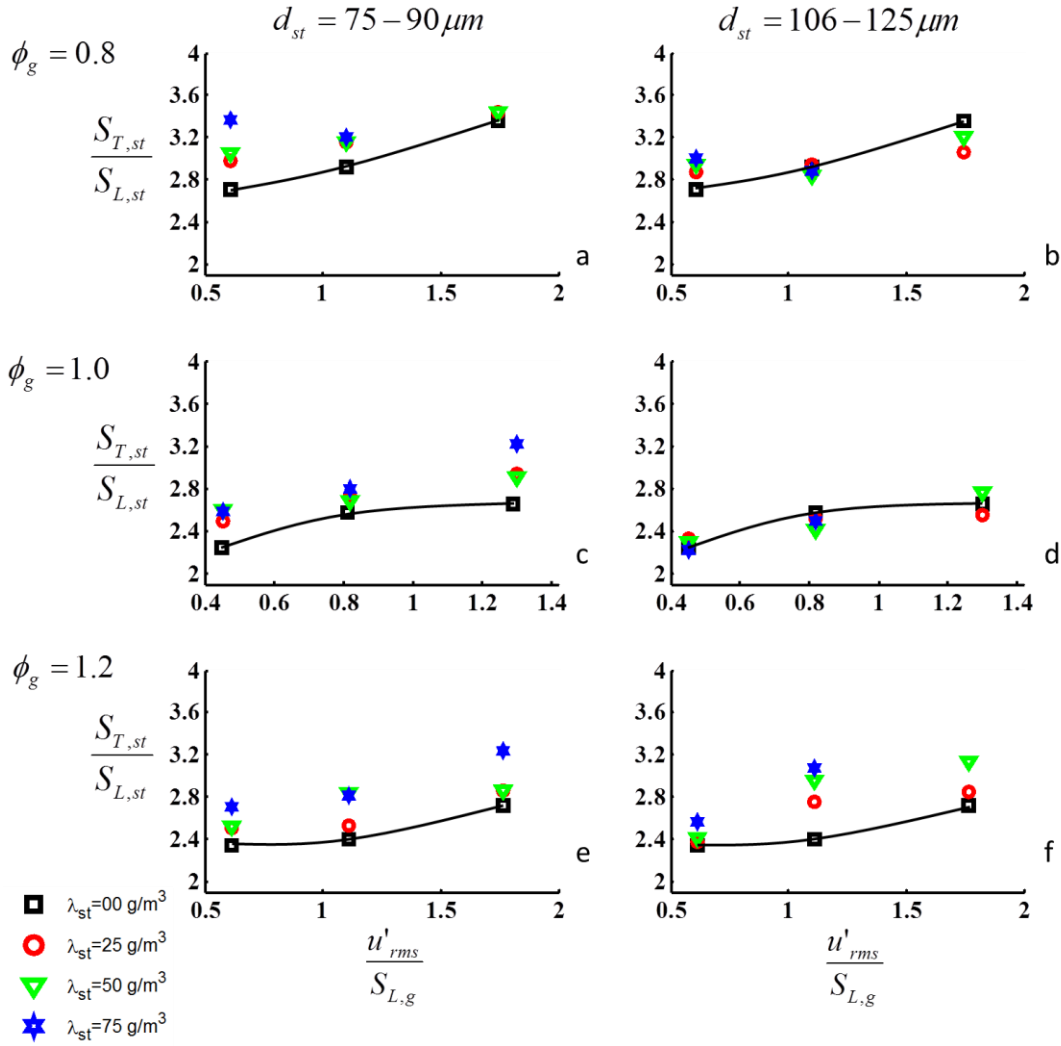


Figure 4.9: Turbulent burning velocity vs. turbulent intensity

In general, Fig. 4.9 shows that the turbulent burning velocity is more than two-times larger than the laminar counter-part for each and every case studied. The turbulent to laminar burning velocity ratio increases as the turbulent intensity is increased for all cases. More interestingly, in most of the cases where smaller particle range is used ($d_{st} = 75-90 \mu m$), as the dust concentration is increased to 75 g/m^3 , at a given intensity, the ratio of turbulent to laminar flame velocity is seen to increase significantly. This is primarily due to the effect of an increase in the

turbulence level due to the interaction of smaller sized particles, which also increases with increased number of particles present at higher concentrations [14]. This enhances the overall heat and mass transfer in the small sized particles and as a result, the burning velocity increases. While the increasing trend is observed for all three equivalence ratios tested, it is highest for the fuel lean cases since there is also an increase in the local equivalence ratio as discussed below.

For a fixed planar flame, sustained by an isotropic turbulent flow of a combustible mixture with a constant c_p , the Favre-averaged one dimensional energy equation is given by [4]:

$$\frac{d^2\bar{T}}{dx^2} + \frac{\bar{\rho}c_p S_L}{l_0 u'_{rms}} \frac{d\bar{T}}{dx} = 0, \quad (4.20)$$

Where, the turbulent thermal conductivity is expressed as the product of the turbulent length scale (l_0) and root mean square of the turbulent velocity fluctuations (u'_{rms}). Equation 4.20 can be solved with the boundary conditions:

$$\begin{aligned} x = 0; \quad T &= T_f \\ x = \infty; \quad T &= T_\infty \end{aligned} \quad (4.21)$$

to obtain,

$$\frac{T - T_\infty}{T_f - T_\infty} = \exp\left(-\frac{\bar{\rho}c_p S_L}{l_0 u'_{rms}} x\right). \quad (4.22)$$

This solution is plotted in Fig. 4.10 to illustrate how the width of the preheat zone depends on the turbulent diffusion of heat into the unburnt mixture ahead of the flame. When the turbulence is intensified, S_L/u'_{rms} decreases and the width of the preheat zone increases. As the preheat zone extends further into the unburnt mixture, the fuel particles are exposed to a higher temperature longer and consequently release more volatiles. This provides an explanation for why the burning velocity increases with the addition of dust particles in the turbulent gas-phase lean case.

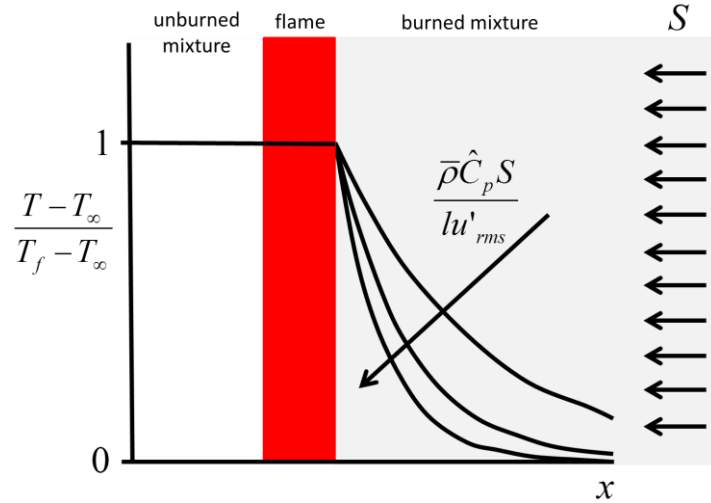


Figure 4.10: The effect of turbulence on the temperature profile in the preheat zone

In the case of higher particle sizes ($d_{st} = 106 - 125 \mu m$), at a given intensity, the injection of the particles either enhances or dissipates the turbulence level. This is also dependent on the size distribution of the particles (mean value of the particle diameter in the injected lot). Therefore, the combined effects of an increase or decrease in the turbulent intensity due to particle injection and the particle size distribution cause a nearly random variation in these cases. However, in this case also, as the intensity is increased, the ratio of turbulent to laminar burning velocity also increases. An increasing trend with concentration of the dust is also observed, however, only at the higher equivalence ratio of 1.2. The influence of concentration on the burning velocity is further analyzed in the next section.

4.2.4 Effect of dust concentration on burning velocity

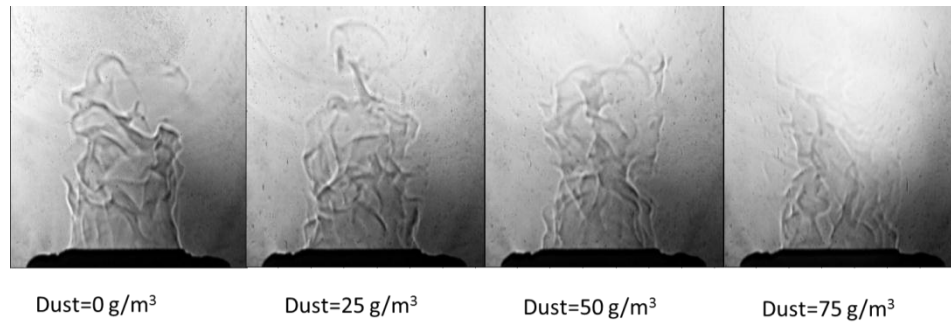


Figure 4.12: Images of turbulent flames at various dust concentrations ($\Phi = 0.8$, $u'_{rms} = 0.185$ m/s and $d_{st} = 75 - 90$ μm)

Figure 4.12 shows sample images over the range of dust concentration used for a lean ($\Phi = 0.8$) conditions. For higher dust concentrations, the shadowgraph intensity is significantly reduced as shown in Fig 4.12 (see image on extreme right). This is mainly because of the increased brightness of the flame due to coal dust particles burning beyond the combustion zone. This reduces the contrast of the shadowgraph image and makes the selection of the flamed edge more difficult at higher dust concentrations.

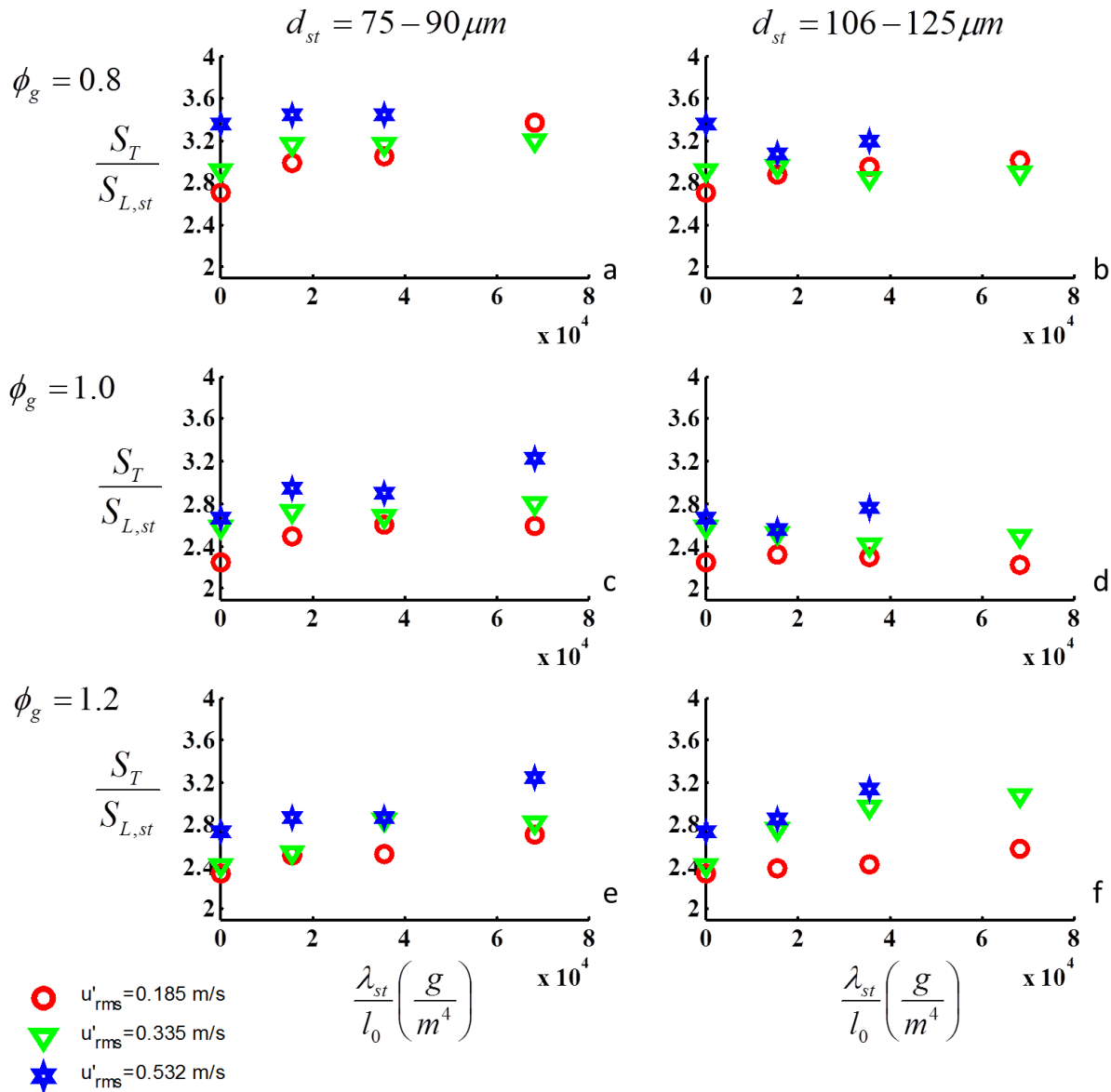


Figure 4.13: Nondimensionalized burning velocity as a function of dust concentration

Figure 4.13 shows the burning velocity with respect to dust concentration while holding turbulent intensity constant. For the smaller particle size ($d_{st} = 75-90 \mu m$) the increase in dust concentration tends to have a varying effect on the burning velocity of the mixture. In the lean case ($\phi_g = 0.8$) the addition of coal dust has a tendency to decrease the burning velocity slightly. This may be due to an increase in the local equivalence ratio from a fuel lean to a fuel rich

condition at higher concentrations and turbulent intensities. In fact, it can be noted that at the highest dust concentration ($\lambda_{st} = 75 \text{ g/m}^3$) and turbulent intensities, the burning velocity for all three equivalence ratios is approximately constant (~ 3.2). A similar trend is also observed with larger particle size range used ($d_{st} = 106 - 120 \text{ }\mu\text{m}$). This result shows that it may be possible that at sufficiently high turbulent intensities, the burning behavior becomes independent of the chemistry of the gas flame but is controlled only by the size and concentration of the dust particles in the flame. The smaller the particles the higher the burning velocity. For the stoichiometric case ($\phi_g = 1.0$) the increase in dust concentration shows a minimal effect on the burning velocity, except for the high turbulent intensity which is slightly increased at the high dust concentration. For the rich case ($\phi_g = 1.2$), the increase in particle concentration also shows minimal effects except for the highest turbulent intensity which is slightly increases.

For the large particle size ($d_{st} = 106 - 125 \text{ }\mu\text{m}$), the effect of the increase in particle loading is more distinct. In the lean case ($\phi_g = 0.8$), the increase in concentration causes a distinct decrease in the burning velocity. For the stoichiometric case ($\phi_g = 1.0$), the burning velocity also causes a decrease in the burning velocity as the concentration is increased but to a lesser extent than for the lean case. For the rich case ($\phi_g = 1.2$), there is no significant effect of on the burning velocity as the dust concentration is increased for the low turbulent intensity but a slight increase for the high turbulent intensity.

4.3 Correlation of turbulent burning velocity

Figure 4.14 shows the turbulent burning velocity versus the turbulent intensity. Using Eq. 4.19, discussed in section 4.2.1,

$$\frac{S_{T,st}}{S_{L,st}} = 1 + C \left(\frac{u'_{rms}}{S_{L,st}} \right)^n, \quad (4.23)$$

two sets of C and n parameters are found based on fuel lean or rich conditions. For gas-phase equivalence ratios less than one the best fit is observed for $C = 2.2$, $n = 0.2$, and equivalence ratios greater than one, $C = 1.7$, $n = 0.2$. Two values of C are used because the volatiles release by the dust in the lean phase boost the burning velocity more than with higher equivalence ratios.

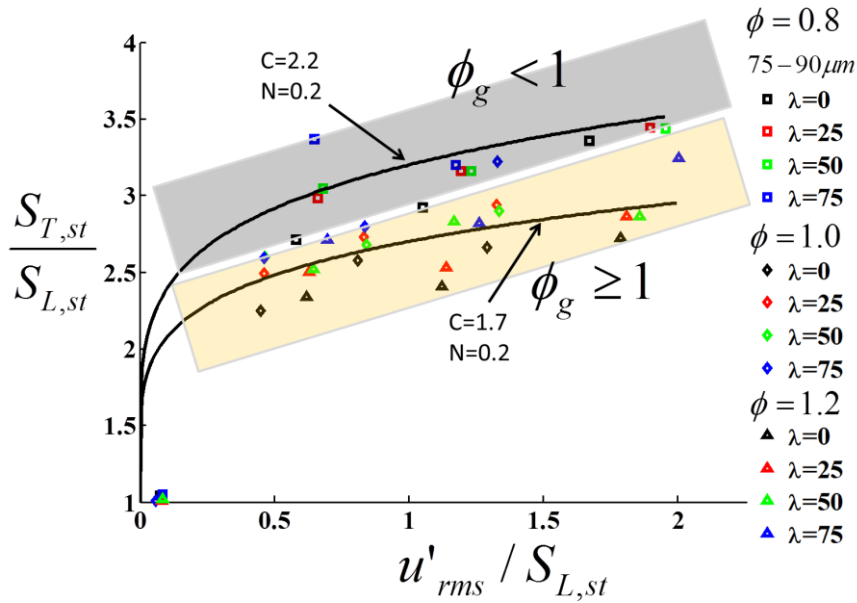


Figure 4.14: Correlation for turbulent burning velocity of hybrid flames.

A similar plot can also be generated for the larger particle size range tested ($d_{st} = 106 - 125 \mu m$) and is shown in Fig. 4.15. In this case, $C = 2.0$ (fuel lean) and $C = 1.65$ (fuel rich) while the exponent n remains the same ($n = 0.2$). Thus, when particle size range increases a similar trend is observed, although the percentage change in the value of C between fuel lean and fuel rich conditions is smaller when compared to the smaller particle size ranges. This is mainly due to the decrease in the pyrolysis rate of coal dust particles with an increase in diameter.

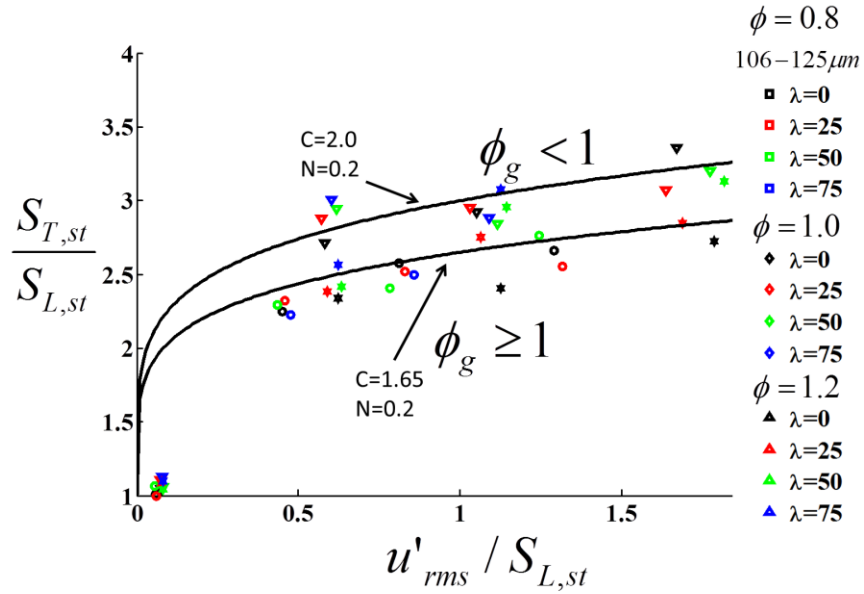


Figure 4.15: Correlations for turbulent burning velocity of hybrid flames.

$$d_{st} = 106 - 125 \mu m$$

The modeling coefficients from Fig. 4.5, 4.14, and 4.15 are listed in table 4.1.

Table 4.1: Modeling coefficients

d_{st}	ϕ	C	n
Gas only	1	1.6	0.3
75-90	<1	2.2	0.2
	≥ 1	1.7	0.2
106-125	<1	2.0	0.2
	≥ 1	1.65	0.2

It is shown that the C coefficient (which includes the turbulence effects) is increasing with the addition of dust; this change is highest in the lean cases when the local equivalence ratio is increased by the addition of fuel vapor from the dust. The n coefficient (known as the bending

coefficient) is lower for the experiments involving dust. This means that due to the influence of the dust particles the burning velocity is not leveling off as much as the pure gas case the turbulent intensity is increased

References

1. Xie, Y., V. Raghavan, and A.S. Rangwala, *Study of interaction of entrained coal dust particles in lean methane-air premixed flames*. Combust. Flame, 2012. **159**: p. 2449-2456.
2. Kobayashi, H., T. Tamura, K. Maruta, T. Niioka, and F.A. Williams, *Burning Velocity of Turbulent Premixed flames in a high Pressure Environment*. Proc. Combust. Inst., 1996. **26**: p. 389-396.
3. Grover, J.H., E.n. Fales, and A.C. Scurlock, Proc. Combust. Inst., 1963. **9**: p. 21-35.
4. Dahoe, A., *Dust Explosions: a Study of Flame Propagation*, in *Applied Sciences*. 2000, Delft University of Technology. p. 298.
5. Damkohler, G., *NACA Tech. Memo 1112*. 1947, National Advisory Committee for Aeronautics: Washington.
6. Schelkin, K.I., *On combustion in a turbulent flow*, *NACA Tech. Memo 1110*. 1947, National Advisory Committee for Aeronautics: Washington.
7. Karlovitz, B., D.W. Denniston, and F.E. Wells, *Investigation of turbulent flames*. Journal of Chemical Physics, 1951. **19**(5): p. 541-547.
8. Taylor, G.I., *Diffusion by continuous movements*. Proceedings of the Royal Society of London. Series A, Mathematical and Physical Sciences, 1921. **20**: p. 196-212.
9. Glassman, I., *Combustion*. 1996: Academic Press San Diego, Calif.
10. Turns, S.R., *An Introduction to Combustion: Concepts and Applications*. 2000, New York: McGraw Hill.
11. Peters, N., *Laminar flamelet concepts in turbulent combustion*. Proc. Combust. Inst., 1986. **21**: p. 1231-1250.
12. Crowe, C., M. Sommerfeld, and Y. Tsuji, *Multiphase Flows with Droplets and Particles*. 1998, Boston: CRC Press.
13. Gore, R.A. and C.T. Crowe, *The effect of particle size on modulating turbulent intensity*. Intl. J. Multiphase Flow, 1989. **15**: p. 279.
14. Crowe, C.T., *On models for turbulence modulation in fluid-particle flows*. International Journal of Multiphase Flow, 2000. **26**: p. 719-727.
15. Rockwell, S.R. and A.S. Rangwala, *Effect of Coal Particles on Turbulent Burning Velocity of Methane-Air Premixed Flames*, in *Technical Meeting of the Eastern States Section of the Combustion Institute*. 2011: Storrs, CT.
16. Bradley, B., *How Fast Can We Burn*. Proc. Combust. Inst., 1992. **24**: p. 247-262.
17. Arntzen, B.J., *Modelling of turbulence and combustion for simulation of gas explosions in complex geometries*, in *Applied Mechanics, Thermodynamics and Fluid Dynamics*. 1998, Norwegian University of Science and Technology.
18. Wingerden, V., B.J. Arntzen, and P. Kosinski, *Modelling of dust explosions*. VDI-Berichte, 2001. **1601**: p. 411.
19. Agreda, A.G., *Study of Hybrid Mixture Explosions*, in *Chemical Engineering*. 2003, Degli Studi di Napoli Federico II.
20. Liu, Y., J. Sun, and D. Chen, *Flame Propagation in Hybrid Mixture of Coal Dust and Methane*. Journal of Loss Prevention in the Process Industries, 2007. **20**: p. 691-697.

21. Chen, D.L., J.H. Sun, Q.S. Wang, and Y. Liu, *Combustion Behaviors and Flame Structure of Methane/Coal Dust Hybrid in a Vertical Rectangle Chamber*. *Combust. Sci. and Tech.*, 2008. **180**: p. 1518-1528.

5. Conclusions and recommendations

Using a combination of experimental methods found in the literature a new apparatus called the Hybrid Flame Analyzer (HFA) is designed, constructed, and used to study the effects of coal dust on the burning velocity of CH₄-air flames as a function of particle size, particle concentration, turbulent intensity, and gas phase equivalence ratio. The burning velocity of the premixed section of the turbulent flames was calculated using the “area method” as found in the literature. The turbulent flow was characterized and shown to fall in the laminar-flamelet regime of the Borghi diagram. The main conclusions based on the experiments are:

1. The turbulent burning velocity is more than two-times larger than the laminar counterpart for each and every case studied. The turbulent to laminar burning velocity ratio increases as the turbulent intensity is increased for all cases.
2. The ratio of turbulent to laminar flame velocity is seen to increase significantly as particle size decreases and dust concentration increases. This is primarily due to the effect of an increase in the turbulence level due to the interaction of smaller sized particles, which also increases with increased number of particles present at higher concentrations.
3. While the increasing trend is observed for all three equivalence ratios tested, it is highest for the fuel lean cases since there is also an increase in the local equivalence ratio.
4. An empirical correlation of the form $\frac{S_{T,st}}{S_{L,st}} = 1 + C \left(\frac{u'_{rms}}{S_{L,st}} \right)^n$ can be used to correlate the experimental data where C & n are functions of the gas phase equivalence ratio, integral length scale and particle size. This relatively crude model is used for the current data to provide a mathematical representation of the trends. Once more testing is done as discussed below a more precise model can be developed.

The author would like to provide a number of recommendations for the continued use of the HFA. First off it is important to show that the instrument can produce reproducible measurements. To do this and produce more data tests could be done at more frequent dust concentrations with the same flow conditions used in this work. The data should fall on the same line. The overall purpose of this work is to help provide industry with a new tool for designing protection systems therefore results from these tests should be compared with large scale explosion experiments to show that the data from the lab scale experiments can be correlated to the large scale explosions. Once the lab scale is shown to match with the full scale, the HFA experimental results should be coupled to industry in two ways. First the empirical models provided through the experimentation should be used in future modeling programs such as DESC [1]. Second, the turbulent burning velocity should be tied into structure vent design as it is tied to K_{st} currently in the design codes and standards [2].

After confidence has been established in this new apparatus and repeatability shown a variety of dust types should be tested such as steel and other metal dusts along with cellulose based dusts like those found the food processing industry. While varying the types of dust the effect of inert particles should be examined which would help explain the effects of the coal dust used in this work. Suppressants should also be added to the flow stream to see what their effects are on the turbulent hybrid flame. The dust concentration should be varied; the range can be increased by changing the size of the helix in the dust feeder. Different dust sizes should be tested, a new helix will be required for the small dusts as they will not feed through the current design. The effect of the integral length scale should be examined next. To do this the author recommends

matching turbulent intensity values with different perforated plates thereby decoupling the effect of the length scale with the turbulent intensity.

Radiations effects should be examined using this apparatus as-well. It is known that radiation plays a much larger role in dust flame than gas flames though this was not discussed in this work. Information about both the fundamental combustion behavior and the risk of flash fires involving condense phase fuels should be studied. This while all of these tasks are important building confidence in the apparatus to show that the measurements are applicable to use in industry and thus a benefit to the fire field is most important.

Several modifications to the HFA are also proposed. The author recommends adding an emergency shutoff switch which will turn off the electronics and the gas flow in the event of a situation in which the user needs to leave the area rapidly. The methane being used is lab grade 99.9% pure and therefore has no odorant; therefor a methane detector should be added to the laboratory area so that any potential leaks can be detected. A nitrogen purge should be added to the exhaust system due to the possibility of a fire caused by a build of coal particles. And lastly an automated image analysis program would significantly speed up the data analysis process.

1. Skjold, T., *Review of the DESC project*. Journal of the Loss Prevention in the Process Industries, 2007. **20**: p. 291-302.
2. *ISO 6184-1 Explosion Protection Systems - Part 1: Determination of explosion indices of combustible dusts in air*. International Organization for Standardization (ISO). 1985.

Appendix 1: Parameters quantifying the hazard associated with a dust

	Name of Parameter (symbol, units)	Description	Established Test Methods or Apparatus*
Thermodynamic Parameters			
1	Heat of combustion (J/g)	Amount of energy released per unit mass undergoing a combustion reaction	Bomb calorimeter
2	Combustion efficiency	Fraction of energy that is utilized in pressure build up	Law of Conservation of Energy
3	Radiant heat fraction	Fraction of total heat released that is transferred via radiation mode	Radiant flux measurements
4	Latent heat of vaporization (J/g)	Amount of heat required to vaporize a unit mass of fuel	Differential Scanning Calorimeter
5	Adiabatic flame temperature (°C)	Maximum possible temperature achieved by the combustion reaction in a constant pressure process	Theoretical Calculations
6	Specific heat of dust (J/g-K)	Amount of energy required per unit mass of dust to increase the temperature of the dust by one unit	Differential Scanning Calorimeter
Thermo-kinetic Parameters			
7	Laminar burning velocity (m/s)	Velocity at which unburned gases move through a combustion front in the direction normal to the front surface	None
8	Propagation speed of smoldering reaction front (m/s)	Rate at which an exothermic oxidation reaction front moves in the direction of non-reactive zone of a dust layer	
9	Rate of reaction in the gas phase (g/s)	Rate at which the reactant gas concentration depletes	
10	Rate of reaction in the solid phase (surface chemical reaction rate) (g/s)	Identifies the smoldering combustion of a dust layer. Smoldering layers can release combustible vapors such as CO, CH ₄ , which can lead to a gas deflagration	
11	Maximum closed volume deflagration pressure (bar)	Maximum pressure reached during a dust deflagration for the optimum concentration of the dust cloud	ASTM E1226
12	Maximum closed volume rate of pressure rise (bar/s)	Rate of pressure rise at maximum pressure reached during a dust deflagration for the optimum concentration of the dust cloud	ASTM E1226
13	Deflagration index, (K _{St}) (bar-m/s)	Rate of pressure rise at maximum pressure during a dust deflagration normalized to unit volume	ASTM E1226
14	Minimum explosion concentration (MEC) (g/m ³)	Minimum concentration of a combustible dust cloud sufficient to increase the pressure by 1 atmosphere (14.7 psi or 1.01bar) due to deflagration. Dust assumed to be well dispersed in air.	ASTM E 1515
15	Minimum ignition energy (MIE) (mJ)	Minimum energy sufficient to ignite most easily ignitable concentration of fuel in air	ASTM E 2019
16	Autoignition temperature of layer (°C)	Lowest set temperature of the surface at which dust layer on it will ignite spontaneously	ASTM E 2021
17	Autoignition temperature of cloud (°C)	Minimum temperature at which a dust cloud will self ignite	ASTM E 1491 06 (Godbert Greenwald Furnace Test)
18	Limiting oxygen	Minimum oxygen concentration at the limit of	ASTM E 2079

	concentration (LOC)	flammability for the worst case (most flammable) fuel concentration	
Physical Parameters			
19	Thermal conductivity of dust (W/m°C)	Amount of heat transmitted through a unit thickness in a direction normal to a surface of unit area caused due to a unit temperature gradient	
20	Mass of combustible particulate solid (g)	Typically a fugitive dust layer can contain inerts which are not combustible. This property accounts for this variable	
21	Particle shape	Quantitatively, shape factors and coefficients are used as parameters in equations governed by particle shape	Pattern recognition techniques
22	Particle size (m)	Characteristic dimension of irregularly shaped particle representing the diameter of equivalent sphere	Image Analysis with Microscope
23	Particle size distribution	Statistical term that quantifies fluctuations in size and shape of particles of given dust sample	ASTM B761 - 06
24	Bulk density (g/cm ³)	Weight of dust per unit volume	
25	Porosity	Measure of difference in densities of dust bulk and dust particle because of void spaces between particles in the bulk	
26	Degree of compaction of powder	Ratio of volume under specified pressure to volume under ambient pressure for a given mass of dust and configuration of dust pile	
27	Moisture content in dust	Weight percentage of water content in given dust sample	
28	Layer thickness (mm)	Minimum thickness of dust layer of a give particle size needed to cause a deflagration	
29	Surface area/volume ratio of dust (1/m)	Ratio of surface area to volume of given dust particles can be used to relate the arbitrary particle shapes to standard shapes like cube, sphere, cylinder etc.	
30	Suspension	Ease with which particles can be suspended in air	
31	Dispersibility	Degree of dispersion in a dust cloud, depends on cohesiveness of particles, settling velocity, moisture content	ASTM E 1945
32	Agglomeration	A mass conserving, number-reducing process that shifts the particle size distribution towards larger sizes	
33	Terminal settling velocity of dust particle (m/s)	Velocity of a particle when the drag force and buoyancy force balance equal the gravitational pull	
34	Speed of sound in dust cloud (m/s)	Plays an important role in all compressible flow phenomena	
Chemical Parameters			
35	Chemical composition	Molecular formula of the sample gives important information like Molecular Weight, acidic or basic nature, special affinity for other chemicals	
36	Reactivity with water		
Electrical Parameters			
37	Volume resistivity	Measure of electrostatic ignition hazard of the dust	IEC 60093
38	Charge relaxation time	Time duration of charge retention in a dust	IEC 61340-2-1:2000
39	Chargeability	Propensity of dust particles to become charged when flowing or air-bourn	IEC 61340-2-1:2000
External Parameters (facility related)			
40	Size of partial volume explosion that can be handled by the construction	This factor will depend on construction type, volume of initial cloud that can be formed, number of vents installed, and nature of dust	

41	Type of construction	Based on NFPA 220 standard on types of building construction	
42	Room volume (m ³)	Total volume of room/enclosure where fugitive dust accumulation is possible	
43	Operating temperature (°C)	Certain facilities could operate at a temperature higher than ambient. Thus possibility of autoignition is higher.	
44	Operating pressure (bar)	Certain facilities can operate at pressures other than atmospheric. Studies have shown that thermodynamic and thermo-kinetic properties vary with pressure.	
45	Relative humidity	Major of quantity of water vapor in ambient air	
46	Confinement	Dimensions of the enclosure which is considered to be at constant temperature and pressure and surrounds given test apparatus or control volume under consideration	
47	Turbulence	Flow-instability represented by chaotic state of fluid motion with dissipative structure	Reynolds number
48	Detonability limit	Condition outside which self-sustained propagation of detonation wave cannot be realized	

* Test methods starting with ASTM and IEC are standard test methods (Some standard test methods are not designed for dust per se but can be easily modified to include dust samples)

- i. ASTM B761 – 06: Standard Test Method for Particle Size Distribution of Metal Powders and Related Compounds by X-ray Monitoring of Gravity Sedimentation
- ii. ASTM E 1226 - 05: Standard Test Method for Pressure and Rate of Pressure Rise for Combustible Dust
- iii. ASTM E 1491 – 06: Standard Test Method for Minimum Autoignition Temperature of Dust Clouds
- iv. ASTM 1515 – 07: Standard Test Method for Minimum Explosible Concentration of Combustible Dusts
- v. ASTM E 1945 – 02(2008): Standard test Method for Percent Dispersibility
- vi. ASTM E 2019 – 03(2007): Standard Test Method for Minimum Ignition Energy of a Dust Cloud in Air
- vii. ASTM E 2021 – 06: Standard Test Method for Hot-Surface Ignition Temperature of Dust Layers
- viii. ASTM E 2079 – 07: Standard Test Methods for Limiting Oxygen (oxidant) Concentration in Gases and Vapors
- ix. IEC 60093: Methods of test for volume resistivity and surface resistivity of solid electrical insulating materials
- x. IEC 61340-2-1 (2002-06): Measurement methods – Ability of materials and products to dissipate static electric charge
- xi. IEC 61340-2-2 (2000-067): Measurements methods – Measurement of chargeability

Appendix 2: HFA User's Manual

Hybrid Flame Analyzer (HFA)

User's Manual - v01

Last revised 2012

Combustion Lab

Salsbury Lab 214

Worcester Polytechnic Institute

Worcester, MA 01609

Potential Dangers of this instrument:

Glass breaking

Electrical shock

Burning

Respiratory Irritation

Explosion

Suffocation

Instructional videos:

15 instructional videos were made to help students learn how to use the HFA. These are available at www.firesciencetools.com on the hybrid flame analyzer page.

16. Hybrid Flame Analyzer startup sequence
17. Hybrid Flame Analyzer shutdown sequence
18. Running laminar flame tests
19. Electrical system for Hybrid Flame Analyzer
20. Exhaust system for Hybrid Flame Analyzer
21. Fuel control system for Hybrid Flame Analyzer
22. Water cooling system for Hybrid Flame Analyzer
23. Building Annular/Ring Pilot Flame for Turbulent Burner - Hybrid Flame Analyzer
24. Simple shadowgraph design description - Hybrid Flame Analyzer
25. Gas analysis for combustion system - Hybrid Flame Analyzer
26. How to use mass flow controllers - Hybrid Flame Analyzer
27. Changing perforated plate in Hybrid Flame Analyzer
28. Calibrating volumetric dust feeder - Hybrid Flame Analyzer
29. Setting up hot wire anemometer for Hybrid Flame Analyzer
30. Checking hotwire anemometer voltage for Hybrid Flame Analyzer

Recommended Personal Protective Equipment (PPE)

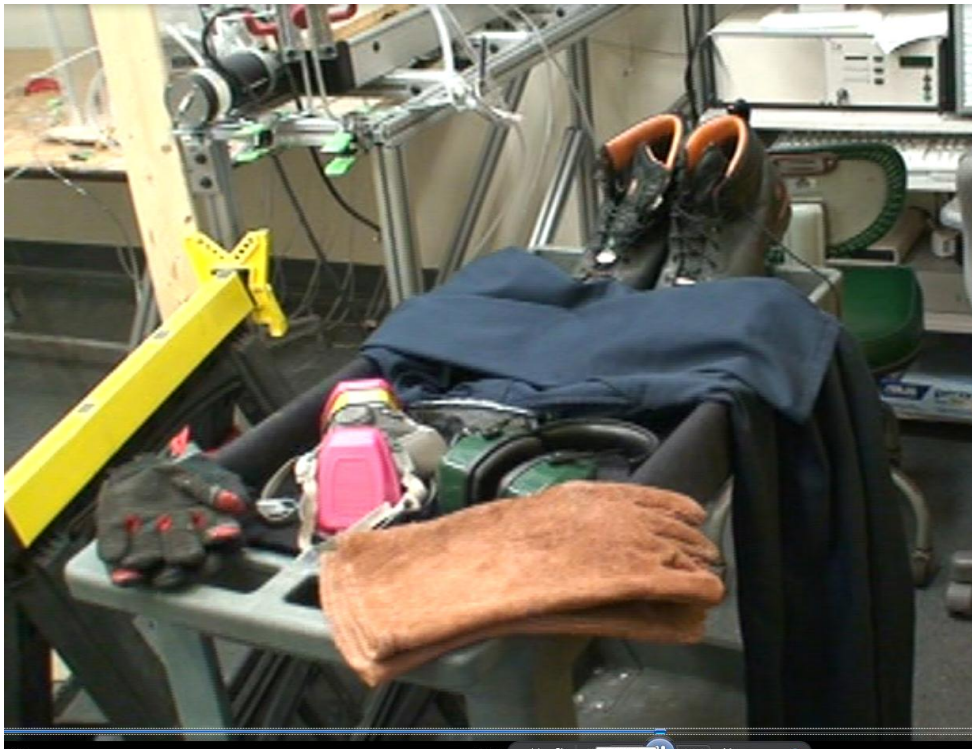
Gloves

Safety Glasses

Lab Coat

Respirator / dust mask

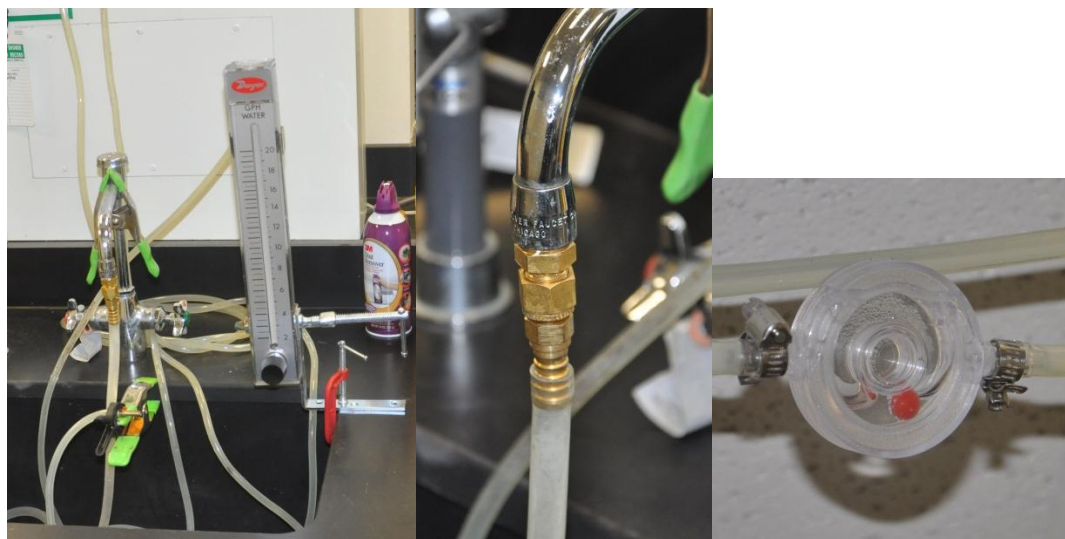
Steel toed boots



Turning on HFA:

Start water cooling - ~10 lph (to much more will rupture water cooling fittings)

The water is controlled using the sink taps. Rotate the knob toward the sink to turn the water on and away from you to turn the water off. It does not need to be turned very far ($<1/8$ turn) to get the recommended flow. The flowmeter clamped to the sink will show the flow going through the tubing, the stainless steel valve can be used to control the flow but it is recommended to use the sink knob itself to avoid building up pressure in the line between the sink and the flowmeter inlet. There is a clear plastic water flow indicator (as shown below). When the red ball is turning it is easy to see the water is flowing without having to look at the flowmeter. Between the output of the flowmeter and the burner nozzle there is a section of $1/8$ " copper tubing as shown below. This is used to keep any potential pressure buildup in the system in the sink area rather than at the nozzle to avoid water leaks un the on the apparatus itself.



Plug in

Black chord for battery power strip

Black chord for mass flow controllers

The HFA has two different power strips to provide power, one is located on the 2nd shelf, the other is located on the lab bench behind the computer.



Turn on exhaust fan

Turn on cooling fan for shadowgraph light point source

Turn on Camera power

Turn on heat sink (if using gas analysis) – it will require time to reach steady state temperature

For ease of use the power for these parts of the experiment are routed through a set of switches (as shown below).



Turn on computer

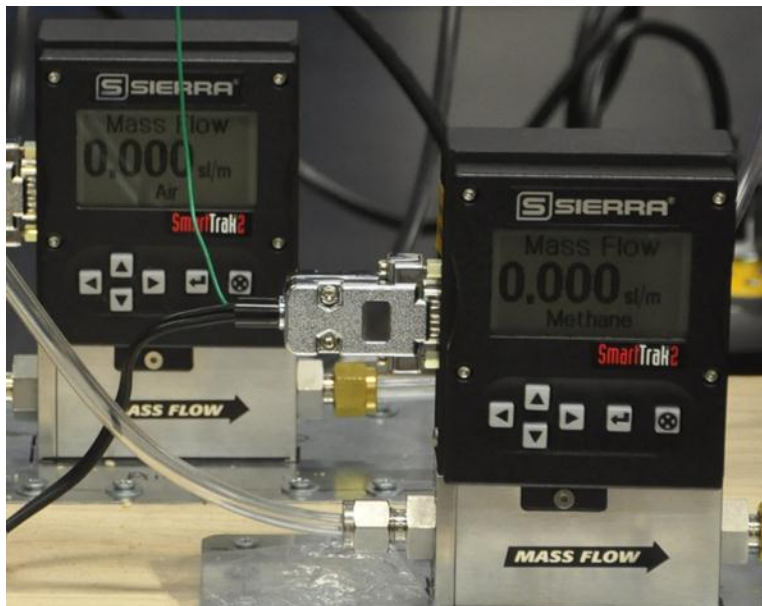
Plug in timing hub usb port

Plug in gas analyzer USB port

Turn off driver for the assumed mouse (if needed)

Start hyperterminal

Turn on Mass flow controllers (allow 15 min to warm up)



Turn on gas bottle valves valves

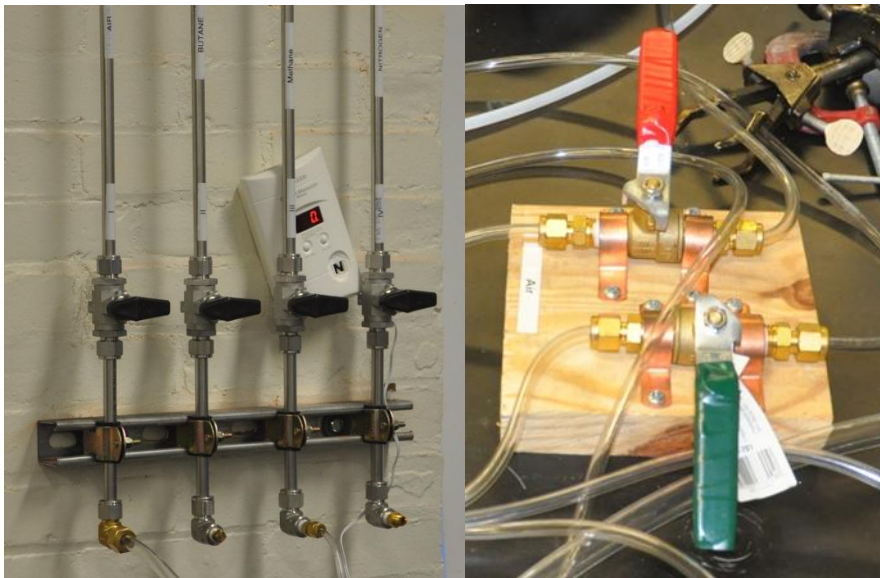
Air – set to 25psi and open shutoff valve all the way

Methane – 10 psi

Oxygen – 10 psi



Open valve chain (SS valve, splitting valve)



Gas analyzer is usually left on



Calibration:

Gas Analyzer:

Nitrogen for zero

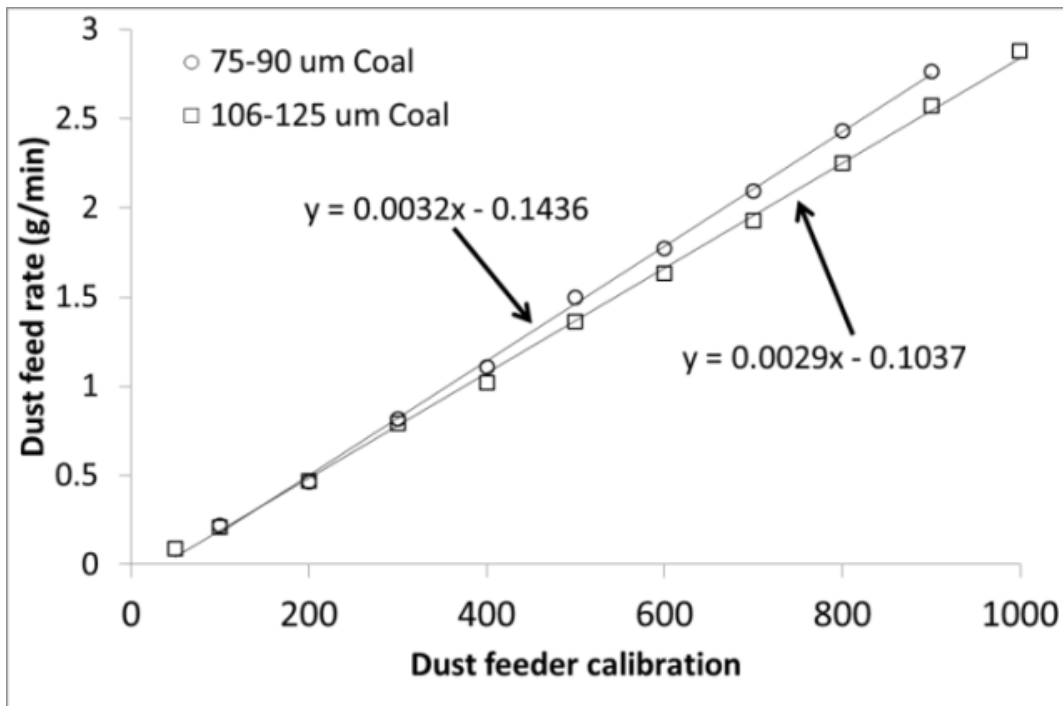
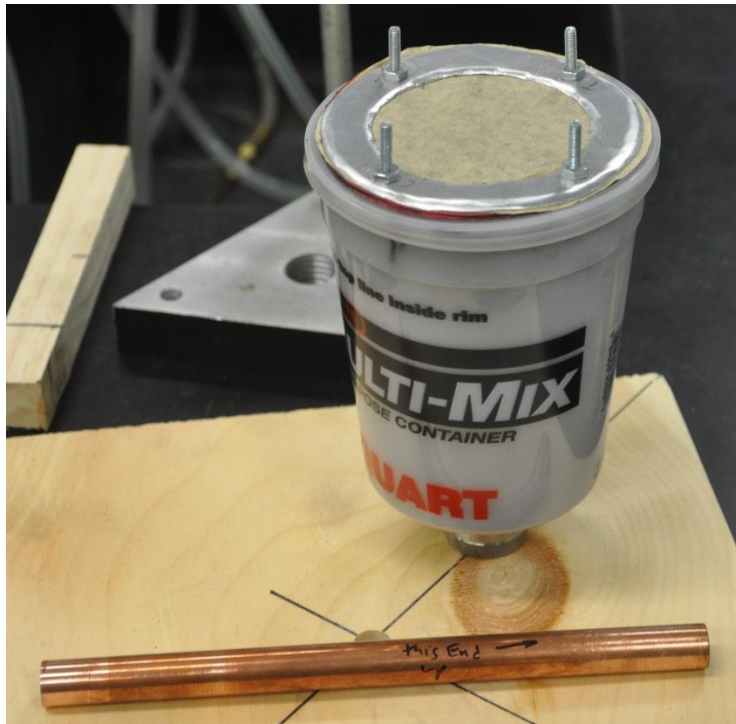
Specialized tanks for various analyzer

Depending on the analyzer the gas sensors need to be calibrated once a day to once a week. See the gas analyzer users manual for instructions on how to do the calibration. The calibration gasses should be tied into the sample line before the heat sink so that the calibration gas goes through the same processing as the sample gas.

Dust Feeder:

A filter topped hopper was built to catch the dust out of the burner after a 1 minute run. Using flow rate of 10 lpm, and running the hopper for 1 minute at every 100 counts a curve fit is made of the dust feeder output.

To do the calibration the burner nozzles need to be replaced with the copper tube shown below, one end of it has been sanded down so that it easily fits into the filter assembly shown below. Run the test for 1 minute, take the dust catch housing off and weight it. Repeat for the full range of the feeder. Two calibration curves are shown below.



Things to check:

Gas bottle levels

- When running a large number of tests it is more efficient to keep more than 1 bottle of air in the lab at one time.

Filter levels

- Acid filter should be changed periodically, it does not have an indicator
- The desiccant should be changed when it turns purple. The absorbed water can be removed using an oven, there is one in the fire lab.
-



Dust hopper level – make sure there is enough dust in the feeder to run tests

Camera memory level – empty before test

The exhaust duct should be vacuumed out periodically to prevent the buildup of dust particles and ash.

Shadowgraph alignment

Water catch shown above, make sure it is empty.

Starting/Running test:

Camera settings:

- Shutter speed=1/8000
- Fstop=2.8
- ISO=800

Align shadowgraph

Install perforate plate and set in desired position

Set mass flow controllers to desired flow rate

Turn on Combustion chamber makeup air (30 lpm)

Turn on methane for pilot (200 cc/min reading on flow meter)

Ignite with spark

Turn on oxygen for pilot (700 cc/min reading on flow meter)

Allow pilot to reach steady state, there will be a distinct high pitch sound

Turn on central burner air

Turn on central burner methane

Turn on Dust

Turn on shadowgraph light

Take 100 pictures (35 seconds using the remote and holding down the large button)

Turn off Dust

Turn off Shadowgraph light

Turn off Central burner methane

Turn off Central burner air

Turn off pilot oxygen and wait for diffusion flame to form

Turn off pilot methane

Briefly turn on main burner air to blow out pilot flame

Wait for picture to copy to compact flash disk in camera

Create new folder on computer with test details

Copy images to folder

Delete images on compact flash disk

Put disk back in camera

Change dust setting

Repeat as needed

Start flowing air through burner and pilot gasses, ignite pilot gasses with spark,
adjust pilot gasses as desired

Start methane flowing at desired rate using mass flow controller

Take the desired number of pictures

Run long enough to get gas analysis data

Set dust feeder settings

Start dust feeder

Take desired number of pictures

Collecting gas analysis data:

Turn on colt trap (orange covered switch)

Turn on Hyperterminal software

Turn off driver for mouse (computer thinks 232 usb adapter is a mouse)

Windows button → drivers & printers → gigaware USB to serial cable (com5) → right click → properties → hardware tab → disable mouse or driver (if I remember right)

Com5

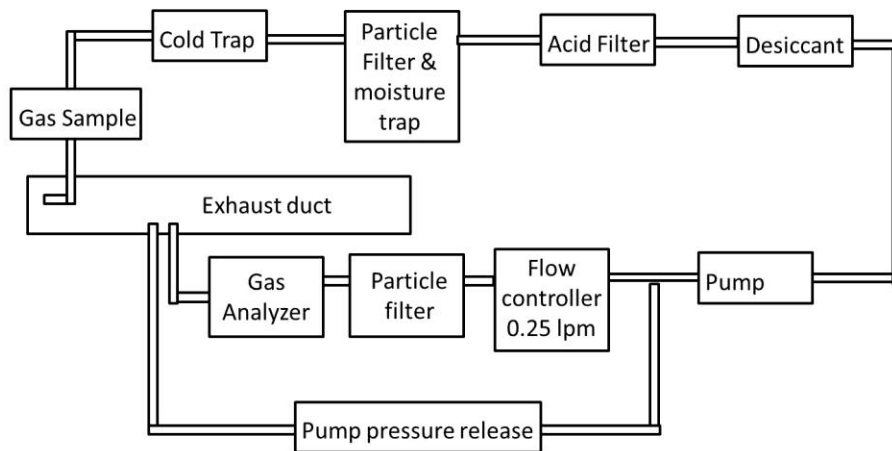
Baud rate 9600, no bias, continuous output (also settings for servomex 4000)

You want to collect hyperterminal data as the experiment occurs use:

Transfer → capture text → name file → stop when done with test

There is approximately a 30 second delay in the gas analyzer measurement

Data is recorded at 1 Hz.



The gas analyzer is connected to the computer using a RS232 extension cable, RS232 to usb adapter and USB adapter extinction cable. This cable is run up and over along the drop ceiling to prevent it from being walked on.

ASTM standards E2058 (for FPA) and E1354 (for Cone Calorimeter) describe the use of gas analyzers and the equations involved.

It is to be noted that the gas analyzer measures a percentage of the selected gas in the exhaust duct. The flow rate in the duct needs to be known to be able to use a percentage. This could be accomplished by adding a bi-directional probe inside the duct. The vane anemometer and hot wire anemometer will be compromised by the as from the coal particles.

The T-connection after the pump releases excess pressure from the pump, if this pressure is not released the gas reading takes about 10 minutes to change.

Currently the gas analyzer is the only part of the analyzer set up for use, due to the high uncertainty in the CO and CO₂. The lab does not currently have gas tanks to calibrate these.

Turning off Experiment:

Make sure all flames are extinguished

Change set point of mass flow controllers to zero

Open combustion chamber

Vacuum combustion chamber clean

Wipe of lens and glass of shadowgraph with lens cleaning wipes

Bleed gas lines

- Turn off gas bottle top valves
- Bleed out gas lines
 - o Methane
 - o Air
 - o Oxygen (do not bleed methane and oxygen into combustion chamber together)
- Close pressure regulator valve
- Close shutoff valve
- Close valves between

Unplug electronics

- Main power strip on instruments
- Power supply for mass flow controllers
-

Check and empty moisture trap if gas analysis was done

Turn off water cooling

Check to make sure there is no combustion in the exhaust hood

MATLAB Scripts

There are several MATLAB scripts created for use with the HFA:

- Image Analysis – pixel point only
- Area of flame based on pixel data
- Turbulent Intensity
- Gas Analyzer data from Hyperterminal

These are shown in Appendix 3

Using Hotwire Anemometer:

For the setup of the hotwire anemometer a video was made.

Naming convention has two parts. In the MiniCTA software, when data is collected, experiments are named:

#_##_#_##_

Where from left to right the numbers correspond to the perforated plate hole size in mm, the flow rate in lpm, the perforate plate position (1-6, one on top), and the height above the burner in cm.

When the data is exported the naming convention is:

YYMMDD_##mm_##lpm_#pos_#cm_###kHz_##sec_S

Where from left to right the numbers correspond to the date, hole diameter, flow rate, perforate plate position, anemometer location above the burner in cm, sampling rate, number of samples of data collection, and the S stands for the smaller anemometer which was the only one not broken at the time this was written.

The probe used is a 55P11, on the bottle the following data was on the bottle:

R20=3.80 ohms

R2=0.5 ohms

Alpha20=0.36%/degC

$R=R_{tot} + \alpha_{20} * R_{20} * (T_{sensor} - T_0)$

To use the CTA software:

Install CTA programs and Drivers on the two provided CD's

Run MiniCTA v4.05

Startup → New Database → put in name

When asked to reate new project click yes → put in name

When asked to configure system now click yes → click 1-D probe → pick type of probe (55P11)
→ 1Dsupporters → 1D straight-short(55H20) → cable 4 meter → click save

When asked would you like to setup hardware click yes, I've been leaving the default

I haven't been doing a calibration but maybe I should.

To collect anemometer data using the MiniCTA

At top of the window click Run → run default setup → type in name → click on setup → click on
A/D box → under measurement set "Sampling frequency" and "Number of Samples"

100000 kHz

300000 samples

Click ok for A/D setup

Click ok for define default setup

Click run to start collecting data

Data file will show up in "Database" window

To view data:

Double click file name in database window

In raw data selection click load → close window

Data will load in new window

To export data:

-load data

Click file → export → set name & location → set type to tab delimited (I think) → click save

(you have to do it for each file individually as far as I can tell)

The hot wire is mounted above the burner exit using a ring stand C-clamped to the experiment frame (see video if I forget to include a picture here)

Turbulent intensity calculations are done using a the matlab code below:

Appendix 3: Matlab scripts used in data analysis

Contents

- A1.1 - Edge selection script
- A1.2 - Edge data analysis script
- A1.3 - Laminar data plotting script for figure 4.1
- A1.4 - Data validation script for figure 4.3, 4.5, and 4.10
- A1.5 - Borghi diagram calculations for figure 4.6
- A1.6 - Plotting all data script for figure 4.9
- A1.7 - Plotting turbulent burning velocity vs. turbulent intensity for Fig. 4.11
- A1.8 - Plotting Normalized burning velocity vs. turbulent intensity for Fig. 4.12
- A1.9 - Plotting burning velocity vs. dust concentration for Fig. 4.14
- A1.10 - Fitting theory script
- A1.11 - Creating arrays of test data as a function of dust concentration

- A1.12 - Turbulent intensity calculation
- A1.13 - Gas analysis data retrieval
- A1.14 - plotAverage_noplot

A3.1 - Edge selection script

```
clear all
close all
clc

% dname_save = ('\0mm,pos0,phi=0.8, dst=000=000g_m3, V=10lpm') ;
directory = ('E:\HFA test data\HFA Test Data');
particleSize = ('106-125 micron coal');
experimentSpecs = ('0mm,pos0, V=010lpm');
dataFileName = ('0mm,pos0,phi=0.8, dst=000=000g_m3, V=10lpm');
dname_save = [directory '/' particleSize '/' experimentSpecs '/' dataFileName];
dname = [dname_save 'Original'];%Default Directory To be Opened
matFileName = [particleSize '_' dataFileName] ;

image_start = 1;
image_end = 25 ; % number of pictures to operate on

%% Operating on individual images
top_file = [dname '\'] ; %Set up main database to open and look inside
ls_top_file = ls(top_file) ; %List Files inside main folder
c = cellstr(ls_top_file) ; %Turn cells from ls function into strings
cc = c(3:length(c)) ; %Set up a matrix without the . and .. produces by the
ls function
S = size(cc) ; %Find the size of matrix containing names of files inside
of main database
a = image_start ; %This counter is set to 3 to account for the . and
.. at the beggining of each matrix created by ls
image = image_start ;

ref_width_check = 0 ;
while image <= image_end
    close all
    file = char(cellstr([top_file char(cc(image))])) ; %File to be operated on
    file_name = char(cc(image)) % display file being operated on in command
window

    %%%%%%%%%%%
    % Put code to operate on each file in a folder here

    fileToRead2 = file ;

    imcmp = imread(fileToRead2) ; %[] colour map of imported image
    imcmp = imrotate(imcmp,90); % Rotate image
    image_magnification = 63 ;

    crop =2;
    if crop == 1
        imcmp = imcrop(imcmp,[500 1300 500 850]);
    elseif crop == 2
        imcmp = imcrop(imcmp,[500 1100 750 1050]);
    end

    imcmp=imcmp(:,:,2); % change to blue channel only
```

```

imcmp = imadjust(imcmp);

[size_y size_x spare] = size(imcmp) ;
dname_x_pix_save = [dname_save 'x_pix_save.txt'] ;
dname_y_pix_save = [dname_save 'y_pix_save.txt'] ;

if ref_width_check == 0

x_pix_save = zeros(4,1);
y_pix_save = zeros(4,1);
save(dname_x_pix_save, 'x_pix_save', '-ascii', '-double', '-tabs')
save(dname_y_pix_save, 'y_pix_save', '-ascii', '-double', '-tabs')
% dname_S_T_save = [dname_save '\S_T_save.txt'] ;
% S_T_save(1) = 0 ;
% save(dname_S_T_save, 'S_T_save', '-ascii', '-double', '-tabs')
end
ref_width_check = 1;

% if ref_width_check ~= 0
% scale_coef= load(dname_scale_coef_save)
% end

load(dname_x_pix_save) ;
load(dname_y_pix_save) ;

count_01_max = 1000 ;
count_01 = 1;

figure
axis on
imshow((imcmp),'InitialMagnification', image_magnification)%, 'Border','tight')
axis on

while count_01 < count_01_max
if count_01 > 1
hold on
plot(x_pix, y_pix)
end
end

[x_pix(count_01),y_pix(count_01)] = ginput(1) ; % Grab x and y

hold on
plot(x_pix, y_pix)
if count_01 > 1
if (x_pix(count_01-1) == x_pix(count_01)) && (y_pix(count_01-1) == y_pix(count_01))
break
end
end
end
count_01 = count_01+1 ;
end

dname_image_save = [ dname_save 'edit_' file_name '.jpg'] ;
saveas(gcf, dname_image_save) ;

close all

```

```

% save text data
x_pix = x_pix(1:end-1);
y_pix = y_pix(1:end-1);

if length(x_pix) >= 1
dist_tot(a) = 1;

x_check = x_pix;
y_check = y_pix;
x_pix_save(1:length(x_pix),a) = x_pix ;
y_pix_save(1:length(y_pix),a) = y_pix ;

save(dname_x_pix_save, 'x_pix_save', '-ascii', '-double', '-tabs')
save(dname_y_pix_save, 'y_pix_save', '-ascii', '-double', '-tabs')
clear x_pix y_pix imcmp
save([matFileName '.mat'] )

    a                = a+1                ;
end

image = image+1

end

```

A3.2 - Edge data analysis script

```
% 1 pixel = 15.88mm/368pix = 0.043152mm/pix
```

```
clear all  
close all  
clc
```

```
% Script to operate on all files in a folder  
% dname = ('C:\Users\Public\Documents\WPI research\Hybrid Flame Analyzer (HFA)\Matlab Codes\Edge  
Analysis\EdgeDataAll_35lpm only');%Default Directory To be Opened
```

```
dname = ('C:\Users\Public\Documents\WPI research\Hybrid Flame Analyzer (HFA)\Matlab Codes\Edge  
Analysis\EdgeDataAll_copyNoDustFiles');%Default Directory To be Opened  
pix_to_m = 15.88./368/1000 ; %mm/pix  
u_prime_all = [0.0241 0.1854 0.3352 0.5323] ; % turbulent intensity for 10,30,35,40 lpm  
u_bar = [1.001 3.03 3.53 4.04] ; % flow velocity  
u_prime_williams = [0 0.0993 0.1995 0.3289 0.4593];  
burning_velocity_williams = [0.3394 0.4931 0.7844 1.096 1.2013];  
l_00 = [0.0027 0.0016 0.0014 0.0011];  
D_per_plate= 0.001 ; % [m] diameter of holes in perforate plate  
% l_0 = (u_prime_all./u_bar).*(l_00./D_per_plate);
```

```
% solution method:  
% 1 - average height of flame edge  
% 2 - using plot average function  
% 3 - fitting average line to shape of cone  
sol_method = 2 ;  
plotAll = 1 ; % value =1 will plot figures of all tests
```

```
%% Set up basic file name path to read  
top_file = [dname '\'] ; %Set up main database to open and look inside  
ls_top_file = ls(top_file) ; %List Files inside main folder  
c = cellstr(ls_top_file) ; %Turn cells from ls function into strings  
cc = c(3:length(c)) ; %Set up a matrix without the . and .. produces by the  
ls function  
S = size(cc) ; %Find the size of matrix containing names of files inside  
of main database  
a = 1 ; %This counter is set to 3 to account for the . and .. at the  
beginning of each matrix created by ls  
ct_3 = 1;ct_4 = 1;ct_5 = 1;ct_6 = 1;ct_7 = 1;ct_8 = 1;ct_9 = 1;ct_10 = 1;ct_11 = 1;  
ct_12 = 1;ct_13 = 1;ct_14 = 1;ct_15 = 1;ct_16 = 1;ct_17 = 1;ct_18 = 1;ct_19 = 1;  
ct_20 = 1;ct_21 = 1;ct_22 = 1;ct_23 = 1;ct_24 = 1;ct_25 = 1;ct_26 = 1;
```

```
while a <= S(1)  
close all  
file = char(cellstr([top_file char(cc(a))])) ; %File to be operated on  
data_n = char(cc(a))  
file_name = char(cc(a)) ;  
  
if str2num(file_name(1:2))==75  
flowRate(a) = str2num(file_name(56:57)) ; dust_conc(a) = str2num(file_name(45:47)) ; phi(a) =  
str2num(file_name(32:34)) ; particleSize = 75 ;  
end  
if str2num(file_name(1:3))==106
```

```

    flowRate(a) = str2num(file_name(58:59)) ; dust_conc(a) = str2num(file_name(47:49)) ; phi(a) =
str2num(file_name(34:36)) ; particleSize = 106 ;
end

if flowRate(a)==10;
    u_prime(a) = u_prime_all(1);
elseif flowRate(a) == 30 ;
    u_prime(a) = u_prime_all(2);
elseif flowRate(a) == 35 ;
    u_prime(a) = u_prime_all(3);
elseif flowRate(a) == 40 ;
    u_prime(a) = u_prime_all(4);
end

fileNameLoad = [top_file file_name];
load(fileNameLoad, '-mat', ['x_pix_save']); load(fileNameLoad, '-mat', ['y_pix_save']);

x_non_zero = nonzeros(x_pix_save);
x_plot = x_pix_save - median(x_non_zero);
y_plot = max(max(y_pix_save)) - y_pix_save ;

SS = size(x_plot) ;

if plotAll == 1
    figure1 = figure; axes1 = axes('Parent',figure1,'YDir','reverse'); hold(axes1,'all');
end
ct_1 = 1 ;
while ct_1 <= SS(2)
    x_plot_nz = nonzeros(x_pix_save(:,ct_1));
    y_plot_nz = y_pix_save(1:length(x_plot_nz),ct_1);

    x = x_plot_nz ;
    y = y_plot_nz ;

    x_left_min(ct_1)=x(1);
    x_right_min(ct_1)=x(end);
    y_left_min(ct_1)= y(1);
    y_right_min(ct_1)=y(end);

    count_02 = 1 ;
    while count_02 < length(x)
        point_dist(count_02) = sqrt((x(count_02+1)-x(count_02))^2+(y(count_02+1)-y(count_02))^2) ;
        count_02 = count_02+1;
    end
    dist_tot(ct_1) = sum(point_dist)*pix_to_m;

    if plotAll == 1
        plot(x_plot_nz,y_plot_nz,'g-')
    end
    height(ct_1) = (max(y_plot_nz)-min(y_plot_nz))*pix_to_m ;

    clear x_plot_nz y_plot_nz
    ct_1 = ct_1+1;
end

```

```

if sol_method == 2
    % [avgH, avgData] = plotAverage ;
    % pause(0.5);
    [avgH, avgData] = plotAverage_noPlot ;
    averageData = cell2mat(avgData) ;
    x_aveDataRow = averageData(:,1);
    y_aveDataRow = averageData(:,2);
    % calculate starting position of flames on each side
    x_start_left = mean(x_left_min);
    x_start_right = mean(x_right_min);
    y_start_left = mean(y_left_min);
    y_start_right = mean(y_right_min);

    if y_start_left > y_start_right
        y_start_right = y_start_left;
    end
    if y_start_right > y_start_left
        y_start_left = y_start_right;
    end

    indicies = find(x_aveDataRow > x_start_left & x_aveDataRow < x_start_right) ;
    num_pt_ave = 20 ;

    % Interpolate between average starting point and first average line point
    x_matrix_Left = [x_start_left, x_aveDataRow(indicies(1))];
    y_matrix_Left = [y_start_left, y_aveDataRow(indicies(1))];
    x_int_left = x_start_left : (x_aveDataRow(indicies(1)) - x_start_left) / (num_pt_ave - 1) : x_aveDataRow(indicies(1));
    y_int_left = interp1(x_matrix_Left, y_matrix_Left, x_int_left);

    x_matrix_Right = [x_start_right, x_aveDataRow(indicies(end))];
    y_matrix_Right = [y_start_right, y_aveDataRow(indicies(end))];

    x_int_right = x_aveDataRow(indicies(end)) : (x_start_right - x_aveDataRow(indicies(end))) / (num_pt_ave - 1) : x_start_right;
    y_int_right = interp1(x_matrix_Right, y_matrix_Right, x_int_right);

    x_curve(1:num_pt_ave) = x_int_left ;
    x_curve(num_pt_ave+1:num_pt_ave+length(indicies)) = x_aveDataRow(indicies);
    x_curve(num_pt_ave+length(indicies)+1:2*num_pt_ave+length(indicies)) = x_int_right;
    y_curve(1:num_pt_ave) = y_int_left ;
    y_curve(num_pt_ave+1:num_pt_ave+length(indicies)) = y_aveDataRow(indicies);
    y_curve(num_pt_ave+length(indicies)+1:2*num_pt_ave+length(indicies)) = y_int_right;

    %% Simple Low Pass Filter
    num_pt_ave = num_pt_ave/2 ;
    CCC1 = x_curve;
    CCC2 = y_curve;
    for ii = num_pt_ave+1:length(CCC1)-(num_pt_ave+1)
        CCC_N1(ii) = mean( CCC1(ii-num_pt_ave : ii+num_pt_ave) );
        CCC_N2(ii) = mean( CCC2(ii-num_pt_ave : ii+num_pt_ave) );
    end

    x_curveSmooth(1:num_pt_ave) = x_curve(1:num_pt_ave);
    x_curveSmooth(num_pt_ave+1:length(CCC_N1)) = CCC_N1(num_pt_ave+1:end);
    x_curveSmooth(length(CCC_N1)+1:length(CCC_N1)+num_pt_ave+1) = x_curve(end-num_pt_ave:end);

```

```

y_curveSmooth(1:num_pt_ave) = y_curve(1:num_pt_ave);
y_curveSmooth(num_pt_ave+1:length(CCC_N1))=CCC_N2(num_pt_ave+1:end);
y_curveSmooth(length(CCC_N1)+1:length(CCC_N1)+num_pt_ave+1)=y_curve(end-num_pt_ave:end);

plot(x_curveSmooth,y_curveSmooth,'LineWidth',4)
axis([0 1000 0 1000])

hold off
if a==1
    pause(0.5)

end

end

height_smooth(a) = (max(y_curveSmooth)-min(y_curveSmooth))*pix_to_m;
% height_ave_clicked_lines(a) = mean(height) ;

dist_tot_median(a) = median(dist_tot);
nozzleDiameter = 0.0145 ; %m
nozzleArea = pi()/4*nozzleDiameter^2;
vel_flow(a) = flowRate(a)/(60000*nozzleArea); % [m/s] velocity based on flow rate in tube

volFlow(a) = flowRate(a)/60000;
flame_area(a) = dist_tot_median(a)/2.*pi()/2*nozzleDiameter;
Burning_velocity_ave_length(a) = volFlow(a)/flame_area(a) ;

height_ave(a) = height_smooth(a);
Burning_velocity_ave_height(a) = vel_flow(a)*sin(atan(0.5*nozzleDiameter/height_ave(a)));

Burning_velocity_all_height = vel_flow(a)*sin(atan(0.5*nozzleDiameter./height));
standard_deviation_BV(a)=std(Burning_velocity_all_height);

Burning_velocity(a) = Burning_velocity_ave_height(a);

%%%%%%%%%%%%%%%%%%%%%%%%%%%%%%%%%%%%%%%%%%%%%%%%%%%%%%%%%%%%%%%%%%%%%%%%
particleSizeSave(a) = particleSize;

clear x_curveSmooth y_curveSmooth CCC_N1 CCC_N2 CCC1 CCC2 x y x_plot_nz y_plot_nz
clear avgH avgData x_curve y_curve x_plot_nz y_plot_nz
clear x_non_zero x_plot y_plot x_aveDataRaw y_aveDataRaw indices
clear x_matrix_Left y_matrix_Left x_int_left y_int_left
clear x_matrix_Right y_matrix_Right x_int_right y_int_right
%%
Burn_vel_func_dst_part_szev01 ;
Plot_funct_part_size_01

if phi(a) == 0.8
    if particleSize == 106 && flowRate(a)==10
        if dust_conc(a) == 0
            burn_vel_08_106_00(1) = Burning_velocity(a) ;
            stanDev_BV_08_106_00(1) = standard_deviation_BV(a);
%             height_ave_08_106_00(1,1) = height_ave(a);
            end
            if dust_conc(a) == 25

```

```

burn_vel_08_106_25(1) = Burning_velocity(a) ;
stanDev_BV_08_106_25(1) = standard_deviation_BV(a);
end
if dust_conc(a) == 50
burn_vel_08_106_50(1) = Burning_velocity(a) ;
stanDev_BV_08_106_50(1) = standard_deviation_BV(a);
end
if dust_conc(a) == 75
burn_vel_08_106_75(1) = Burning_velocity(a) ;
stanDev_BV_08_106_75(1) = standard_deviation_BV(a);
end
end
if particleSize == 106 && flowRate(a)==30
if dust_conc(a) == 0
burn_vel_08_106_00(2) = Burning_velocity(a) ;
stanDev_BV_08_106_00(2) = standard_deviation_BV(a);
end
if dust_conc(a) == 25
burn_vel_08_106_25(2) = Burning_velocity(a) ;
stanDev_BV_08_106_25(2) = standard_deviation_BV(a);
end
if dust_conc(a) == 50
burn_vel_08_106_50(2) = Burning_velocity(a) ;
stanDev_BV_08_106_50(2) = standard_deviation_BV(a);
end
if dust_conc(a) == 75
burn_vel_08_106_75(2) = Burning_velocity(a) ;
stanDev_BV_08_106_75(2) = standard_deviation_BV(a);
end
end
if particleSize == 106 && flowRate(a)==35
if dust_conc(a) == 0
burn_vel_08_106_00(3) = Burning_velocity(a) ;
stanDev_BV_08_106_00(3) = standard_deviation_BV(a);
end
if dust_conc(a) == 25
burn_vel_08_106_25(3) = Burning_velocity(a) ;
stanDev_BV_08_106_25(3) = standard_deviation_BV(a);
end
if dust_conc(a) == 50
burn_vel_08_106_50(3) = Burning_velocity(a) ;
stanDev_BV_08_106_50(3) = standard_deviation_BV(a);
end
if dust_conc(a) == 75
burn_vel_08_106_75(3) = Burning_velocity(a) ;
stanDev_BV_08_106_75(3) = standard_deviation_BV(a);
end
end
if particleSize == 106 && flowRate(a)==40
if dust_conc(a) == 0
burn_vel_08_106_00(4) = Burning_velocity(a) ;
stanDev_BV_08_106_00(4) = standard_deviation_BV(a);
end
if dust_conc(a) == 25
burn_vel_08_106_25(4) = Burning_velocity(a) ;
stanDev_BV_08_106_25(4) = standard_deviation_BV(a);

```

```

end
if dust_conc(a) == 50
burn_vel_08_106_50(4) = Burning_velocity(a) ;
stanDev_BV_08_106_50(4) = standard_deviation_BV(a);
end
if dust_conc(a) == 75
burn_vel_08_106_75(4) = Burning_velocity(a) ;
stanDev_BV_08_106_75(4) = standard_deviation_BV(a);
end
end

if particleSize == 75 && flowRate(a)==10
if dust_conc(a) == 0
burn_vel_08_75_00(1) = Burning_velocity(a) ;
stanDev_BV_08_75_00(1) = standard_deviation_BV(a);
end
if dust_conc(a) == 25
burn_vel_08_75_25(1) = Burning_velocity(a) ;
stanDev_BV_08_75_25(1) = standard_deviation_BV(a);
end
if dust_conc(a) == 50
burn_vel_08_75_50(1) = Burning_velocity(a) ;
stanDev_BV_08_75_50(1) = standard_deviation_BV(a);
end
if dust_conc(a) == 75
burn_vel_08_75_75(1) = Burning_velocity(a) ;
stanDev_BV_08_75_75(1) = standard_deviation_BV(a);
end
end

if particleSize == 75 && flowRate(a)==30
if dust_conc(a) == 0
burn_vel_08_75_00(2) = Burning_velocity(a) ;
stanDev_BV_08_75_00(2) = standard_deviation_BV(a);
end
if dust_conc(a) == 25
burn_vel_08_75_25(2) = Burning_velocity(a) ;
stanDev_BV_08_75_25(2) = standard_deviation_BV(a);
end
if dust_conc(a) == 50
burn_vel_08_75_50(2) = Burning_velocity(a) ;
stanDev_BV_08_75_50(2) = standard_deviation_BV(a);
end
if dust_conc(a) == 75
burn_vel_08_75_75(2) = Burning_velocity(a) ;
stanDev_BV_08_75_75(2) = standard_deviation_BV(a);
end
end

if particleSize == 75 && flowRate(a)==35
if dust_conc(a) == 0
burn_vel_08_75_00(3) = Burning_velocity(a) ;
stanDev_BV_08_75_00(3) = standard_deviation_BV(a);
end
if dust_conc(a) == 25
burn_vel_08_75_25(3) = Burning_velocity(a) ;
stanDev_BV_08_75_25(3) = standard_deviation_BV(a);

```

```

end
if dust_conc(a) == 50
burn_vel_08_75_50(3) = Burning_velocity(a) ;
stanDev_BV_08_75_50(3) = standard_deviation_BV(a);
end
if dust_conc(a) == 75
burn_vel_08_75_75(3) = Burning_velocity(a) ;
stanDev_BV_08_75_75(3) = standard_deviation_BV(a);
end
end
if particleSize == 75 && flowRate(a)==40
if dust_conc(a) == 0
burn_vel_08_75_00(4) = Burning_velocity(a) ;
stanDev_BV_08_75_00(4) = standard_deviation_BV(a);
end
if dust_conc(a) == 25
burn_vel_08_75_25(4) = Burning_velocity(a) ;
stanDev_BV_08_75_25(4) = standard_deviation_BV(a);
end
if dust_conc(a) == 50
burn_vel_08_75_50(4) = Burning_velocity(a) ;
stanDev_BV_08_75_50(4) = standard_deviation_BV(a);
end
if dust_conc(a) == 75
burn_vel_08_75_75(4) = Burning_velocity(a) ;
stanDev_BV_08_75_75(4) = standard_deviation_BV(a);
end
end
end
if phi(a) == 1.0
if particleSize == 106 && flowRate(a)==10
if dust_conc(a) == 0
burn_vel_10_106_00(1) = Burning_velocity(a) ;
stanDev_BV_10_106_00(1) = standard_deviation_BV(a);
end
if dust_conc(a) == 25
burn_vel_10_106_25(1) = Burning_velocity(a) ;
stanDev_BV_10_106_25(1) = standard_deviation_BV(a);
end
if dust_conc(a) == 50
burn_vel_10_106_50(1) = Burning_velocity(a) ;
stanDev_BV_10_106_50(1) = standard_deviation_BV(a);
end
if dust_conc(a) == 75
burn_vel_10_106_75(1) = Burning_velocity(a) ;
stanDev_BV_10_106_75(1) = standard_deviation_BV(a);
end
end
if particleSize == 106 && flowRate(a)==30
if dust_conc(a) == 0
burn_vel_10_106_00(2) = Burning_velocity(a) ;
stanDev_BV_10_106_00(2) = standard_deviation_BV(a);
end
if dust_conc(a) == 25
burn_vel_10_106_25(2) = Burning_velocity(a) ;

```

```

stanDev_BV_10_106_25(2) = standard_deviation_BV(a);
end
if dust_conc(a) == 50
burn_vel_10_106_50(2) = Burning_velocity(a) ;
stanDev_BV_10_106_50(2) = standard_deviation_BV(a);
end
if dust_conc(a) == 75
burn_vel_10_106_75(2) = Burning_velocity(a) ;
stanDev_BV_10_106_75(2) = standard_deviation_BV(a);
end
end
if particleSize == 106 && flowRate(a)==35
if dust_conc(a) == 0
burn_vel_10_106_00(3) = Burning_velocity(a) ;
stanDev_BV_10_106_00(3) = standard_deviation_BV(a);
end
if dust_conc(a) == 25
burn_vel_10_106_25(3) = Burning_velocity(a) ;
stanDev_BV_10_106_25(3) = standard_deviation_BV(a);
end
if dust_conc(a) == 50
burn_vel_10_106_50(3) = Burning_velocity(a) ;
stanDev_BV_10_106_50(3) = standard_deviation_BV(a);
end
if dust_conc(a) == 75
burn_vel_10_106_75(3) = Burning_velocity(a) ;
stanDev_BV_10_106_75(3) = standard_deviation_BV(a);
end
end
if particleSize == 106 && flowRate(a)==40
if dust_conc(a) == 0
burn_vel_10_106_00(4) = Burning_velocity(a) ;
stanDev_BV_10_106_00(4) = standard_deviation_BV(a);
end
if dust_conc(a) == 25
burn_vel_10_106_25(4) = Burning_velocity(a) ;
stanDev_BV_10_106_25(4) = standard_deviation_BV(a);
end
if dust_conc(a) == 50
burn_vel_10_106_50(4) = Burning_velocity(a) ;
stanDev_BV_10_106_50(4) = standard_deviation_BV(a);
end
if dust_conc(a) == 75
burn_vel_10_106_75(4) = Burning_velocity(a) ;
stanDev_BV_10_106_75(4) = standard_deviation_BV(a);
end
end
if particleSize == 75 && flowRate(a)==10
if dust_conc(a) == 0
burn_vel_10_75_00(1) = Burning_velocity(a) ;
stanDev_BV_10_75_00(1) = standard_deviation_BV(a);
end
if dust_conc(a) == 25
burn_vel_10_75_25(1) = Burning_velocity(a) ;
stanDev_BV_10_75_25(1) = standard_deviation_BV(a);

```

```

end
if dust_conc(a) == 50
burn_vel_10_75_50(1) = Burning_velocity(a) ;
stanDev_BV_10_75_50(1) = standard_deviation_BV(a);
end
if dust_conc(a) == 75
burn_vel_10_75_75(1) = Burning_velocity(a) ;
stanDev_BV_10_75_75(1) = standard_deviation_BV(a);
end
end

if particleSize == 75 && flowRate(a)==30
if dust_conc(a) == 0
burn_vel_10_75_00(2) = Burning_velocity(a) ;
stanDev_BV_10_75_00(2) = standard_deviation_BV(a);
end
if dust_conc(a) == 25
burn_vel_10_75_25(2) = Burning_velocity(a) ;
stanDev_BV_10_75_25(2) = standard_deviation_BV(a);
end
if dust_conc(a) == 50
burn_vel_10_75_50(2) = Burning_velocity(a) ;
stanDev_BV_10_75_50(2) = standard_deviation_BV(a);
end
if dust_conc(a) == 75
burn_vel_10_75_75(2) = Burning_velocity(a) ;
stanDev_BV_10_75_75(2) = standard_deviation_BV(a);
end
end
if particleSize == 75 && flowRate(a)==35
if dust_conc(a) == 0
burn_vel_10_75_00(3) = Burning_velocity(a) ;
stanDev_BV_10_75_00(3) = standard_deviation_BV(a);
end
if dust_conc(a) == 25
burn_vel_10_75_25(3) = Burning_velocity(a) ;
stanDev_BV_10_75_25(3) = standard_deviation_BV(a);
end
if dust_conc(a) == 50
burn_vel_10_75_50(3) = Burning_velocity(a) ;
stanDev_BV_10_75_50(3) = standard_deviation_BV(a);
end
if dust_conc(a) == 75
burn_vel_10_75_75(3) = Burning_velocity(a) ;
stanDev_BV_10_75_75(3) = standard_deviation_BV(a);
end
end
if particleSize == 75 && flowRate(a)==40
if dust_conc(a) == 0
burn_vel_10_75_00(4) = Burning_velocity(a) ;
stanDev_BV_10_75_00(4) = standard_deviation_BV(a);
end
if dust_conc(a) == 25
burn_vel_10_75_25(4) = Burning_velocity(a) ;
stanDev_BV_10_75_25(4) = standard_deviation_BV(a);
end
end

```

```

    if dust_conc(a) == 50
    burn_vel_10_75_50(4) = Burning_velocity(a) ;
    stanDev_BV_10_75_50(4) = standard_deviation_BV(a);
    end
    if dust_conc(a) == 75
    burn_vel_10_75_75(4) = Burning_velocity(a) ;
    stanDev_BV_10_75_75(4) = standard_deviation_BV(a);
    end
  end
end

if phi(a) == 1.2
  if particleSize == 106 && flowRate(a)==10
    if dust_conc(a) == 0
    burn_vel_12_106_00(1) = Burning_velocity(a) ;
    stanDev_BV_12_106_00(1) = standard_deviation_BV(a);
    end
    if dust_conc(a) == 25
    burn_vel_12_106_25(1) = Burning_velocity(a) ;
    stanDev_BV_12_106_25(1) = standard_deviation_BV(a);
    end
    if dust_conc(a) == 50
    burn_vel_12_106_50(1) = Burning_velocity(a) ;
    stanDev_BV_12_106_50(1) = standard_deviation_BV(a);
    end
    if dust_conc(a) == 75
    burn_vel_12_106_75(1) = Burning_velocity(a) ;
    stanDev_BV_12_106_75(1) = standard_deviation_BV(a);
    end
  end
  if particleSize == 106 && flowRate(a)==30
    if dust_conc(a) == 0
    burn_vel_12_106_00(2) = Burning_velocity(a) ;
    stanDev_BV_12_106_00(2) = standard_deviation_BV(a);
    end
    if dust_conc(a) == 25
    burn_vel_12_106_25(2) = Burning_velocity(a) ;
    stanDev_BV_12_106_25(2) = standard_deviation_BV(a);
    end
    if dust_conc(a) == 50
    burn_vel_12_106_50(2) = Burning_velocity(a) ;
    stanDev_BV_12_106_50(2) = standard_deviation_BV(a);
    end
    if dust_conc(a) == 75
    burn_vel_12_106_75(2) = Burning_velocity(a) ;
    stanDev_BV_12_106_75(2) = standard_deviation_BV(a);
    end
  end
  if particleSize == 106 && flowRate(a)==35
    if dust_conc(a) == 0
    burn_vel_12_106_00(3) = Burning_velocity(a) ;
    stanDev_BV_12_106_00(3) = standard_deviation_BV(a);
    end
    if dust_conc(a) == 25
    burn_vel_12_106_25(3) = Burning_velocity(a) ;
    stanDev_BV_12_106_25(3) = standard_deviation_BV(a);

```

```

end
if dust_conc(a) == 50
burn_vel_12_106_50(3) = Burning_velocity(a) ;
stanDev_BV_12_106_50(3) = standard_deviation_BV(a);
end
if dust_conc(a) == 75
burn_vel_12_106_75(3) = Burning_velocity(a) ;
stanDev_BV_12_106_75(3) = standard_deviation_BV(a);
end
end
if particleSize == 106 && flowRate(a)==40
if dust_conc(a) == 0
burn_vel_12_106_00(4) = Burning_velocity(a) ;
stanDev_BV_12_106_00(4) = standard_deviation_BV(a);
end
if dust_conc(a) == 25
burn_vel_12_106_25(4) = Burning_velocity(a) ;
stanDev_BV_12_106_25(4) = standard_deviation_BV(a);
end
if dust_conc(a) == 50
burn_vel_12_106_50(4) = Burning_velocity(a) ;
stanDev_BV_12_106_50(4) = standard_deviation_BV(a);
end
if dust_conc(a) == 75
burn_vel_12_106_75(4) = Burning_velocity(a) ;
stanDev_BV_12_106_75(4) = standard_deviation_BV(a);
end
end

if particleSize == 75 && flowRate(a)==10
if dust_conc(a) == 0
burn_vel_12_75_00(1) = Burning_velocity(a) ;
stanDev_BV_12_75_00(1) = standard_deviation_BV(a);
end
if dust_conc(a) == 25
burn_vel_12_75_25(1) = Burning_velocity(a) ;
stanDev_BV_12_75_25(1) = standard_deviation_BV(a);
end
if dust_conc(a) == 50
burn_vel_12_75_50(1) = Burning_velocity(a) ;
stanDev_BV_12_75_50(1) = standard_deviation_BV(a);
end
if dust_conc(a) == 75
burn_vel_12_75_75(1) = Burning_velocity(a) ;
stanDev_BV_12_75_75(1) = standard_deviation_BV(a);
end
end

if particleSize == 75 && flowRate(a)==30
if dust_conc(a) == 0
burn_vel_12_75_00(2) = Burning_velocity(a) ;
stanDev_BV_12_75_00(2) = standard_deviation_BV(a);
end
if dust_conc(a) == 25
burn_vel_12_75_25(2) = Burning_velocity(a) ;
stanDev_BV_12_75_25(2) = standard_deviation_BV(a);

```

```

end
if dust_conc(a) == 50
burn_vel_12_75_50(2) = Burning_velocity(a) ;
stanDev_BV_12_75_50(2) = standard_deviation_BV(a);
end
if dust_conc(a) == 75
burn_vel_12_75_75(2) = Burning_velocity(a) ;
stanDev_BV_12_75_75(2) = standard_deviation_BV(a);
end
end
if particleSize == 75 && flowRate(a)==35
if dust_conc(a) == 0
burn_vel_12_75_00(3) = Burning_velocity(a) ;
stanDev_BV_12_75_00(3) = standard_deviation_BV(a);
end
if dust_conc(a) == 25
burn_vel_12_75_25(3) = Burning_velocity(a) ;
stanDev_BV_12_75_25(3) = standard_deviation_BV(a);
end
if dust_conc(a) == 50
burn_vel_12_75_50(3) = Burning_velocity(a) ;
stanDev_BV_12_75_50(3) = standard_deviation_BV(a);
end
if dust_conc(a) == 75
burn_vel_12_75_75(3) = Burning_velocity(a) ;
stanDev_BV_12_75_75(3) = standard_deviation_BV(a);
end
end
if particleSize == 75 && flowRate(a)==40
if dust_conc(a) == 0
burn_vel_12_75_00(4) = Burning_velocity(a) ;
stanDev_BV_12_75_00(4) = standard_deviation_BV(a);
end
if dust_conc(a) == 25
burn_vel_12_75_25(4) = Burning_velocity(a) ;
stanDev_BV_12_75_25(4) = standard_deviation_BV(a);
end
if dust_conc(a) == 50
burn_vel_12_75_50(4) = Burning_velocity(a) ;
stanDev_BV_12_75_50(4) = standard_deviation_BV(a);
end
if dust_conc(a) == 75
burn_vel_12_75_75(4) = Burning_velocity(a) ;
stanDev_BV_12_75_75(4) = standard_deviation_BV(a);
end
end
end
a = a+1 ;
end

```

```

l_0_08 = (u_prime_all(2:end))./burn_vel_08_75_00(1);
l_0_10 = (u_prime_all(2:end))./burn_vel_10_75_00(1);
l_0_12 = (u_prime_all(2:end))./burn_vel_12_75_00(1);

```

```

plotMarkerSize = 10;

```

```
plotLineWidth = 3 ;
textSize = 16 ;
```

```
figure2 = figure;
testSize2 = 14 ;
axes2 = axes('Parent',figure2,...
    'YMinorTick','on',...
    'XMinorTick','on',...
    'FontSize',testSize2);
```

```
hold on
```

```
%dummy plots to get the legend to have data markers and fitted curve lines
```

```
plot(-1,-1,'ks-', 'MarkerSize',plotMarkerSize, 'LineWidth',plotLineWidth)
plot(-1,-1,'rs-', 'MarkerSize',plotMarkerSize, 'LineWidth',plotLineWidth)
plot(-1,-1,'gs-', 'MarkerSize',plotMarkerSize, 'LineWidth',plotLineWidth)
plot(-1,-1,'bs-', 'MarkerSize',plotMarkerSize, 'LineWidth',plotLineWidth)
plot(-1,-1,'kv-', 'MarkerSize',plotMarkerSize, 'LineWidth',plotLineWidth)
plot(-1,-1,'rv-', 'MarkerSize',plotMarkerSize, 'LineWidth',plotLineWidth)
plot(-1,-1,'gv-', 'MarkerSize',plotMarkerSize, 'LineWidth',plotLineWidth)
plot(-1,-1,'bv-', 'MarkerSize',plotMarkerSize, 'LineWidth',plotLineWidth)
plot(-1,-1,'k+-', 'MarkerSize',plotMarkerSize, 'LineWidth',plotLineWidth)
plot(-1,-1,'r+-', 'MarkerSize',plotMarkerSize, 'LineWidth',plotLineWidth)
plot(-1,-1,'g+-', 'MarkerSize',plotMarkerSize, 'LineWidth',plotLineWidth)
plot(-1,-1,'b+-', 'MarkerSize',plotMarkerSize, 'LineWidth',plotLineWidth)
plot(-1,-1,'ko-', 'MarkerSize',plotMarkerSize, 'LineWidth',plotLineWidth)
plot(-1,-1,'ro-', 'MarkerSize',plotMarkerSize, 'LineWidth',plotLineWidth)
plot(-1,-1,'go-', 'MarkerSize',plotMarkerSize, 'LineWidth',plotLineWidth)
plot(-1,-1,'bo-', 'MarkerSize',plotMarkerSize, 'LineWidth',plotLineWidth)
plot(-1,-1,'kx-', 'MarkerSize',plotMarkerSize, 'LineWidth',plotLineWidth)
plot(-1,-1,'rx-', 'MarkerSize',plotMarkerSize, 'LineWidth',plotLineWidth)
plot(-1,-1,'gx-', 'MarkerSize',plotMarkerSize, 'LineWidth',plotLineWidth)
plot(-1,-1,'bx-', 'MarkerSize',plotMarkerSize, 'LineWidth',plotLineWidth)
plot(-1,-1,'kh-', 'MarkerSize',plotMarkerSize, 'LineWidth',plotLineWidth)
plot(-1,-1,'rh-', 'MarkerSize',plotMarkerSize, 'LineWidth',plotLineWidth)
plot(-1,-1,'gh-', 'MarkerSize',plotMarkerSize, 'LineWidth',plotLineWidth)
plot(-1,-1,'bh-', 'MarkerSize',plotMarkerSize, 'LineWidth',plotLineWidth)
```

```
legend('\phi=0.8,d=75,d_st=00','\phi=0.8,d=75,d_st=25','\phi=0.8,d=75,d_st=50','\phi=0.8,d=75,d_st=75',...
    '\phi=1.0,d=75,d_st=00','\phi=1.0,d=75,d_st=25','\phi=1.0,d=75,d_st=50','\phi=1.0,d=75,d_st=75',...
    '\phi=1.2,d=75,d_st=00','\phi=1.2,d=75,d_st=25','\phi=1.2,d=75,d_st=50','\phi=1.2,d=75,d_st=75',...
    '\phi=0.8,d=106,d_st=00','\phi=0.8,d=106,d_st=25','\phi=0.8,d=106,d_st=50','\phi=0.8,d=106,d_st=75',...
    '\phi=1.0,d=106,d_st=00','\phi=1.0,d=106,d_st=25','\phi=1.0,d=106,d_st=50','\phi=1.0,d=106,d_st=75',...
    '\phi=1.2,d=106,d_st=00','\phi=1.2,d=106,d_st=25','\phi=1.2,d=106,d_st=50','\phi=1.2,d=106,d_st=75',...
    'Location','eastoutside')
```

```
%% Linear fit for laminar data
```

```
dust_concFit=[0 25 50 75];
lam_fit_08=polyfit(dust_concFit,burn_vel_08_75_10_dst_size_orig,1);
lam_fit_10=polyfit(dust_concFit,burn_vel_10_75_10_dst_size_orig,1);
lam_fit_12=polyfit(dust_concFit,burn_vel_12_75_10_dst_size_orig,1);
burn_vel_08_75_10_dst_size_origFit=dust_concFit.*lam_fit_08(1)+lam_fit_08(2);
burn_vel_10_75_10_dst_size_origFit=dust_concFit.*lam_fit_10(1)+lam_fit_10(2);
burn_vel_12_75_10_dst_size_origFit=dust_concFit.*lam_fit_12(1)+lam_fit_12(2);
```

```
%% normalizing data
```

```
burn_vel_08_75_00_orig = burn_vel_08_75_00;
```

```
burn_vel_08_75_25_orig = burn_vel_08_75_25 ;
burn_vel_08_75_50_orig = burn_vel_08_75_50 ;
burn_vel_08_75_75_orig = burn_vel_08_75_75 ;
burn_vel_08_106_00_orig = burn_vel_08_106_00 ;
burn_vel_08_106_25_orig = burn_vel_08_106_25 ;
burn_vel_08_106_50_orig = burn_vel_08_106_50 ;
burn_vel_08_106_75_orig = burn_vel_08_106_75 ;
```

```
burn_vel_10_75_00_orig = burn_vel_10_75_00 ;
burn_vel_10_75_25_orig = burn_vel_10_75_25 ;
burn_vel_10_75_50_orig = burn_vel_10_75_50 ;
burn_vel_10_75_75_orig = burn_vel_10_75_75 ;
burn_vel_10_106_00_orig = burn_vel_10_106_00 ;
burn_vel_10_106_25_orig = burn_vel_10_106_25 ;
burn_vel_10_106_50_orig = burn_vel_10_106_50 ;
burn_vel_10_106_75_orig = burn_vel_10_106_75 ;
```

```
burn_vel_12_75_00_orig = burn_vel_12_75_00 ;
burn_vel_12_75_25_orig = burn_vel_12_75_25 ;
burn_vel_12_75_50_orig = burn_vel_12_75_50 ;
burn_vel_12_75_75_orig = burn_vel_12_75_75 ;
burn_vel_12_106_00_orig = burn_vel_12_106_00 ;
burn_vel_12_106_25_orig = burn_vel_12_106_25 ;
burn_vel_12_106_50_orig = burn_vel_12_106_50 ;
burn_vel_12_106_75_orig = burn_vel_12_106_75 ;
```

```
lam_data = 1; % if =1 include laminar data, if 2 exclude laminar data
lam_data_dst_size = 1 ;
```

```
burn_vel_08_75_00 = burn_vel_08_75_00_orig(lam_data:end)./burn_vel_08_75_00_orig(lam_data:end);
burn_vel_08_75_25 = burn_vel_08_75_25_orig(lam_data:end)./burn_vel_08_75_00_orig(lam_data:end);
burn_vel_08_75_50 = burn_vel_08_75_50_orig(lam_data:end)./burn_vel_08_75_00_orig(lam_data:end);
burn_vel_08_75_75 = burn_vel_08_75_75_orig(lam_data:end)./burn_vel_08_75_00_orig(lam_data:end-1);
burn_vel_08_106_00 = burn_vel_08_106_00_orig(lam_data:end)./burn_vel_08_106_00_orig(lam_data:end);
burn_vel_08_106_25 = burn_vel_08_106_25_orig(lam_data:end)./burn_vel_08_106_00_orig(lam_data:end);
burn_vel_08_106_50 = burn_vel_08_106_50_orig(lam_data:end)./burn_vel_08_106_00_orig(lam_data:end);
burn_vel_08_106_75 = burn_vel_08_106_75_orig(lam_data:end)./burn_vel_08_106_00_orig(lam_data:end-1);
```

```
burn_vel_10_75_00 = burn_vel_10_75_00_orig(lam_data:end)./burn_vel_10_75_00_orig(lam_data:end);
burn_vel_10_75_25 = burn_vel_10_75_25_orig(lam_data:end)./burn_vel_10_75_00_orig(lam_data:end);
burn_vel_10_75_50 = burn_vel_10_75_50_orig(lam_data:end)./burn_vel_10_75_00_orig(lam_data:end);
burn_vel_10_75_75 = burn_vel_10_75_75_orig(lam_data:end)./burn_vel_10_75_00_orig(lam_data:end);
burn_vel_10_106_00 = burn_vel_10_106_00_orig(lam_data:end)./burn_vel_10_106_00_orig(lam_data:end);
burn_vel_10_106_25 = burn_vel_10_106_25_orig(lam_data:end)./burn_vel_10_106_00_orig(lam_data:end);
burn_vel_10_106_50 = burn_vel_10_106_50_orig(lam_data:end)./burn_vel_10_106_00_orig(lam_data:end);
burn_vel_10_106_75 = burn_vel_10_106_75_orig(lam_data:end)./burn_vel_10_106_00_orig(lam_data:end-1);
```

```
burn_vel_12_75_00 = burn_vel_12_75_00_orig(lam_data:end)./burn_vel_12_75_00_orig(lam_data:end);
burn_vel_12_75_25 = burn_vel_12_75_25_orig(lam_data:end)./burn_vel_12_75_00_orig(lam_data:end);
burn_vel_12_75_50 = burn_vel_12_75_50_orig(lam_data:end)./burn_vel_12_75_00_orig(lam_data:end);
burn_vel_12_75_75 = burn_vel_12_75_75_orig(lam_data:end)./burn_vel_12_75_00_orig(lam_data:end);
burn_vel_12_106_00 = burn_vel_12_106_00_orig(lam_data:end)./burn_vel_12_106_00_orig(lam_data:end);
burn_vel_12_106_25 = burn_vel_12_106_25_orig(lam_data:end)./burn_vel_12_106_00_orig(lam_data:end);
burn_vel_12_106_50 = burn_vel_12_106_50_orig(lam_data:end)./burn_vel_12_106_00_orig(lam_data:end);
```

```
burn_vel_12_106_75 = burn_vel_12_106_75_orig(lam_data:end)/burn_vel_12_106_00_orig(lam_data:end-1);
```

```
% l_0_all = l_0_10;  
% l_0 = l_0(lam_data:end);
```

```
burn_vel_08_75_10_dst_size_orig = burn_vel_08_75_10_dst_size;  
burn_vel_08_75_30_dst_size_orig = burn_vel_08_75_30_dst_size ;  
burn_vel_08_75_35_dst_size_orig = burn_vel_08_75_35_dst_size ;  
burn_vel_08_75_40_dst_size_orig = burn_vel_08_75_40_dst_size ;
```

```
burn_vel_08_106_10_dst_size_orig = burn_vel_08_106_10_dst_size ;  
burn_vel_08_106_30_dst_size_orig = burn_vel_08_106_30_dst_size ;  
burn_vel_08_106_35_dst_size_orig = burn_vel_08_106_35_dst_size ;  
burn_vel_08_106_40_dst_size_orig = burn_vel_08_106_40_dst_size ;
```

```
burn_vel_10_75_10_dst_size_orig = burn_vel_10_75_10_dst_size ;  
burn_vel_10_75_30_dst_size_orig = burn_vel_10_75_30_dst_size ;  
burn_vel_10_75_35_dst_size_orig = burn_vel_10_75_35_dst_size ;  
burn_vel_10_75_40_dst_size_orig = burn_vel_10_75_40_dst_size ;
```

```
burn_vel_10_106_10_dst_size_orig = burn_vel_10_106_10_dst_size ;  
burn_vel_10_106_30_dst_size_orig = burn_vel_10_106_30_dst_size ;  
burn_vel_10_106_35_dst_size_orig = burn_vel_10_106_35_dst_size ;  
burn_vel_10_106_40_dst_size_orig = burn_vel_10_106_40_dst_size ;
```

```
burn_vel_12_75_10_dst_size_orig = burn_vel_12_75_10_dst_size ;  
burn_vel_12_75_30_dst_size_orig = burn_vel_12_75_30_dst_size ;  
burn_vel_12_75_35_dst_size_orig = burn_vel_12_75_35_dst_size ;  
burn_vel_12_75_40_dst_size_orig = burn_vel_12_75_40_dst_size ;
```

```
burn_vel_12_106_10_dst_size_orig = burn_vel_12_106_10_dst_size ;  
burn_vel_12_106_30_dst_size_orig = burn_vel_12_106_30_dst_size ;  
burn_vel_12_106_35_dst_size_orig = burn_vel_12_106_35_dst_size ;  
burn_vel_12_106_40_dst_size_orig = burn_vel_12_106_40_dst_size ;
```

```
burn_vel_08_75_10_dst_size = burn_vel_08_75_10_dst_size(1:end)/burn_vel_08_75_10_dst_size_orig(1);  
burn_vel_08_75_30_dst_size =  
burn_vel_08_75_30_dst_size(lam_data_dst_size:end)/burn_vel_08_75_10_dst_size_orig(2);  
burn_vel_08_75_35_dst_size =  
burn_vel_08_75_35_dst_size(lam_data_dst_size:end)/burn_vel_08_75_10_dst_size_orig(3);  
burn_vel_08_75_40_dst_size =  
burn_vel_08_75_40_dst_size(lam_data_dst_size:end)/burn_vel_08_75_10_dst_size_orig(4);  
burn_vel_08_106_10_dst_size = burn_vel_08_106_10_dst_size(1:end)/burn_vel_08_106_10_dst_size_orig(1);  
burn_vel_08_106_30_dst_size =  
burn_vel_08_106_30_dst_size(lam_data_dst_size:end)/burn_vel_08_106_10_dst_size_orig(2);  
burn_vel_08_106_35_dst_size =  
burn_vel_08_106_35_dst_size(lam_data_dst_size:end)/burn_vel_08_106_10_dst_size_orig(3);  
burn_vel_08_106_40_dst_size =  
burn_vel_08_106_40_dst_size(lam_data_dst_size:end)/burn_vel_08_106_10_dst_size_orig(4);
```

```
burn_vel_10_75_10_dst_size = burn_vel_10_75_10_dst_size(1:end)/burn_vel_10_75_10_dst_size_orig(1);
```

```

burn_vel_10_75_30_dst_size =
burn_vel_10_75_30_dst_size(lam_data_dst_size:end)/burn_vel_10_75_10_dst_size_orig(2);
burn_vel_10_75_35_dst_size =
burn_vel_10_75_35_dst_size(lam_data_dst_size:end)/burn_vel_10_75_10_dst_size_orig(3);
burn_vel_10_75_40_dst_size =
burn_vel_10_75_40_dst_size(lam_data_dst_size:end)/burn_vel_10_75_10_dst_size_orig(4);

burn_vel_10_106_10_dst_size = burn_vel_10_106_10_dst_size(1:end)/burn_vel_10_106_10_dst_size_orig(1);
burn_vel_10_106_30_dst_size =
burn_vel_10_106_30_dst_size(lam_data_dst_size:end)/burn_vel_10_106_10_dst_size_orig(2);
burn_vel_10_106_35_dst_size =
burn_vel_10_106_35_dst_size(lam_data_dst_size:end)/burn_vel_10_106_10_dst_size_orig(3);
burn_vel_10_106_40_dst_size =
burn_vel_10_106_40_dst_size(lam_data_dst_size:end)/burn_vel_10_106_10_dst_size_orig(4);

burn_vel_12_75_10_dst_size = burn_vel_12_75_10_dst_size(1:end)/burn_vel_12_75_10_dst_size_orig(1);
burn_vel_12_75_30_dst_size =
burn_vel_12_75_30_dst_size(lam_data_dst_size:end)/burn_vel_12_75_10_dst_size_orig(2);
burn_vel_12_75_35_dst_size =
burn_vel_12_75_35_dst_size(lam_data_dst_size:end)/burn_vel_12_75_10_dst_size_orig(3);
burn_vel_12_75_40_dst_size =
burn_vel_12_75_40_dst_size(lam_data_dst_size:end)/burn_vel_12_75_10_dst_size_orig(4);

burn_vel_12_106_10_dst_size = burn_vel_12_106_10_dst_size(1:end)/burn_vel_12_106_10_dst_size_orig(1);
burn_vel_12_106_30_dst_size =
burn_vel_12_106_30_dst_size(lam_data_dst_size:end)/burn_vel_12_106_10_dst_size_orig(2);
burn_vel_12_106_35_dst_size =
burn_vel_12_106_35_dst_size(lam_data_dst_size:end)/burn_vel_12_106_10_dst_size_orig(3);
burn_vel_12_106_40_dst_size =
burn_vel_12_106_40_dst_size(lam_data_dst_size:end)/burn_vel_12_106_10_dst_size_orig(4);

```

% Standard deviation

```

stanDev_BV_08_75_00_orig = stanDev_BV_08_75_00;
stanDev_BV_08_75_25_orig = stanDev_BV_08_75_25 ;
stanDev_BV_08_75_50_orig = stanDev_BV_08_75_50 ;
stanDev_BV_08_75_75_orig = stanDev_BV_08_75_75 ;
stanDev_BV_08_106_00_orig = stanDev_BV_08_106_00 ;
stanDev_BV_08_106_25_orig = stanDev_BV_08_106_25 ;
stanDev_BV_08_106_50_orig = stanDev_BV_08_106_50 ;
stanDev_BV_08_106_75_orig = stanDev_BV_08_106_75 ;

stanDev_BV_10_75_00_orig = stanDev_BV_10_75_00 ;
stanDev_BV_10_75_25_orig = stanDev_BV_10_75_25 ;
stanDev_BV_10_75_50_orig = stanDev_BV_10_75_50 ;
stanDev_BV_10_75_75_orig = stanDev_BV_10_75_75 ;
stanDev_BV_10_106_00_orig = stanDev_BV_10_106_00 ;
stanDev_BV_10_106_25_orig = stanDev_BV_10_106_25 ;
stanDev_BV_10_106_50_orig = stanDev_BV_10_106_50 ;
stanDev_BV_10_106_75_orig = stanDev_BV_10_106_75 ;

stanDev_BV_12_75_00_orig = stanDev_BV_12_75_00 ;
stanDev_BV_12_75_25_orig = stanDev_BV_12_75_25 ;
stanDev_BV_12_75_50_orig = stanDev_BV_12_75_50 ;
stanDev_BV_12_75_75_orig = stanDev_BV_12_75_75 ;

```

```
stanDev_BV_12_106_00_orig = stanDev_BV_12_106_00 ;
stanDev_BV_12_106_25_orig = stanDev_BV_12_106_25 ;
stanDev_BV_12_106_50_orig = stanDev_BV_12_106_50 ;
stanDev_BV_12_106_75_orig = stanDev_BV_12_106_75 ;
```

```
close all
```

```
%% plotting functions
```

```
% plot_ND_SLv01
```

```
% plot_ND_SL_dst_sev01
```

```
% plot_ND_SLdivSLgasOnlyv01
```

```
% plot_ND_SL_dst_sev02_lamOnly
```

```
% plot_williams_data_v01
```

```
% plot_SL_02_lamOnly
```

```
% plot_ND_SL_dst_sev02_lamOnly
```

```
% plot_ND_SLv03_6fig
```

```
% plot_ND_SLdivSLgasOnlyv04_6fig
```

```
%
```

```
% plot_ND_SL_dst_sev03_turbOnly
```

A3.3 - Plotting figure 4.9

```
% plot_ND_SLdivSLgasOnlyv01
% plot_ND_SLdivSLgasOnlyv02_6fig
% plot_ND_SLv03_6fig

legend_plot=0 ;
plotMarkerSize = 10;
plotLineWidth = 3 ;
testSize2 = 14 ;

% x_axisMin = 0 ;
% x_axisMax = 80 ;
y_axisMin = 1.9;
y_axisMax = 4 ;

l_0_08_00 = (u_prime_all(2:end)./burn_vel_08_75_10_dst_size_origFit(1));
l_0_08_25 = (u_prime_all(2:end)./burn_vel_08_75_10_dst_size_origFit(1));
l_0_08_50 = (u_prime_all(2:end)./burn_vel_08_75_10_dst_size_origFit(1));
l_0_08_75 = (u_prime_all(2:end)./burn_vel_08_75_10_dst_size_origFit(1));

l_0_10_00 = (u_prime_all(2:end)./burn_vel_10_75_10_dst_size_origFit(1));
l_0_10_25 = (u_prime_all(2:end)./burn_vel_10_75_10_dst_size_origFit(1));
l_0_10_50 = (u_prime_all(2:end)./burn_vel_10_75_10_dst_size_origFit(1));
l_0_10_75 = (u_prime_all(2:end)./burn_vel_10_75_10_dst_size_origFit(1));

l_0_12_00 = (u_prime_all(2:end)./burn_vel_12_75_10_dst_size_origFit(1));
l_0_12_25 = (u_prime_all(2:end)./burn_vel_12_75_10_dst_size_origFit(1));
l_0_12_50 = (u_prime_all(2:end)./burn_vel_12_75_10_dst_size_origFit(1));
l_0_12_75 = (u_prime_all(2:end)./burn_vel_12_75_10_dst_size_origFit(1));

% phi 0.8 ;
figure1 = figure('Name','NDim turbulent velocity');
% axes2 = axes('Parent',figure1,...
% 'YMinorTick','on',...
% 'XMinorTick','on',...
% 'FontSize',testSize2);

hold on

%
subplot1 = subplot(3,2,1,'Parent',figure1,'YTick',[2 2.4 2.8 3.2 3.6 4],...
'LineWidth',2,...
'FontWeight','bold',...
'FontSize',14,...
'FontName','Times New Roman');
hold on
plot(l_0_08_00,burn_vel_08_75_00_orig(lam_data:end)./burn_vel_08_75_10_dst_size_origFit(1),'ks','LineWidth',plotLineWidth);
plot(l_0_08_25,burn_vel_08_75_25_orig(lam_data:end)./burn_vel_08_75_10_dst_size_origFit(2),'ro','LineWidth',plotLineWidth);
plot(l_0_08_50,burn_vel_08_75_50_orig(lam_data:end)./burn_vel_08_75_10_dst_size_origFit(3),'gv','LineWidth',plotLineWidth);
```

```

plot(l_0_08_75(1:length(burn_vel_08_75_75)),burn_vel_08_75_75_orig(lam_data:end)./burn_vel_08_75_10_dst_size_origFit(4),'bh','LineWidth',plotLineWidth);
ylim([y_axisMin y_axisMax]);
hold off
% axis tight

subplot1 = subplot(3,2,2,'Parent',figure1,'YTick',[2 2.4 2.8 3.2 3.6 4],...
    'LineWidth',2,...
    'FontWeight','bold',...
    'FontSize',14,...
    'FontName','Times New Roman');
% subplot(3,2,2);
hold on
plot(l_0_08_00,burn_vel_08_106_00_orig(lam_data:end)./burn_vel_08_75_10_dst_size_origFit(1),'ks','LineWidth',plotLineWidth);
plot(l_0_08_25,burn_vel_08_106_25_orig(lam_data:end)./burn_vel_08_75_10_dst_size_origFit(2),'ro','LineWidth',plotLineWidth);
plot(l_0_08_50,burn_vel_08_106_50_orig(lam_data:end)./burn_vel_08_75_10_dst_size_origFit(3),'gv','LineWidth',plotLineWidth);
plot(l_0_08_75(1:length(burn_vel_08_106_75)),burn_vel_08_106_75_orig(lam_data:end)./burn_vel_08_75_10_dst_size_origFit(4),'bh','LineWidth',plotLineWidth);
ylim([y_axisMin y_axisMax]);
hold off

subplot1 = subplot(3,2,3,'Parent',figure1,'YTick',[2 2.4 2.8 3.2 3.6 4],...
    'LineWidth',2,...
    'FontWeight','bold',...
    'FontSize',14,...
    'FontName','Times New Roman');
% subplot(3,2,3);
hold on
plot(l_0_10,burn_vel_10_75_00_orig(lam_data:end)./burn_vel_10_75_10_dst_size_origFit(1),'ks','LineWidth',plotLineWidth);
plot(l_0_10_25,burn_vel_10_75_25_orig(lam_data:end)./burn_vel_10_75_10_dst_size_origFit(2),'ro','LineWidth',plotLineWidth);
plot(l_0_10_50,burn_vel_10_75_50_orig(lam_data:end)./burn_vel_10_75_10_dst_size_origFit(3),'gv','LineWidth',plotLineWidth);
plot(l_0_10_75,burn_vel_10_75_75_orig(lam_data:end)./burn_vel_10_75_10_dst_size_origFit(4),'bh','LineWidth',plotLineWidth);
ylim([y_axisMin y_axisMax]);
xlim([0.4 1.42])

subplot1 = subplot(3,2,4,'Parent',figure1,'XTick',[0.4 0.6 0.8 1 1.2 1.4],'YTick',[2 2.4 2.8 3.2 3.6 4],...
    'LineWidth',2,...
    'FontWeight','bold',...
    'FontSize',14,...
    'FontName','Times New Roman');
% subplot(3,2,4);
hold on
plot(l_0_10_00,burn_vel_10_106_00_orig(lam_data:end)./burn_vel_10_75_10_dst_size_origFit(1),'ks','LineWidth',plotLineWidth);
plot(l_0_10_25,burn_vel_10_106_25_orig(lam_data:end)./burn_vel_10_75_10_dst_size_origFit(2),'ro','LineWidth',plotLineWidth);
plot(l_0_10_50,burn_vel_10_106_50_orig(lam_data:end)./burn_vel_10_75_10_dst_size_origFit(3),'gv','LineWidth',plotLineWidth);

```

```

plot(l_0_10_75(1:length(burn_vel_10_106_75)),burn_vel_10_106_75_orig(lam_data:end)./burn_vel_10_75_10_dst
_size_origFit(4),'bh','LineWidth',plotLineWidth);
ylim([y_axisMin y_axisMax]);
xlim([0.4 1.42])
hold off

```

```

subplot1 = subplot(3,2,5,'Parent',figure1,'YTick',[2 2.4 2.8 3.2 3.6 4],...
'LineWidth',2,...
'FontWeight','bold',...
'FontSize',14,...
'FontName','Times New Roman');
% subplot(3,2,5);
hold on
plot(l_0_12_00,burn_vel_12_75_00_orig(lam_data:end)./burn_vel_12_75_10_dst_size_origFit(1),'ks','LineWidth',pl
otLineWidth);
plot(l_0_12_25,burn_vel_12_75_25_orig(lam_data:end)./burn_vel_12_75_10_dst_size_origFit(2),'ro','LineWidth',pl
otLineWidth);
plot(l_0_12_50,burn_vel_12_75_50_orig(lam_data:end)./burn_vel_12_75_10_dst_size_origFit(3),'gv','LineWidth',pl
otLineWidth);
plot(l_0_12_75,burn_vel_12_75_75_orig(lam_data:end)./burn_vel_12_75_10_dst_size_origFit(4),'bh','LineWidth',pl
otLineWidth);
ylim([y_axisMin y_axisMax]);
hold off

```

```

subplot1 = subplot(3,2,6,'Parent',figure1,'YTick',[2 2.4 2.8 3.2 3.6 4],...
'LineWidth',2,...
'FontWeight','bold',...
'FontSize',14,...
'FontName','Times New Roman');
% subplot(3,2,6);
hold on
plot(l_0_12_00,burn_vel_12_106_00_orig(lam_data:end)./burn_vel_12_75_10_dst_size_origFit(1),'ks','LineWidth',p
lotLineWidth);
plot(l_0_12_25,burn_vel_12_106_25_orig(lam_data:end)./burn_vel_12_75_10_dst_size_origFit(2),'ro','LineWidth',p
lotLineWidth);
plot(l_0_12_50,burn_vel_12_106_50_orig(lam_data:end)./burn_vel_12_75_10_dst_size_origFit(3),'gv','LineWidth',
plotLineWidth);
plot(l_0_12_75(1:length(burn_vel_12_106_75)),burn_vel_12_106_75_orig(lam_data:end)./burn_vel_12_75_10_dst
_size_origFit(4),'bh','LineWidth',plotLineWidth);
ylim([y_axisMin y_axisMax]);
hold off

```

```

p=[1 1 1000 450;...
100 -120 850 2750];
set(gcf,'position',p(2,:)) ;

```

%dummy plots to get the legend to have data markers and fitted curve lines

```

if legend_plot==1
plot(-1,-1,'rs','MarkerSize',plotMarkerSize,'LineWidth',plotLineWidth)
plot(-1,-1,'gs','MarkerSize',plotMarkerSize,'LineWidth',plotLineWidth)
plot(-1,-1,'bs','MarkerSize',plotMarkerSize,'LineWidth',plotLineWidth)

plot(-1,-1,'rv','MarkerSize',plotMarkerSize,'LineWidth',plotLineWidth)
plot(-1,-1,'gv','MarkerSize',plotMarkerSize,'LineWidth',plotLineWidth)
plot(-1,-1,'bv','MarkerSize',plotMarkerSize,'LineWidth',plotLineWidth)
legend('d=75,d_{st}=25','d=75,d_{st}=50','d=75,d_{st}=75',...

```

```
'd=106,d_{st}=25','d=106,d_{st}=50','d=106,d_{st}=75',...  
'Location','eastoutside')  
end
```

A3.4 - Plotting figure 4.13

```
plot_legend=0;
plotMarkerSize = 10;
plotLineWidth = 3 ;
testSize2 = 18 ;

y_axisMin = 1.9;
y_axisMax = 4 ;

particleSize=[75 106];

figure3 = figure('Name','Dust concentration'); %plotting laminar data
axes2 = axes('Parent',figure3,'YMinorTick','on','XTick',[0 25 50 75],'XMinorTick','on','FontSize',testSize2);
hold on

if plot_legend==1
%dummy plots to get the legend to have data markers and fitted curve lines
plot(-1,-1,'ks-', 'MarkerSize',plotMarkerSize, 'LineWidth',plotLineWidth)
plot(-1,-1,'kv-', 'MarkerSize',plotMarkerSize, 'LineWidth',plotLineWidth)
plot(-1,-1,'gs-', 'MarkerSize',plotMarkerSize, 'LineWidth',plotLineWidth)
plot(-1,-1,'gv--', 'MarkerSize',plotMarkerSize, 'LineWidth',plotLineWidth)
plot(-1,-1,'bs--', 'MarkerSize',plotMarkerSize, 'LineWidth',plotLineWidth)
plot(-1,-1,'gv--', 'MarkerSize',plotMarkerSize, 'LineWidth',plotLineWidth)
legend('\phi=0.8,106', '\phi=0.8,75',...
        '\phi=1.0,106', '\phi=1.0,75',...
        '\phi=1.2,106', '\phi=1.2,75', 'Location','northwest', 'Orientation', 'horizontal');
end

subplot1 = subplot(3,2,1, 'Parent',figure3, 'YTick',[2 2.4 2.8 3.2 3.6 4],...
        'LineWidth',2,...
        'FontWeight', 'bold',...
        'FontSize',14,...
        'FontName','Times New Roman');
% subplot(3,2,1);
hold on
%
plot(dust_conc_08_75_10_dst_size, burn_vel_08_75_10_dst_size, 'ks', 'MarkerSize',plotMarkerSize, 'LineWidth',plotLi
neWidth);
plot(dust_conc_08_75_30_dst_size(lam_data_dst_size:end)/.1_00(lam_data_dst_size:end), burn_vel_08_75_30_dst_sz
e_orig./burn_vel_08_75_10_dst_size_origFit, 'ro', 'MarkerSize',plotMarkerSize, 'LineWidth',plotLineWidth);
plot(dust_conc_08_75_35_dst_size(lam_data_dst_size:end)/.1_00(lam_data_dst_size:end), burn_vel_08_75_35_dst_sz
e_orig./burn_vel_08_75_10_dst_size_origFit, 'gv', 'MarkerSize',plotMarkerSize, 'LineWidth',plotLineWidth);
plot(dust_conc_08_75_40_dst_size(lam_data_dst_size:end)/.1_00(lam_data_dst_size:end-
1), burn_vel_08_75_40_dst_size_orig./burn_vel_08_75_10_dst_size_origFit(lam_data_dst_size:end-
1), 'bh', 'MarkerSize',plotMarkerSize, 'LineWidth',plotLineWidth);
ylim([y_axisMin y_axisMax]);
hold off

subplot1 = subplot(3,2,2, 'Parent',figure3, 'YTick',[2 2.4 2.8 3.2 3.6 4],...
        'LineWidth',2,...
        'FontWeight', 'bold',...
        'FontSize',14,...
        'FontName','Times New Roman');
% subplot(3,2,2);
```

```

hold on
%
plot(dust_conc_08_106_10_dst_size,burn_vel_08_106_10_dst_size,'kv','MarkerSize',plotMarkerSize,'LineWidth',plot
LineWidth);
plot(dust_conc_08_106_30_dst_size(lam_data_dst_size:end)./1_00(lam_data_dst_size:end),burn_vel_08_106_30_dst_
size_orig./burn_vel_08_75_10_dst_size_origFit,'ro','MarkerSize',plotMarkerSize,'LineWidth',plotLineWidth);
plot(dust_conc_08_106_35_dst_size(lam_data_dst_size:end)./1_00(lam_data_dst_size:end),burn_vel_08_106_35_dst_
size_orig./burn_vel_08_75_10_dst_size_origFit,'gv','MarkerSize',plotMarkerSize,'LineWidth',plotLineWidth);
plot(dust_conc_08_106_40_dst_size(lam_data_dst_size:end)./1_00(lam_data_dst_size:end-
1),burn_vel_08_106_40_dst_size_orig./burn_vel_08_75_10_dst_size_origFit(lam_data_dst_size:end-
1),'bh','MarkerSize',plotMarkerSize,'LineWidth',plotLineWidth);

ylim([y_axisMin y_axisMax]);
hold off

subplot1 = subplot(3,2,3,'Parent',figure3,'YTick',[2 2.4 2.8 3.2 3.6 4],...
'LineWidth',2,...
'FontWeight','bold',...
'FontSize',14,...
'FontName','Times New Roman');
% subplot(3,2,3);
hold on
%
plot(dust_conc_10_75_10_dst_size,burn_vel_10_75_10_dst_size,'ks','MarkerSize',plotMarkerSize,'LineWidth',plotLi
neWidth);
plot(dust_conc_10_75_30_dst_size(lam_data_dst_size:end)./1_00(lam_data_dst_size:end),burn_vel_10_75_30_dst_sz
e_orig./burn_vel_10_75_10_dst_size_origFit,'ro','MarkerSize',plotMarkerSize,'LineWidth',plotLineWidth);
plot(dust_conc_10_75_35_dst_size(lam_data_dst_size:end)./1_00(lam_data_dst_size:end),burn_vel_10_75_35_dst_sz
e_orig./burn_vel_10_75_10_dst_size_origFit,'gv','MarkerSize',plotMarkerSize,'LineWidth',plotLineWidth);
plot(dust_conc_10_75_40_dst_size(lam_data_dst_size:end)./1_00(lam_data_dst_size:end),burn_vel_10_75_40_dst_sz
e_orig./burn_vel_10_75_10_dst_size_origFit,'bh','MarkerSize',plotMarkerSize,'LineWidth',plotLineWidth);
ylim([y_axisMin y_axisMax]);
hold off

subplot1 = subplot(3,2,4,'Parent',figure3,'YTick',[2 2.4 2.8 3.2 3.6 4],...
'LineWidth',2,...
'FontWeight','bold',...
'FontSize',14,...
'FontName','Times New Roman');
% subplot(3,2,4);
hold on
%
plot(dust_conc_10_106_10_dst_size,burn_vel_10_106_10_dst_size,'kv','MarkerSize',plotMarkerSize,'LineWidth',plot
LineWidth);
plot(dust_conc_10_106_30_dst_size(lam_data_dst_size:end)./1_00(lam_data_dst_size:end),burn_vel_10_106_30_dst_
size_orig./burn_vel_10_75_10_dst_size_origFit,'ro','MarkerSize',plotMarkerSize,'LineWidth',plotLineWidth);
plot(dust_conc_10_106_35_dst_size(lam_data_dst_size:end)./1_00(lam_data_dst_size:end),burn_vel_10_106_35_dst_
size_orig./burn_vel_10_75_10_dst_size_origFit,'gv','MarkerSize',plotMarkerSize,'LineWidth',plotLineWidth);
plot(dust_conc_10_106_40_dst_size(lam_data_dst_size:end)./1_00(lam_data_dst_size:end-
1),burn_vel_10_106_40_dst_size_orig./burn_vel_10_75_10_dst_size_origFit(lam_data_dst_size:end-
1),'bh','MarkerSize',plotMarkerSize,'LineWidth',plotLineWidth);

ylim([y_axisMin y_axisMax]);
hold off

subplot1 = subplot(3,2,5,'Parent',figure3,'YTick',[2 2.4 2.8 3.2 3.6 4],...

```

```

'LineWidth',2,...
'FontWeight','bold',...
'FontSize',14,...
'FontName','Times New Roman');
% subplot(3,2,5);
hold on
%
plot(dust_conc_12_75_10_dst_size, burn_vel_12_75_10_dst_size, 'ks', 'MarkerSize', plotMarkerSize, 'LineWidth', plotLineWidth);
plot(dust_conc_12_75_30_dst_size(lam_data_dst_size:end)/1_00(lam_data_dst_size:end), burn_vel_12_75_30_dst_size_orig./burn_vel_12_75_10_dst_size_origFit, 'ro', 'MarkerSize', plotMarkerSize, 'LineWidth', plotLineWidth);
plot(dust_conc_12_75_35_dst_size(lam_data_dst_size:end)/1_00(lam_data_dst_size:end), burn_vel_12_75_35_dst_size_orig./burn_vel_12_75_10_dst_size_origFit, 'gv', 'MarkerSize', plotMarkerSize, 'LineWidth', plotLineWidth);
plot(dust_conc_12_75_40_dst_size(lam_data_dst_size:end)/1_00(lam_data_dst_size:end), burn_vel_12_75_40_dst_size_orig./burn_vel_12_75_10_dst_size_origFit, 'bh', 'MarkerSize', plotMarkerSize, 'LineWidth', plotLineWidth);
ylim([y_axisMin y_axisMax]);
hold off

subplot1 = subplot(3,2,6, 'Parent', figure3, 'YTick', [2 2.4 2.8 3.2 3.6 4], ...
'LineWidth',2,...
'FontWeight','bold',...
'FontSize',14,...
'FontName','Times New Roman');
% subplot(3,2,6);
hold on
%
plot(dust_conc_12_106_10_dst_size, burn_vel_12_106_10_dst_size, 'kv', 'MarkerSize', plotMarkerSize, 'LineWidth', plotLineWidth);
plot(dust_conc_12_106_30_dst_size(lam_data_dst_size:end)/1_00(lam_data_dst_size:end), burn_vel_12_106_30_dst_size_orig./burn_vel_12_75_10_dst_size_origFit, 'ro', 'MarkerSize', plotMarkerSize, 'LineWidth', plotLineWidth);
plot(dust_conc_12_106_35_dst_size(lam_data_dst_size:end)/1_00(lam_data_dst_size:end), burn_vel_12_106_35_dst_size_orig./burn_vel_12_75_10_dst_size_origFit, 'gv', 'MarkerSize', plotMarkerSize, 'LineWidth', plotLineWidth);
plot(dust_conc_12_106_40_dst_size(lam_data_dst_size:end)/1_00(lam_data_dst_size:end)-1, burn_vel_12_106_40_dst_size_orig./burn_vel_12_75_10_dst_size_origFit(lam_data_dst_size:end-1), 'bh', 'MarkerSize', plotMarkerSize, 'LineWidth', plotLineWidth);

ylim([y_axisMin y_axisMax]);
hold off

% p = get(0, 'monitorpositions')
p=[1 1 1000 450;...
100 -270 850 2750];
set(gcf, 'position', p(2,:));

```

A3.5 - Plotting figure 4.14

```
% plot_ND_SLdivSLgasOnlyv01
% plot_ND_SLdivSLgasOnlyv02_6fig
% plot_ND_SLv03_6fig

legend_plot=0 ;
plotMarkerSize = 10;
plotLineWidth = 3 ;
testSize2 = 14 ;

% phi 0.8 ;
figure1 = figure('Name','NDim turbulent velocity');
axes1 = axes('Parent',figure1,'LineWidth',2,'FontWeight','bold',...
    'FontSize',22,...
    'FontName','Times New Roman');

hold on
%dummy plots to get the legend to have data markers and fitted curve lines
if legend_plot==1
plot(-1,-1,'rs','MarkerSize',plotMarkerSize,'LineWidth',plotLineWidth)
plot(-1,-1,'gs','MarkerSize',plotMarkerSize,'LineWidth',plotLineWidth)
plot(-1,-1,'bs','MarkerSize',plotMarkerSize,'LineWidth',plotLineWidth)

plot(-1,-1,'rv','MarkerSize',plotMarkerSize,'LineWidth',plotLineWidth)
plot(-1,-1,'gv','MarkerSize',plotMarkerSize,'LineWidth',plotLineWidth)
plot(-1,-1,'bv','MarkerSize',plotMarkerSize,'LineWidth',plotLineWidth)
legend('d=75,d_{st}=25','d=75,d_{st}=50','d=75,d_{st}=75',...
    'd=106,d_{st}=25','d=106,d_{st}=50','d=106,d_{st}=75',...
    'Location','eastoutside')
end
%

hold on

plot(u_prime_all./burn_vel_08_75_00_orig(1),burn_vel_08_75_00_orig./burn_vel_08_75_10_dst_size_origFit(1),'ks',
'LineWidth',plotLineWidth);
plot(u_prime_all./burn_vel_08_75_25_orig(1),burn_vel_08_75_25_orig./burn_vel_08_75_10_dst_size_origFit(2),'rs',
'LineWidth',plotLineWidth);
plot(u_prime_all./burn_vel_08_75_50_orig(1),burn_vel_08_75_50_orig./burn_vel_08_75_10_dst_size_origFit(3),'gs',
'LineWidth',plotLineWidth);
plot(u_prime_all(1:length(burn_vel_08_75_75_orig))./burn_vel_08_75_75_orig(1),burn_vel_08_75_75_orig./burn_
vel_08_75_10_dst_size_origFit(4),'bs','LineWidth',plotLineWidth);

plot(u_prime_all./burn_vel_10_75_00_orig(1),burn_vel_10_75_00_orig./burn_vel_10_75_10_dst_size_origFit(1),'k
d','LineWidth',plotLineWidth);
plot(u_prime_all./burn_vel_10_75_25_orig(1),burn_vel_10_75_25_orig./burn_vel_10_75_10_dst_size_origFit(2),'rd
','LineWidth',plotLineWidth);
plot(u_prime_all./burn_vel_10_75_50_orig(1),burn_vel_10_75_50_orig./burn_vel_10_75_10_dst_size_origFit(3),'g
d','LineWidth',plotLineWidth);
plot(u_prime_all./burn_vel_10_75_75_orig(1),burn_vel_10_75_75_orig./burn_vel_10_75_10_dst_size_origFit(4),'b
d','LineWidth',plotLineWidth);

plot(u_prime_all./burn_vel_12_75_00_orig(1),burn_vel_12_75_00_orig./burn_vel_12_75_10_dst_size_origFit(1),'k
^','LineWidth',plotLineWidth);
```

```

plot(u_prime_all./burn_vel_12_75_25_orig(1),burn_vel_12_75_25_orig./burn_vel_12_75_10_dst_size_origFit(2),'r^
','LineWidth',plotLineWidth);
plot(u_prime_all./burn_vel_12_75_50_orig(1),burn_vel_12_75_50_orig./burn_vel_12_75_10_dst_size_origFit(3),'g
^','LineWidth',plotLineWidth);
plot(u_prime_all./burn_vel_12_75_75_orig(1),burn_vel_12_75_75_orig./burn_vel_12_75_10_dst_size_origFit(4),'b
^','LineWidth',plotLineWidth);

ylim([1 4]);

C = 1.70;
n = .20;
u_prime_smooth = 0:(max(u_prime_all)-min(u_prime_all))/200:max(u_prime_all);
u_primeDivS_L=u_prime_smooth./burn_vel_12_75_75_orig(1);
S_T_eq_148=(1+C.*(u_primeDivS_L).^n);
plot(u_primeDivS_L,S_T_eq_148,'k-','LineWidth',plotLineWidth)

C = 2.2;
n = .20;
u_primeDivS_L=u_prime_smooth./burn_vel_08_75_50_orig(1);
S_T_eq_148=(1+C.*(u_primeDivS_L).^n);
plot(u_primeDivS_L,S_T_eq_148,'k-','LineWidth',plotLineWidth)

% axis([0.15 0.55 0.65 1.31])

% legend('08,75,00','08,75,25','08,75,50','08,75,75',...
% '08,106,00','08,106,25','08,106,50','08,106,75',...
% '10,75,00','10,75,25','10,75,50','10,75,75',...
% '10,106,00','10,106,25','10,106,50','10,106,75',...
% '12,75,00','12,75,25','12,75,50','12,75,75',...
% '12,106,00','12,106,25','12,106,50','12,106,75')
% legend('\lambda_{st}=0','\lambda_{st}=25','\lambda_{st}=50','\lambda_{st}=75 ',...
% '\lambda_{st}=0','\lambda_{st}=25','\lambda_{st}=50','\lambda_{st}=75 ',...
% '\lambda_{st}=0','\lambda_{st}=25','\lambda_{st}=50','\lambda_{st}=75 ',...
% '\lambda_{st}=0','\lambda_{st}=25','\lambda_{st}=50','\lambda_{st}=75 ',...
% '\lambda_{st}=0','\lambda_{st}=25','\lambda_{st}=50','\lambda_{st}=75 ')

% legend('\lambda=0','\lambda=25','\lambda=50','\lambda=75 ',...
% '\lambda=0','\lambda=25','\lambda=50','\lambda=75 ',...
% '\lambda=0','\lambda=25','\lambda=50','\lambda=75 ',...
% '\lambda=0','\lambda=25','\lambda=50','\lambda=75 ',...
% '\lambda=0','\lambda=25','\lambda=50','\lambda=75 ')

% p=[1 1 1000 450;...
% 1600 -270 1000 650];
p=[1 1 1000 450;...
10 -270 1000 650];
set(gcf,'position',p(2,:)) ;

error('autobreak')

```

```

plot(l_00,burn_vel_08_75_00_orig,'ks','LineWidth',plotLineWidth);
plot(l_00,burn_vel_08_75_25_orig,'ro','LineWidth',plotLineWidth);
plot(l_00,burn_vel_08_75_50_orig,'gv','LineWidth',plotLineWidth);
plot(l_00(1:length(burn_vel_08_75_75_orig)),burn_vel_08_75_75_orig,'bh','LineWidth',plotLineWidth);

% xlabel('(u"/u_{bar})(l_0/D_{pp})','FontSize',textSize);
% ylabel('(S_T/S_L)/(S_T/S_L)_{gas only} (phi=0.8)','FontSize',textSize)
%
errorbar(l_0,burn_vel_08_75_25./burn_vel_08_75_00,stanDev_BV_08_75_25./burn_vel_08_75_00,'rs','LineWidth',
plotLineWidth);
%
errorbar(l_0,burn_vel_08_75_50./burn_vel_08_75_00,stanDev_BV_08_75_50./burn_vel_08_75_00,'gs','LineWidth',
,plotLineWidth);
%
errorbar(l_0(1:length(burn_vel_08_75_75)),burn_vel_08_75_75./burn_vel_08_75_00(1:length(burn_vel_08_75_75)
),stanDev_BV_08_75_75./burn_vel_08_75_00(1:length(burn_vel_08_75_75)), 'bs','LineWidth',plotLineWidth);
%
%
errorbar(l_0,burn_vel_08_106_25./burn_vel_08_75_00,stanDev_BV_08_106_25./burn_vel_08_75_00,'rv','LineWid
th',plotLineWidth);
%
errorbar(l_0,burn_vel_08_106_50./burn_vel_08_75_00,stanDev_BV_08_106_50./burn_vel_08_75_00,'gv','LineWi
dth',plotLineWidth);
%
errorbar(l_0(1:length(burn_vel_08_106_75)),burn_vel_08_106_75./burn_vel_08_75_00(1:length(burn_vel_08_75_
75)),stanDev_BV_08_106_75./burn_vel_08_75_00(1:length(burn_vel_08_106_75)), 'bv','LineWidth',plotLineWid
th);

plot(l_0,burn_vel_08_106_00_orig,'ks','LineWidth',plotLineWidth);
plot(l_0,burn_vel_08_106_25_orig,'ro','LineWidth',plotLineWidth);
plot(l_0,burn_vel_08_106_50_orig,'gv','LineWidth',plotLineWidth);
plot(l_0(1:length(burn_vel_08_106_75_orig)),burn_vel_08_106_75_orig,'bh','LineWidth',plotLineWidth);

plot(l_0,burn_vel_10_75_00_orig,'ks','LineWidth',plotLineWidth);
plot(l_0,burn_vel_10_75_25_orig,'ro','LineWidth',plotLineWidth);
plot(l_0,burn_vel_10_75_50_orig,'gv','LineWidth',plotLineWidth);
plot(l_0,burn_vel_10_75_75_orig,'bh','LineWidth',plotLineWidth);

plot(l_00,burn_vel_10_106_00_orig,'ks','LineWidth',plotLineWidth);
plot(l_00,burn_vel_10_106_25_orig,'ro','LineWidth',plotLineWidth);
plot(l_00,burn_vel_10_106_50_orig,'gv','LineWidth',plotLineWidth);
plot(l_00(1:length(burn_vel_10_106_75_orig)),burn_vel_10_106_75_orig,'bh','LineWidth',plotLineWidth);

% plot(xfit_data,yfit_10_75_00,'k-', 'LineWidth',plotLineWidth)

% % plot(xfit_data,yfit_10_75_25./yfit_10_75_00,'r--','LineWidth',plotLineWidth)

```

```

% % plot(xfit_data,yfit_10_75_50./yfit_10_75_00,'g-', 'LineWidth',plotLineWidth)
% % plot(xfit_data,yfit_10_75_75./yfit_10_75_00,'b-', 'LineWidth',plotLineWidth)

% plot(xfit_data,yfit_10_106_25./yfit_10_75_00,'r--', 'LineWidth',plotLineWidth)
% plot(xfit_data,yfit_10_106_50./yfit_10_75_00,'g-', 'LineWidth',plotLineWidth)
% plot(xfit_data,yfit_10_106_75./yfit_10_75_00,'b-', 'LineWidth',plotLineWidth)
hold off
% xlabel('(u"/u_{bar})(l_0/D_{pp})',FontSize,textSize);
% ylabel('(S_T/S_L)/(S_T/S_L)_{gas only} (phi=1.0)',FontSize,textSize)
% axis([0.09 0.15 1 1.25])

% figure2 = figure;
% axes2 = axes('Parent',figure2,...
%   'YMinorTick','on',...
%   'XMinorTick','on',...
%   'FontSize',testSize2);
% hold on

if legend_plot==1
plot(-1,-1,'ks-', 'MarkerSize',plotMarkerSize, 'LineWidth',plotLineWidth)
plot(-1,-1,'rs--', 'MarkerSize',plotMarkerSize, 'LineWidth',plotLineWidth)
plot(-1,-1,'gs-', 'MarkerSize',plotMarkerSize, 'LineWidth',plotLineWidth)
plot(-1,-1,'bs-', 'MarkerSize',plotMarkerSize, 'LineWidth',plotLineWidth)
plot(-1,-1,'rv--', 'MarkerSize',plotMarkerSize, 'LineWidth',plotLineWidth)
plot(-1,-1,'gv-', 'MarkerSize',plotMarkerSize, 'LineWidth',plotLineWidth)
plot(-1,-1,'bv-', 'MarkerSize',plotMarkerSize, 'LineWidth',plotLineWidth)
legend('gas-only', 'd=75,d_{st}=25', 'd=75,d_{st}=50', 'd=75,d_{st}=75',...
      'd=106,d_{st}=25', 'd=106,d_{st}=50', 'd=106,d_{st}=75',...
      'Location','eastoutside')
end

%
subplot(3,2,5);
hold on
plot(l_0_12,burn_vel_12_75_00,'ks', 'LineWidth',plotLineWidth);
plot(l_0_12,burn_vel_12_75_25,'ro', 'LineWidth',plotLineWidth);
plot(l_0_12,burn_vel_12_75_50,'gv', 'LineWidth',plotLineWidth);
plot(l_0_12,burn_vel_12_75_75,'bh', 'LineWidth',plotLineWidth);

% C_12_00 = 40; n_12_00 = .25 ;
% Su_L_12_00 = burn_vel_12_75_00_orig(1) ;
% S_TL_12_00=((1+C_12_00.*(u_prime_all(2:end))./Su_L_12_00)).^n_12_00);
% plot(l_0_12,S_TL_12_00,'k-', 'LineWidth',plotLineWidth);
hold off
subplot(3,2,6);
hold on
plot(l_0_12,burn_vel_12_106_00,'ks', 'LineWidth',plotLineWidth);
plot(l_0_12,burn_vel_12_106_25,'ro', 'LineWidth',plotLineWidth);
plot(l_0_12,burn_vel_12_106_50,'gv', 'LineWidth',plotLineWidth);
plot(l_0_12(1:length(burn_vel_12_106_75)),burn_vel_12_106_75,'bh', 'LineWidth',plotLineWidth);
hold off

% p = get(0,'monitorpositions')
p=[1 1 1000 450;...
   1600 -270 1000 950];
set(gcf,'position',p(2,:)) ;

```

```

% plot(xfit_data,yfit_12_75_00,'k-', 'LineWidth',plotLineWidth)

% % plot(xfit_data,yfit_12_75_25./yfit_12_75_00,'r--','LineWidth',plotLineWidth)
% % plot(xfit_data,yfit_12_75_50./yfit_12_75_00,'g-', 'LineWidth',plotLineWidth)
% % plot(xfit_data,yfit_12_75_75./yfit_12_75_00,'b-', 'LineWidth',plotLineWidth)
% plot(xfit_data,yfit_12_106_25./yfit_12_75_00,'r--','LineWidth',plotLineWidth)
% plot(xfit_data,yfit_12_106_50./yfit_12_75_00,'g-', 'LineWidth',plotLineWidth)
% plot(xfit_data,yfit_12_106_75./yfit_12_75_00,'b-', 'LineWidth',plotLineWidth)

hold off
% xlabel('(u"/u_{bar})(l_0/D_{pp})','FontSize',textSize);
% ylabel('(S_T/S_L)/(S_T/S_L)_{gas only} (phi=1.2)','FontSize',textSize)
% axis([0.09 0.15 1 1.25])

```

A3.6 - Plotting figure 4.15

```
% plot_ND_SLdivSLgasOnlyv01
% plot_ND_SLdivSLgasOnlyv02_6fig
% plot_ND_SLv03_6fig

legend_plot=0 ;
plotMarkerSize = 10;
plotLineWidth = 3 ;
testSize2 = 14 ;

% phi 0.8 ;
figure1 = figure('Name','NDim turbulent velocity');
axes1 = axes('Parent',figure1,'LineWidth',2,'FontWeight','bold',...
    'FontSize',22,...
    'FontName','Times New Roman');

hold on
%dummy plots to get the legend to have data markers and fitted curve lines
if legend_plot==1
plot(-1,-1,'rs','MarkerSize',plotMarkerSize,'LineWidth',plotLineWidth)
plot(-1,-1,'gs','MarkerSize',plotMarkerSize,'LineWidth',plotLineWidth)
plot(-1,-1,'bs','MarkerSize',plotMarkerSize,'LineWidth',plotLineWidth)

plot(-1,-1,'rv','MarkerSize',plotMarkerSize,'LineWidth',plotLineWidth)
plot(-1,-1,'gv','MarkerSize',plotMarkerSize,'LineWidth',plotLineWidth)
plot(-1,-1,'bv','MarkerSize',plotMarkerSize,'LineWidth',plotLineWidth)
legend('d=75,d_{st}=25','d=75,d_{st}=50','d=75,d_{st}=75',...
    'd=106,d_{st}=25','d=106,d_{st}=50','d=106,d_{st}=75',...
    'Location','eastoutside')
end
%

hold on

%
plot(u_prime_all./burn_vel_08_75_00_orig(1),burn_vel_08_75_00_orig./burn_vel_08_75_00_orig(1),'ks','LineWidht
h',plotLineWidth);
%
plot(u_prime_all./burn_vel_08_75_25_orig(1),burn_vel_08_75_25_orig./burn_vel_08_75_25_orig(1),'rs','LineWidht
h',plotLineWidth);
%
plot(u_prime_all./burn_vel_08_75_50_orig(1),burn_vel_08_75_50_orig./burn_vel_08_75_50_orig(1),'gs','LineWidht
h',plotLineWidth);
%
plot(u_prime_all(1:length(burn_vel_08_75_75_orig))./burn_vel_08_75_75_orig(1),burn_vel_08_75_75_orig./burn_
vel_08_75_75_orig(1),'bs','LineWidth',plotLineWidth);

plot(u_prime_all./burn_vel_08_106_00_orig(1),burn_vel_08_106_00_orig./burn_vel_08_75_10_dst_size_origFit(1),
'kv','LineWidth',plotLineWidth);
plot(u_prime_all./burn_vel_08_106_25_orig(1),burn_vel_08_106_25_orig./burn_vel_08_75_10_dst_size_origFit(2),
'rv','LineWidth',plotLineWidth);
plot(u_prime_all./burn_vel_08_106_50_orig(1),burn_vel_08_106_50_orig./burn_vel_08_75_10_dst_size_origFit(3),
'gv','LineWidth',plotLineWidth);
```

```

plot(u_prime_all(1:length(burn_vel_08_106_75_orig))./burn_vel_08_106_75_orig(1),burn_vel_08_106_75_orig./bu
rn_vel_08_75_10_dst_size_origFit(4),'bv','LineWidth',plotLineWidth);

%
plot(u_prime_all./burn_vel_10_75_00_orig(1),burn_vel_10_75_00_orig./burn_vel_10_75_00_orig(1),'kd','LineWidt
h',plotLineWidth);
%
plot(u_prime_all./burn_vel_10_75_25_orig(1),burn_vel_10_75_25_orig./burn_vel_10_75_25_orig(1),'rd','LineWidt
h',plotLineWidth);
%
plot(u_prime_all./burn_vel_10_75_50_orig(1),burn_vel_10_75_50_orig./burn_vel_10_75_50_orig(1),'gd','LineWidt
h',plotLineWidth);
%
plot(u_prime_all./burn_vel_10_75_75_orig(1),burn_vel_10_75_75_orig./burn_vel_10_75_75_orig(1),'bd','LineWidt
h',plotLineWidth);

plot(u_prime_all./burn_vel_10_106_00_orig(1),burn_vel_10_106_00_orig./burn_vel_10_75_10_dst_size_origFit(1),
'ko','LineWidth',plotLineWidth);
plot(u_prime_all./burn_vel_10_106_25_orig(1),burn_vel_10_106_25_orig./burn_vel_10_75_10_dst_size_origFit(2),
'ro','LineWidth',plotLineWidth);
plot(u_prime_all./burn_vel_10_106_50_orig(1),burn_vel_10_106_50_orig./burn_vel_10_75_10_dst_size_origFit(3),
'go','LineWidth',plotLineWidth);
plot(u_prime_all(1:length(burn_vel_10_106_75_orig))./burn_vel_10_106_75_orig(1),burn_vel_10_106_75_orig./bu
rn_vel_10_75_10_dst_size_origFit(4),'bo','LineWidth',plotLineWidth);

%
plot(u_prime_all./burn_vel_12_75_00_orig(1),burn_vel_12_75_00_orig./burn_vel_12_75_00_orig(1),'k^','LineWidt
h',plotLineWidth);
%
plot(u_prime_all./burn_vel_12_75_25_orig(1),burn_vel_12_75_25_orig./burn_vel_12_75_25_orig(1),'r^','LineWidt
h',plotLineWidth);
%
plot(u_prime_all./burn_vel_12_75_50_orig(1),burn_vel_12_75_50_orig./burn_vel_12_75_50_orig(1),'g^','LineWidt
h',plotLineWidth);
%
plot(u_prime_all./burn_vel_12_75_75_orig(1),burn_vel_12_75_75_orig./burn_vel_12_75_75_orig(1),'b^','LineWidt
h',plotLineWidth);

plot(u_prime_all./burn_vel_12_106_00_orig(1),burn_vel_12_106_00_orig./burn_vel_12_75_10_dst_size_origFit(1),
'kh','LineWidth',plotLineWidth);
plot(u_prime_all./burn_vel_12_106_25_orig(1),burn_vel_12_106_25_orig./burn_vel_12_75_10_dst_size_origFit(2),
'rh','LineWidth',plotLineWidth);
plot(u_prime_all./burn_vel_12_106_50_orig(1),burn_vel_12_106_50_orig./burn_vel_12_75_10_dst_size_origFit(3),
'gh','LineWidth',plotLineWidth);
plot(u_prime_all(1:length(burn_vel_12_106_75_orig))./burn_vel_12_106_75_orig(1),burn_vel_12_106_75_orig./bu
rn_vel_12_75_10_dst_size_origFit(4),'bh','LineWidth',plotLineWidth);

C = 1.65;
n = .20;
u_prime_smooth = 0:(max(u_prime_all)-min(u_prime_all))/200:max(u_prime_all);
u_primeDivS_L=u_prime_smooth./burn_vel_12_75_75_orig(1);
S_T_eq_148=(1+C.*(u_primeDivS_L).^n);

```

```

plot(u_primeDivS_L,S_T_eq_148,'k-', 'LineWidth',plotLineWidth)

C = 2.00;
n = .20;
u_primeDivS_L=u_prime_smooth./burn_vel_08_75_50_orig(1);
S_T_eq_148=(1+C.*(u_primeDivS_L).^n);
plot(u_primeDivS_L,S_T_eq_148,'k-', 'LineWidth',plotLineWidth)

% axis([0.15 0.55 0.65 1.31])

% legend('08,75,00','08,75,25','08,75,50','08,75,75',...
% '08,106,00','08,106,25','08,106,50','08,106,75',...
% '10,75,00','10,75,25','10,75,50','10,75,75',...
% '10,106,00','10,106,25','10,106,50','10,106,75',...
% '12,75,00','12,75,25','12,75,50','12,75,75',...
% '12,106,00','12,106,25','12,106,50','12,106,75')
% legend('\lambda_{st}=0','\lambda_{st}=25','\lambda_{st}=50','\lambda_{st}=75 ',...
% '\lambda_{st}=0','\lambda_{st}=25','\lambda_{st}=50','\lambda_{st}=75 ')

% legend('\lambda=0','\lambda=25','\lambda=50','\lambda=75 ',...
% '\lambda=0','\lambda=25','\lambda=50','\lambda=75 ',...
% '\lambda=0','\lambda=25','\lambda=50','\lambda=75 ',...
% '\lambda=0','\lambda=25','\lambda=50','\lambda=75 ',...
% '\lambda=0','\lambda=25','\lambda=50','\lambda=75 ')

axis([0 2 1 4])
p=[1 1 1000 450;...
1600 -270 1000 650];
set(gcf,'position',p(2,:));

error('autobreak')

plot(l_00,burn_vel_08_75_00_orig,'ks','LineWidth',plotLineWidth);
plot(l_00,burn_vel_08_75_25_orig,'ro','LineWidth',plotLineWidth);
plot(l_00,burn_vel_08_75_50_orig,'gv','LineWidth',plotLineWidth);
plot(l_00(1:length(burn_vel_08_75_75_orig)),burn_vel_08_75_75_orig,'bh','LineWidth',plotLineWidth);

% xlabel('(u"/u_{bar})(l_0/D_{pp})','FontSize',textSize);
% ylabel('(S_T/S_L)/(S_T/S_L)_{gas only} (phi=0.8)','FontSize',textSize)
%
errorbar(l_0,burn_vel_08_75_25./burn_vel_08_75_00,stanDev_BV_08_75_25./burn_vel_08_75_00,'rs','LineWidth',
plotLineWidth);

```

```

%
errorbar(l_0,burn_vel_08_75_50./burn_vel_08_75_00,stanDev_BV_08_75_50./burn_vel_08_75_00,'gs','LineWidth'
,plotLineWidth);
%
errorbar(l_0(1:length(burn_vel_08_75_75)),burn_vel_08_75_75./burn_vel_08_75_00(1:length(burn_vel_08_75_75)
),stanDev_BV_08_75_75./burn_vel_08_75_00(1:length(burn_vel_08_75_75)),'bs','LineWidth',plotLineWidth);
%
%
errorbar(l_0,burn_vel_08_106_25./burn_vel_08_75_00,stanDev_BV_08_106_25./burn_vel_08_75_00,'rv','LineWid
th',plotLineWidth);
%
errorbar(l_0,burn_vel_08_106_50./burn_vel_08_75_00,stanDev_BV_08_106_50./burn_vel_08_75_00,'gv','LineWi
dth',plotLineWidth);
%
errorbar(l_0(1:length(burn_vel_08_106_75)),burn_vel_08_106_75./burn_vel_08_75_00(1:length(burn_vel_08_75_
75)),stanDev_BV_08_106_75./burn_vel_08_75_00(1:length(burn_vel_08_106_75)),'bv','LineWidth',plotLineWid
th);

plot(l_0,burn_vel_08_106_00_orig,'ks','LineWidth',plotLineWidth);
plot(l_0,burn_vel_08_106_25_orig,'ro','LineWidth',plotLineWidth);
plot(l_0,burn_vel_08_106_50_orig,'gv','LineWidth',plotLineWidth);
plot(l_0(1:length(burn_vel_08_106_75_orig)),burn_vel_08_106_75_orig,'bh','LineWidth',plotLineWidth);

plot(l_0,burn_vel_10_75_00_orig,'ks','LineWidth',plotLineWidth);
plot(l_0,burn_vel_10_75_25_orig,'ro','LineWidth',plotLineWidth);
plot(l_0,burn_vel_10_75_50_orig,'gv','LineWidth',plotLineWidth);
plot(l_0,burn_vel_10_75_75_orig,'bh','LineWidth',plotLineWidth);

plot(l_00,burn_vel_10_106_00_orig,'ks','LineWidth',plotLineWidth);
plot(l_00,burn_vel_10_106_25_orig,'ro','LineWidth',plotLineWidth);
plot(l_00,burn_vel_10_106_50_orig,'gv','LineWidth',plotLineWidth);
plot(l_00(1:length(burn_vel_10_106_75_orig)),burn_vel_10_106_75_orig,'bh','LineWidth',plotLineWidth);

% plot(xfit_data,yfit_10_75_00,'k-', 'LineWidth',plotLineWidth)

% % plot(xfit_data,yfit_10_75_25./yfit_10_75_00,'r--','LineWidth',plotLineWidth)
% % plot(xfit_data,yfit_10_75_50./yfit_10_75_00,'g-', 'LineWidth',plotLineWidth)
% % plot(xfit_data,yfit_10_75_75./yfit_10_75_00,'b:', 'LineWidth',plotLineWidth)

% plot(xfit_data,yfit_10_106_25./yfit_10_75_00,'r--','LineWidth',plotLineWidth)
% plot(xfit_data,yfit_10_106_50./yfit_10_75_00,'g-', 'LineWidth',plotLineWidth)
% plot(xfit_data,yfit_10_106_75./yfit_10_75_00,'b:', 'LineWidth',plotLineWidth)
hold off
% xlabel('(u"/u_{bar})(l_0/D_{pp})','FontSize',textSize);
% ylabel('(S_T/S_L)/(S_T/S_L)_{gas only} (phi=1.0)','FontSize',textSize)
% axis([0.09 0.15 1 1.25])

% figure2 = figure;
% axes2 = axes('Parent',figure2,...
% 'YMinorTick','on',...
% 'XMinorTick','on',...
% 'FontSize',testSize2);

```

```

% hold on

if legend_plot==1
plot(-1,-1,'ks-', 'MarkerSize',plotMarkerSize, 'LineWidth',plotLineWidth)
plot(-1,-1,'rs--', 'MarkerSize',plotMarkerSize, 'LineWidth',plotLineWidth)
plot(-1,-1,'gs-', 'MarkerSize',plotMarkerSize, 'LineWidth',plotLineWidth)
plot(-1,-1,'bs:', 'MarkerSize',plotMarkerSize, 'LineWidth',plotLineWidth)
plot(-1,-1,'rv--', 'MarkerSize',plotMarkerSize, 'LineWidth',plotLineWidth)
plot(-1,-1,'gv-', 'MarkerSize',plotMarkerSize, 'LineWidth',plotLineWidth)
plot(-1,-1,'bv:', 'MarkerSize',plotMarkerSize, 'LineWidth',plotLineWidth)
legend('gas-only', 'd=75,d_{st}=25', 'd=75,d_{st}=50', 'd=75,d_{st}=75',...
      'd=106,d_{st}=25', 'd=106,d_{st}=50', 'd=106,d_{st}=75',...
      'Location','eastoutside')
end

%
subplot(3,2,5);
hold on
plot(l_0_12,burn_vel_12_75_00,'ks', 'LineWidth',plotLineWidth);
plot(l_0_12,burn_vel_12_75_25,'ro', 'LineWidth',plotLineWidth);
plot(l_0_12,burn_vel_12_75_50,'gv', 'LineWidth',plotLineWidth);
plot(l_0_12,burn_vel_12_75_75,'bh', 'LineWidth',plotLineWidth);

% C_12_00 = 40; n_12_00 = .25 ;
% Su_L_12_00 = burn_vel_12_75_00_orig(1) ;
% S_TL_12_00=((1+C_12_00.*(u_prime_all(2:end)/Su_L_12_00)).^n_12_00);
% plot(l_0_12,S_TL_12_00,'k-', 'LineWidth',plotLineWidth);
hold off
subplot(3,2,6);
hold on
plot(l_0_12,burn_vel_12_106_00,'ks', 'LineWidth',plotLineWidth);
plot(l_0_12,burn_vel_12_106_25,'ro', 'LineWidth',plotLineWidth);
plot(l_0_12,burn_vel_12_106_50,'gv', 'LineWidth',plotLineWidth);
plot(l_0_12(1:length(burn_vel_12_106_75)),burn_vel_12_106_75,'bh', 'LineWidth',plotLineWidth);
hold off

% p = get(0,'monitorpositions')
p=[1 1 1000 450;...
   1600 -270 1000 950];
set(gcf,'position',p(2,:)) ;

% plot(xfit_data,yfit_12_75_00,'k-', 'LineWidth',plotLineWidth)

% % plot(xfit_data,yfit_12_75_25./yfit_12_75_00,'r--', 'LineWidth',plotLineWidth)
% % plot(xfit_data,yfit_12_75_50./yfit_12_75_00,'g-', 'LineWidth',plotLineWidth)
% % plot(xfit_data,yfit_12_75_75./yfit_12_75_00,'b:', 'LineWidth',plotLineWidth)
% plot(xfit_data,yfit_12_106_25./yfit_12_75_00,'r--', 'LineWidth',plotLineWidth)
% plot(xfit_data,yfit_12_106_50./yfit_12_75_00,'g-', 'LineWidth',plotLineWidth)
% plot(xfit_data,yfit_12_106_75./yfit_12_75_00,'b:', 'LineWidth',plotLineWidth)

hold off
% xlabel('(u"/u_{bar})(l_0/D_{pp})', 'FontSize',textSize);
% ylabel('(S_T/S_L)/(S_T/S_L)_{gas only} (phi=1.2)', 'FontSize',textSize)
% axis([0.09 0.15 1 1.25])

```

A3.7 - Creating arrays of test data as a function of dust concentration (Burn_vel_func_dst_part_sizev01)

```
% Burn_vel_func_dst_sizev01

if phi(a) == 0.8
    if particleSize == 106 && flowRate(a)==10
        dust_conc_08_106_10_dst_size(ct_3) = dust_conc(a) ;
        burn_vel_08_106_10_dst_size(ct_3) = Burning_velocity(a) ;
        ct_3 = ct_3 + 1;
    end
    if particleSize == 106 && flowRate(a)==30
        dust_conc_08_106_30_dst_size(ct_4) = dust_conc(a) ;
        burn_vel_08_106_30_dst_size(ct_4) = Burning_velocity(a) ;
        ct_4 = ct_4 + 1;
    end
    if particleSize == 106 && flowRate(a)==35
        dust_conc_08_106_35_dst_size(ct_5) = dust_conc(a) ;
        burn_vel_08_106_35_dst_size(ct_5) = Burning_velocity(a) ;
        ct_5 = ct_5 + 1;
    end
    if particleSize == 106 && flowRate(a)==40
        dust_conc_08_106_40_dst_size(ct_6) = dust_conc(a) ;
        burn_vel_08_106_40_dst_size(ct_6) = Burning_velocity(a) ;
        ct_6 = ct_6 + 1;
    end

    if particleSize == 75 && flowRate(a)==10
        dust_conc_08_75_10_dst_size(ct_7) = dust_conc(a) ;
        burn_vel_08_75_10_dst_size(ct_7) = Burning_velocity(a) ;
        ct_7 = ct_7 + 1;
    end
    if particleSize == 75 && flowRate(a)==30
        dust_conc_08_75_30_dst_size(ct_8) = dust_conc(a) ;
        burn_vel_08_75_30_dst_size(ct_8) = Burning_velocity(a) ;
        ct_8 = ct_8 + 1;
    end
    if particleSize == 75 && flowRate(a)==35
        dust_conc_08_75_35_dst_size(ct_9) = dust_conc(a) ;
        burn_vel_08_75_35_dst_size(ct_9) = Burning_velocity(a) ;
        ct_9 = ct_9 + 1;
    end
    if particleSize == 75 && flowRate(a)==40
        dust_conc_08_75_40_dst_size(ct_10) = dust_conc(a) ;
        burn_vel_08_75_40_dst_size(ct_10) = Burning_velocity(a) ;
        ct_10 = ct_10 + 1;
    end

end

if phi(a) == 1.0
    if particleSize == 106 && flowRate(a)==10
        dust_conc_10_106_10_dst_size(ct_11) = dust_conc(a) ;
        burn_vel_10_106_10_dst_size(ct_11) = Burning_velocity(a) ;
        ct_11 = ct_11 + 1;
    end
end
```

```

end
if particleSize == 106 && flowRate(a)==30
    dust_conc_10_106_30_dst_size(ct_12) = dust_conc(a) ;
    burn_vel_10_106_30_dst_size(ct_12) = Burning_velocity(a) ;
    ct_12 = ct_12 + 1;
end
if particleSize == 106 && flowRate(a)==35
    dust_conc_10_106_35_dst_size(ct_13) = dust_conc(a) ;
    burn_vel_10_106_35_dst_size(ct_13) = Burning_velocity(a) ;
    ct_13 = ct_13 + 1;
end
if particleSize == 106 && flowRate(a)==40
    dust_conc_10_106_40_dst_size(ct_14) = dust_conc(a) ;
    burn_vel_10_106_40_dst_size(ct_14) = Burning_velocity(a) ;
    ct_14 = ct_14 + 1;
end

if particleSize == 75 && flowRate(a)==10
    dust_conc_10_75_10_dst_size(ct_15) = dust_conc(a) ;
    burn_vel_10_75_10_dst_size(ct_15) = Burning_velocity(a) ;
    ct_15 = ct_15 + 1;
end
if particleSize == 75 && flowRate(a)==30
    dust_conc_10_75_30_dst_size(ct_16) = dust_conc(a) ;
    burn_vel_10_75_30_dst_size(ct_16) = Burning_velocity(a) ;
    ct_16 = ct_16 + 1;
end
if particleSize == 75 && flowRate(a)==35
    dust_conc_10_75_35_dst_size(ct_17) = dust_conc(a) ;
    burn_vel_10_75_35_dst_size(ct_17) = Burning_velocity(a) ;
    ct_17 = ct_17 + 1;
end
if particleSize == 75 && flowRate(a)==40
    dust_conc_10_75_40_dst_size(ct_18) = dust_conc(a) ;
    burn_vel_10_75_40_dst_size(ct_18) = Burning_velocity(a) ;
    ct_18 = ct_18 + 1;
end

if phi(a) == 1.2
    if particleSize == 106 && flowRate(a)==10
        dust_conc_12_106_10_dst_size(ct_19) = dust_conc(a) ;
        burn_vel_12_106_10_dst_size(ct_19) = Burning_velocity(a) ;
        ct_19 = ct_19 + 1;
    end
    if particleSize == 106 && flowRate(a)==30
        dust_conc_12_106_30_dst_size(ct_20) = dust_conc(a) ;
        burn_vel_12_106_30_dst_size(ct_20) = Burning_velocity(a) ;
        ct_20 = ct_20 + 1;
    end
    if particleSize == 106 && flowRate(a)==35
        dust_conc_12_106_35_dst_size(ct_21) = dust_conc(a) ;
        burn_vel_12_106_35_dst_size(ct_21) = Burning_velocity(a) ;
        ct_21 = ct_21 + 1;
    end
    if particleSize == 106 && flowRate(a)==40

```

```

dust_conc_12_106_40_dst_size(ct_22) = dust_conc(a) ;
burn_vel_12_106_40_dst_size(ct_22) = Burning_velocity(a) ;
ct_22 = ct_22 + 1;
end

if particleSize == 75 && flowRate(a)==10
dust_conc_12_75_10_dst_size(ct_23) = dust_conc(a) ;
burn_vel_12_75_10_dst_size(ct_23) = Burning_velocity(a) ;
ct_23 = ct_23 + 1;
end
if particleSize == 75 && flowRate(a)==30
dust_conc_12_75_30_dst_size(ct_24) = dust_conc(a) ;
burn_vel_12_75_30_dst_size(ct_24) = Burning_velocity(a) ;
ct_24 = ct_24 + 1;
end
if particleSize == 75 && flowRate(a)==35
dust_conc_12_75_35_dst_size(ct_25) = dust_conc(a) ;
burn_vel_12_75_35_dst_size(ct_25) = Burning_velocity(a) ;
ct_25 = ct_25 + 1;
end
if particleSize == 75 && flowRate(a)==40
dust_conc_12_75_40_dst_size(ct_26) = dust_conc(a) ;
burn_vel_12_75_40_dst_size(ct_26) = Burning_velocity(a) ;
ct_26 = ct_26 + 1;
end
end
end

```

A3.8 - Turbulent intensity calculation

```
clear all
close all
clc
format long

folderName = ('1mm perf plate - test data only');
filePath = ('E:\HFA test data\Turbulent Intensity measurements');

dname = [filePath '\ folderName] ;

%% Set up basic file name path to read
top_file      = [dname '\']           ; %Set up main database to open and look inside
ls_top_file   = ls(top_file)         ; %List Files inside main folder
c             = cellstr(ls_top_file)  ; %Turn cells from ls function into strings
cc           = c(3:length(c))        ; %Set up a matrix without the . and .. produces by the
ls function
S             = size(cc)              ; %Find the size of matrix containing names of files inside
of main database
a             = 1                    ; %This counter is set to 3 to account for the . and .. at the
beginning of each matrix created by ls
ct_01 = 1 ;
ct_02 = 1 ;
ct_03 = 1 ;
ct_04 = 1 ;
ct_05 = 1 ;
ct_06 = 1 ;
while a <= S(1)
    close all
    file      = char(cellstr([top_file char(cc(a))])) ; %File to be operated on
    data_n    = char(cc(a))
    fileName  = char(cc(a))           ;

    nozzleDiameter = 0.0145 ; %m
    flowRate = str2num(fileName(12:13)) ;
    position = str2num(fileName(17));
    height = str2num(fileName(22:23));

    nozzleArea = pi()/4*nozzleDiameter^2;
    vel_flow = flowRate./(60000*nozzleArea); % [m/s] velocity based on flow rate in tube
    vel_flow_save(a,1) = vel_flow ;
    fileToRead1 = [dname '\ fileName] ;
    newData1 = importdata(fileToRead1);
    vars = fieldnames(newData1);
    for i = 1:length(vars)
        assignin('base', vars{i}, newData1.(vars{i}));
    end

    %% calculate rms value
    num_samples = 100000;
```

```

time = data(1:num_samples,1); %[s] time stamp
E_all = data(1:num_samples,2); %[volts] voltage from anemometer
E = E_all ;
E_bar = mean(E); %[volts] average voltage
E_bar_save(a,1) = E_bar ;
% cal_factor = vel_flow./E_bar ; % [(m/s)/volts]

u = 0.000215*exp(7.918735*E) ; %[m/s]
u_bar = mean(u) ;

u_prime = u - u_bar ;

u_prime_max = max(abs(u_prime));
% RMS_TIME=sqrt(sum(T_Time.*T_Time)/length(T_Time))

% u_prime_rms2 = sqrt(sum(u_prime.*u_prime)/length(u_prime))
u_prime_rms = sqrt(mean(u_prime.^2)) ;
u_prime_rms_save(a)=u_prime_rms ;
% [ACF] = acf(u_prime, (1000)) ;
% l_0 = u_bar.*sum(ACF);

% auto_corr=xcorr(u_prime,u_prime,10000);
% l_0 = u_bar.*sum(auto_corr(length(auto_corr)/2:end))*1/100000

T_1 = u' ;
T_2 = T_1 ;
% offset = 0 ;
% T_1 = sin(0:0.01:pi()) ; %C First temperature profile - left
% T_2(offset+1:length(T_1)) = T_1(1:(length(T_1)-offset)) ;
%
maxlag = 1000 ; % maximum size of sampling lag
window_size = length(T_1)-2*(maxlag+1) ; % length of data profile to use

T_1s = T_1(maxlag+1:maxlag+window_size) ; % create 1st correlated profile
T_1s = T_1s - mean(T_1) ; % Normalizing the temperature profile
sigma_13 = std(T_1)*std(T_2) ; % Calculating standard deviation

CCC1 = zeros(maxlag+1,1) ; % create initial CC coefficient matrix
%% Cross Correlation claculations
for i = 0:maxlag
    T_2s = T_2(i+maxlag+1:i+maxlag+window_size) ;
    T_2s = T_2s - mean(T_2) ;

    CCC1(i+maxlag+1) = (T_2s*T_1s)/(length(T_2s)*sigma_13) ; % Cross correlation 1st side
% CCC1(i+1) = (T_2s*T_1s)/(mean(T_1)^2) ; % Cross correlation 1st side

end

% lag_spacing = (1:2*maxlag+1) - (maxlag+1) ; % Create matrix is lag spacings

%% Plot Comparison
close all
figure
plot(CCC1)
ylabel('Correlation Coefficient')

```

```

pause(0.2)

l_02(a) = u_bar.*sum(CCC1)*1/100000 ;
l_0=l_02(a);

if position == 1 && height==0
    Turb_int_pos1_ht0(ct_01,1) = u_prime_rms ;
    u_prime_max_pos1_ht0(ct_01,1) = u_prime_max ;
    l_0_pos1_ht0(ct_01,1)=l_0;
    ct_01 = ct_01 +1;
elseif position == 3 && height==0
    Turb_int_pos3_ht0(ct_02,1) = u_prime_rms ;
    u_prime_max_pos3_ht0(ct_02,1) = u_prime_max ;
    l_0_pos3_ht0(ct_02,1)=l_0;
    ct_02 = ct_02 +1;
elseif position == 6 && height==0
    Turb_int_pos6_ht0(ct_03,1) = u_prime_rms ;
    u_prime_max_pos6_ht0(ct_03,1) = u_prime_max ;
    l_0_pos6_ht0(ct_03,1)=l_0;
    ct_03 = ct_03 +1;
elseif position == 1 && height==3
    Turb_int_pos1_ht3(ct_04,1) = u_prime_rms ;
    u_prime_max_pos1_ht3(ct_04,1) = u_prime_max ;
    l_0_pos1_ht3(ct_04,1)=l_0;
    ct_04 = ct_04 +1;
elseif position == 3 && height==3
    Turb_int_pos3_ht3(ct_05,1) = u_prime_rms ;
    u_prime_max_pos3_ht3(ct_05,1) = u_prime_max ;
    l_0_pos3_ht3(ct_05,1)=l_0;
    ct_05 = ct_05 +1;
elseif position == 6 && height==3
    Turb_int_pos6_ht3(ct_06,1) = u_prime_rms ;
    u_prime_max_pos6_ht3(ct_06,1) = u_prime_max ;
    l_0_pos6_ht3(ct_06,1)=l_0;
    ct_06 = ct_06 +1;
end

%%%%%%%%%%%%%%%%%%%%%%%%%%%%%%%%%%%%%%%%%%%%%%%%%%%%%%%%%%%%%%%%%%%%%%%%

a                = a+1
end

```

A3.9 - Gas analysis data retrieval

```
% Pulls in max of 3600 header lines used to get data, shouldn't been  
% collecting for more than an hour anyway.
```

```
clear all  
close all  
clc
```

```
fileName = ('120411_phi_1_test_matlab_capture.TXT');  
filePath = ('J:\Terribite Drive Documents\My Documents Folder - Copied\2 WPI research\Turbulent flame\Hybrid  
Flame Analyzer (HFA)\Gas Analyser - Hyperterminal');
```

```
fileToRead1 = [filePath '\ ' fileName];
```

```
DELIMITER = '\t';  
HEADERLINES = 3600;
```

```
% Import the file
```

```
rawData1 = importdata(fileToRead1, DELIMITER, HEADERLINES);  
rawData1_cell = cellstr(rawData1);
```

```
for ct_1 = 1:length(rawData1_cell)  
    dataOneLine = cell2mat(rawData1_cell(ct_1));  
    oxygenPercent(ct_1,1) = str2num(dataOneLine(46:50)) ;  
end
```

A3.10 - plotAverage_noplot

Note: This is a modified code from the matlab central exchange and was not originally written by the author.

```
function [avgH, avgData] = plotAverage(handleOrData, avgPoints, varargin)
%PLOT AVERAGE plots an average line into a plot (and more)
%
% SYNOPSIS: [avgH, avgData] = plotAverage(handleOrData, avgPoints, parameterName, parameterValue, ...)
%
% INPUT handleOrData: handle to figure or axes of the plot to average. Can
%     be vectors of figures or of axes handles. In a figure with
%     multiple subplots, the average is calculated for each subplot
%     individually.
%     Alternatively, provide a cell array with {x1,y1,x2,y2...},
%     where xi/yi are vectors of different data sets. With the latter
%     form, a plot is generated with figure,plot(x1,y1,x2,y2...).
%     Optional. If empty, plotAverage calls(gcf) to find the current
%     figure.
% avgPoints: points on the x-axis (or y-axis, see below) where the
%     average is to be calculated.
%     If empty, the points are selected by locally clustering data
%     points and robustly averaging of the position within each
%     cluster. This works best if the data on the corresponding axes
%     indeed cluster into more or less evenly spaced clusters. If
%     this is not the case, it is probably better to input avgPoints.
%     If avgPoints is a scalar N, the axis is split into N equally
%     spaced points between the minimum and the maximum of the data
%     (excluding the minimum and maximum).
%     Note: If you want to specify separate avgPoints for each of the
%     axes handles passed to plotAverage, pass avgPoints as a cell
%     array.
%
% plotAverage supports the following parameterName/parameterValue
%     pairs
% addErrorBars: if 1, error bars are added, if 0, not. Default: 1
% horzAvg: if 1, average is calculated horizontally (along x) instead
%     of vertically. Default: 0.
% interpMethod: interpolation method for estimating data values in
%     between support points. See 'help interp1' for supported
%     methods. Default: 'linear'.
%     Use interpMethod='hist' if you want to take the average of
%     all points in the vicinity of the data (good for scattered data
%     points)
% plot2NewFigure: if 1, average is plotted in separate figure. If 0,
%     average is plotted on top of the individual data lines. If 2
%     (or an axes handle), the average lines of all the plots are
%     collected in the same figure. Default: 0.
% useRobustMean: if 1, the robust mean is taken (discarding outliers)
%     for the average curve. If 0, the normal mean is used.
%     Default: 1.
% plotSEM: if 1, SEM, if 0, the standard deviation is plotted.
%     Default: 1
%
% OUTPUT avgH: handle(s) to average line, plus errorbar handle if
%     applicable
%     avgData: cell array with [x,y,err,n] array of x-values, y-values,
```



```

        legendIdx = strcmp('legend',get(chH,'Tag'));
        ahList = [ahList;chH(~legendIdx)]; %#ok<*AGROW>
    end
end
end
if isempty(ahList)
    error('no valid axes handles found in handleOrData or children thereof')
end

% check for other optional inputs
if nargin < 2
    avgPoints = [];
end

if ~isEven(length(varargin))
    error('options must be specified as parameter name/parameter value pairs')
end
for i=1:2:length(varargin)
    opt.(varargin{i}) = varargin{i+1};
end

% turn off robutsMean-warning
oldWarn = warning;
warning off ROBUSTMEAN:INSUFFICIENTDATA

%% CALCULATE AVERAGE

nAh = length(ahList);
data(1:nAh) = struct('xData',[],'yData',[],'avgPoints',avgPoints,'ahIn',num2cell(ahList),'ahOut',[],'avgData',[]);

for ia = nAh:-1:1 % count down in case we remove entries
    % find data in axes
    chH = get(data(ia).ahIn,'Children');
    % remove errorBars, not-lines
    chH(~strcmp('line',get(chH,'Type')) | ismember(get(chH,'Tag',{'errorBar':'avg'}))) = [];
    if isempty(chH)
        % if no valid children, discard axes
        data(ia) = [];
    else
        % get data
        if length(chH) == 1
            data(ia).xData = {get(chH,'XData')};
            data(ia).yData = {get(chH,'YData')};
        else
            data(ia).xData = get(chH,'XData');
            data(ia).yData = get(chH,'YData');
        end
    end
end
end

nData = length(data);
if nData < 1
    error('no line plots found in the axes provided')
end
end

```

```

% determine x- (or y-) points for calculating the average
for id = 1:nData
    if isempty(data(id).avgPoints)
        if opt.horzAvg
            % collect y
            pts = cat(2,data(id).yData{:});
        else
            % collect x
            pts = cat(2,data(id).xData{:});
        end
        % cluster - keep multiples for averaging
        % pts = unique(pts);
        d = pdist(pts); % follow TMW notation
        Z = linkage(d);
        % cutoff is half the average step size
        % Of course, this could theoretically lead to too wide spacing.
        % However, if there are many points that overlap REALLY well,
        % robustMean gives a cutoff that is way too low.
        cutoff = mean(diff(unique(pts)))/2;
        clust = cluster(Z,'cutoff',cutoff,'criterion','distance');
        % for every cluster, calculate mean
        tmp = NaN(max(clust),1);
        for c=1:max(clust)
            tmp(c) = robustMean(pts(clust==c));
        end
        % remove NaN, sort
        data(id).avgPoints = sort(tmp(isfinite(tmp)));
    elseif isscalar(data(id).avgPoints)
        if opt.horzAvg
            % collect y
            pts = cat(2,data(id).yData{:});
        else
            % collect x
            pts = cat(2,data(id).xData{:});
        end
        % linearly space N points
        data(id).avgPoints = linspace(min(pts),max(pts),data(id).avgPoints+2);
        data(id).avgPoints([1,end]) = [];
    end

    % now that we know the location, get the value of the average
    nLines = length(data(id).xData);
    avgTmp = NaN(length(data(id).avgPoints),nLines);
    stdTmp = avgTmp;
    for d = 1:nLines
        % if there are multiple 'abscissa'-points with the same value,
        % interpolation fails. Thus, pick the first point if necessary
        if opt.horzAvg
            xx = data(id).yData{d};yy=data(id).xData{d};
        else
            xx = data(id).xData{d};yy=data(id).yData{d};
        end

        if strcmp(opt.interpMethod,'hist')
            % associate points in xx with averagePoints.
            avgPoints = data(id).avgPoints(:);

```

```

meanDelta = mean(diff(avgPoints));
avgPoints = [avgPoints-meanDelta/2;avgPoints(end)+meanDelta/2];
[n,binIdx] = histc(xx,avgPoints);
goodIdx = binIdx>0;

% use accumarray to get average (yes!)
if opt.useRobustMean
    avgTmp(:,d) = accumarray(binIdx(goodIdx)',yy(goodIdx)',[],@robustMean);
    stdTmp(:,d) = accumarray(binIdx(goodIdx)',yy(goodIdx)',[],@robustStd);
else
    avgTmp(:,d) = accumarray(binIdx(goodIdx)',yy(goodIdx)',[],@mean);
    stdTmp(:,d) = accumarray(binIdx(goodIdx)',yy(goodIdx)',[],@std);
end
end
else
% make unique
[xx,uidx] = unique(xx);
yy = yy(uidx);
% remove NaNs
anyNaN = isnan(xx) | isnan(yy);
xx(anyNaN) = [];
yy(anyNaN) = [];
% interpolate
if length(xx)>3 && length(yy)>3
avgTmp(:,d) = interp1(xx,yy,data(id).avgPoints',opt.interpMethod)';
end
end
end
if nLines == 1 && strcmp(opt.interpMethod,'hist')
    data(id).avgData(:,1) = avgTmp;
    data(id).avgData(:,2) = stdTmp;
    data(id).avgData(:,3) = 1;
elseif opt.useRobustMean && nLines > 4
    [data(id).avgData(:,1),data(id).avgData(:,2),iid] = robustMean(avgTmp,2);
    ctMat = zeros(size(avgTmp));
    ctMat(iid) = 1;
    data(id).avgData(:,3) = sum(ctMat,2);
else
    data(id).avgData(:,1) = nanmean(avgTmp,2);
    data(id).avgData(:,2) = nanstd(avgTmp,0,2);
    data(id).avgData(:,3) = nLines;
end
end
end

%% PLOT AVERAGE

% open a global figure if necessary, otherwise start the plotting loop
if opt.plot2NewFigure == 2
    %outFh = figure('name','collected averages');
    outAh = axes('nextPlot','add');
end
avgH = zeros(nData,1 + opt.addErrorBars);

for id = 1:nData
    % find out where to plot
    switch opt.plot2NewFigure
        case 0

```

```

    data(id).ahOut = data(id).ahIn;
    set(data(id).ahOut,'NextPlot','add');
case 1
    %outFh = figure;
    data(id).ahOut = axes;
case 2
    data(id).ahOut = outAh;
otherwise
    % check whether an axes handle has been supplied
    if ishandle(opt.plot2NewFigure) && strcmp(get(opt.plot2NewFigure,'type'),'axes')
        data(id).ahOut = opt.plot2NewFigure;
    else
        error('unsupported option for plot2newFigure')
    end
end

% plot
if opt.addErrorBars
    err = data(id).avgData(:,2);
    if opt.plotSEM
        err = err ./ sqrt(data(id).avgData(:,3));
    end
end
if opt.horzAvg
%     avgH(id,1) = plot(data(id).ahOut,data(id).avgData(:,1),data(id).avgPoints,'k','LineWidth',2,'Tag','avg');
    if opt.addErrorBars
%         errH =
myErrorbar(data(id).ahOut,data(id).avgData(:,1),data(id).avgPoints,[err;NaN(length(data(id).avgPoints),1);]);
        delete(errH(1));
        avgH(id,2) = errH(2);
    end
else
%     avgH(id,1) = plot(data(id).ahOut,data(id).avgPoints,data(id).avgData(:,1),'k','LineWidth',2,'Tag','avg');
    if opt.addErrorBars
%         avgH(id,2) = myErrorbar(data(id).ahOut,data(id).avgPoints,data(id).avgData(:,1),err);
    end
end

% set legend name
% set(avgH(id,1),'DisplayName','Average line')

end % loop data to plot

%% CLEANUP
warning(oldWarn)
if nargout == 0
    clear avgH
end
if nargout > 1
    for id = nData:-1:1
        avgData{id} = [data(id).avgPoints(:),data(id).avgData];
    end
end
end

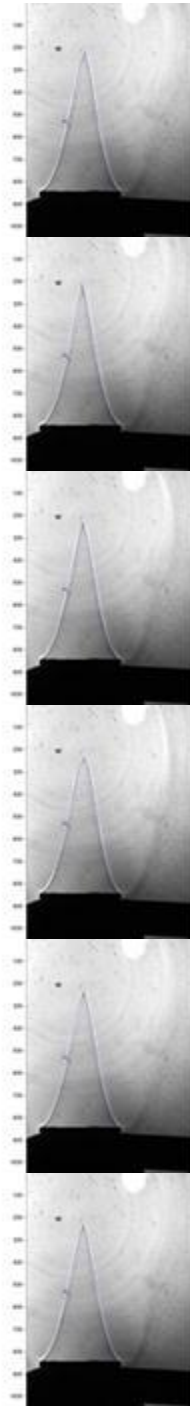
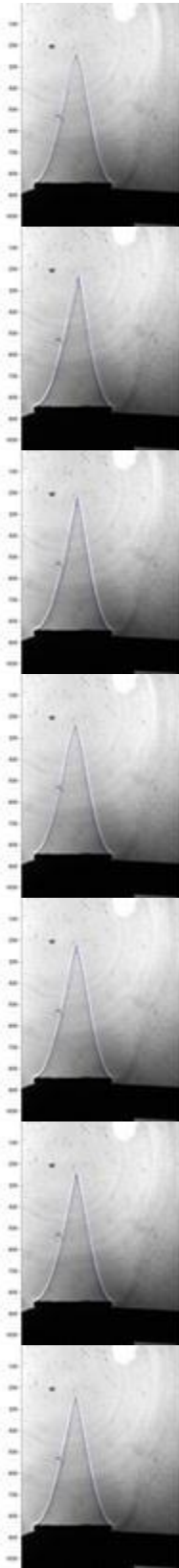
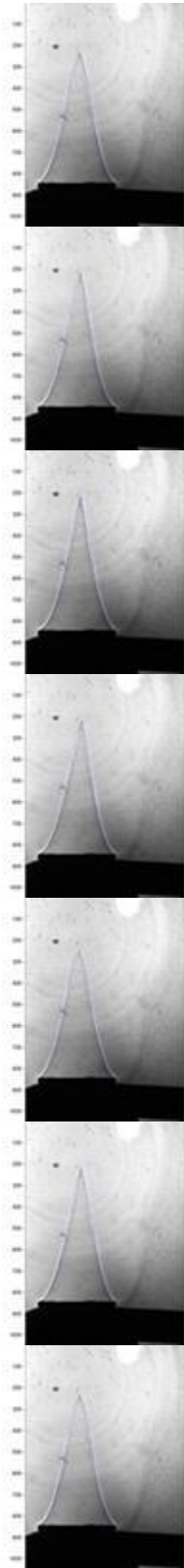
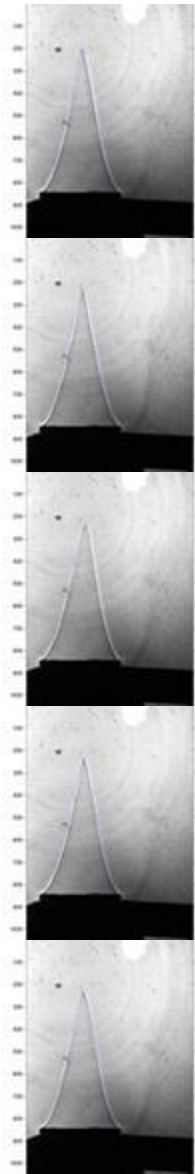
```

Appendix 4: Error Bar values – standard deviation of velocity calculation

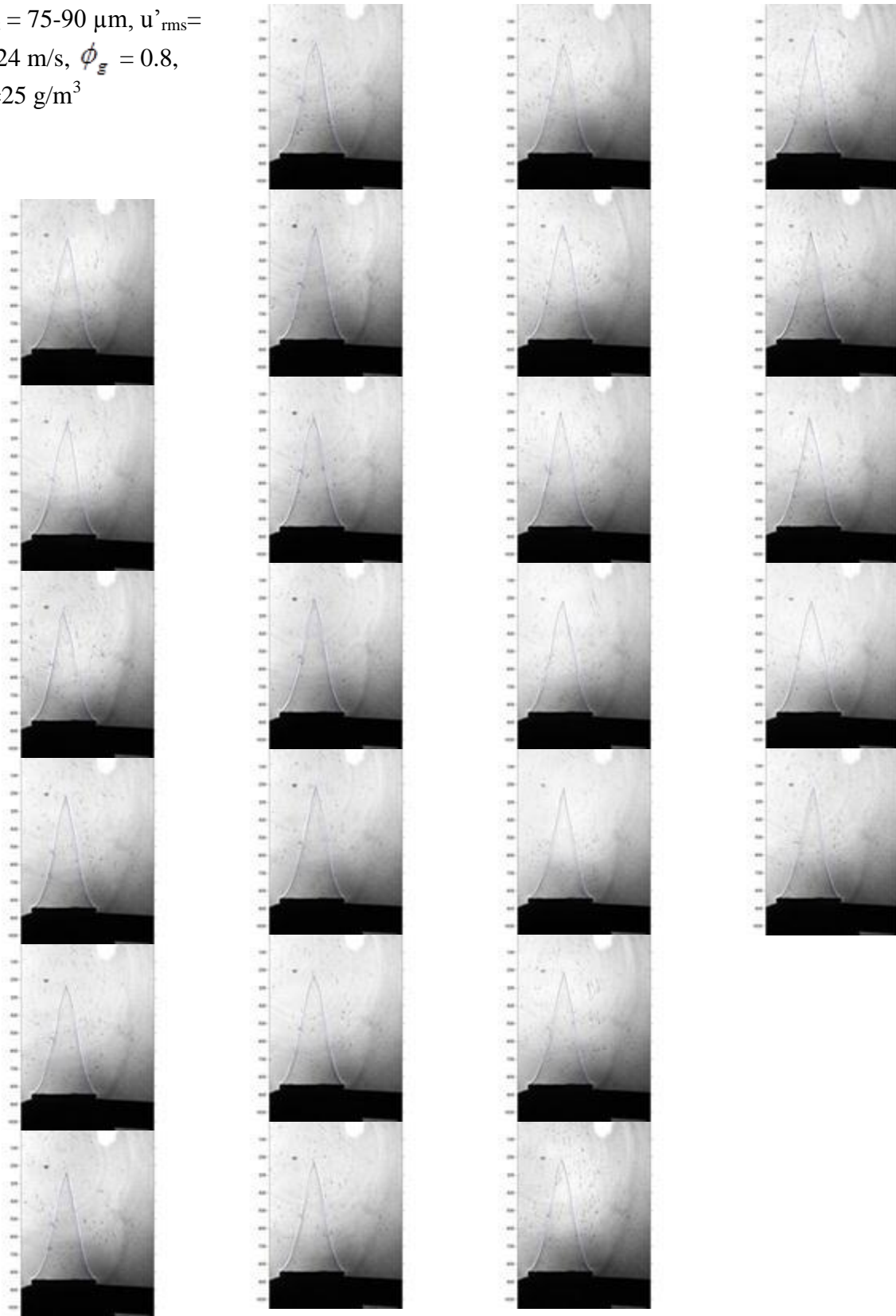
			Velocity (m/s)				Standard Deviation			
			Turbulent Intensity				Turbulent Intensity			
λ_{st}	d_{st}	ϕ_g	0.021	0.185	0.3352	0.532	0.021	0.185	0.3352	0.532
(g/m3)	(μm)		(m/s)				(m/s)			
0	75-90	0.8	0.319	0.827	0.891	1.024	0.007	0.078	0.166	0.096
		1	0.413	0.921	1.053	1.088	0.008	0.108	0.116	0.090
		1.2	0.298	0.706	0.726	0.821	0.006	0.107	0.054	0.063
	106-125	0.8	0.319	0.827	0.891	1.024	0.007	0.078	0.166	0.096
		1	0.413	0.921	1.053	1.088	0.008	0.108	0.116	0.090
		1.2	0.298	0.706	0.726	0.821	0.006	0.107	0.054	0.063
25	75-90	0.8	0.280	0.878	0.931	1.014	0.005	0.096	0.308	0.102
		1	0.401	1.008	1.105	1.190	0.010	0.085	0.157	0.115
		1.2	0.294	0.728	0.737	0.835	0.010	0.074	0.048	0.084
	106-125	0.8	0.325	0.847	0.868	0.903	0.006	0.075	0.106	0.117
		1	0.404	0.941	1.020	1.035	0.008	0.127	0.099	0.076
		1.2	0.315	0.694	0.801	0.829	0.007	0.074	0.076	0.093
50	75-90	0.8	0.272	0.864	0.896	0.975	0.006	0.099	0.098	0.081
		1	0.398	1.042	1.073	1.162	0.011	0.154	0.071	0.125
		1.2	0.286	0.707	0.796	0.805	0.007	0.071	0.087	0.170
	106-125	0.8	0.300	0.835	0.806	0.908	0.009	0.082	0.061	0.071
		1	0.427	0.919	0.964	1.108	0.208	0.077	0.113	0.087
		1.2	0.293	0.678	0.830	0.880	0.007	0.059	0.080	0.075
75	75-90	0.8	0.285	0.919	0.873		0.010	0.098	0.109	
		1	0.400	1.028	1.109	1.279	0.011	0.427	0.084	0.119
		1.2	0.266	0.733	0.762	0.877	0.011	0.461	0.732	0.093
	106-125	0.8	0.308	0.821	0.787		0.016	0.082	0.061	
		1	0.390	0.883	0.991		0.196	0.070	0.057	
		1.2	0.297	0.693	0.832		0.014	0.075	0.067	

Appendix 5:

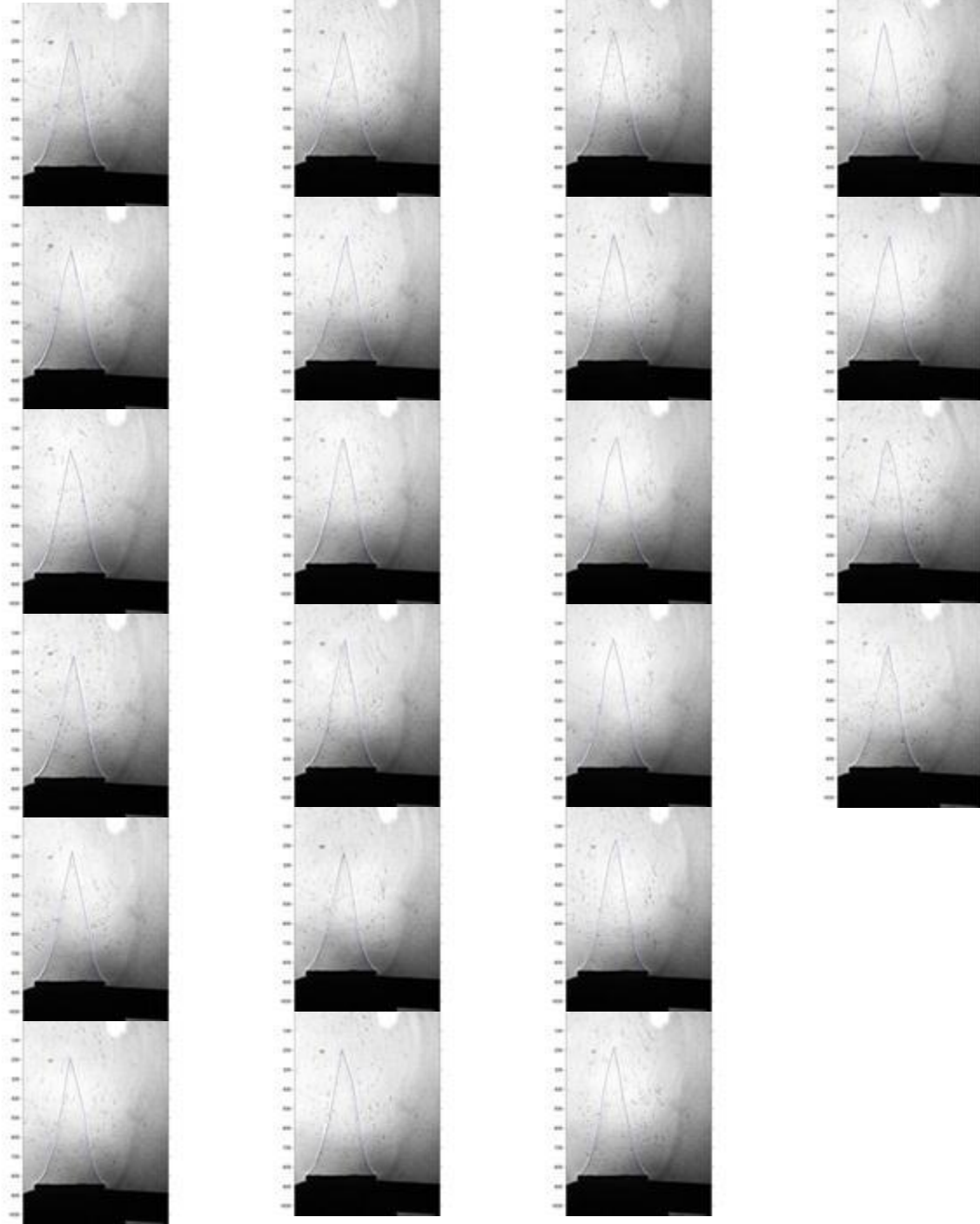
Flame Images $d_{st} = 75-90 \mu\text{m}$, $u'_{rms} = 0.024$ m/s, $\phi_g = 0.8$, $\lambda_{st} = 0$ g/m³



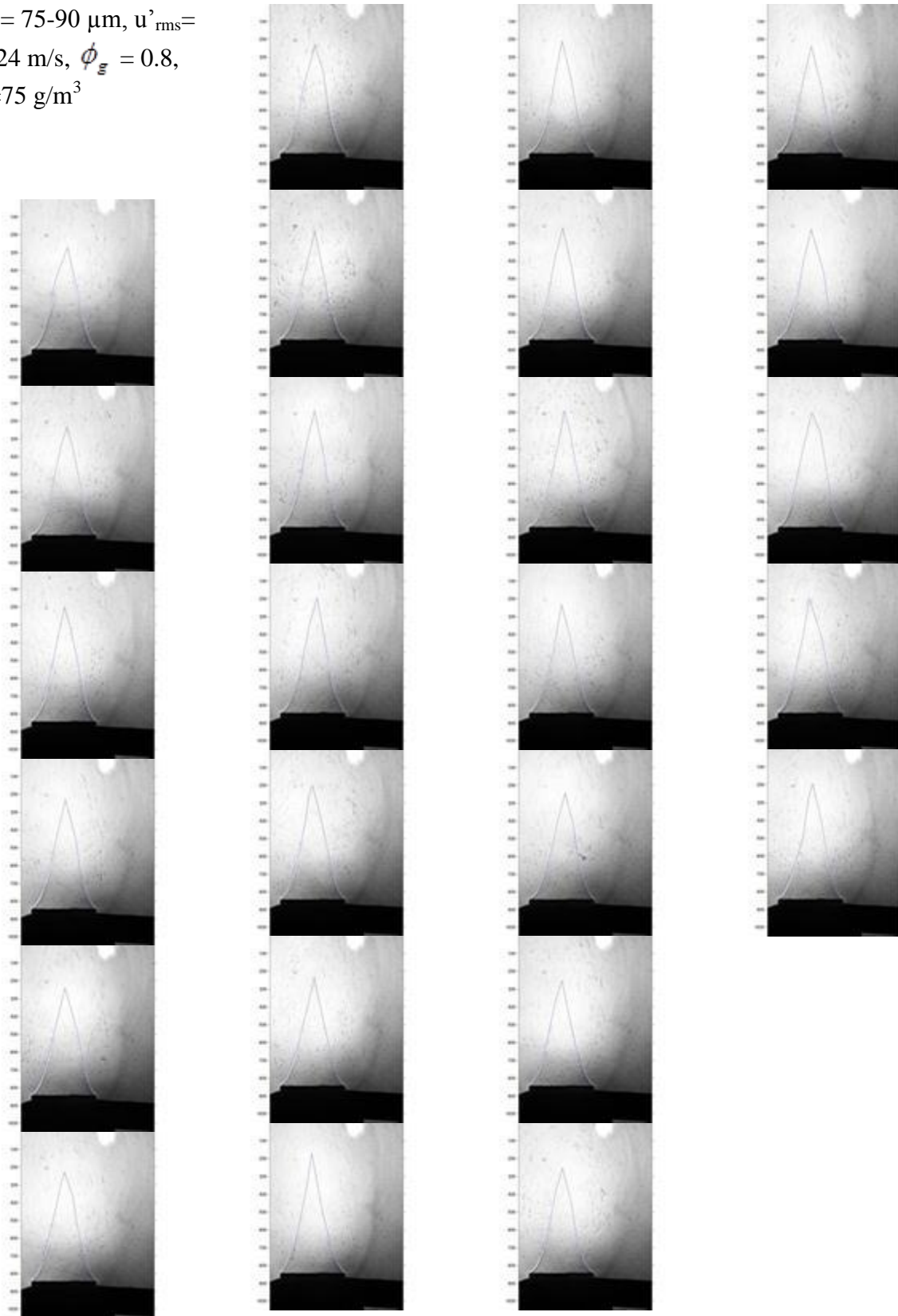
$d_{st} = 75-90 \mu\text{m}$, $u'_{rms} =$
 0.024 m/s , $\phi_g = 0.8$,
 $\lambda_{st} = 25 \text{ g/m}^3$



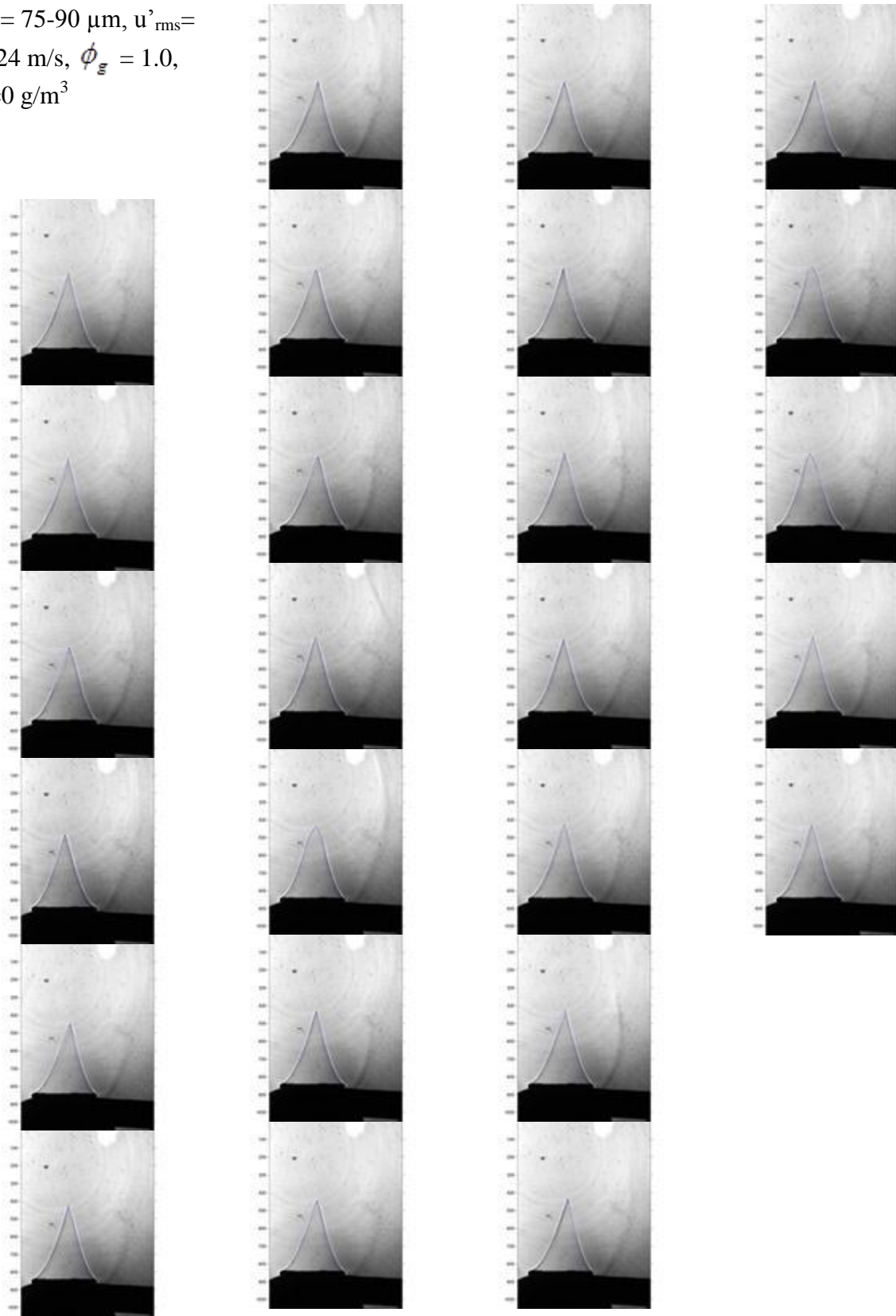
$d_{st} = 75-90 \mu\text{m}$, $u'_{rms} =$
 0.024 m/s , $\phi_g = 0.8$,
 $\lambda_{st} = 50 \text{ g/m}^3$



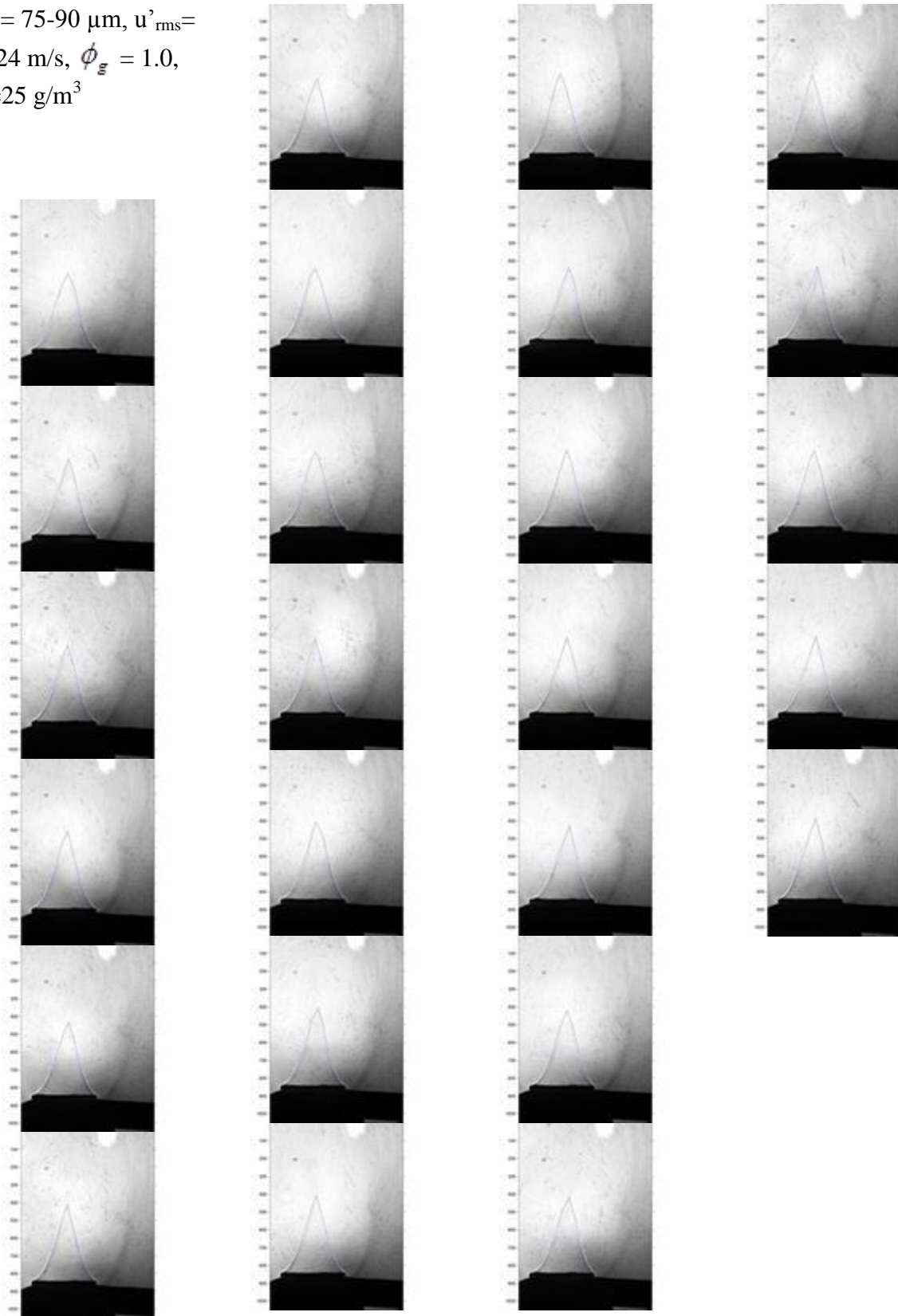
$d_{st} = 75-90 \mu\text{m}$, $u'_{\text{rms}} =$
 0.024 m/s , $\phi_g = 0.8$,
 $\lambda_{st} = 75 \text{ g/m}^3$



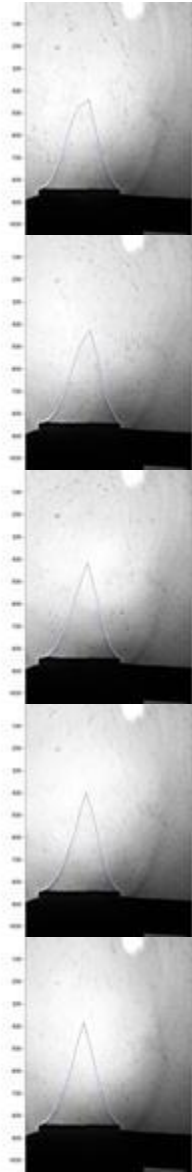
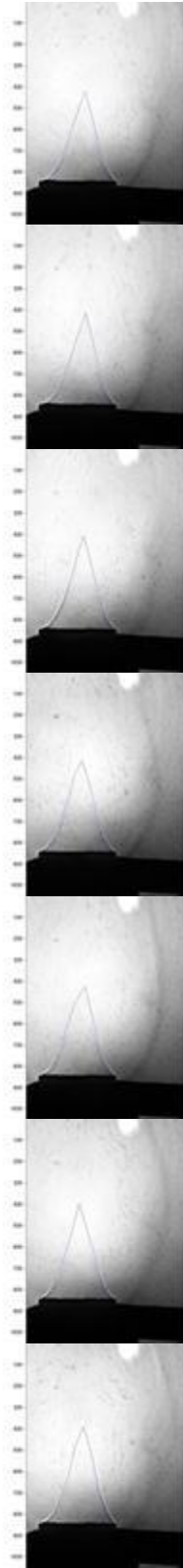
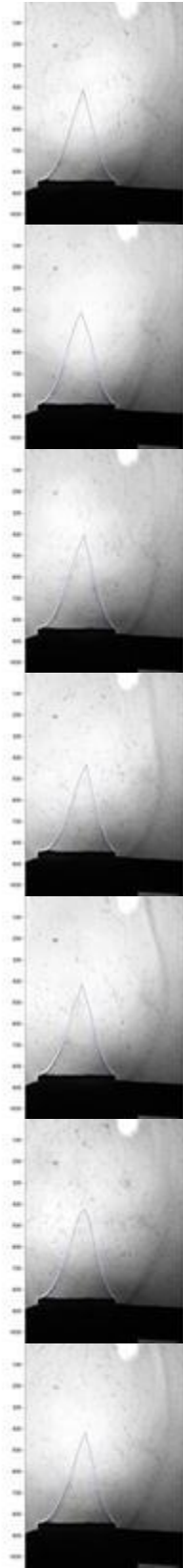
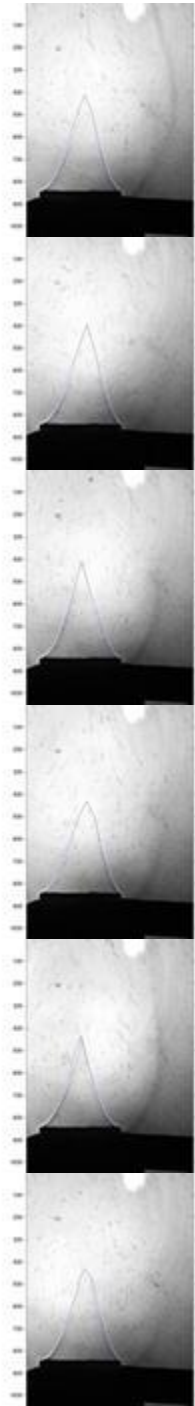
$d_{st} = 75-90 \mu\text{m}$, $u'_{\text{rms}} =$
 0.024 m/s , $\phi_g = 1.0$,
 $\lambda_{st} = 0 \text{ g/m}^3$



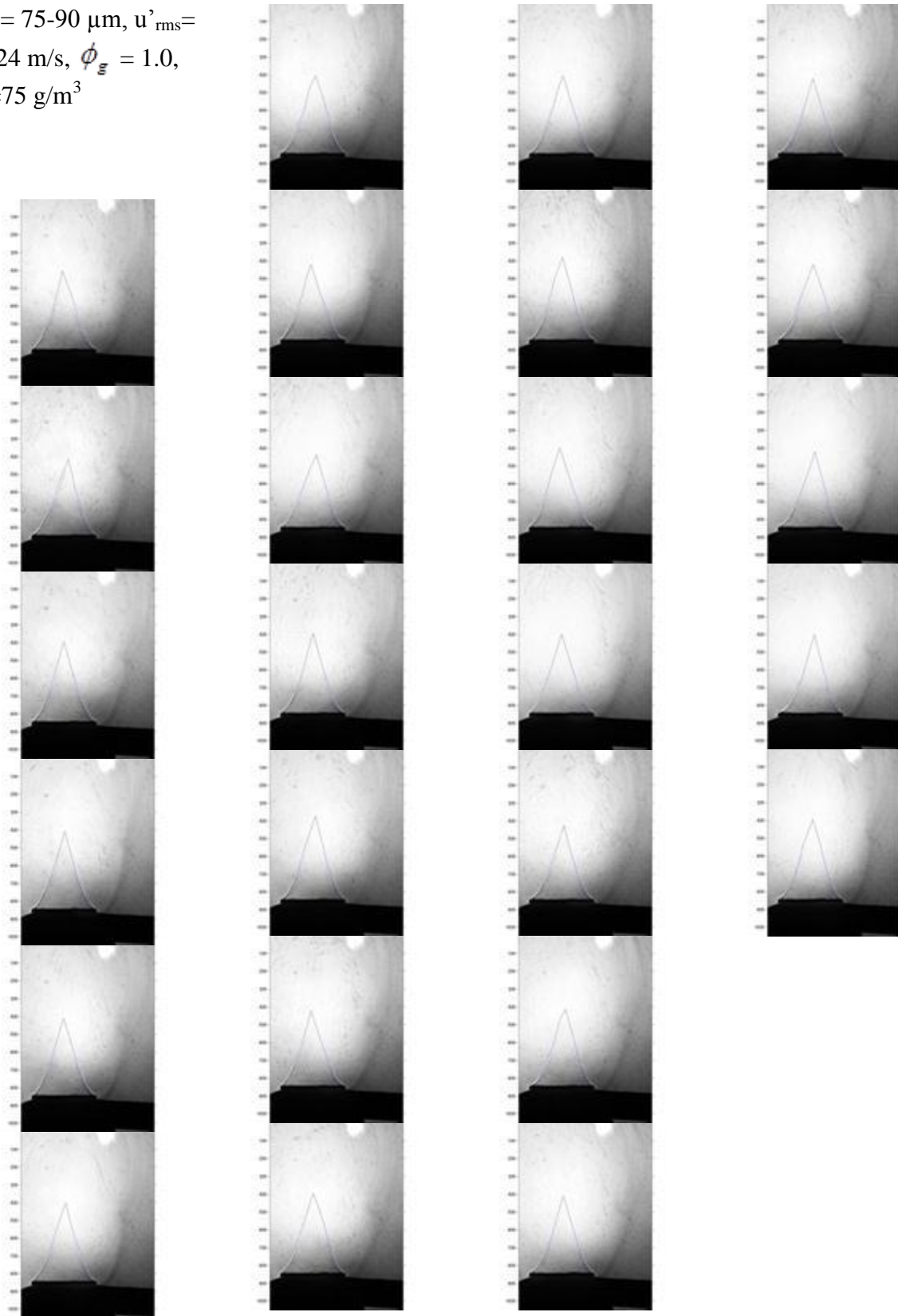
$d_{st} = 75-90 \mu\text{m}$, $u'_{rms} =$
 0.024 m/s , $\phi_g = 1.0$,
 $\lambda_{st} = 25 \text{ g/m}^3$



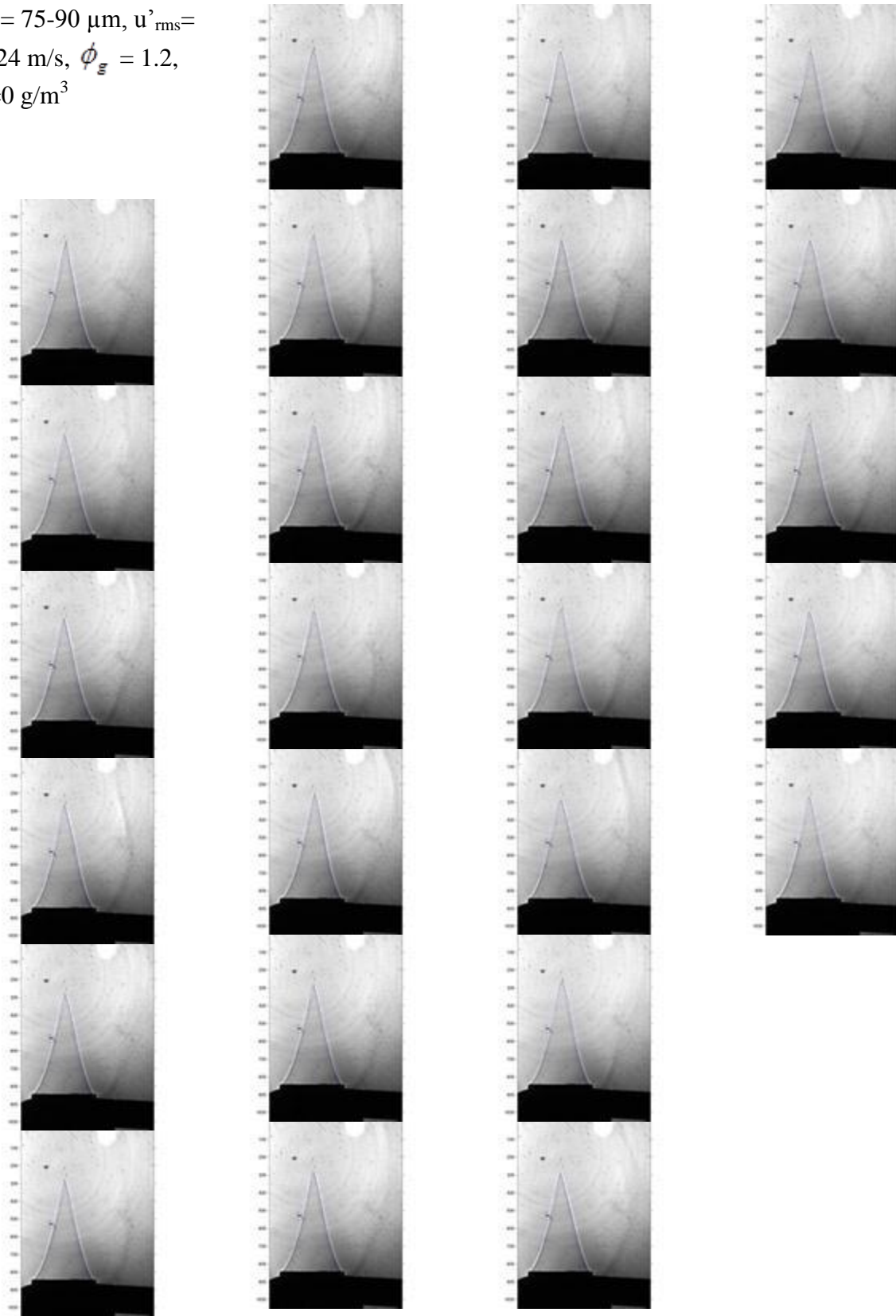
$d_{st} = 75-90 \mu\text{m}$, $u'_{\text{rms}} =$
 0.024 m/s , $\phi_g = 1.0$,
 $\lambda_{st} = 50 \text{ g/m}^3$



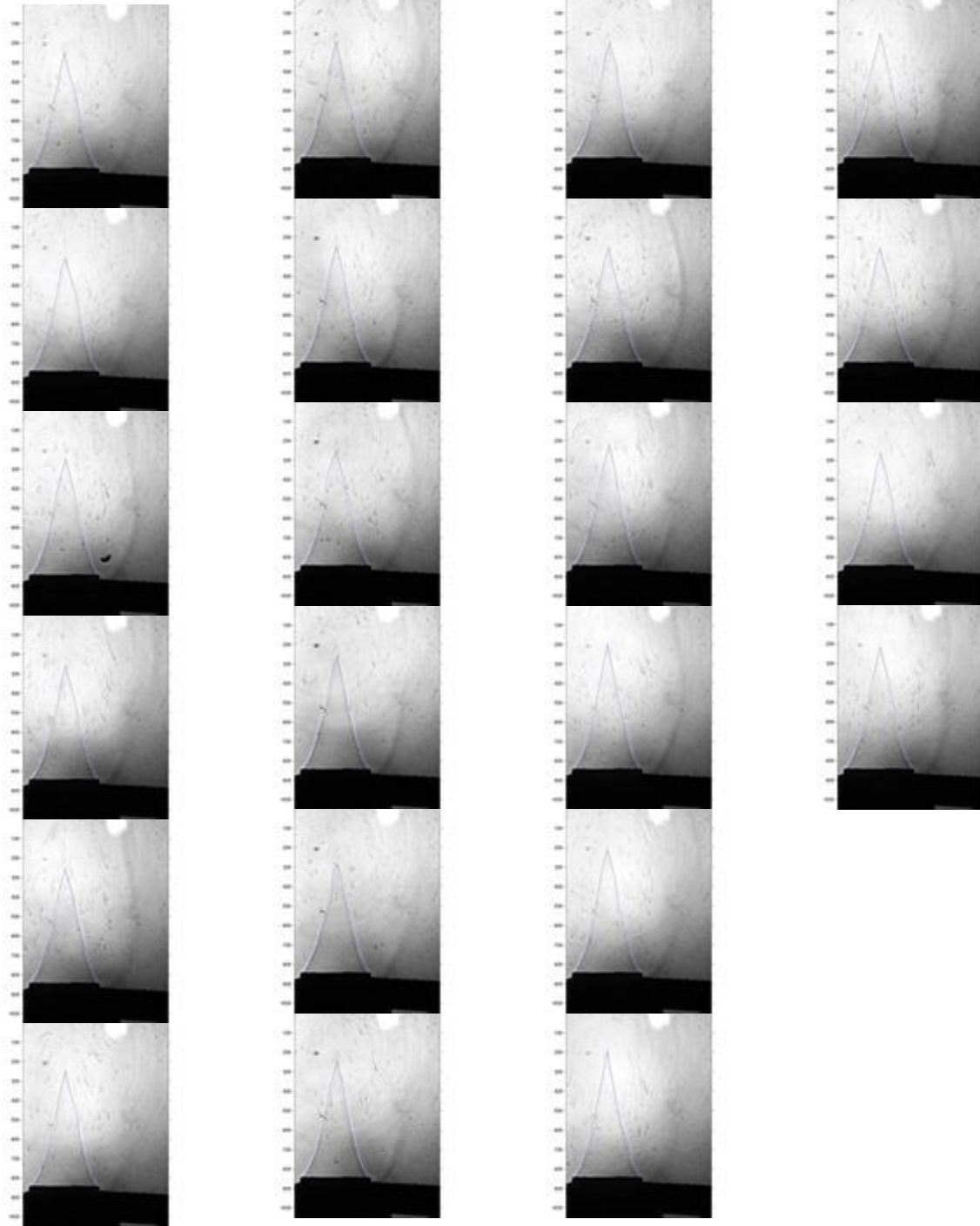
$d_{st} = 75-90 \mu\text{m}$, $u'_{rms} =$
 0.024 m/s , $\phi_g = 1.0$,
 $\lambda_{st} = 75 \text{ g/m}^3$



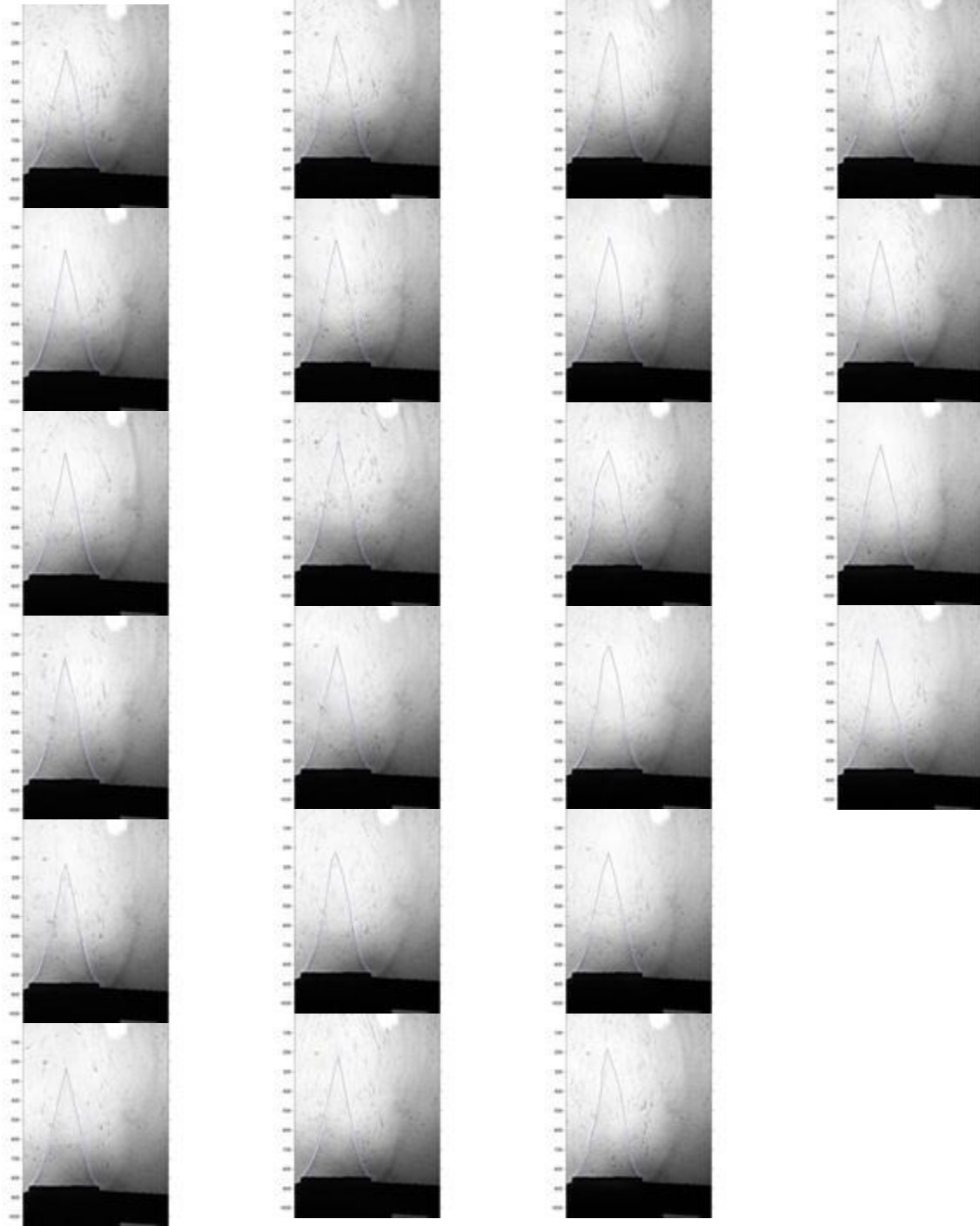
$d_{st} = 75-90 \mu\text{m}$, $u'_{rms} =$
 0.024 m/s , $\phi_g = 1.2$,
 $\lambda_{st} = 0 \text{ g/m}^3$



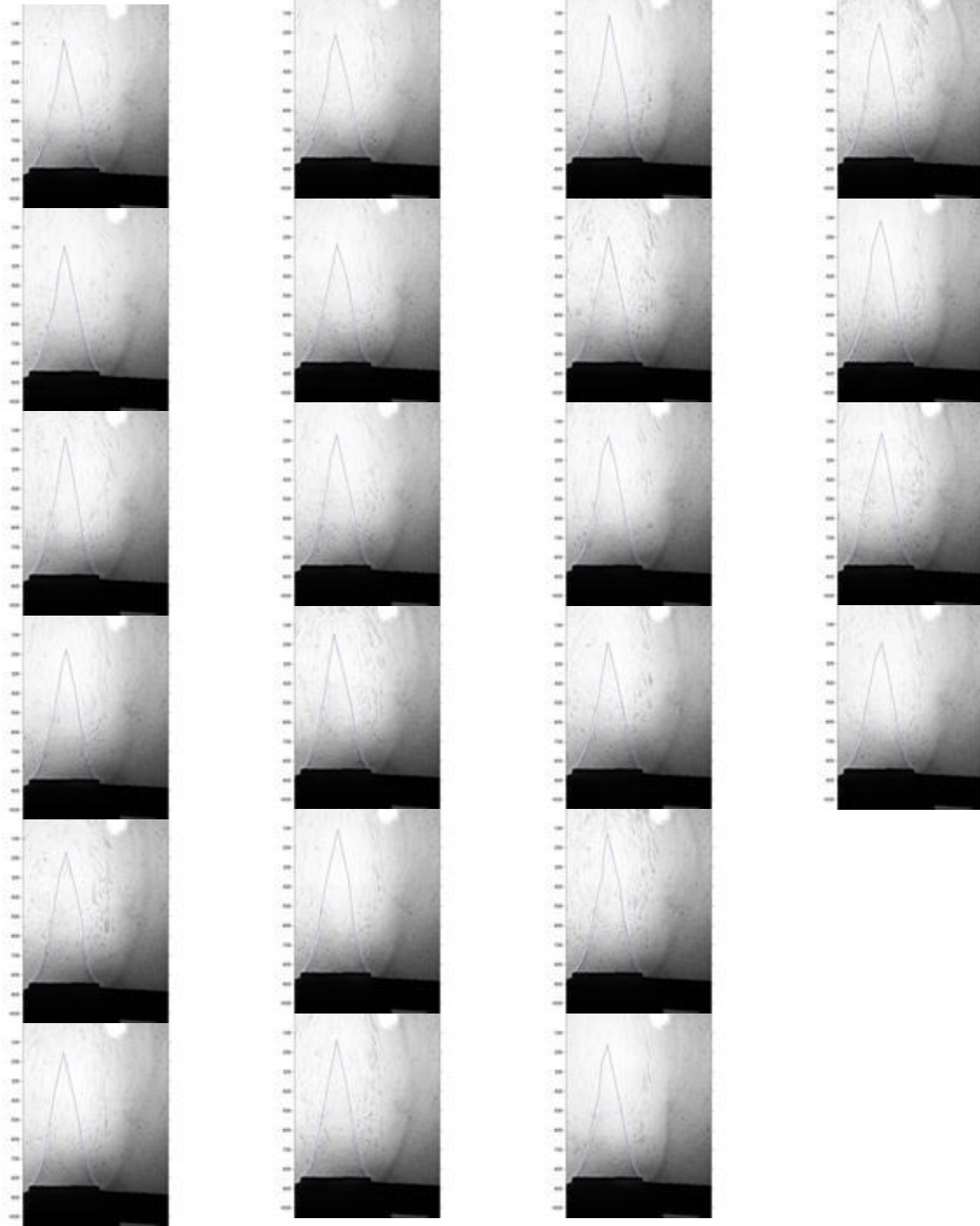
$d_{st} = 75-90 \mu\text{m}$, $u'_{rms} =$
 0.024 m/s , $\phi_g = 1.2$,
 $\lambda_{st} = 25 \text{ g/m}^3$



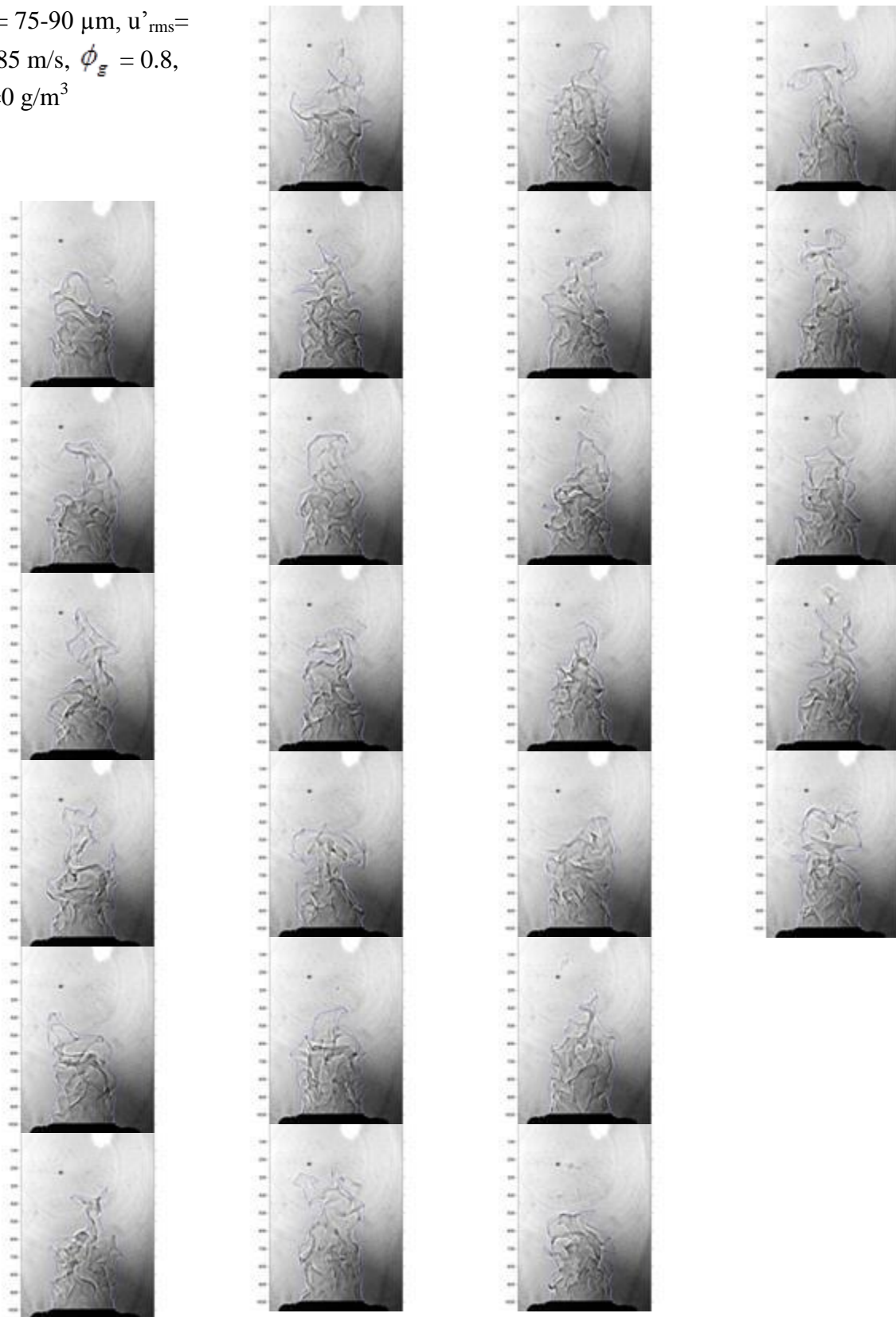
$d_{st} = 75-90 \mu\text{m}$, $u'_{rms} =$
 0.024 m/s , $\phi_g = 1.2$,
 $\lambda_{st} = 50 \text{ g/m}^3$



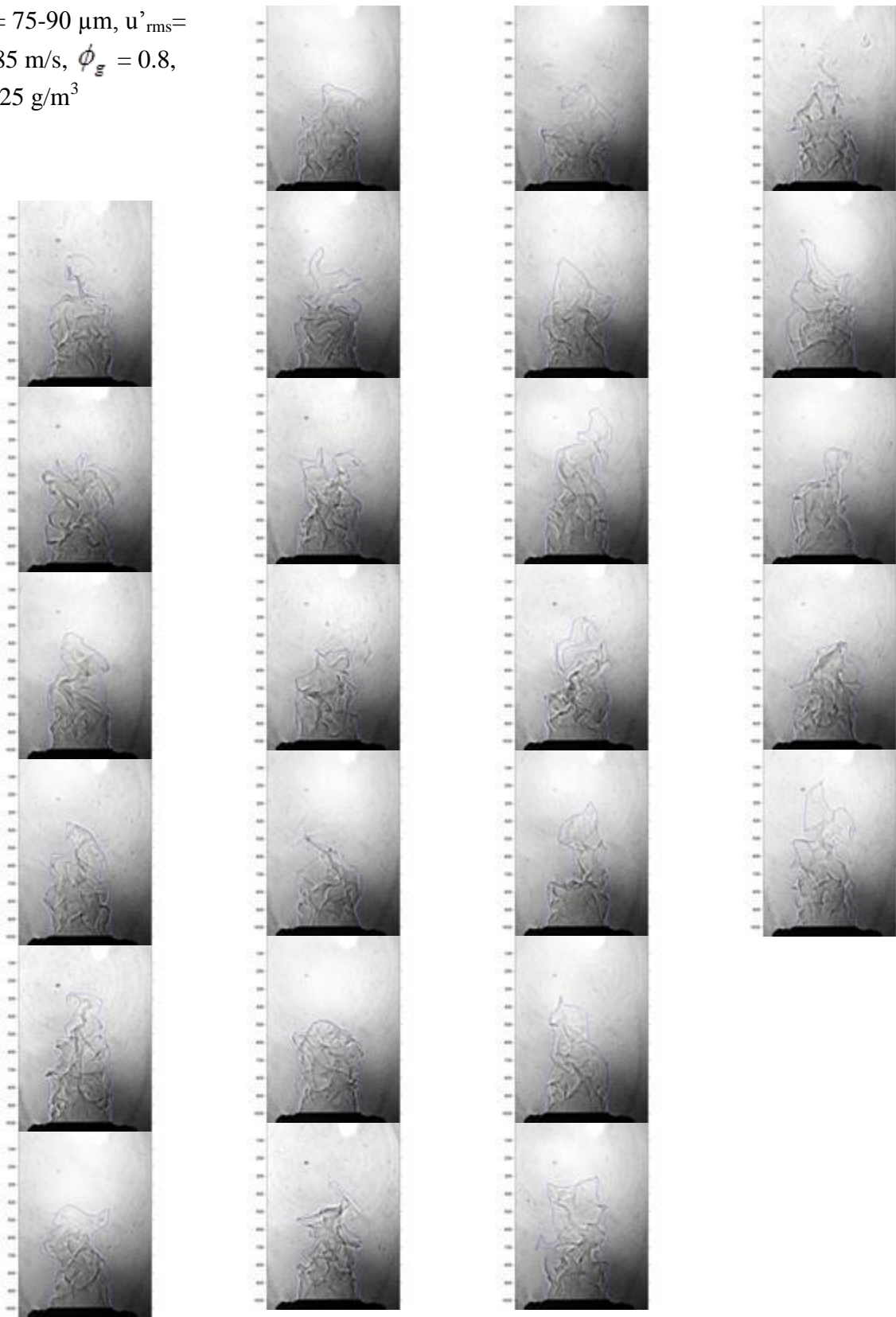
$d_{st} = 75-90 \mu\text{m}$, $u'_{rms} =$
 0.024 m/s , $\phi_g = 1.2$,
 $\lambda_{st} = 75 \text{ g/m}^3$



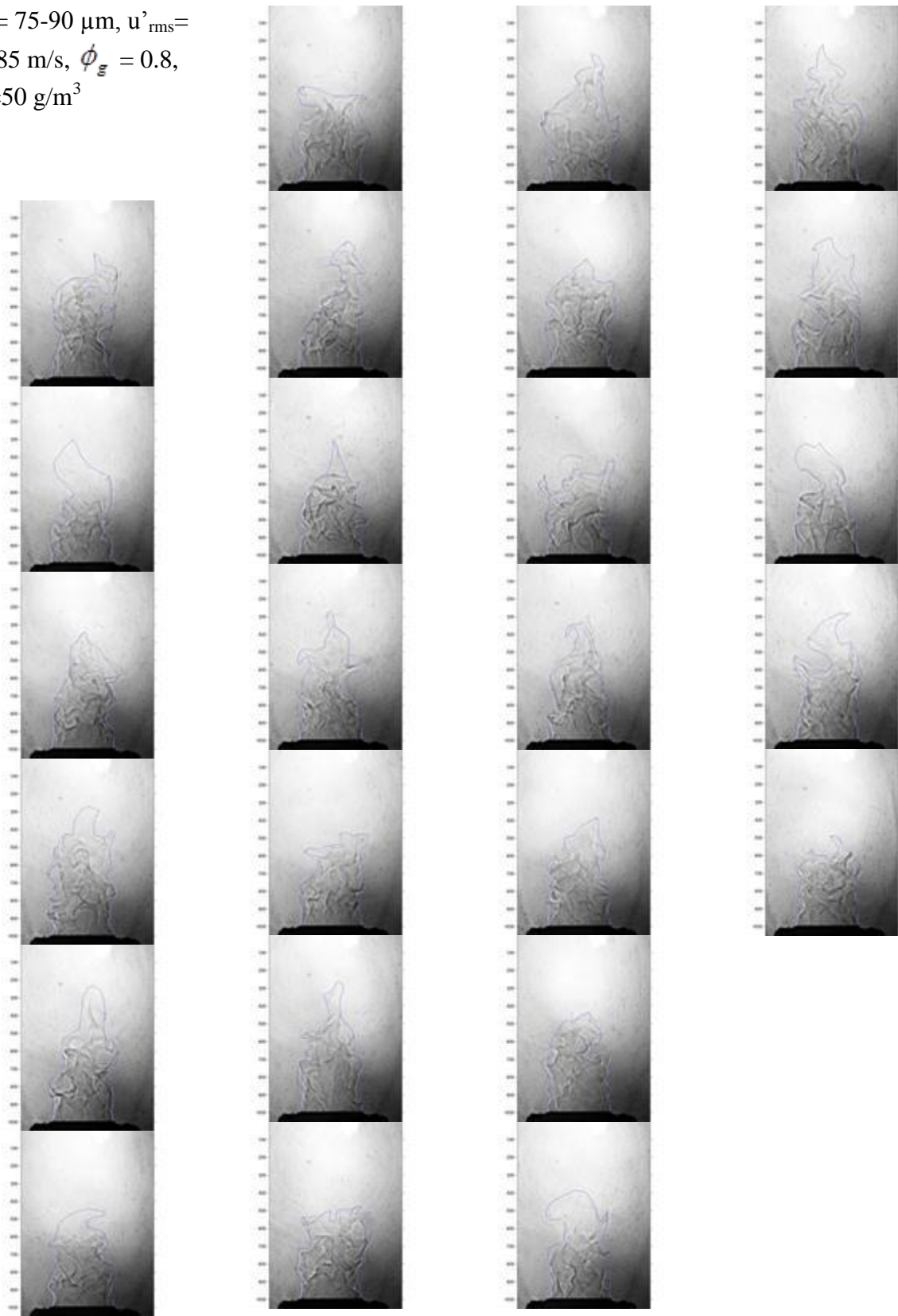
$d_{st} = 75-90 \mu\text{m}$, $u'_{rms} =$
 0.185 m/s , $\phi_g = 0.8$,
 $\lambda_{st} = 0 \text{ g/m}^3$



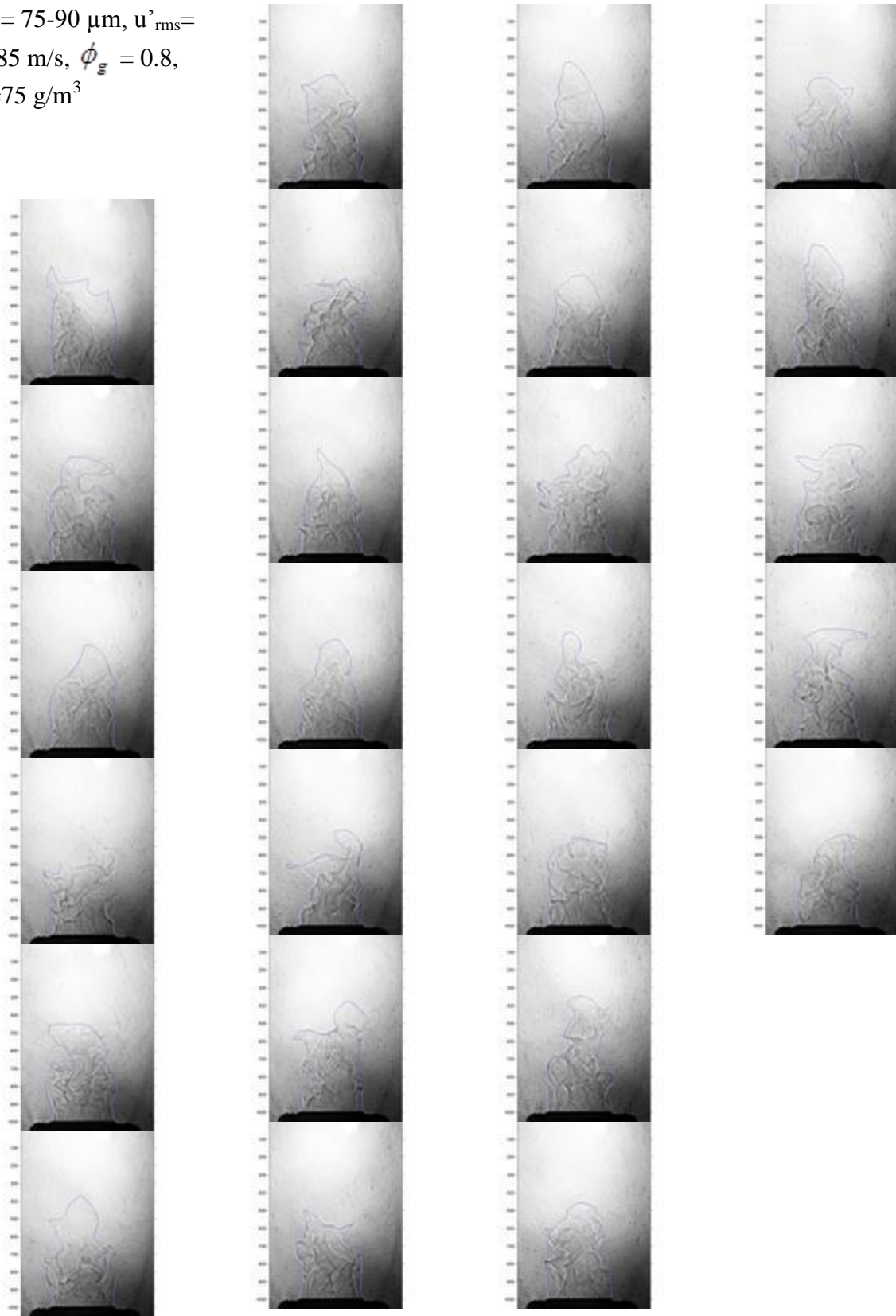
$d_{st} = 75-90 \mu\text{m}$, $u'_{rms} =$
 0.185 m/s , $\phi_g = 0.8$,
 $\lambda_{st} = 25 \text{ g/m}^3$



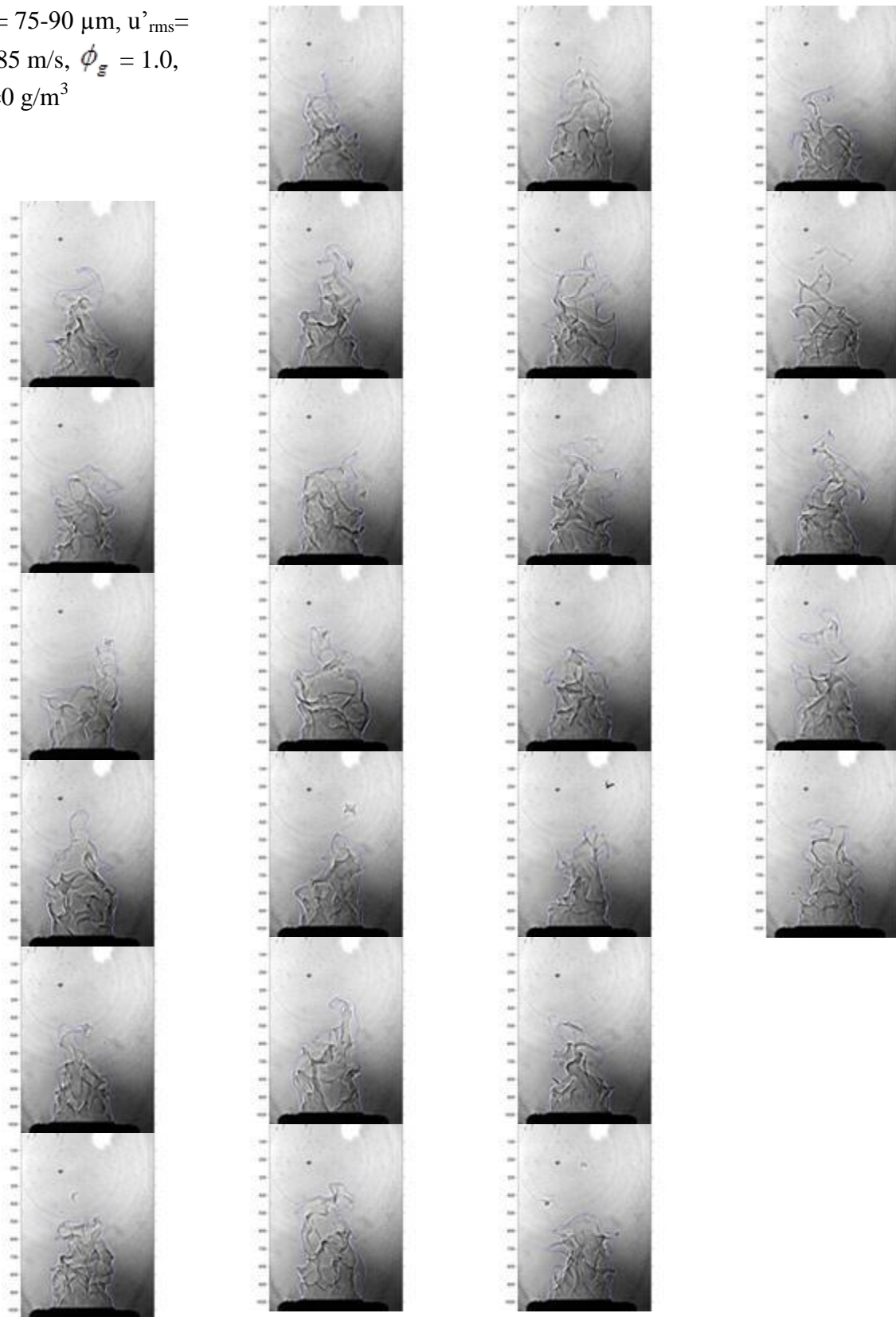
$d_{st} = 75-90 \mu\text{m}$, $u'_{rms} =$
 0.185 m/s , $\phi_g = 0.8$,
 $\lambda_{st} = 50 \text{ g/m}^3$



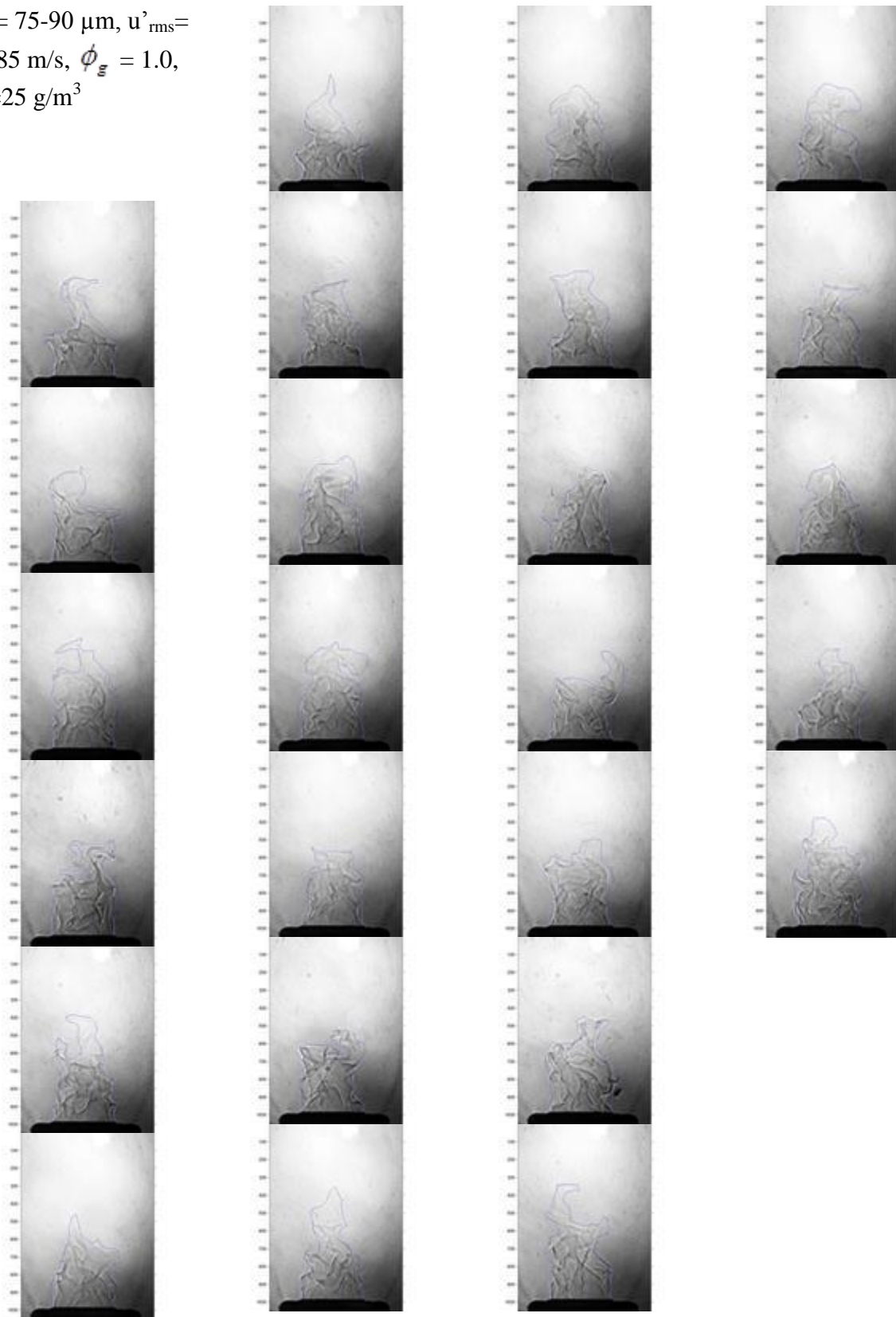
$d_{st} = 75-90 \mu\text{m}$, $u'_{\text{rms}} =$
 0.185 m/s , $\phi_g = 0.8$,
 $\lambda_{st} = 75 \text{ g/m}^3$



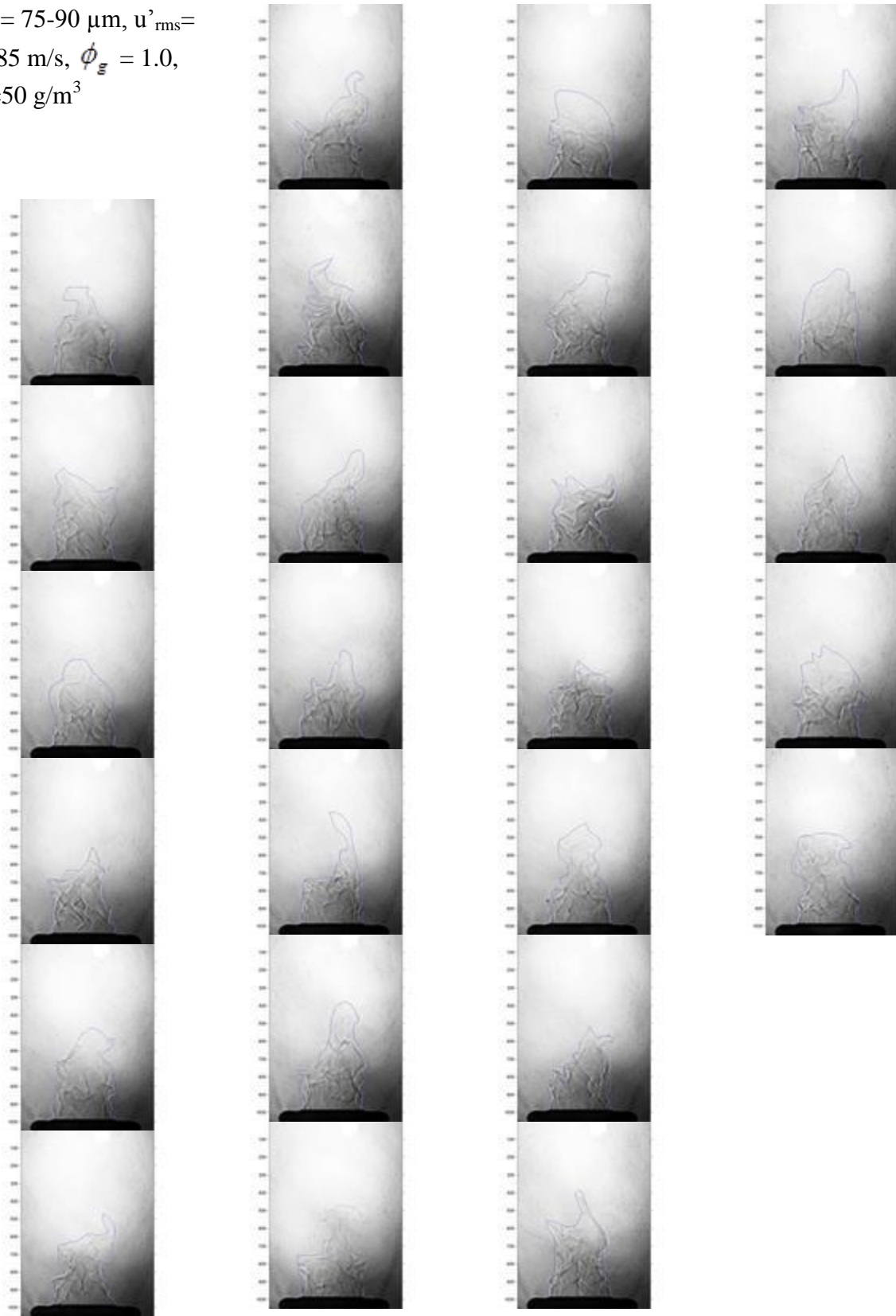
$d_{st} = 75-90 \mu\text{m}$, $u'_{rms} =$
 0.185 m/s , $\phi_g = 1.0$,
 $\lambda_{st} = 0 \text{ g/m}^3$



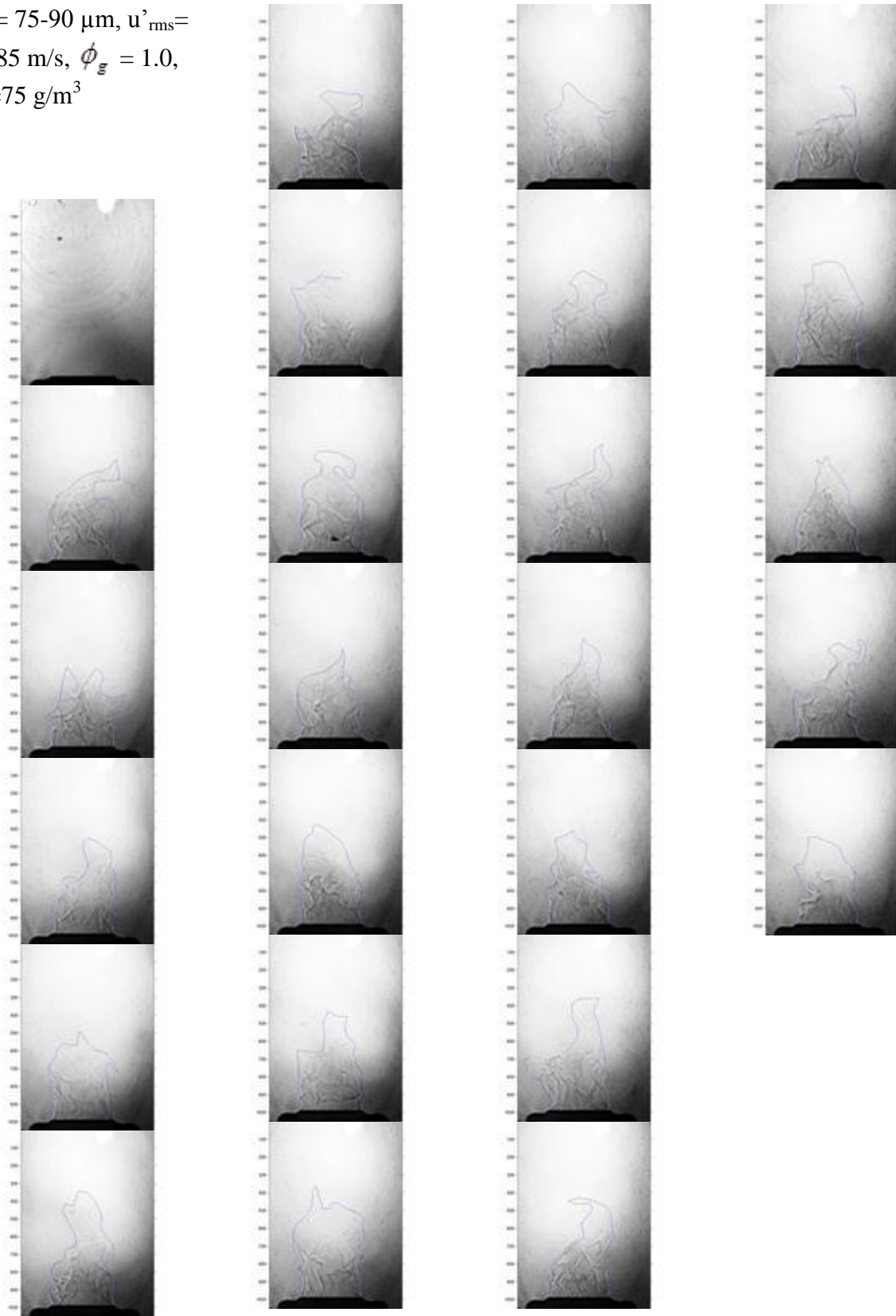
$d_{st} = 75-90 \mu\text{m}$, $u'_{rms} =$
 0.185 m/s , $\phi_g = 1.0$,
 $\lambda_{st} = 25 \text{ g/m}^3$



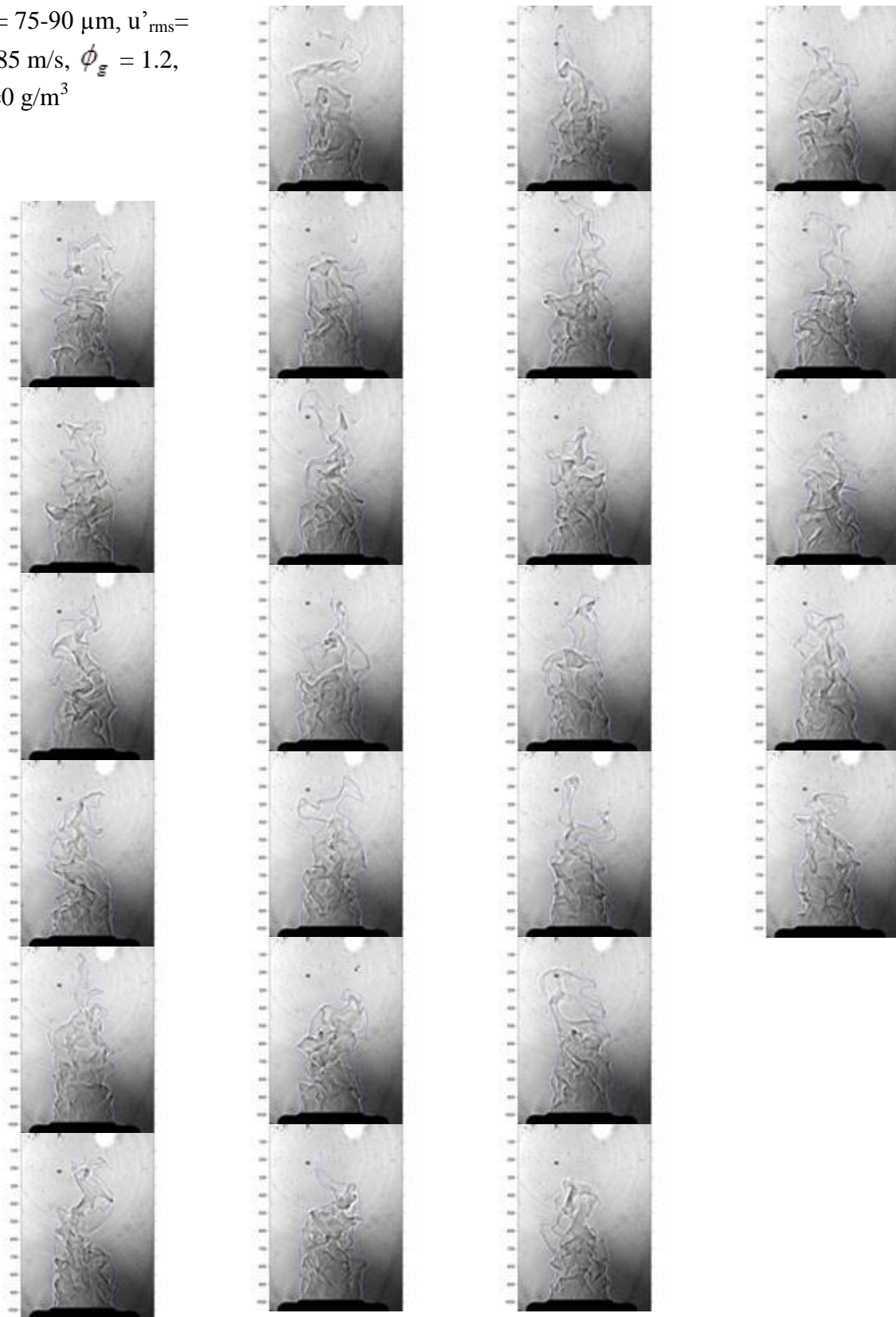
$d_{st} = 75-90 \mu\text{m}$, $u'_{rms} =$
 0.185 m/s , $\phi_g = 1.0$,
 $\lambda_{st} = 50 \text{ g/m}^3$



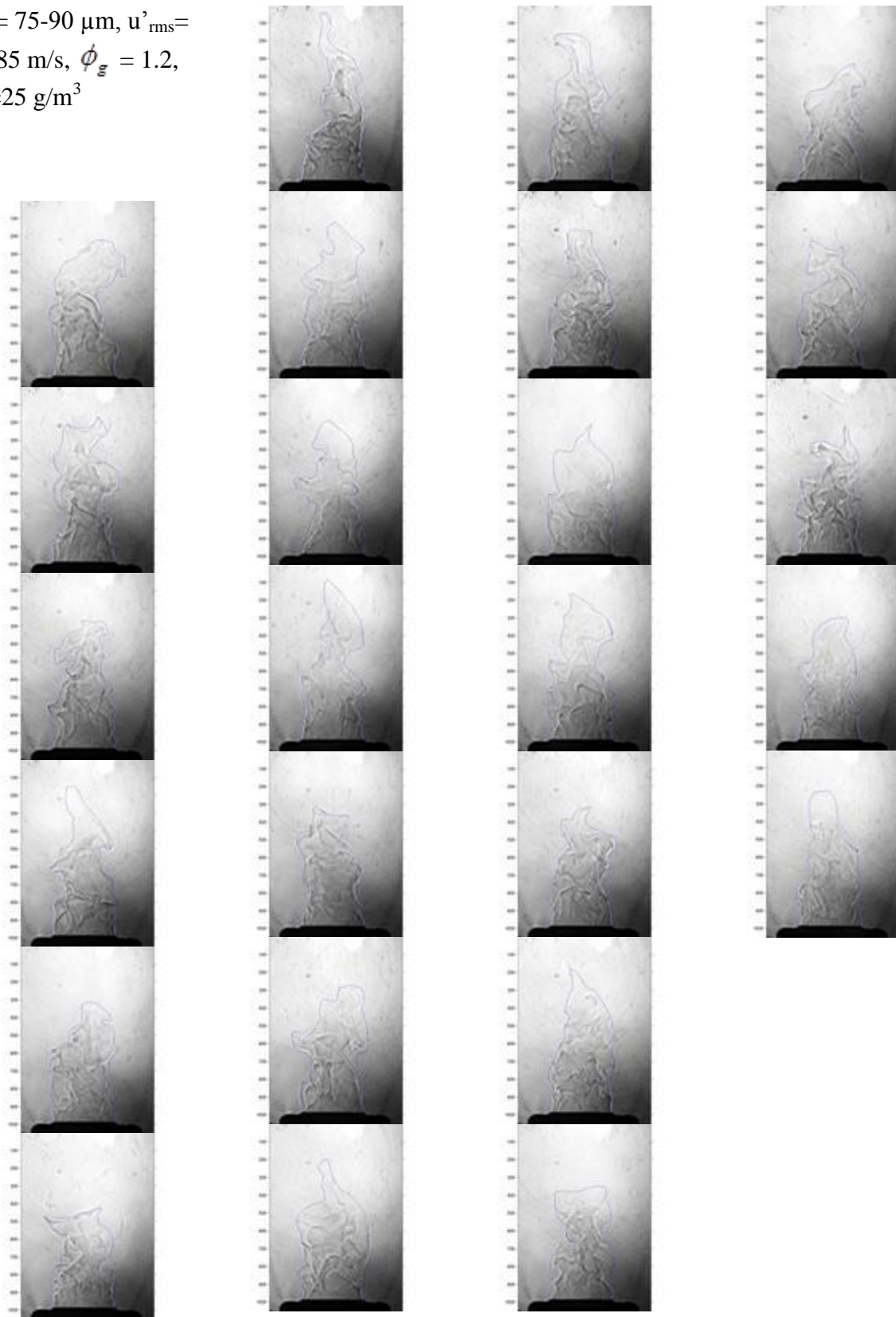
$d_{st} = 75-90 \mu\text{m}$, $u'_{rms} =$
 0.185 m/s , $\phi_g = 1.0$,
 $\lambda_{st} = 75 \text{ g/m}^3$



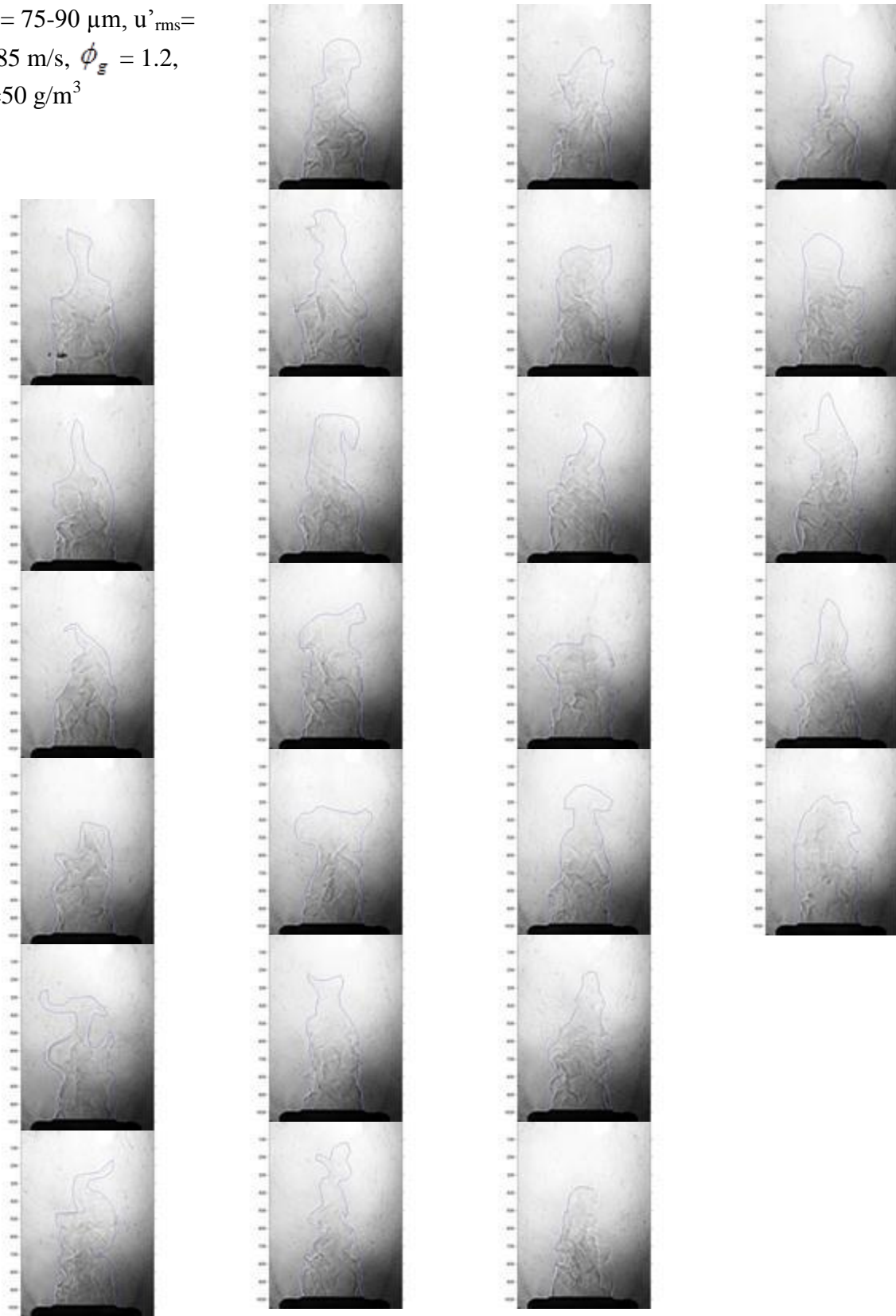
$d_{st} = 75-90 \mu\text{m}$, $u'_{rms} =$
 0.185 m/s , $\phi_g = 1.2$,
 $\lambda_{st} = 0 \text{ g/m}^3$



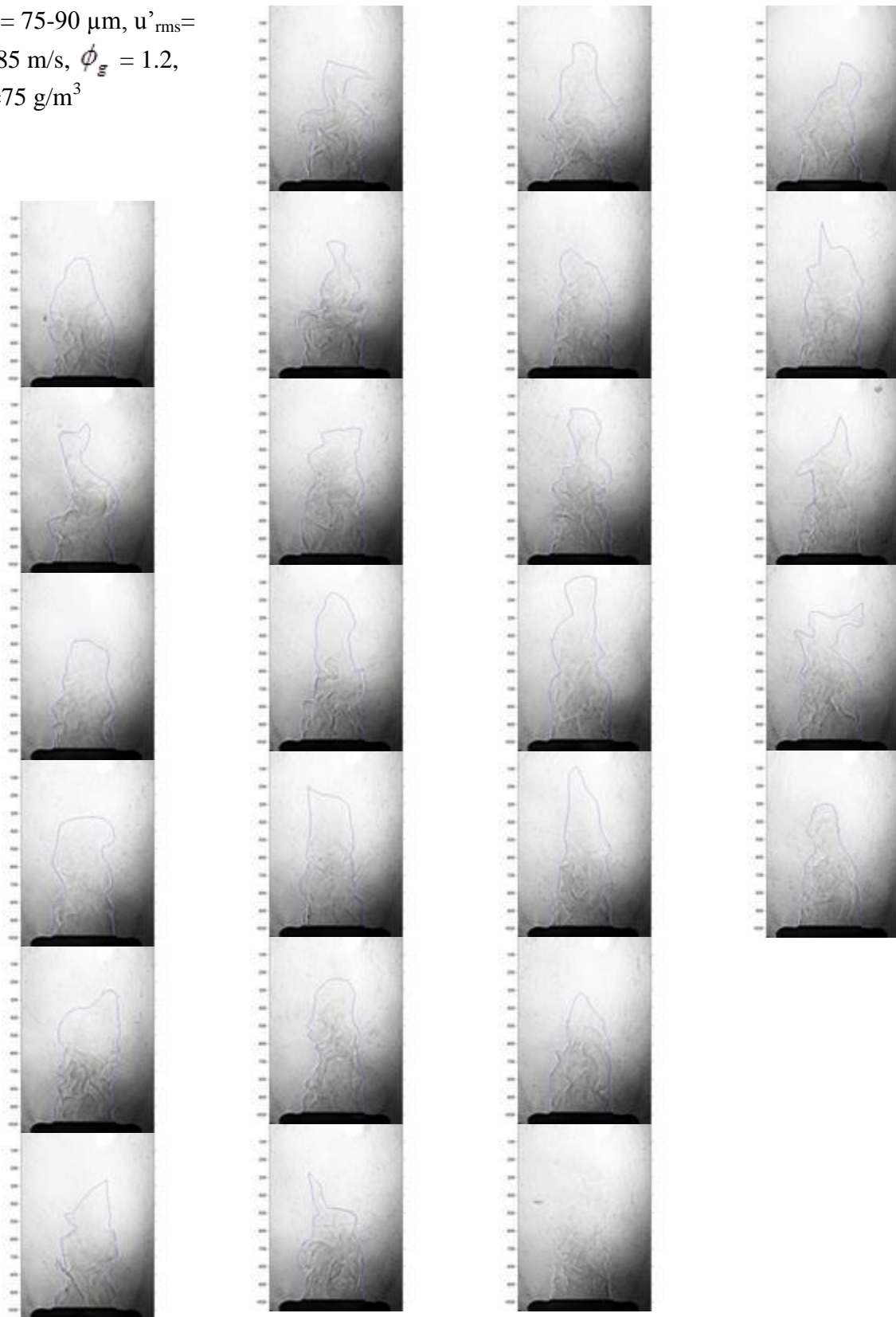
$d_{st} = 75-90 \mu\text{m}$, $u'_{rms} =$
 0.185 m/s , $\phi_g = 1.2$,
 $\lambda_{st} = 25 \text{ g/m}^3$



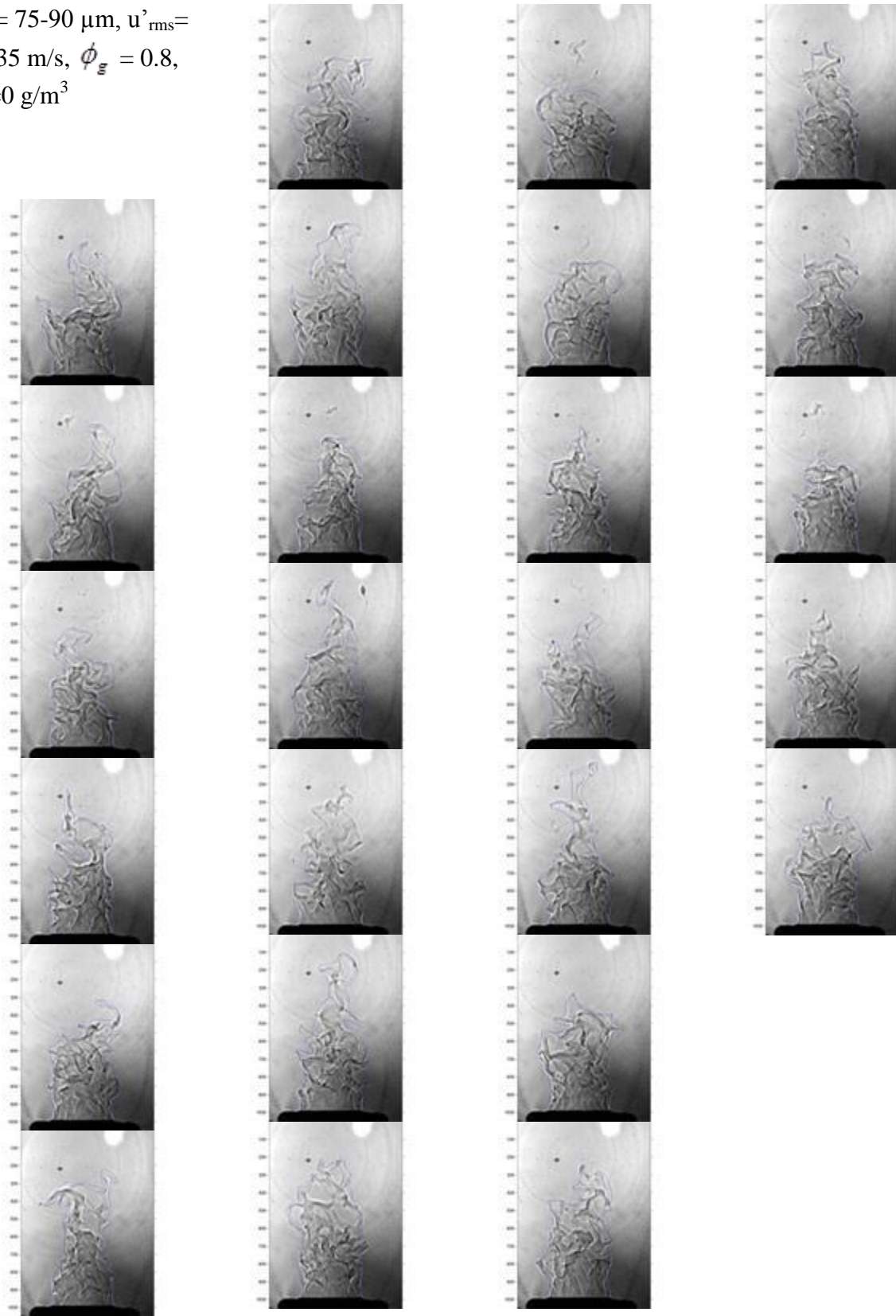
$d_{st} = 75-90 \mu\text{m}$, $u'_{rms} =$
 0.185 m/s , $\phi_g = 1.2$,
 $\lambda_{st} = 50 \text{ g/m}^3$



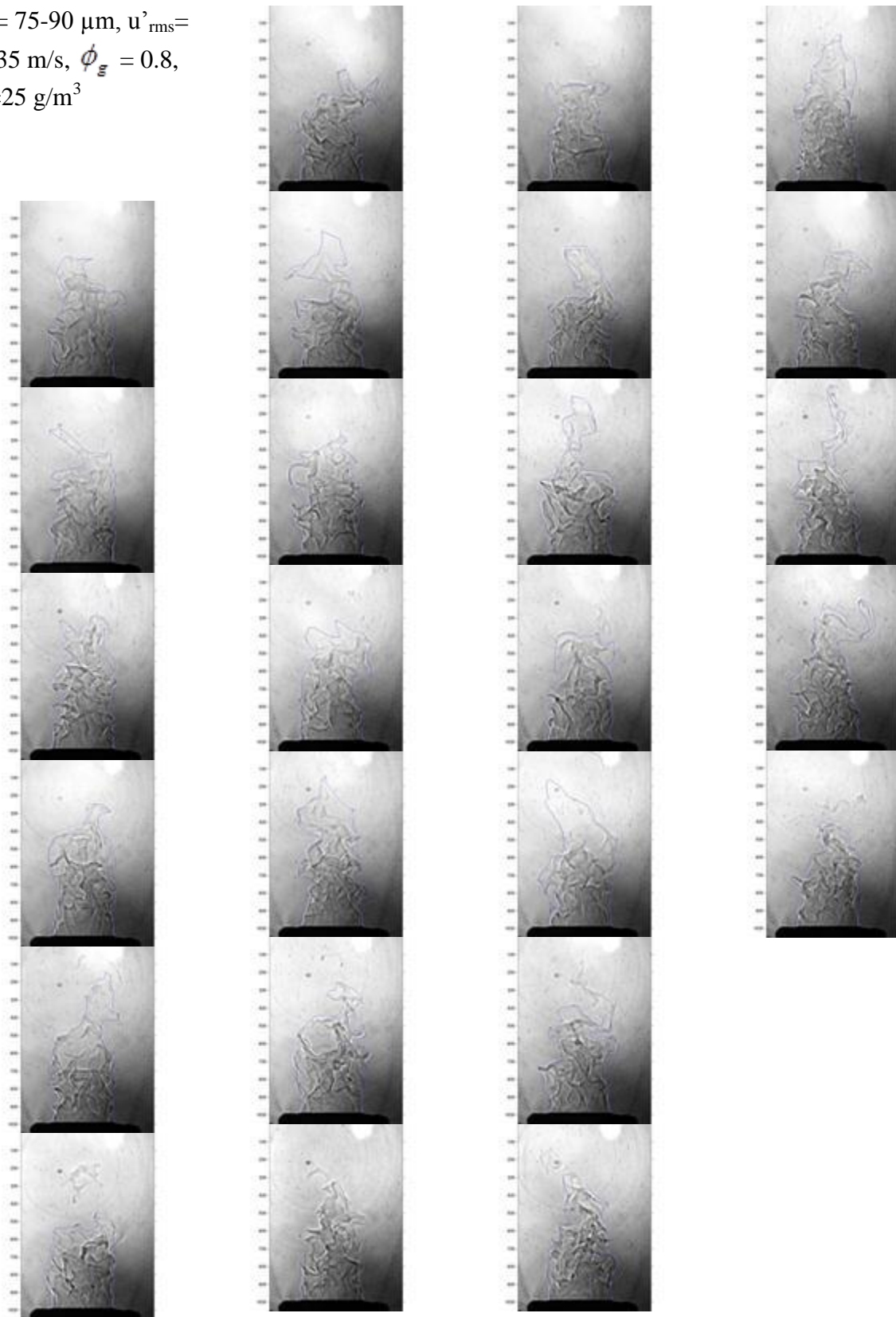
$d_{st} = 75-90 \mu\text{m}$, $u'_{rms} =$
 0.185 m/s , $\phi_g = 1.2$,
 $\lambda_{st} = 75 \text{ g/m}^3$



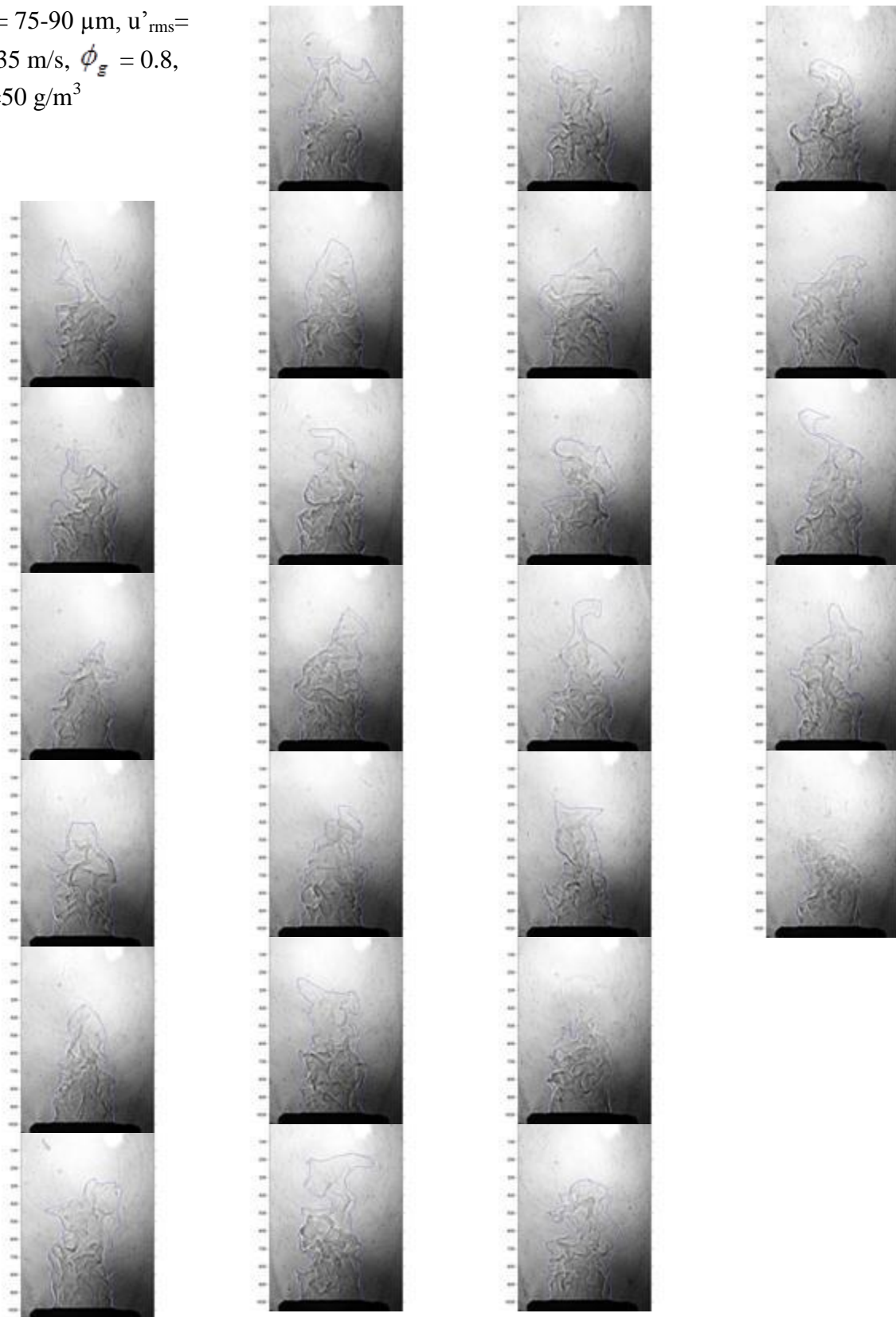
$d_{st} = 75-90 \mu\text{m}$, $u'_{rms} =$
 0.335 m/s , $\phi_g = 0.8$,
 $\lambda_{st} = 0 \text{ g/m}^3$



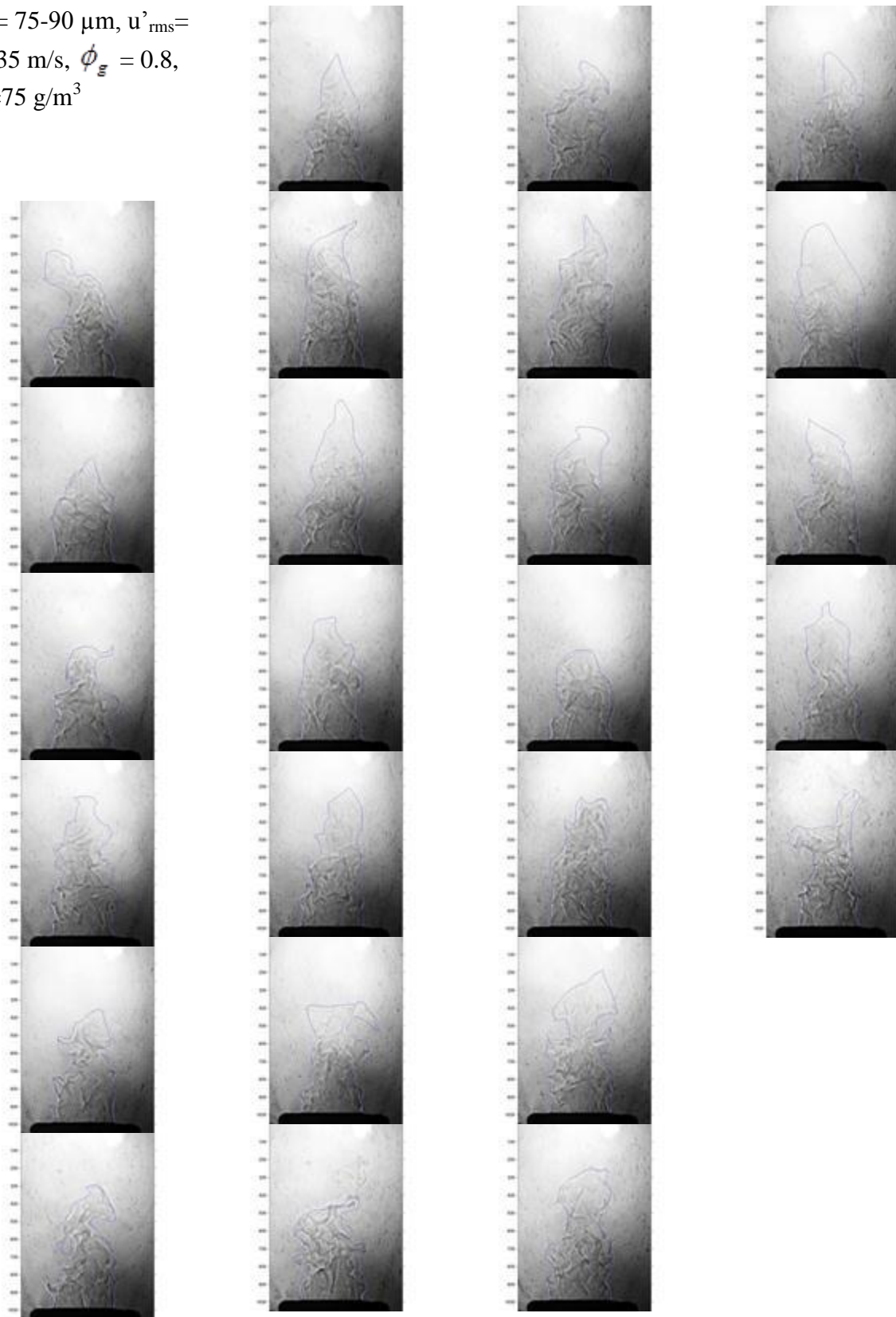
$d_{st} = 75-90 \mu\text{m}$, $u'_{rms} =$
 0.335 m/s , $\phi_g = 0.8$,
 $\lambda_{st} = 25 \text{ g/m}^3$



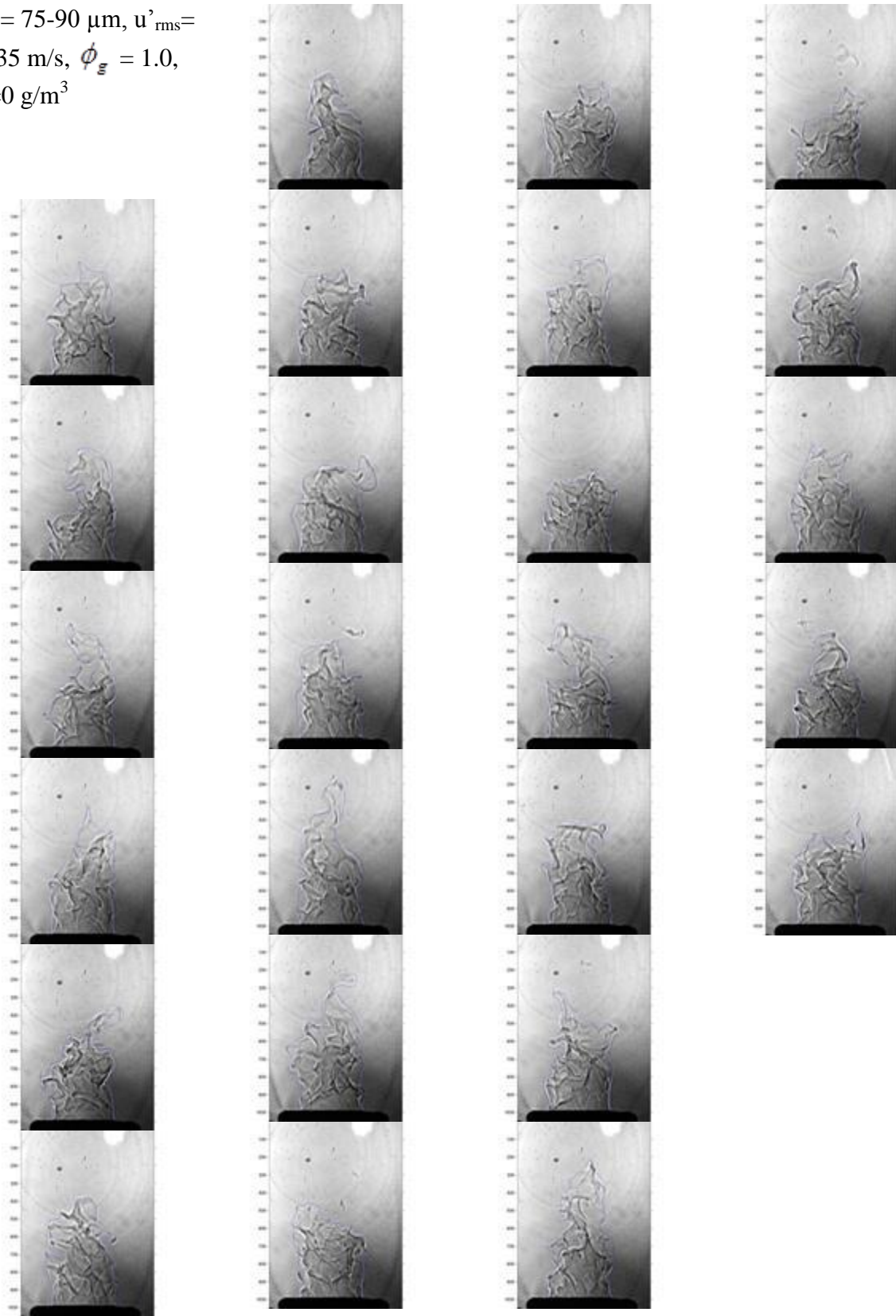
$d_{st} = 75-90 \mu\text{m}$, $u'_{rms} =$
 0.335 m/s , $\phi_g = 0.8$,
 $\lambda_{st} = 50 \text{ g/m}^3$



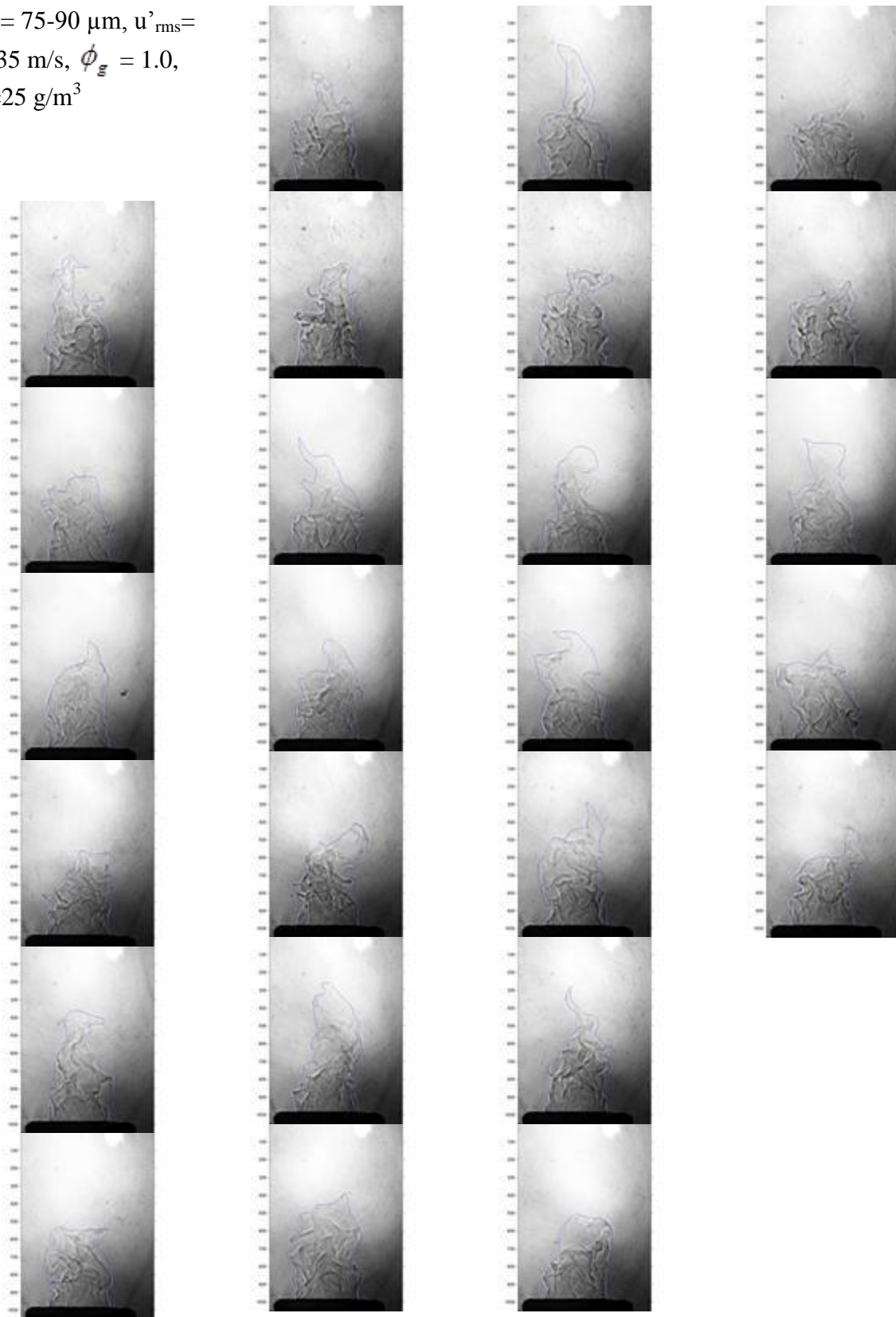
$d_{st} = 75-90 \mu\text{m}$, $u'_{rms} =$
 0.335 m/s , $\phi_g = 0.8$,
 $\lambda_{st} = 75 \text{ g/m}^3$



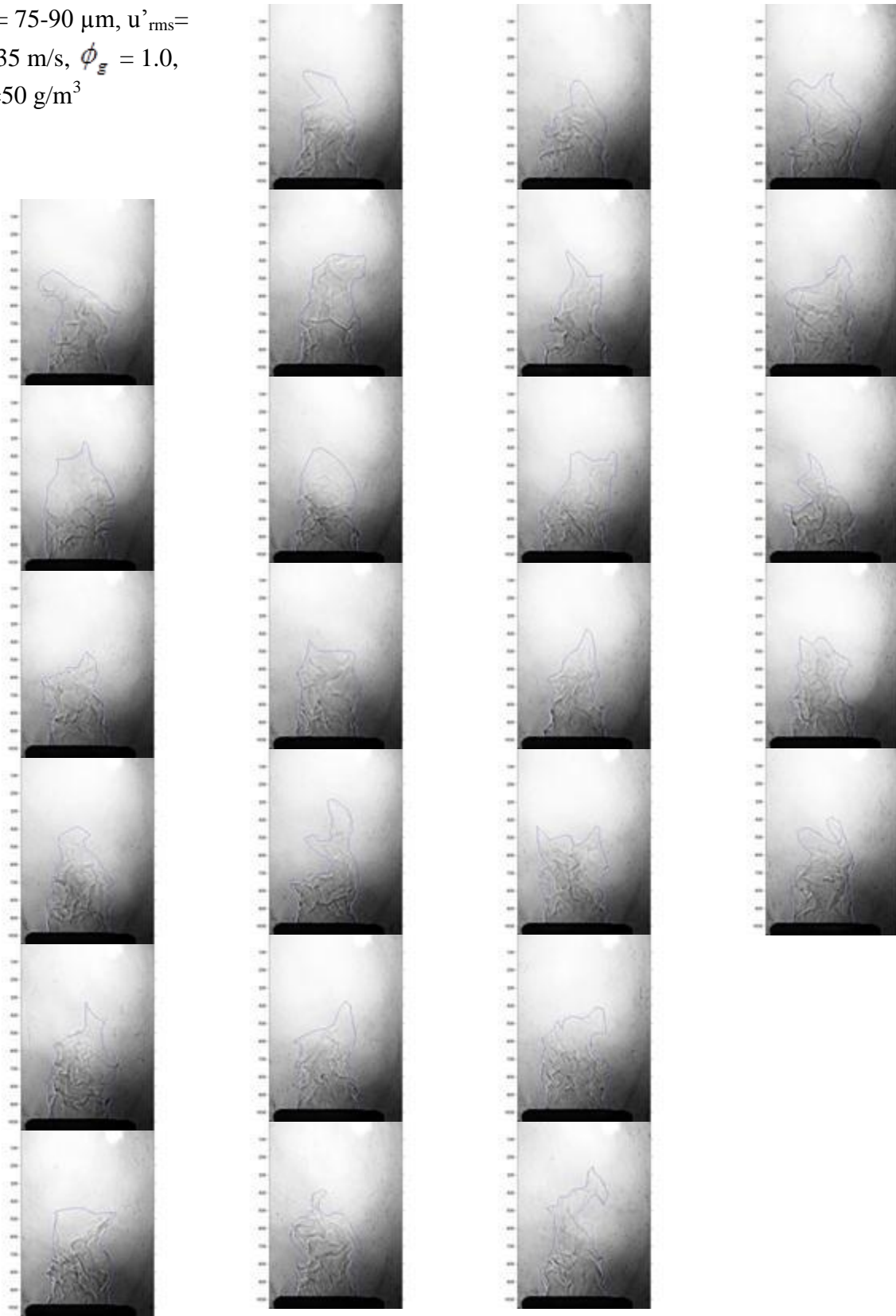
$d_{st} = 75-90 \mu\text{m}$, $u'_{rms} =$
 0.335 m/s , $\phi_g = 1.0$,
 $\lambda_{st} = 0 \text{ g/m}^3$



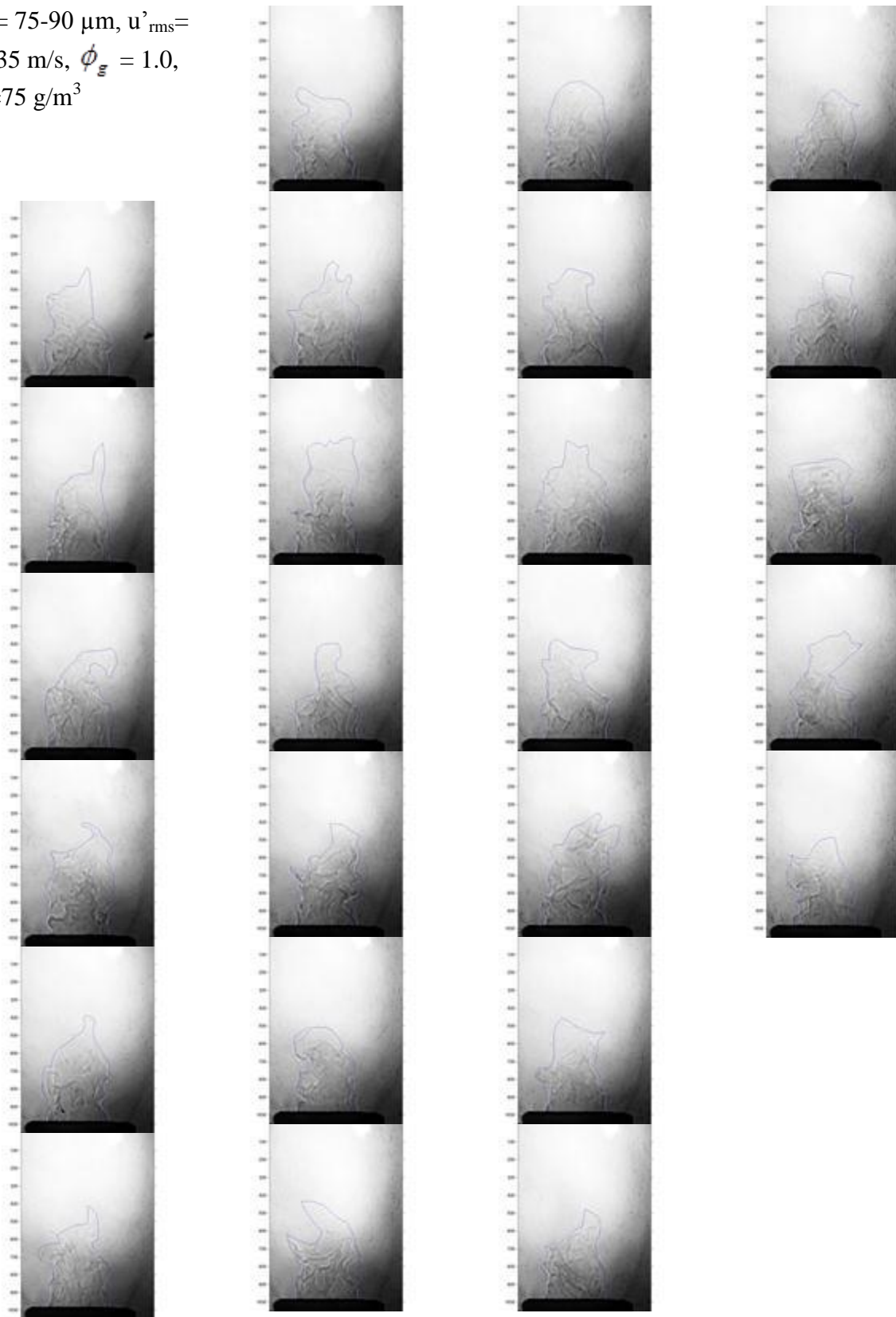
$d_{st} = 75-90 \mu\text{m}$, $u'_{rms} =$
 0.335 m/s , $\phi_g = 1.0$,
 $\lambda_{st} = 25 \text{ g/m}^3$



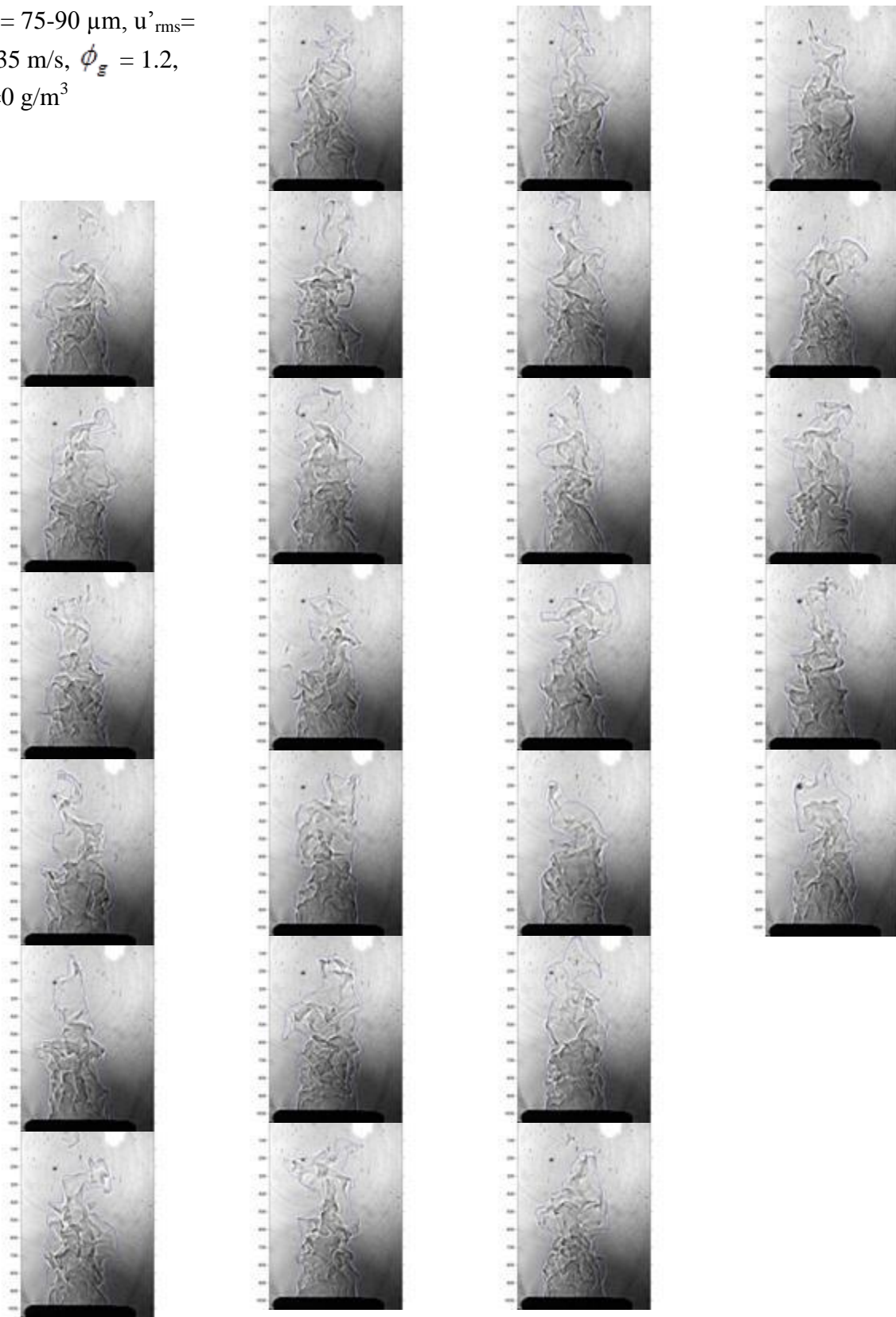
$d_{st} = 75-90 \mu\text{m}$, $u'_{rms} =$
 0.335 m/s , $\phi_g = 1.0$,
 $\lambda_{st} = 50 \text{ g/m}^3$



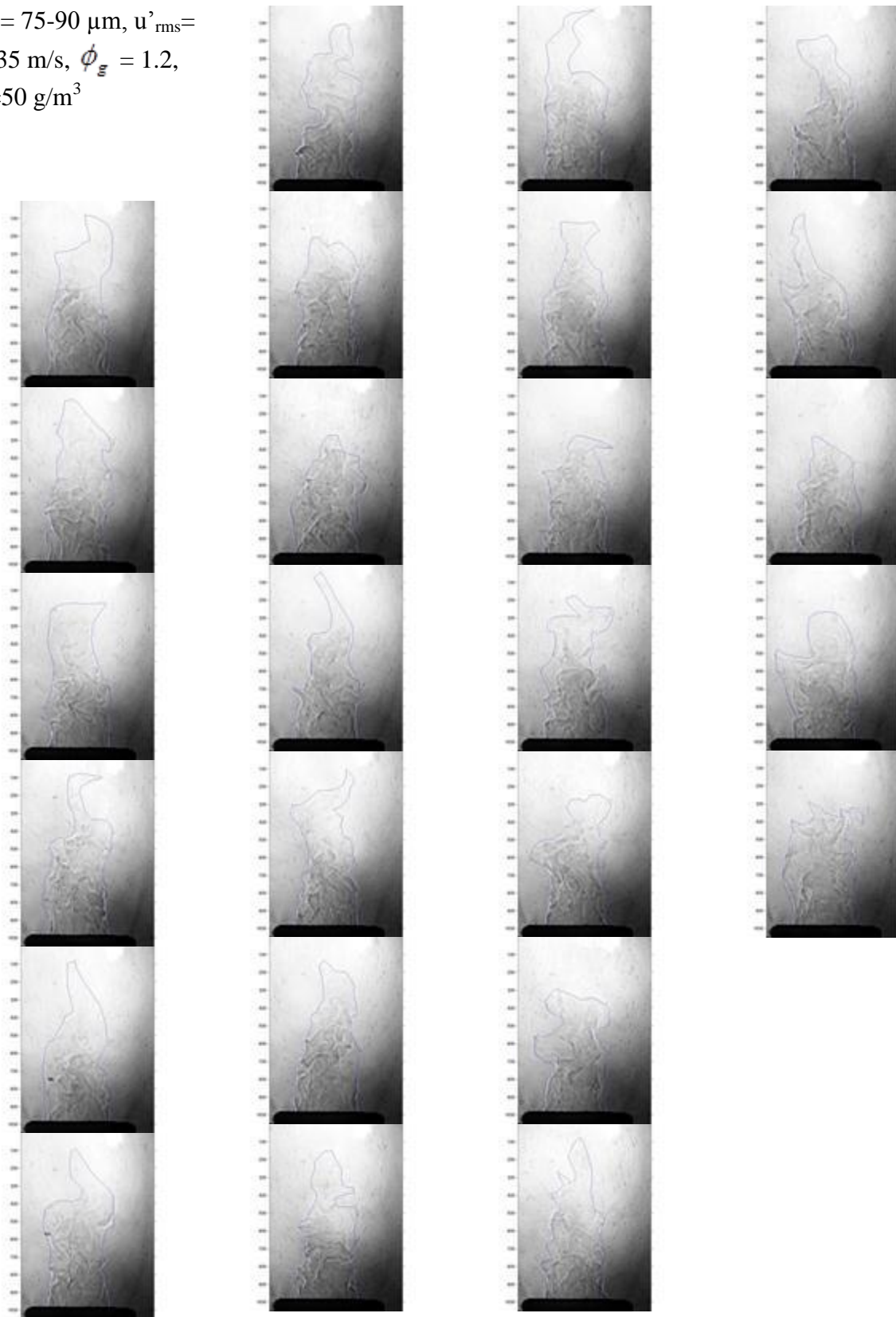
$d_{st} = 75-90 \mu\text{m}$, $u'_{rms} =$
 0.335 m/s , $\phi_g = 1.0$,
 $\lambda_{st} = 75 \text{ g/m}^3$



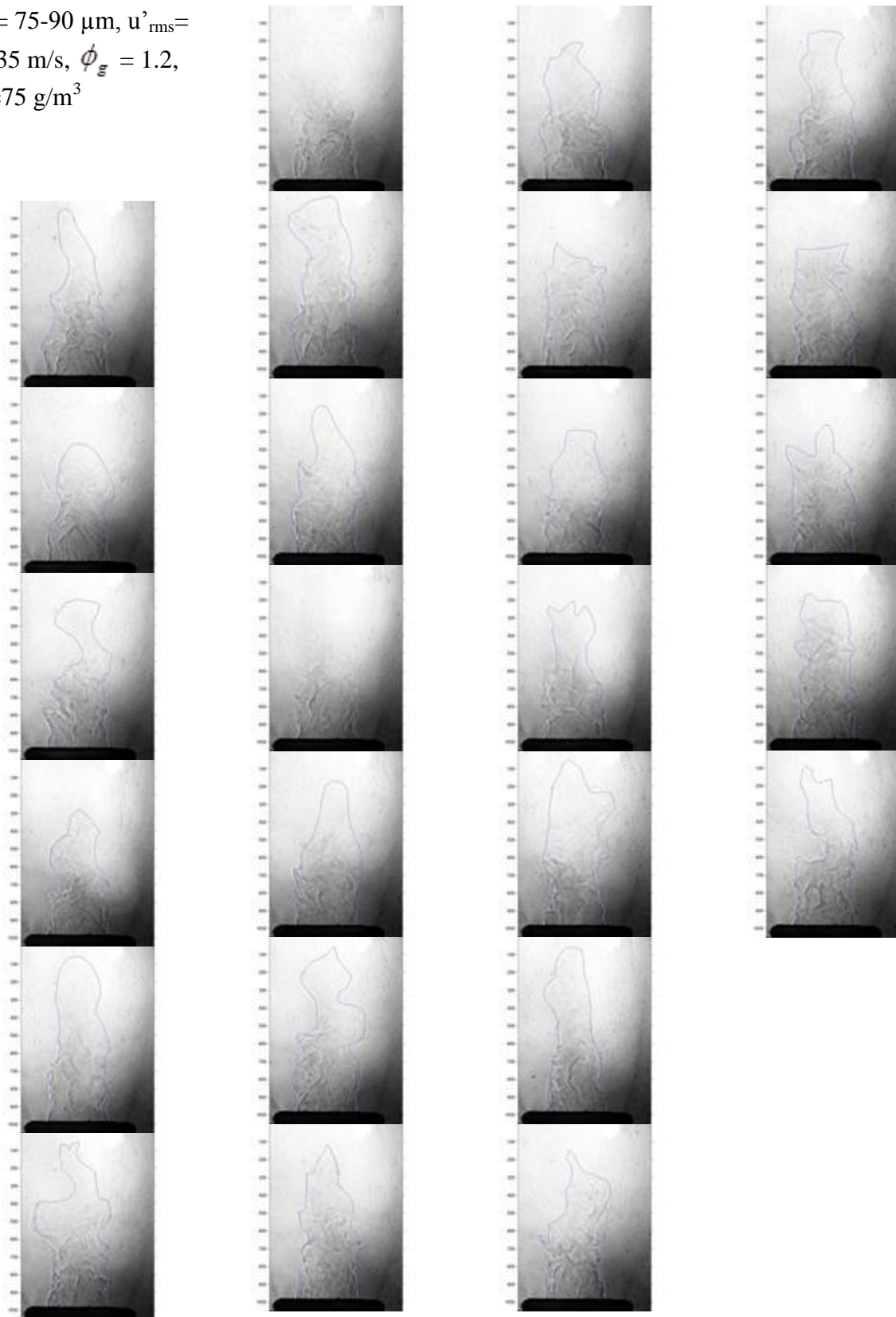
$d_{st} = 75-90 \mu\text{m}$, $u'_{rms} =$
 0.335 m/s , $\phi_g = 1.2$,
 $\lambda_{st} = 0 \text{ g/m}^3$



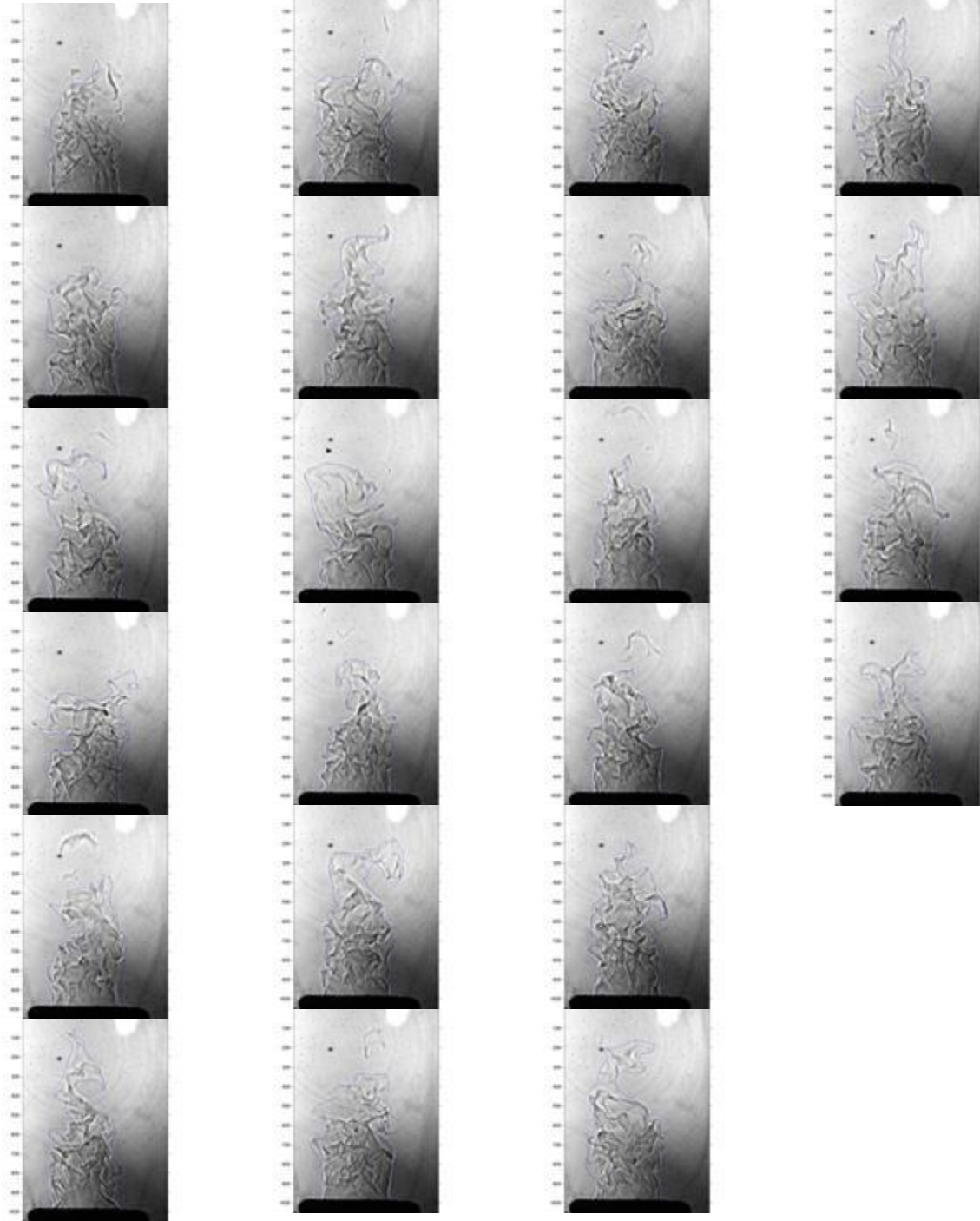
$d_{st} = 75-90 \mu\text{m}$, $u'_{rms} =$
 0.335 m/s , $\phi_g = 1.2$,
 $\lambda_{st} = 50 \text{ g/m}^3$



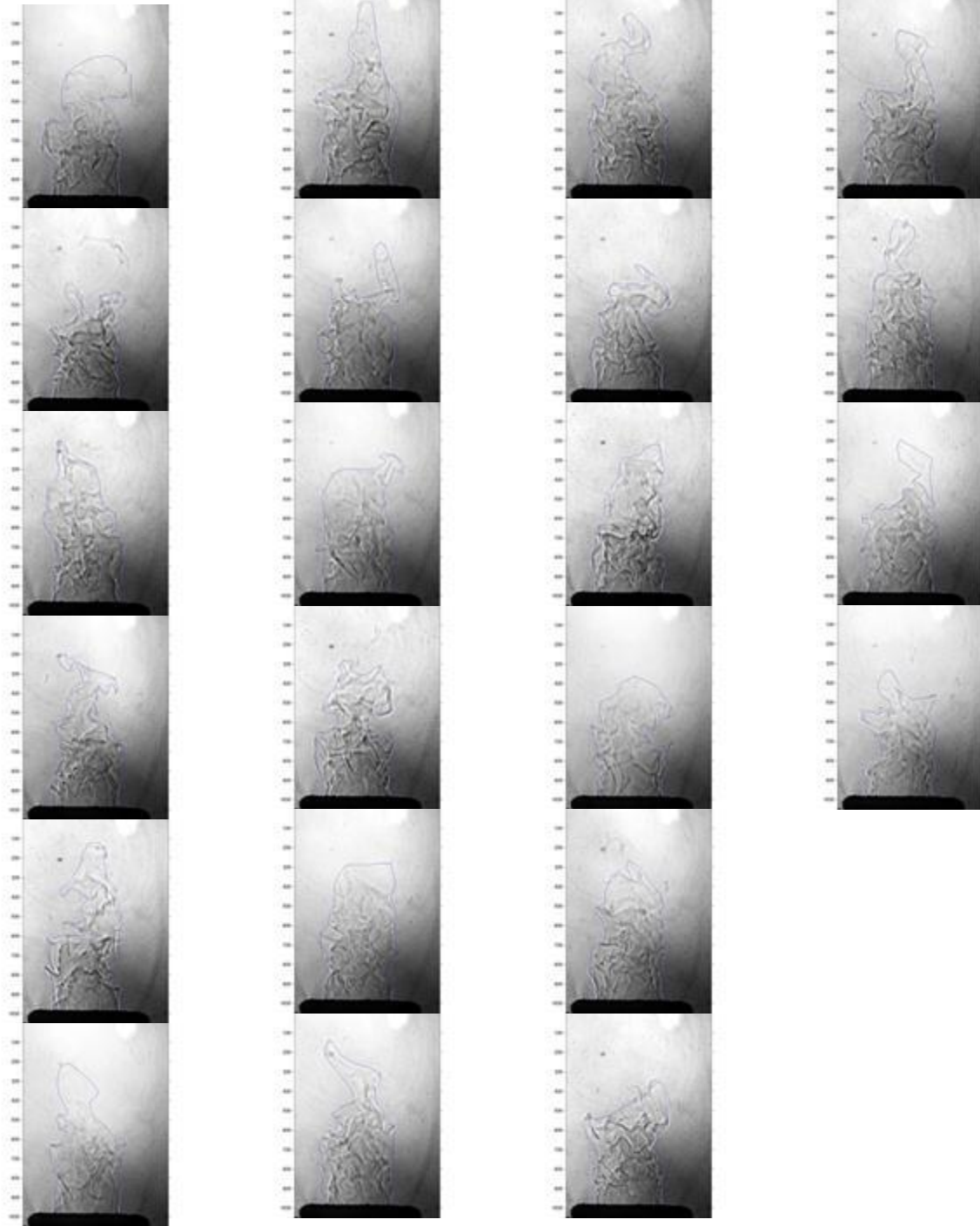
$d_{st} = 75-90 \mu\text{m}$, $u'_{rms} =$
 0.335 m/s , $\phi_g = 1.2$,
 $\lambda_{st} = 75 \text{ g/m}^3$



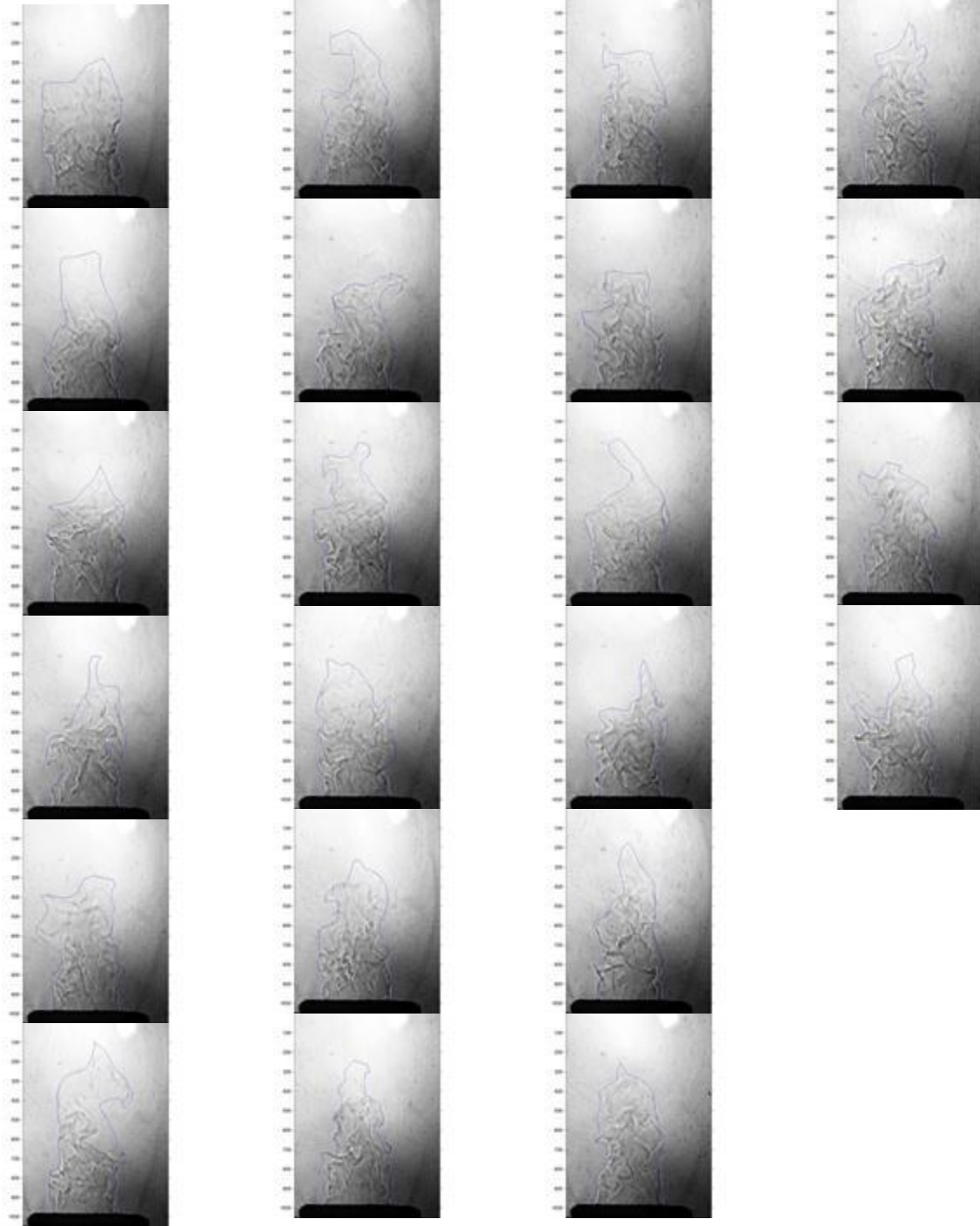
$d_{st} = 75-90 \mu\text{m}$, $u'_{rms} =$
 0.532 m/s , $\phi_g = 0.8$,
 $\lambda_{st} = 0 \text{ g/m}^3$



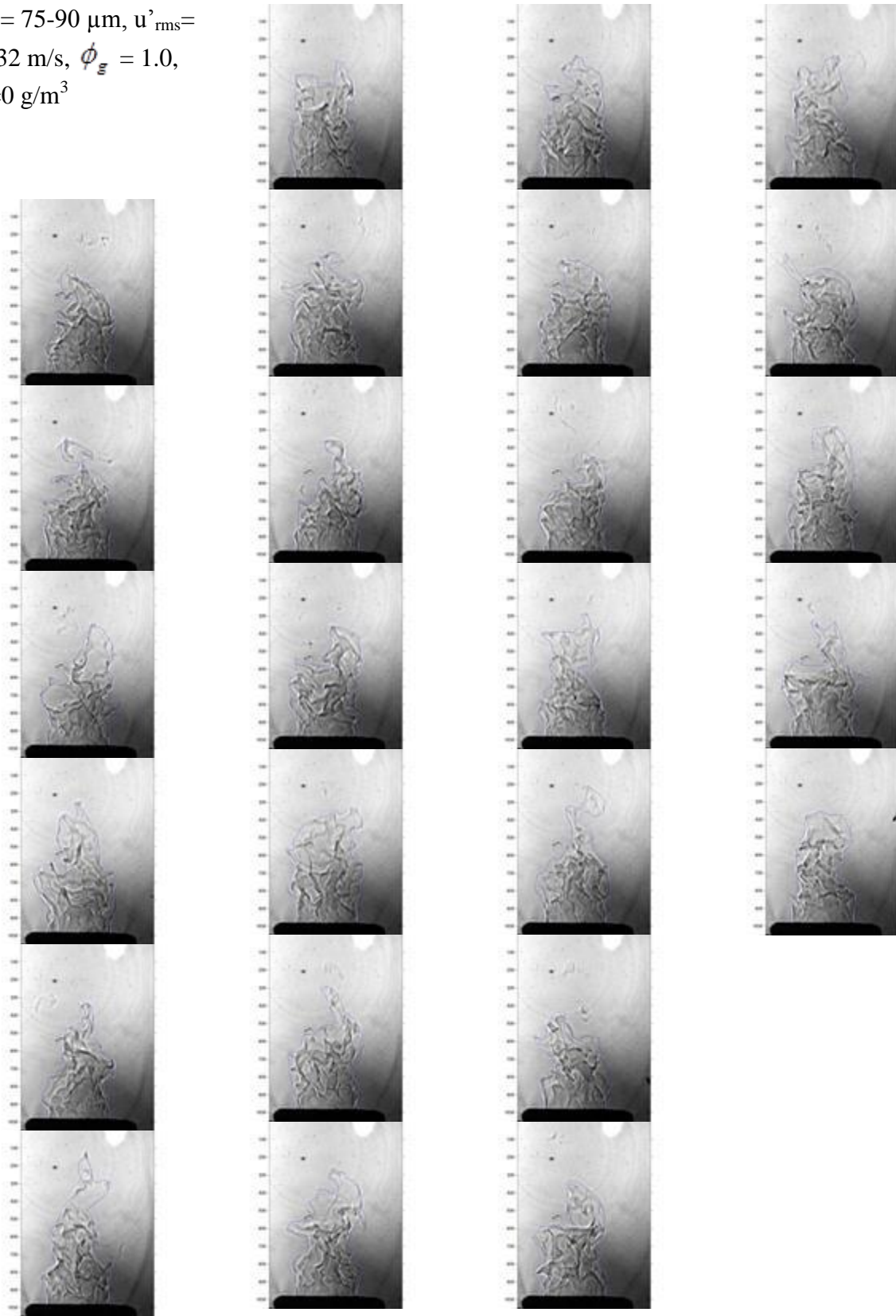
$d_{st} = 75-90 \mu\text{m}$, $u'_{\text{rms}} =$
 0.532 m/s , $\phi_g = 0.8$,
 $\lambda_{st} = 25 \text{ g/m}^3$



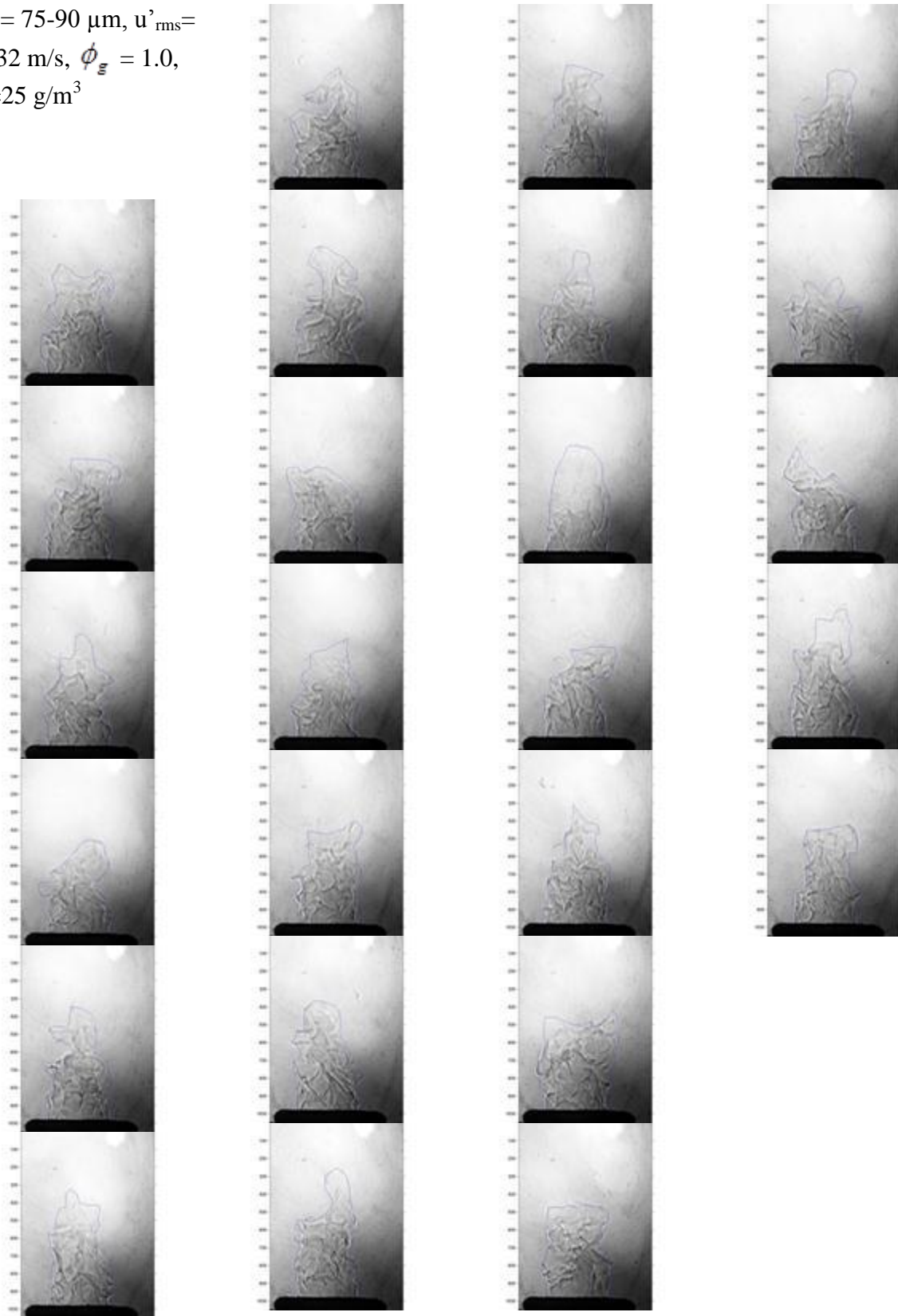
$d_{st} = 75-90 \mu\text{m}$, $u'_{rms} =$
 0.532 m/s , $\phi_g = 0.8$,
 $\lambda_{st} = 50 \text{ g/m}^3$



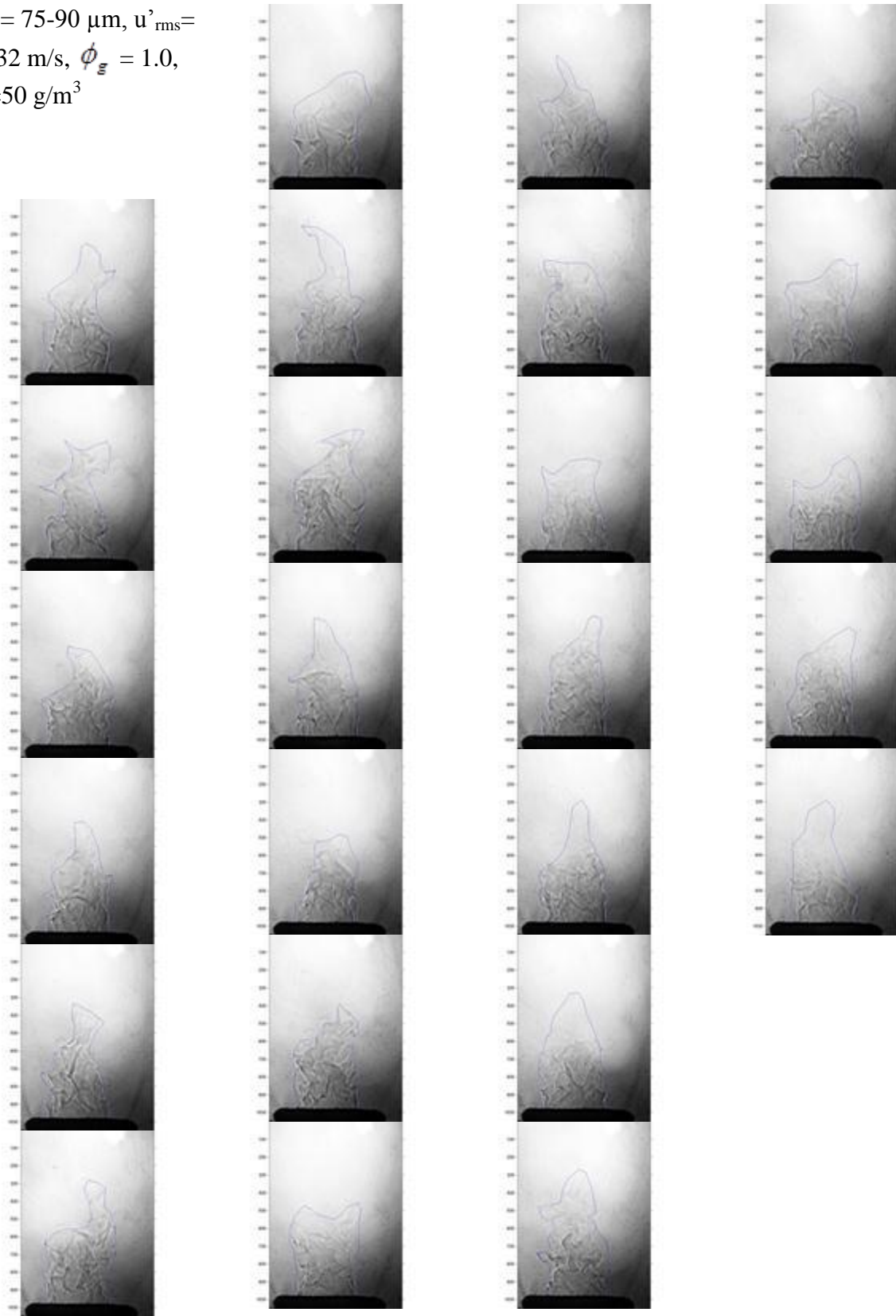
$d_{st} = 75-90 \mu\text{m}$, $u'_{\text{rms}} =$
 0.532 m/s , $\phi_g = 1.0$,
 $\lambda_{st} = 0 \text{ g/m}^3$



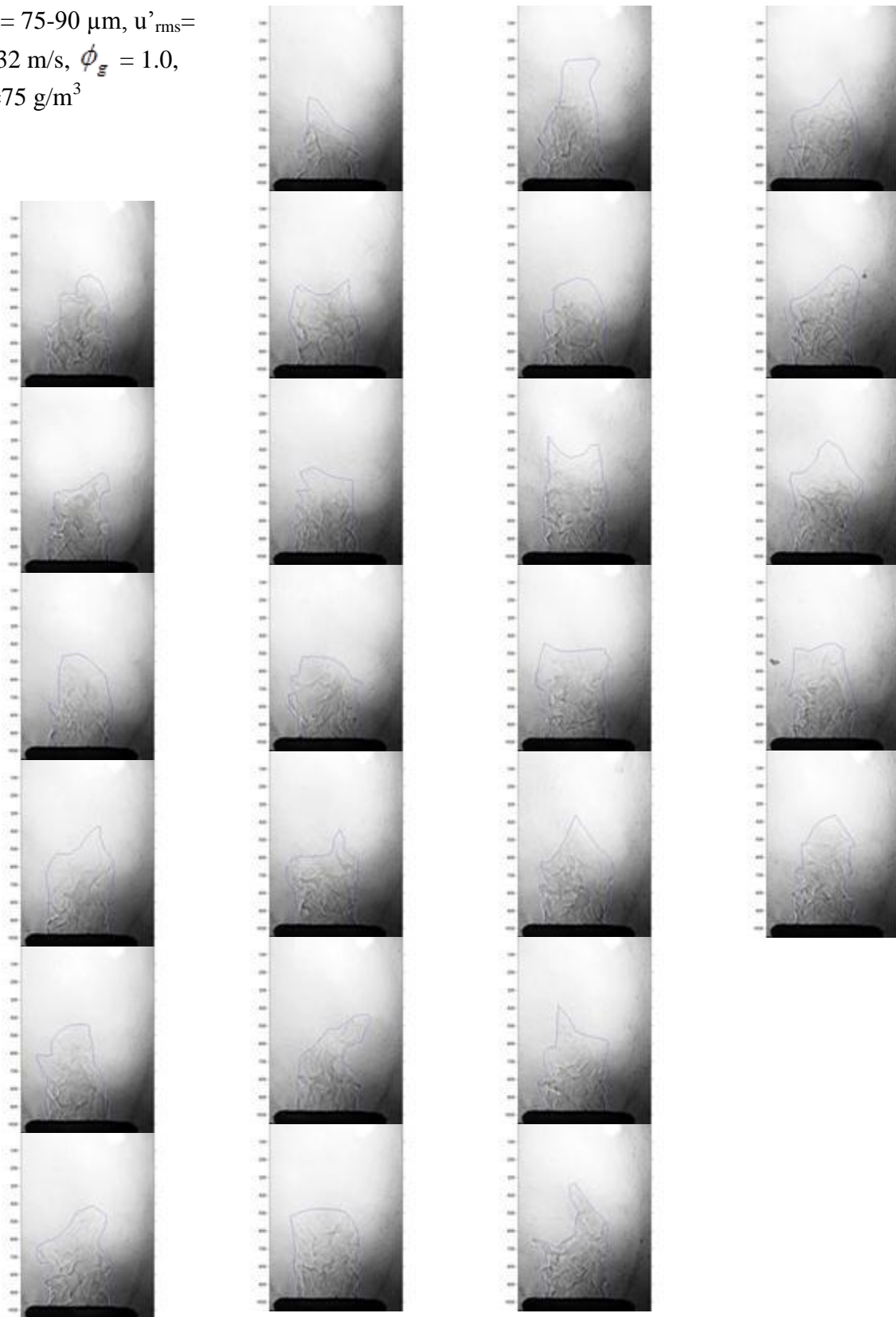
$d_{st} = 75-90 \mu\text{m}$, $u'_{rms} =$
 0.532 m/s , $\phi_g = 1.0$,
 $\lambda_{st} = 25 \text{ g/m}^3$



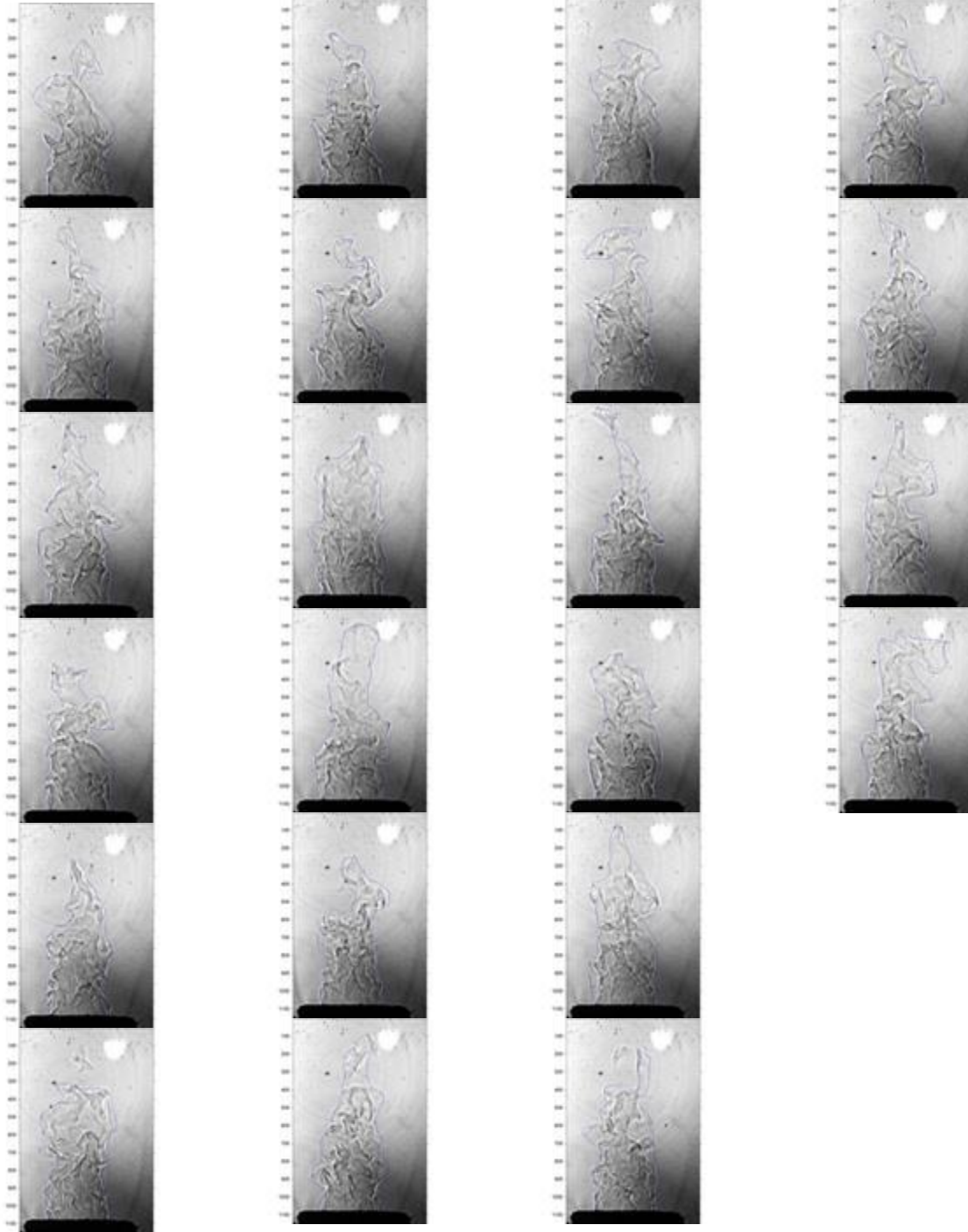
$d_{st} = 75-90 \mu\text{m}$, $u'_{rms} =$
 0.532 m/s , $\phi_g = 1.0$,
 $\lambda_{st} = 50 \text{ g/m}^3$



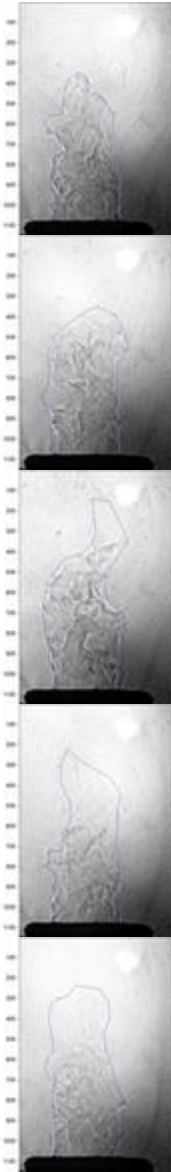
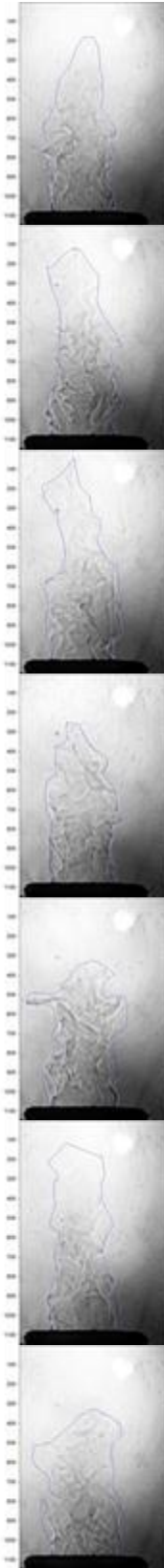
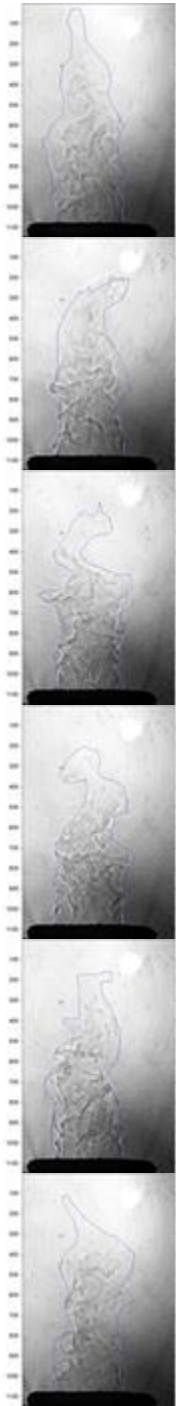
$d_{st} = 75-90 \mu\text{m}$, $u'_{rms} =$
 0.532 m/s , $\phi_g = 1.0$,
 $\lambda_{st} = 75 \text{ g/m}^3$



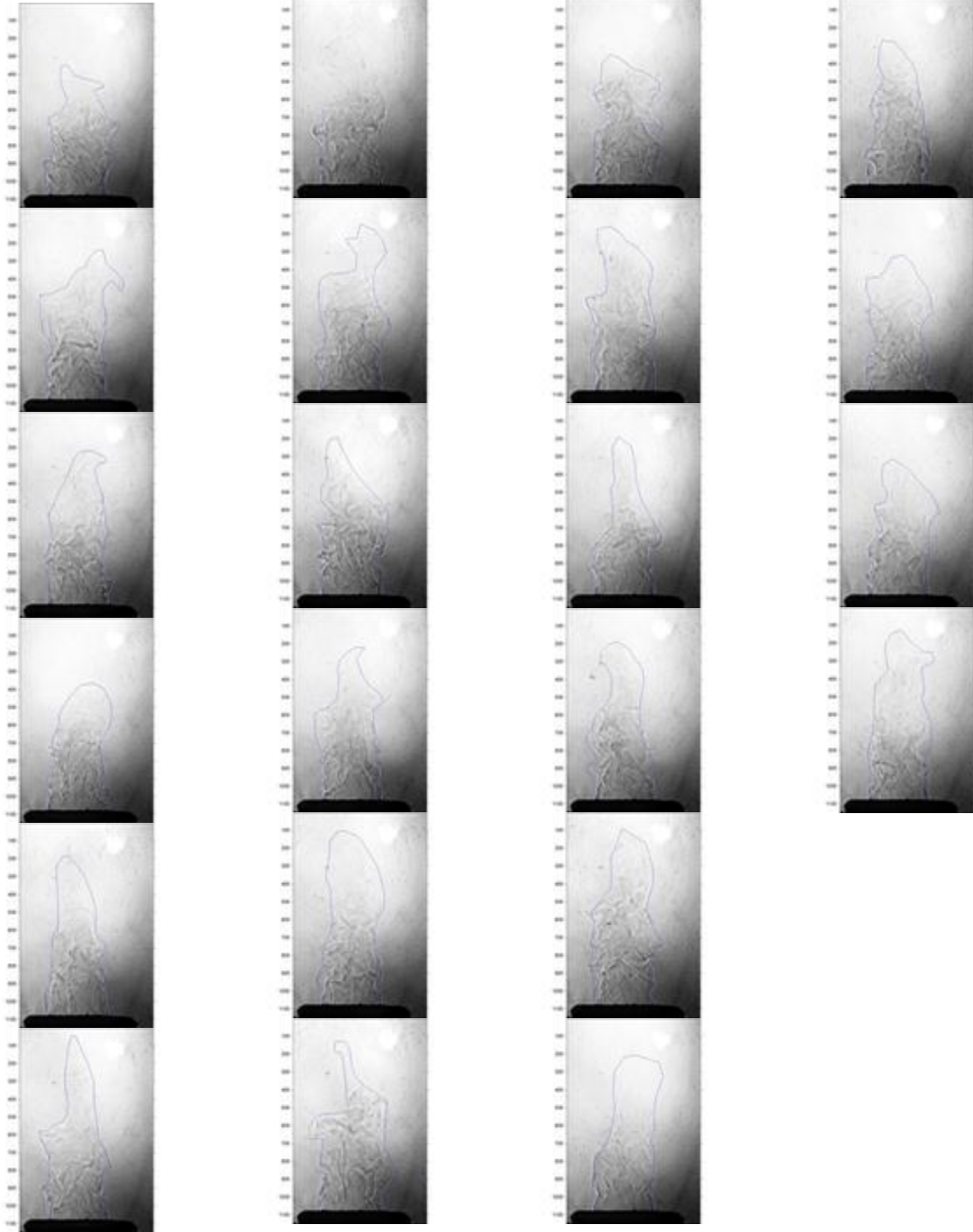
$d_{st} = 75-90 \mu\text{m}$, $u'_{\text{rms}} =$
 0.532 m/s , $\phi_g = 1.2$,
 $\lambda_{st} = 0 \text{ g/m}^3$



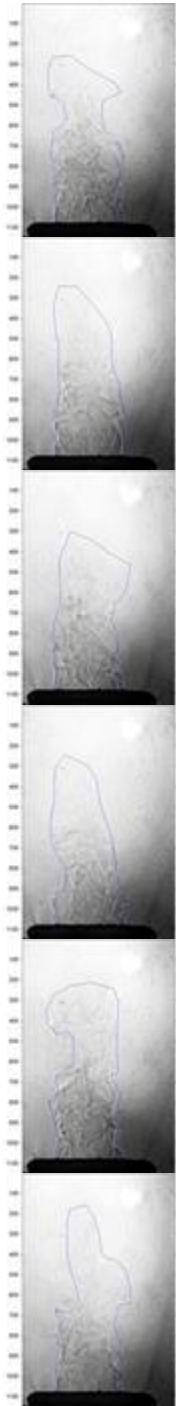
$d_{st} = 75-90 \mu\text{m}$, $u'_{rms} =$
 0.532 m/s , $\phi_g = 1.2$,
 $\lambda_{st} = 25 \text{ g/m}^3$



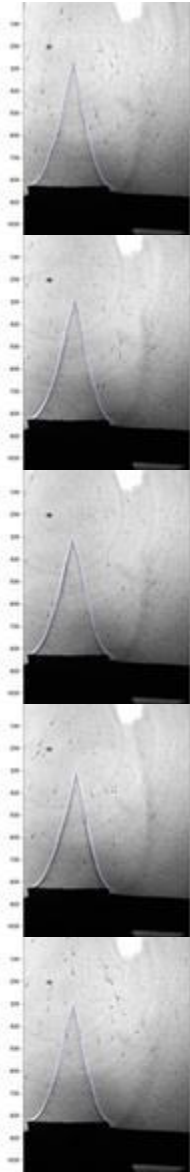
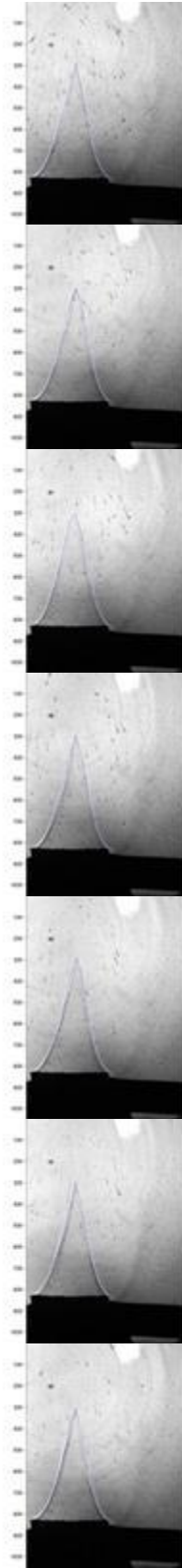
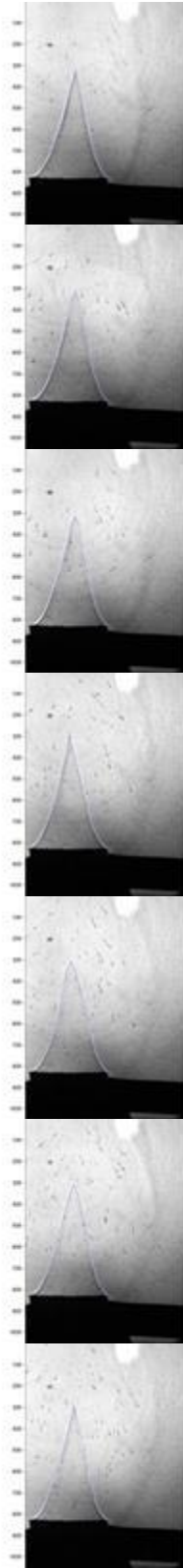
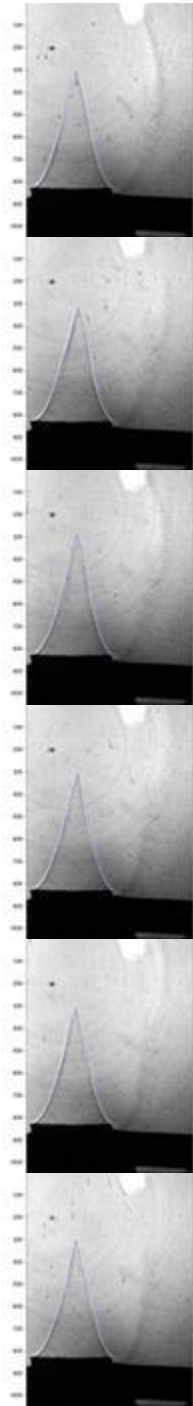
$d_{st} = 75-90 \mu\text{m}$, $u'_{rms} =$
 0.532 m/s , $\phi_g = 1.2$,
 $\lambda_{st} = 50 \text{ g/m}^3$



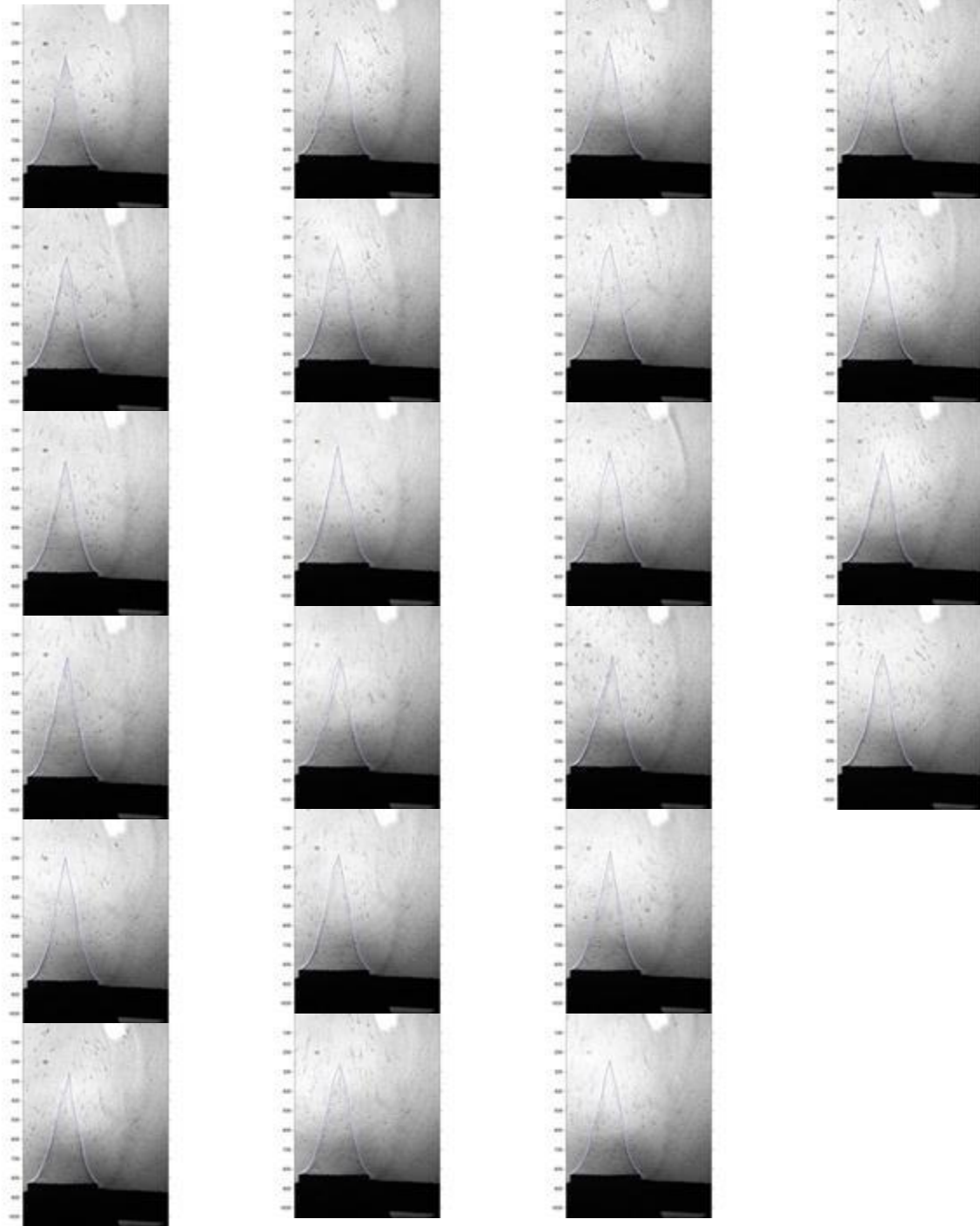
$d_{st} = 75-90 \mu\text{m}$, $u'_{rms} =$
 0.532 m/s , $\phi_g = 1.2$,
 $\lambda_{st} = 75 \text{ g/m}^3$



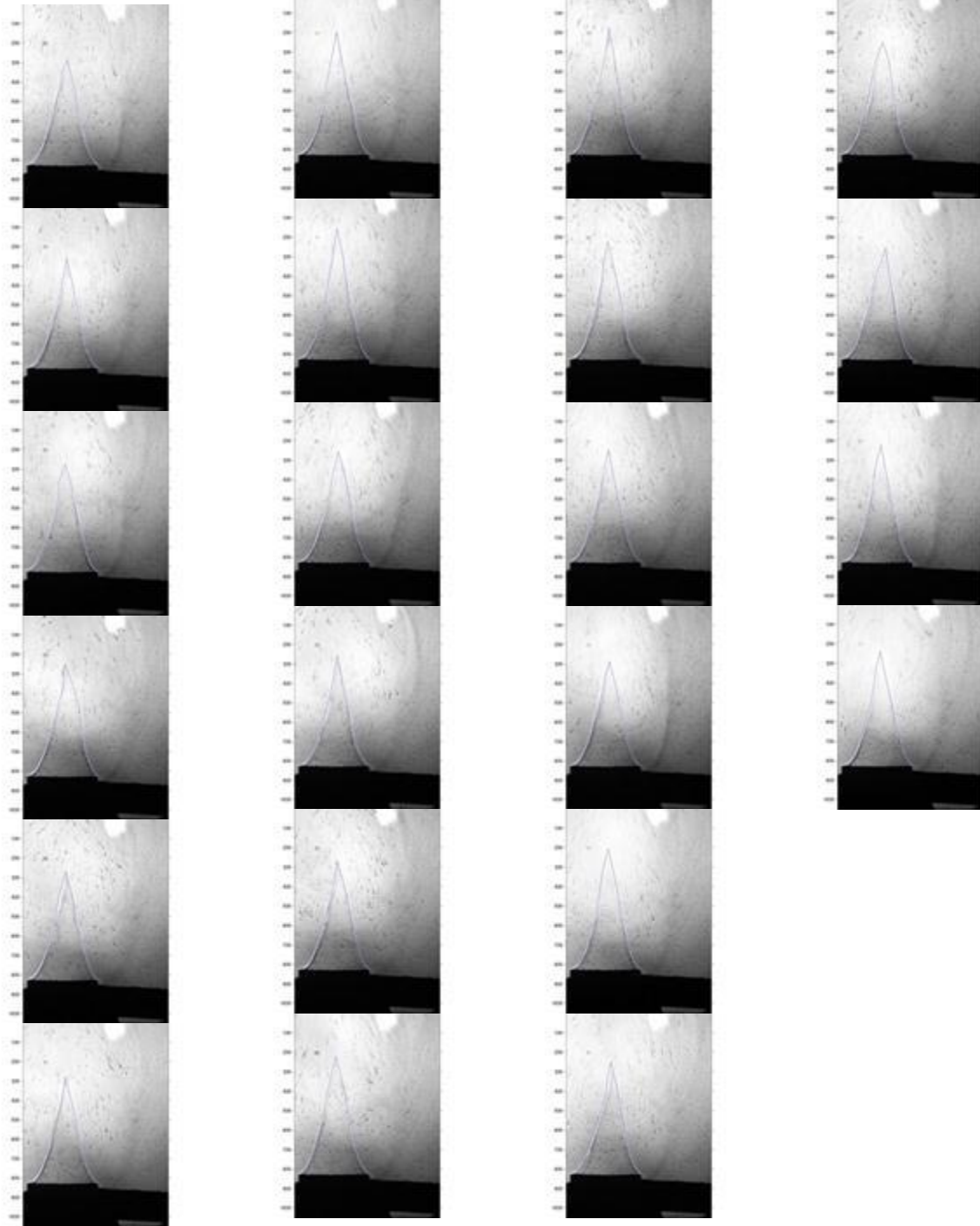
$d_{st} = 75-90 \mu\text{m}$, $u'_{rms} =$
 0.024 m/s , $\phi_g = 0.8$,
 $\lambda_{st} = 25 \text{ g/m}^3$



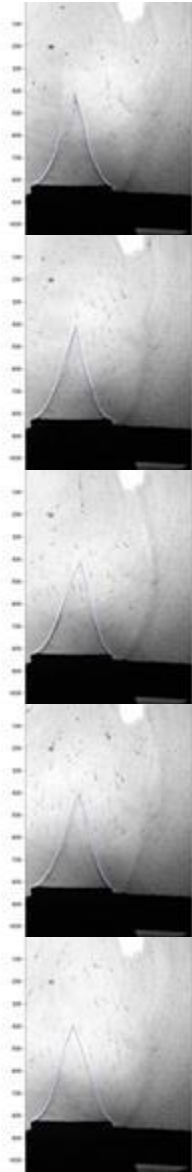
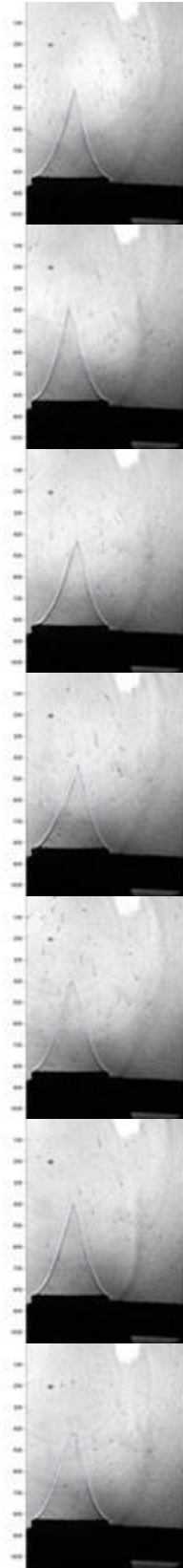
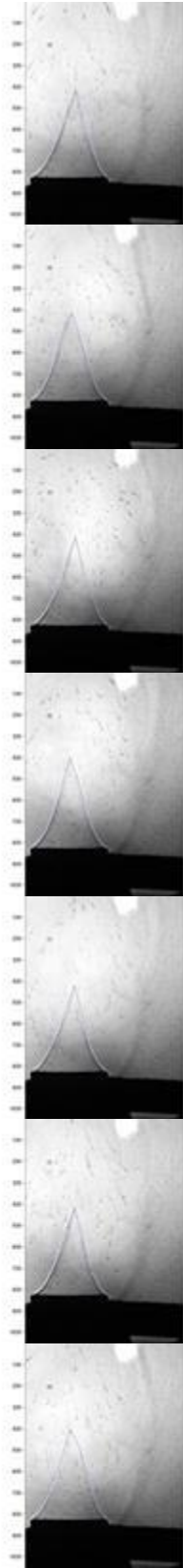
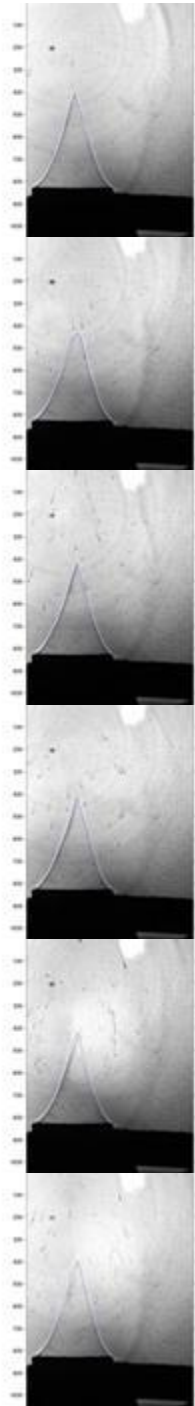
$d_{st} = 75-90 \mu\text{m}$, $u'_{rms} =$
 0.024 m/s , $\phi_g = 0.8$,
 $\lambda_{st} = 50 \text{ g/m}^3$



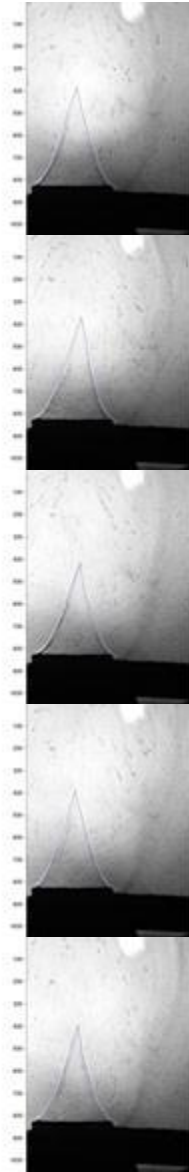
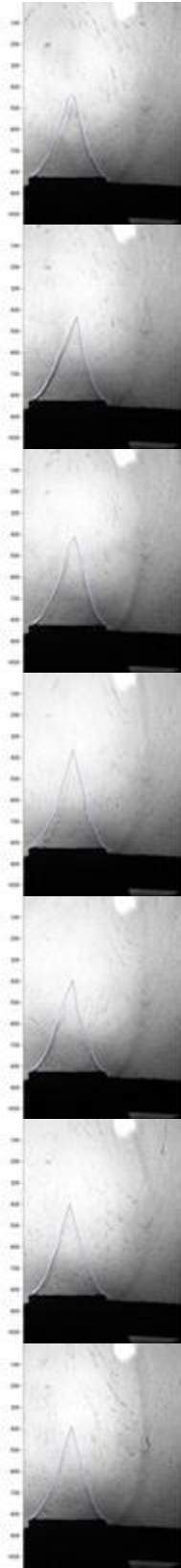
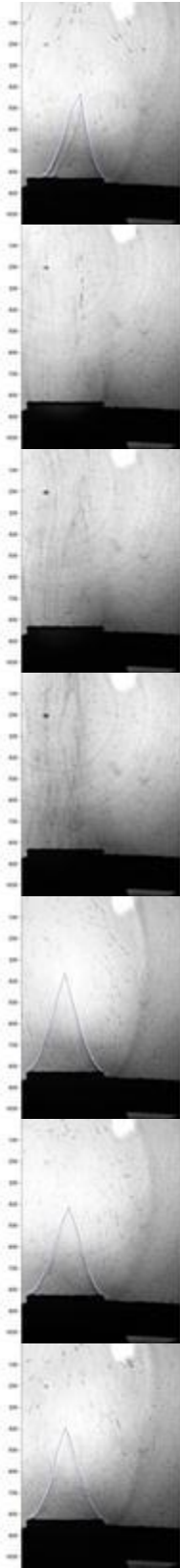
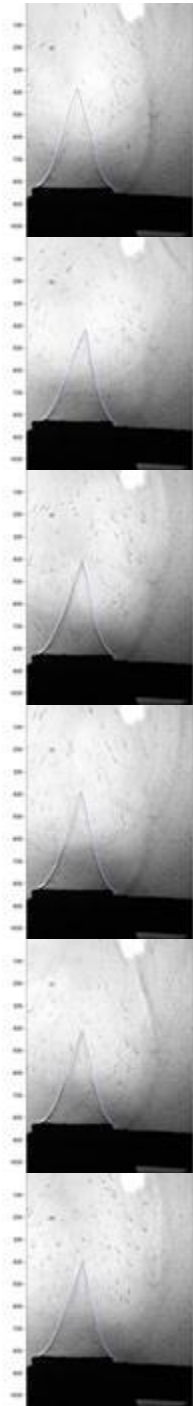
$d_{st} = 75-90 \mu\text{m}$, $u'_{rms} =$
 0.024 m/s , $\phi_g = 0.8$,
 $\lambda_{st} = 75 \text{ g/m}^3$



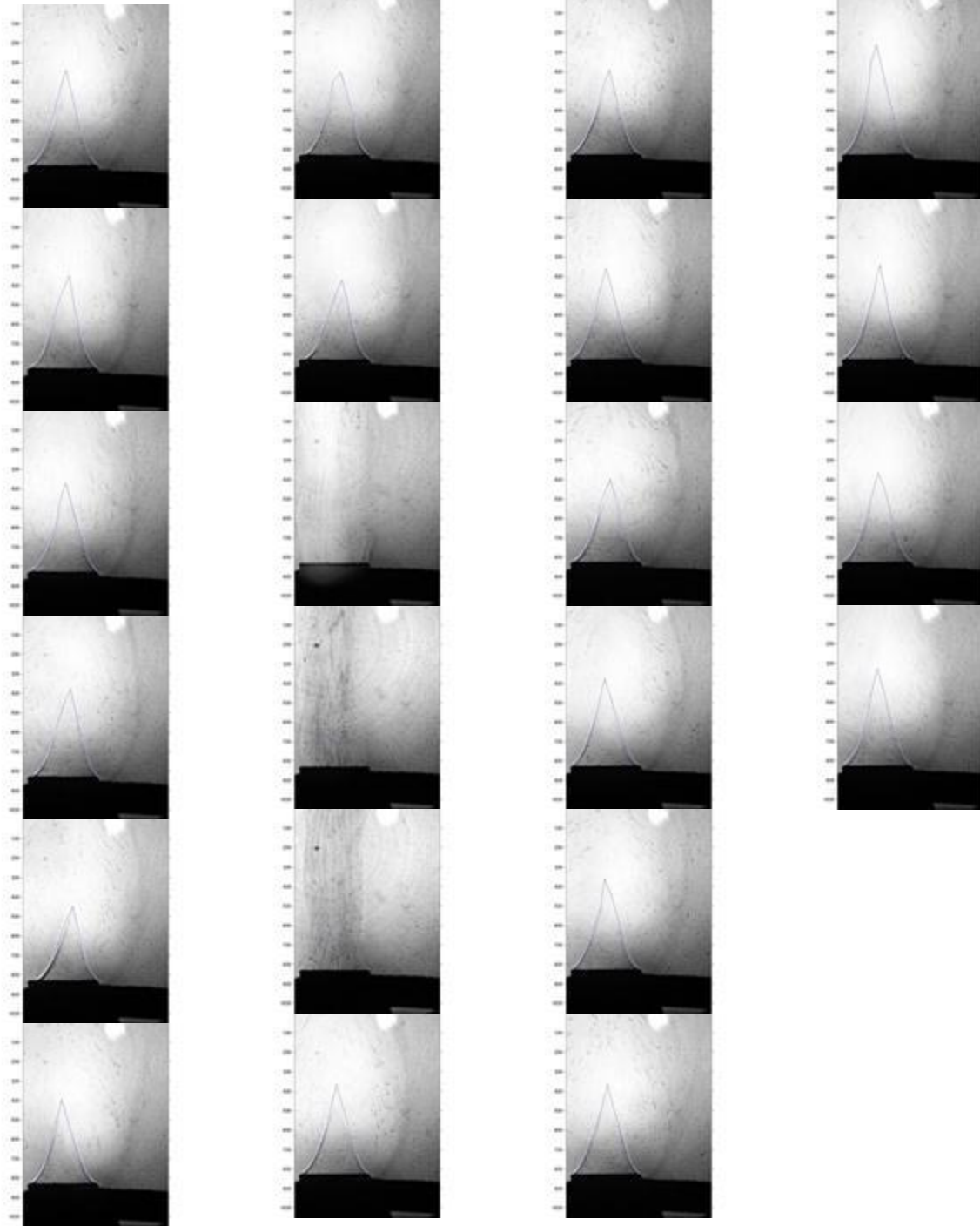
$d_{st} = 75-90 \mu\text{m}$, $u'_{rms} =$
 0.024 m/s , $\phi_g = 1.0$,
 $\lambda_{st} = 25 \text{ g/m}^3$



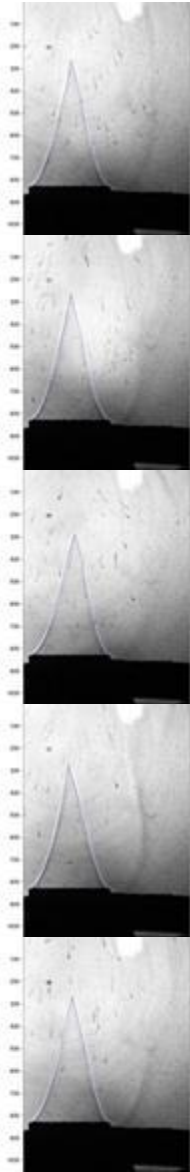
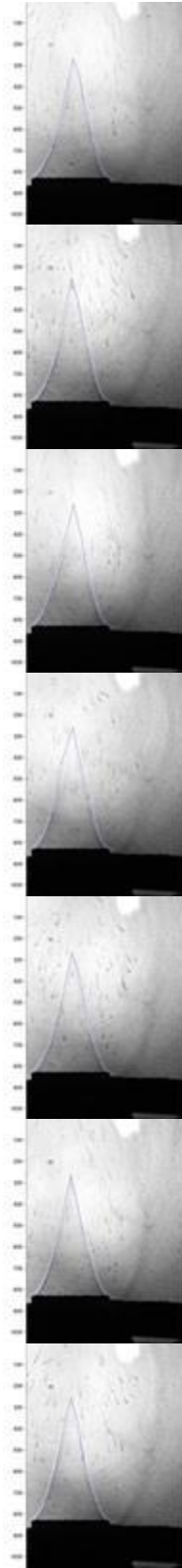
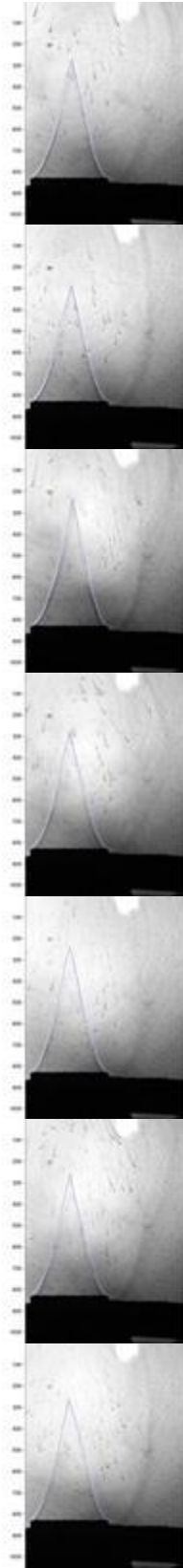
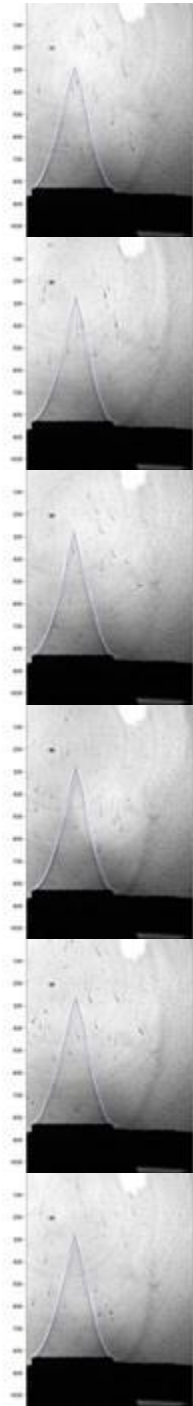
$d_{st} = 75-90 \mu\text{m}$, $u'_{rms} =$
 0.024 m/s , $\phi_g = 1.0$,
 $\lambda_{st} = 50 \text{ g/m}^3$



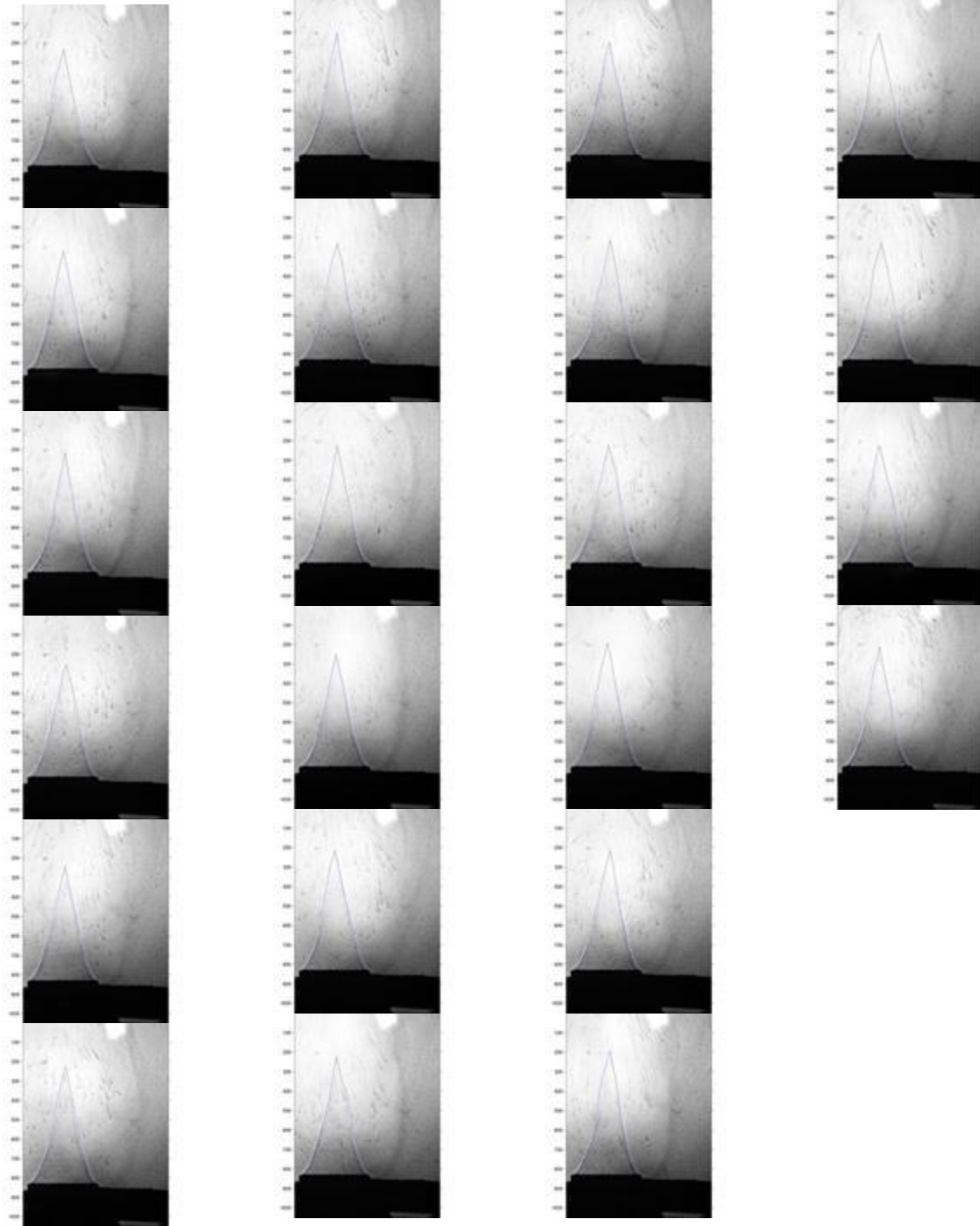
$d_{st} = 75-90 \mu\text{m}$, $u'_{rms} =$
 0.024 m/s , $\phi_g = 1.0$,
 $\lambda_{st} = 75 \text{ g/m}^3$



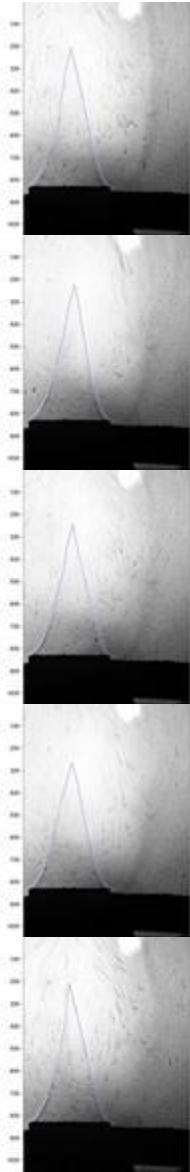
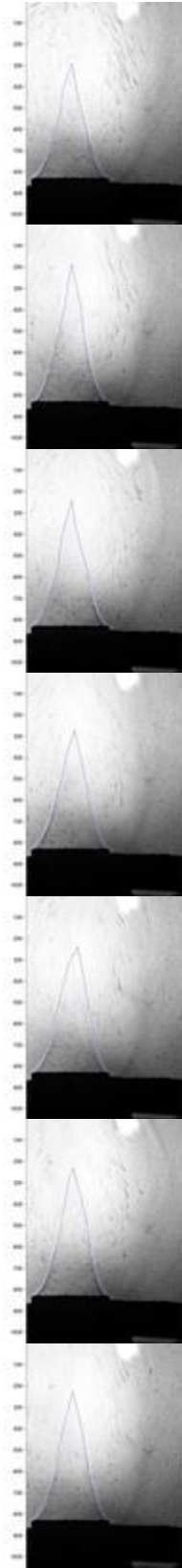
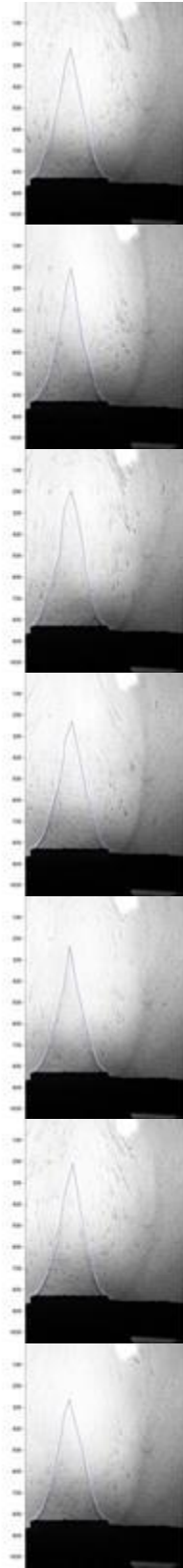
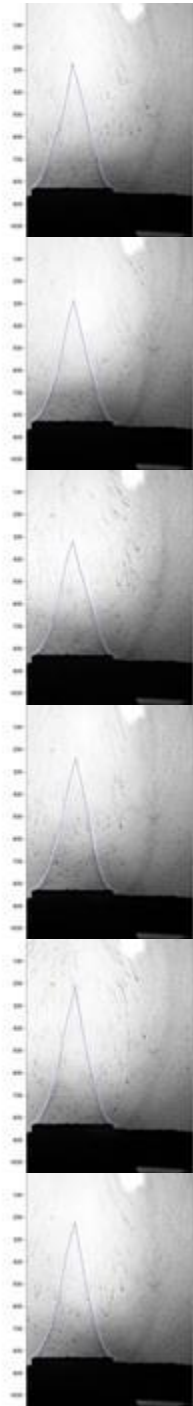
$d_{st} = 75-90 \mu\text{m}$, $u'_{rms} =$
 0.024 m/s , $\phi_g = 1.2$,
 $\lambda_{st} = 25 \text{ g/m}^3$



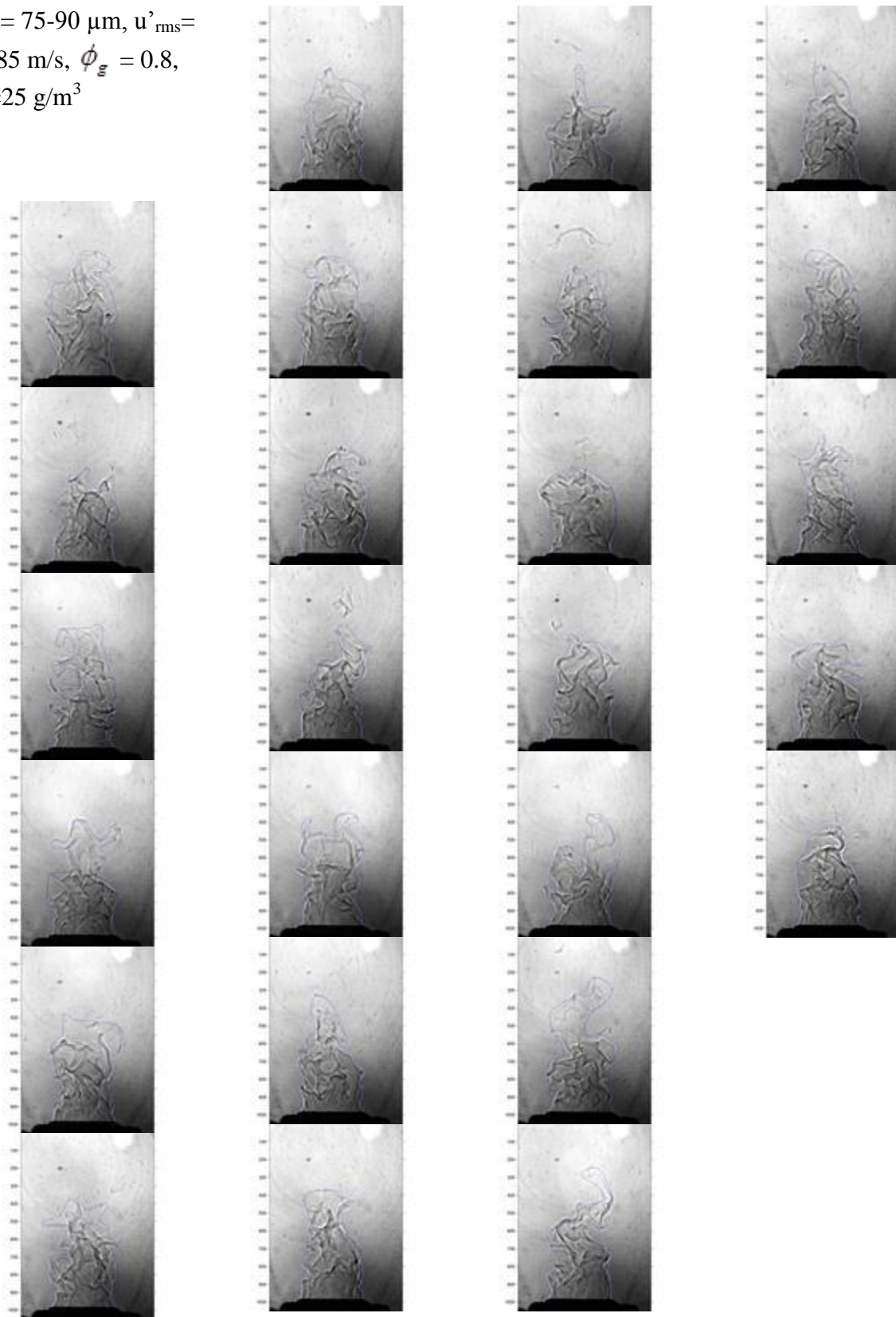
$d_{st} = 75-90 \mu\text{m}$, $u'_{rms} =$
 0.024 m/s , $\phi_g = 1.2$,
 $\lambda_{st} = 50 \text{ g/m}^3$



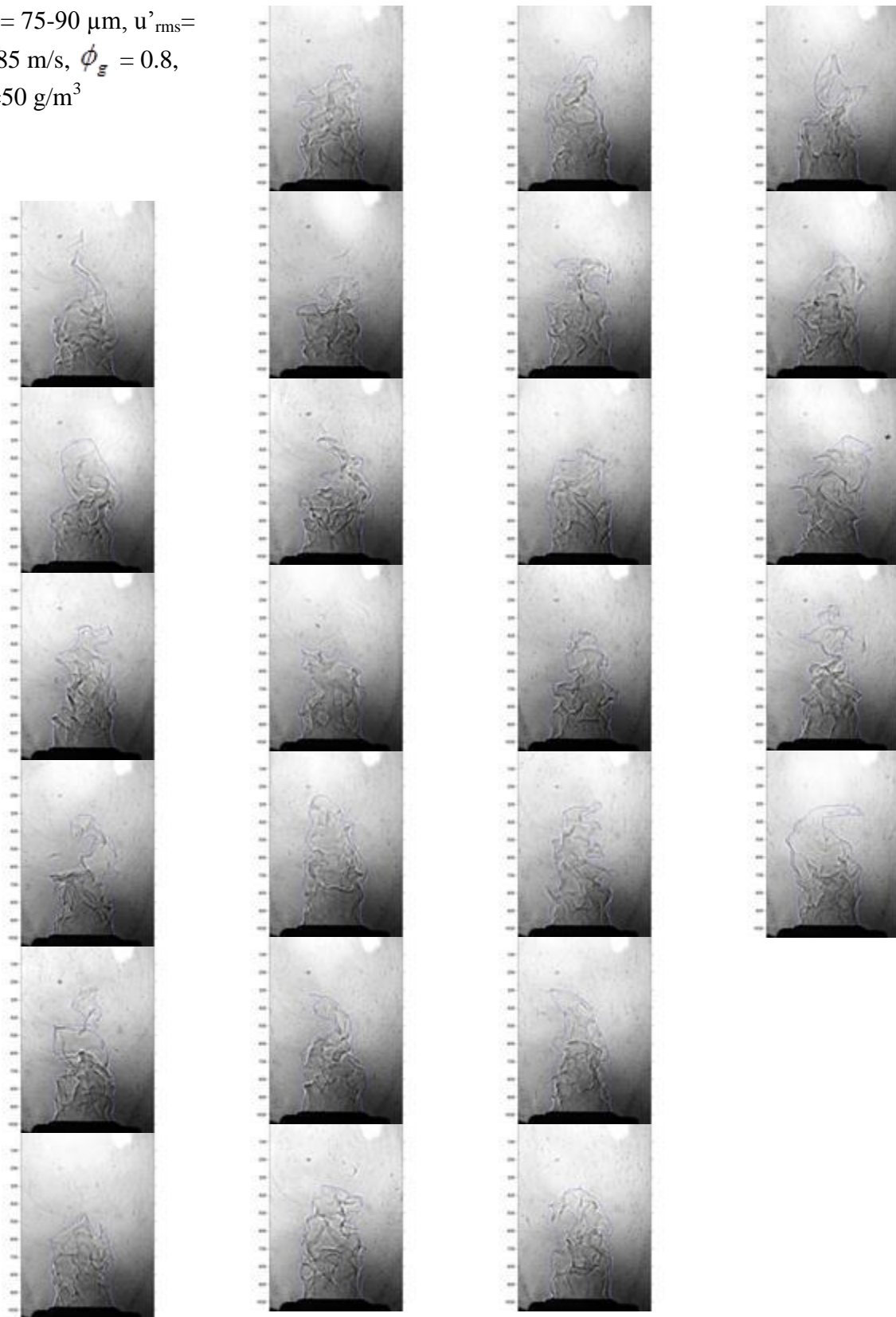
$d_{st} = 75-90 \mu\text{m}$, $u'_{rms} =$
 0.024 m/s , $\phi_g = 1.2$,
 $\lambda_{st} = 75 \text{ g/m}^3$



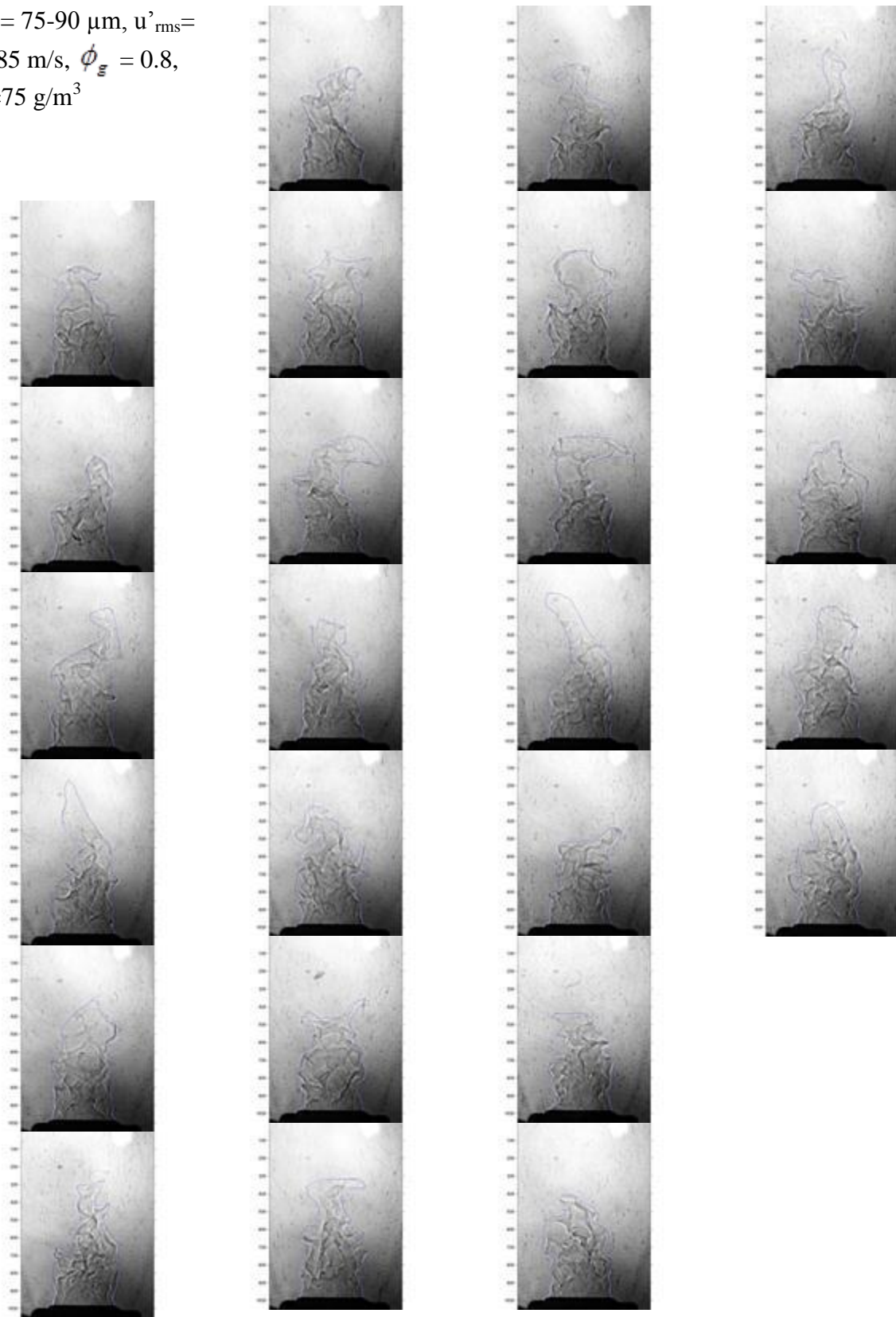
$d_{st} = 75-90 \mu\text{m}$, $u'_{\text{rms}} =$
 0.185 m/s , $\phi_g = 0.8$,
 $\lambda_{st} = 25 \text{ g/m}^3$



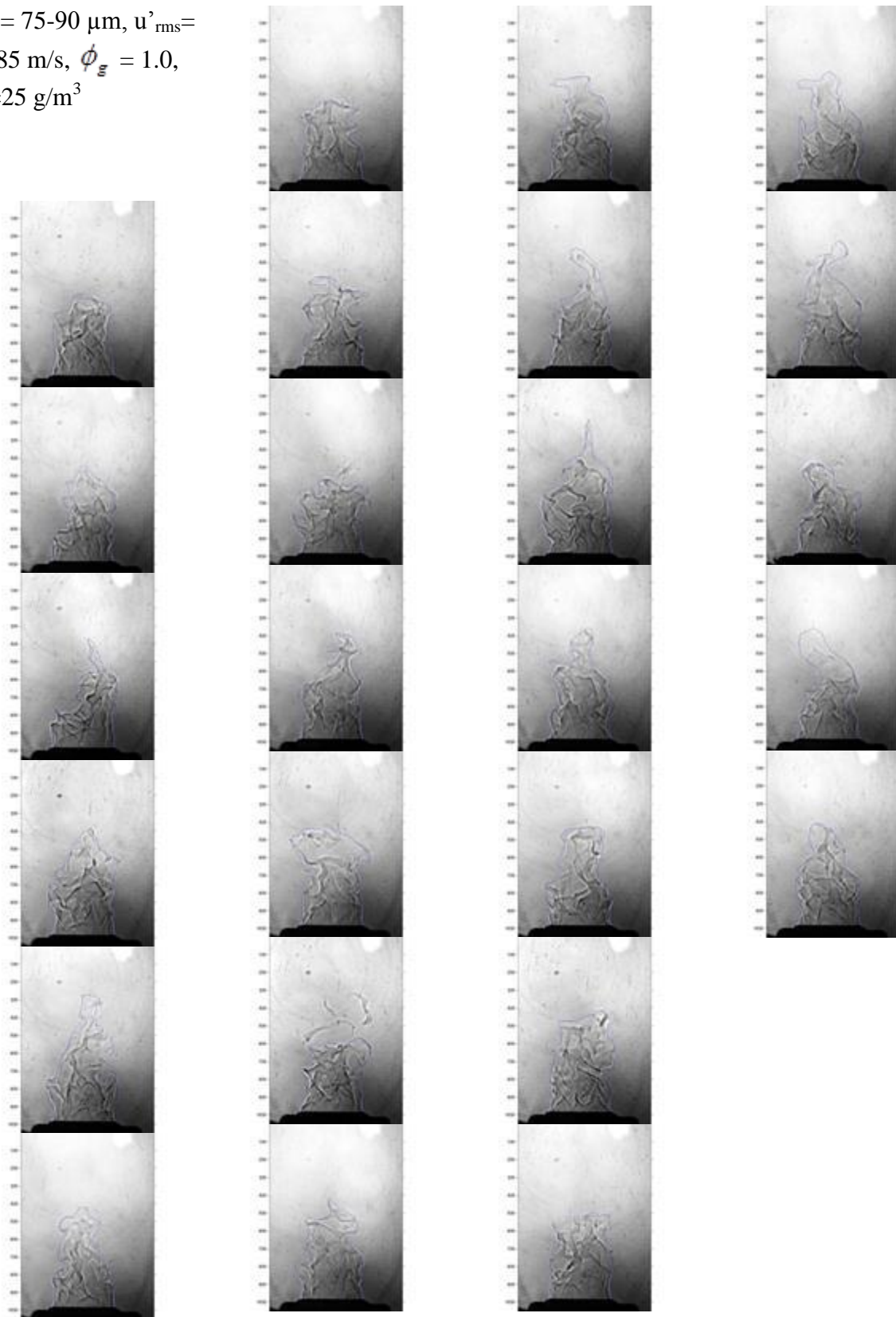
$d_{st} = 75-90 \mu\text{m}$, $u'_{rms} =$
 0.185 m/s , $\phi_g = 0.8$,
 $\lambda_{st} = 50 \text{ g/m}^3$



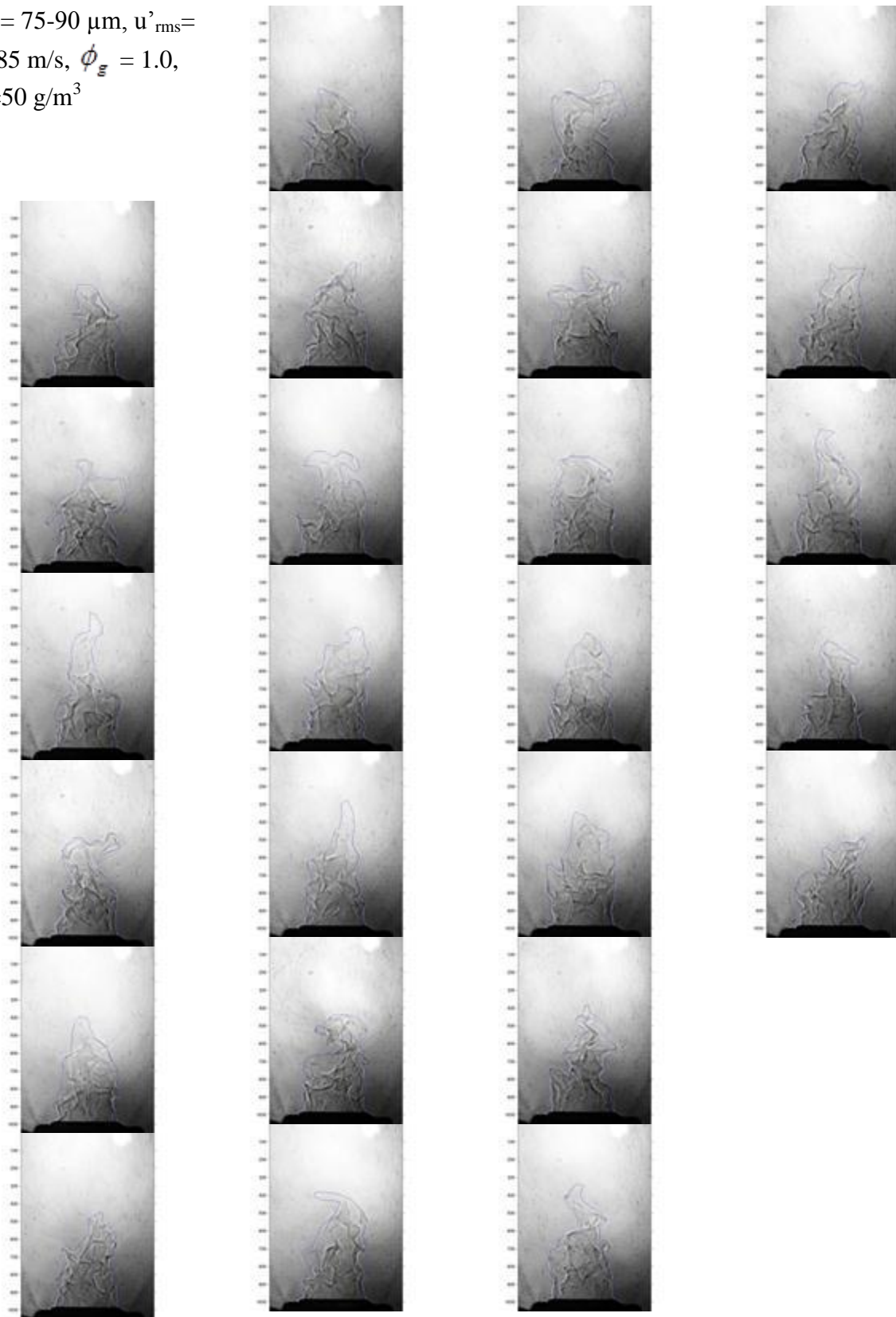
$d_{st} = 75-90 \mu\text{m}$, $u'_{rms} =$
 0.185 m/s , $\phi_g = 0.8$,
 $\lambda_{st} = 75 \text{ g/m}^3$



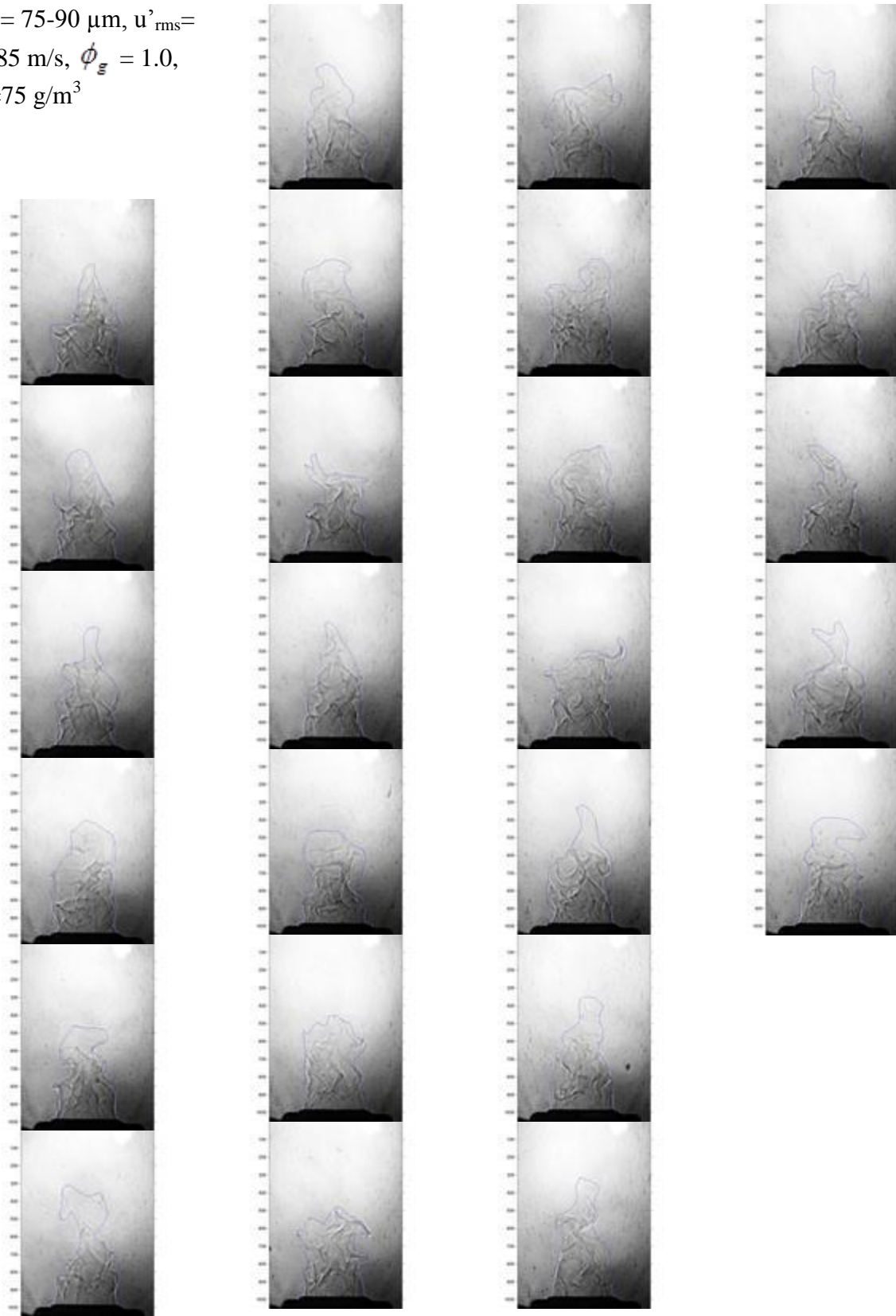
$d_{st} = 75-90 \mu\text{m}$, $u'_{\text{rms}} =$
 0.185 m/s , $\phi_g = 1.0$,
 $\lambda_{st} = 25 \text{ g/m}^3$



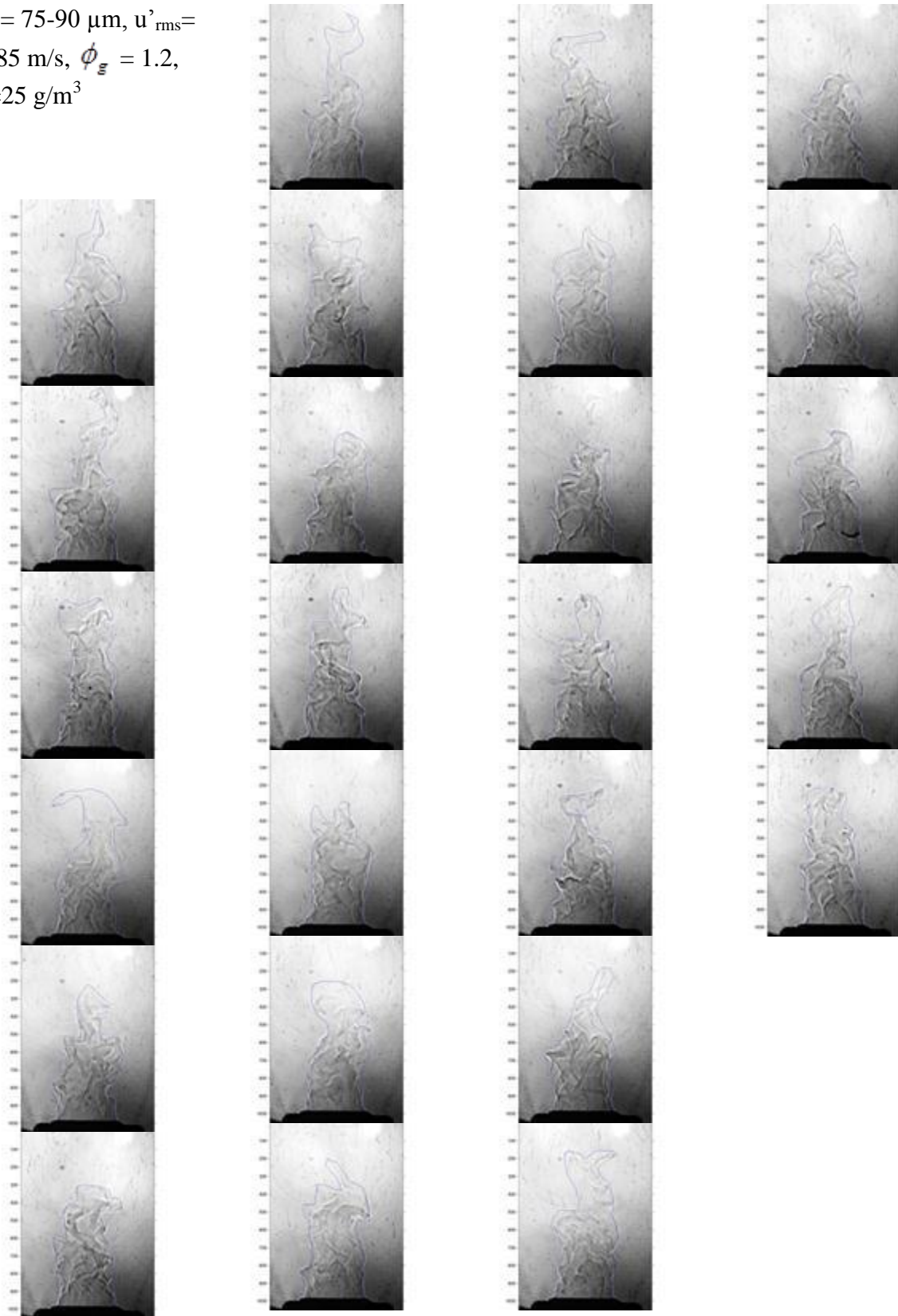
$d_{st} = 75-90 \mu\text{m}$, $u'_{\text{rms}} =$
 0.185 m/s , $\phi_g = 1.0$,
 $\lambda_{st} = 50 \text{ g/m}^3$



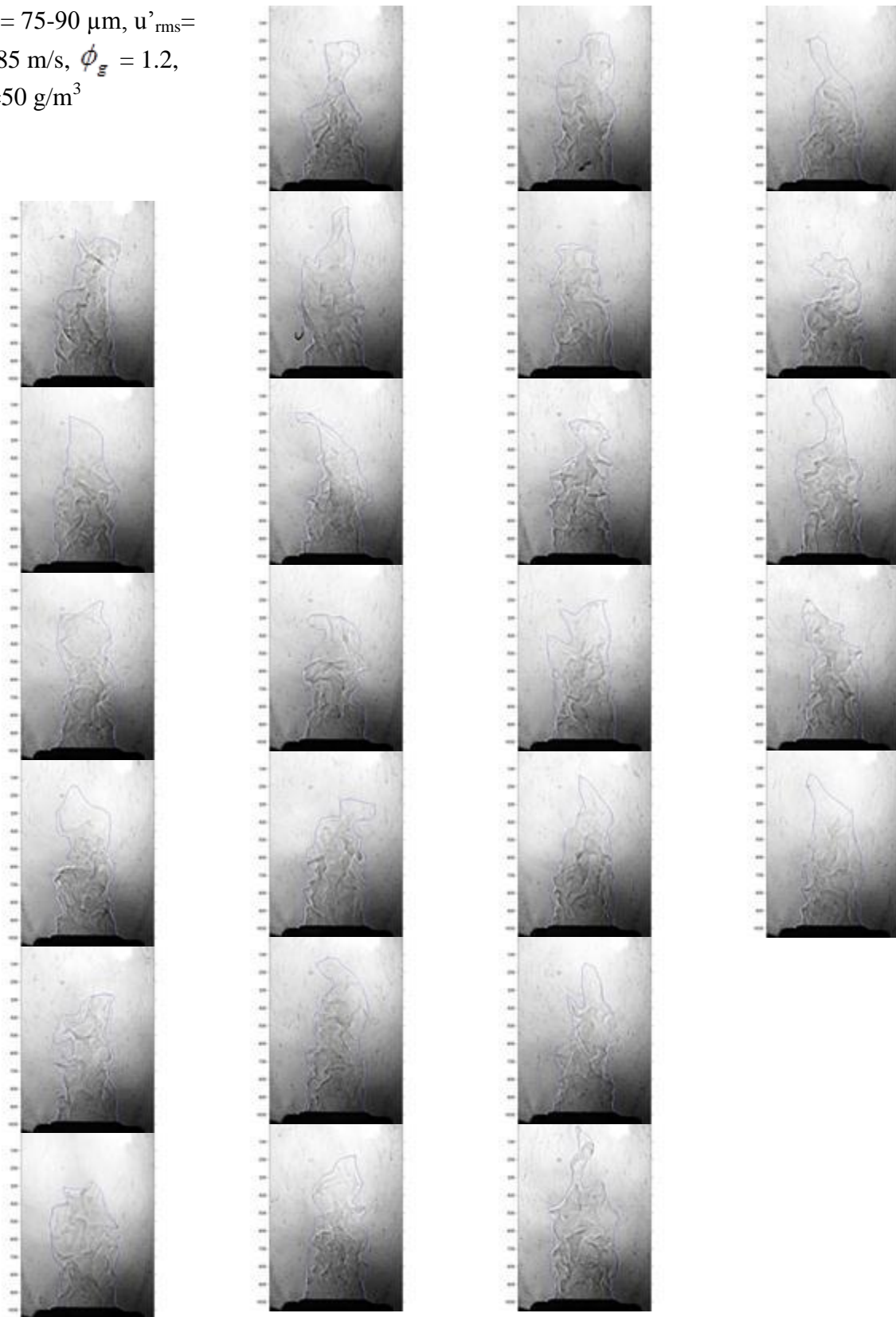
$d_{st} = 75-90 \mu\text{m}$, $u'_{rms} =$
 0.185 m/s , $\phi_g = 1.0$,
 $\lambda_{st} = 75 \text{ g/m}^3$



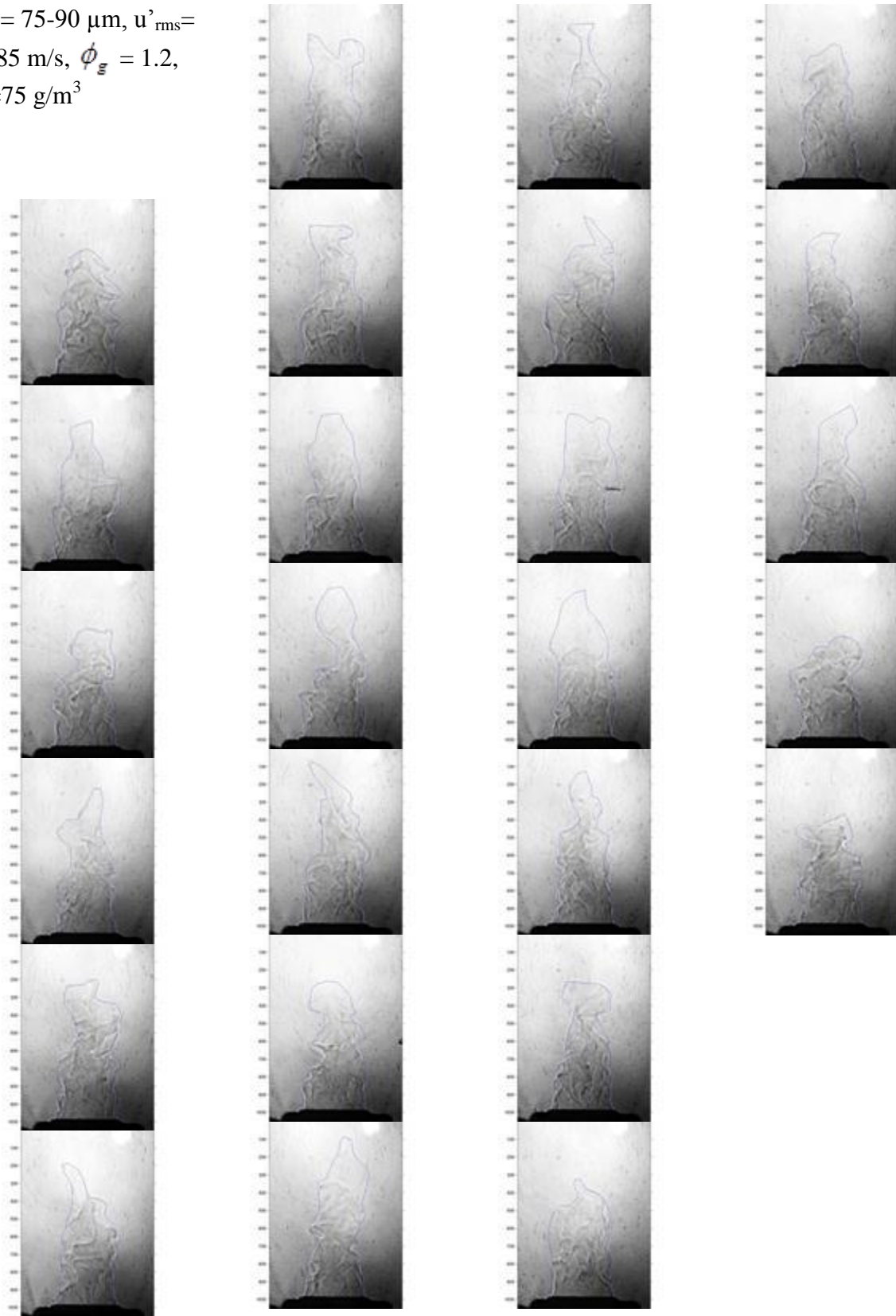
$d_{st} = 75-90 \mu\text{m}$, $u'_{rms} =$
 0.185 m/s , $\phi_g = 1.2$,
 $\lambda_{st} = 25 \text{ g/m}^3$



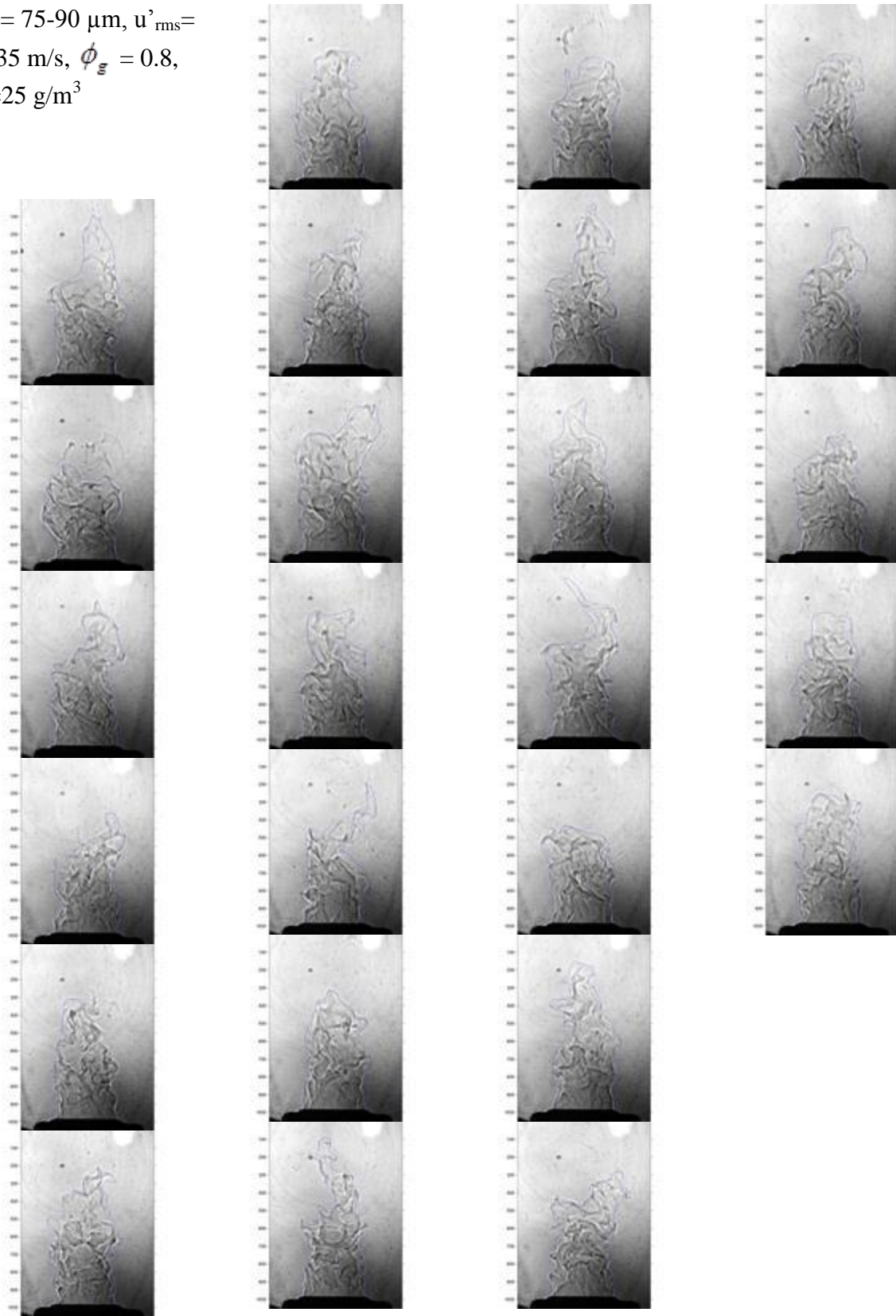
$d_{st} = 75-90 \mu\text{m}$, $u'_{rms} =$
 0.185 m/s , $\phi_g = 1.2$,
 $\lambda_{st} = 50 \text{ g/m}^3$



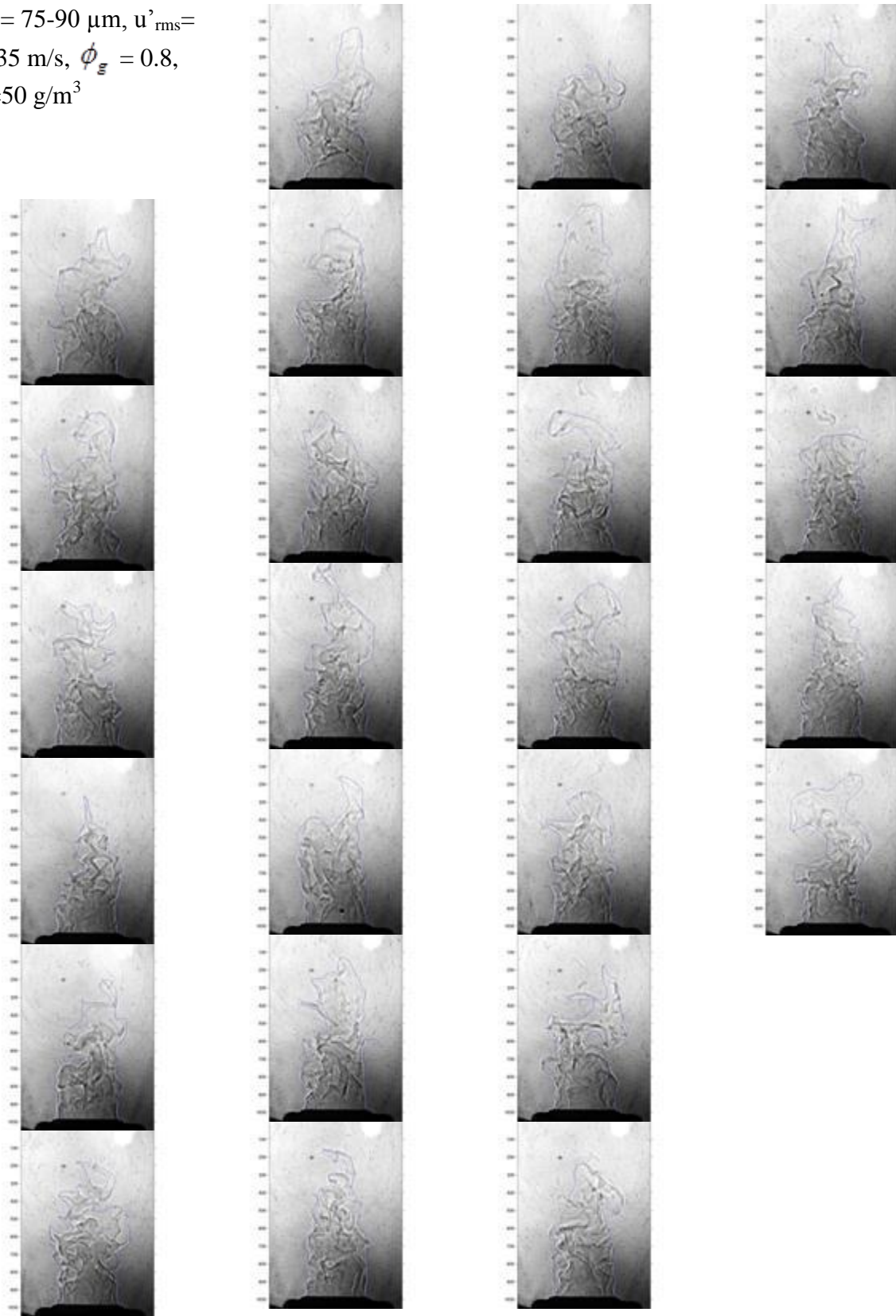
$d_{st} = 75-90 \mu\text{m}$, $u'_{rms} =$
 0.185 m/s , $\phi_g = 1.2$,
 $\lambda_{st} = 75 \text{ g/m}^3$



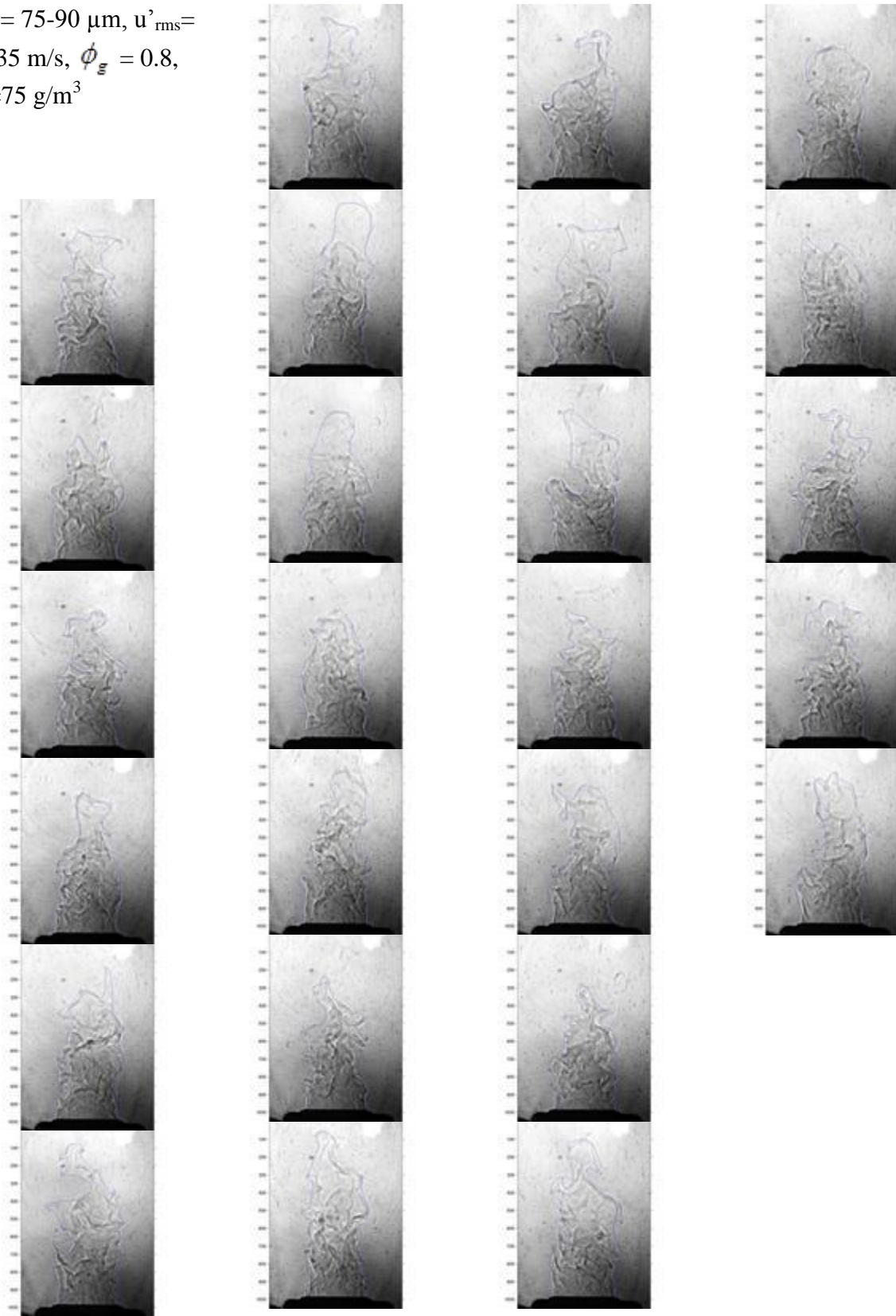
$d_{st} = 75-90 \mu\text{m}$, $u'_{rms} =$
 0.335 m/s , $\phi_g = 0.8$,
 $\lambda_{st} = 25 \text{ g/m}^3$



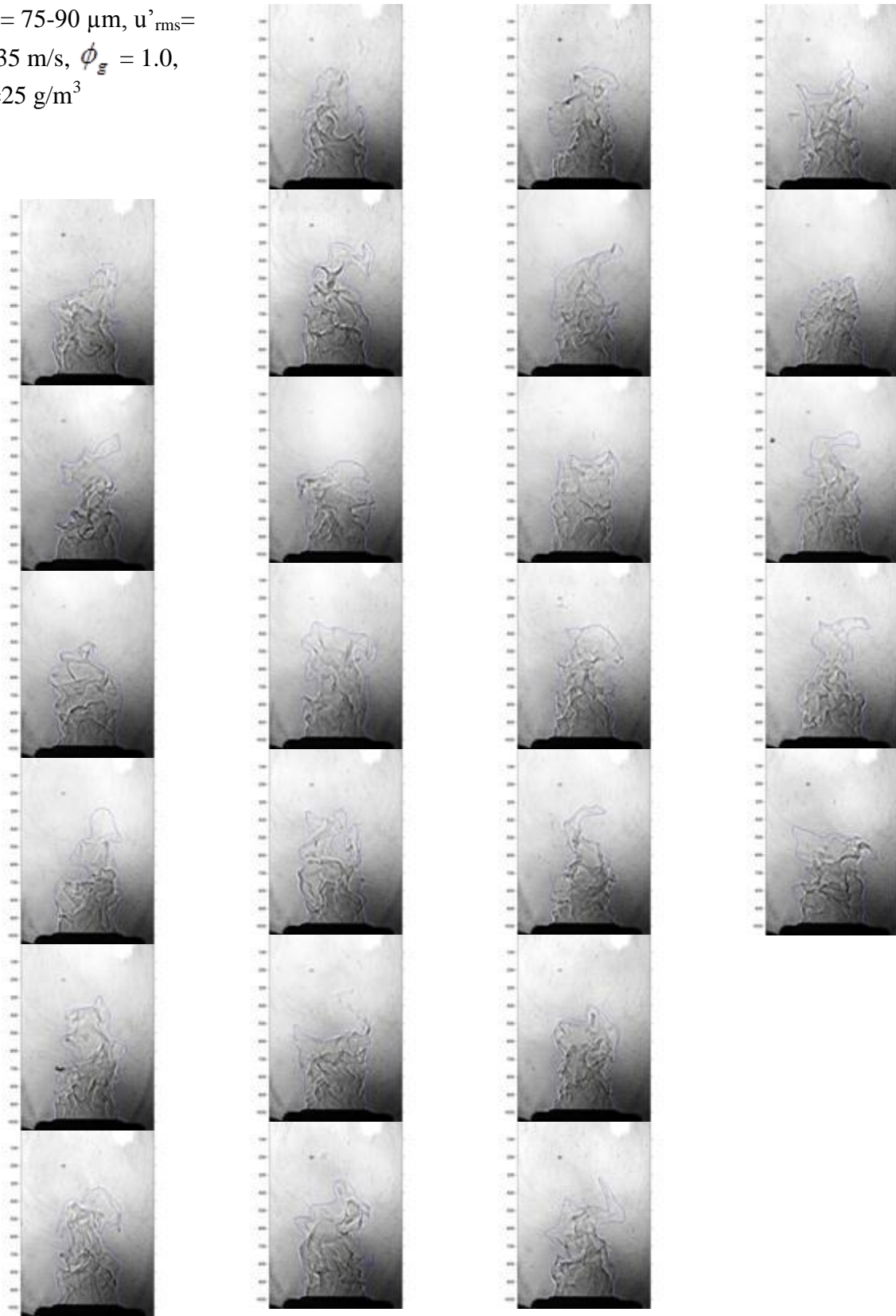
$d_{st} = 75-90 \mu\text{m}$, $u'_{rms} =$
 0.335 m/s , $\phi_g = 0.8$,
 $\lambda_{st} = 50 \text{ g/m}^3$



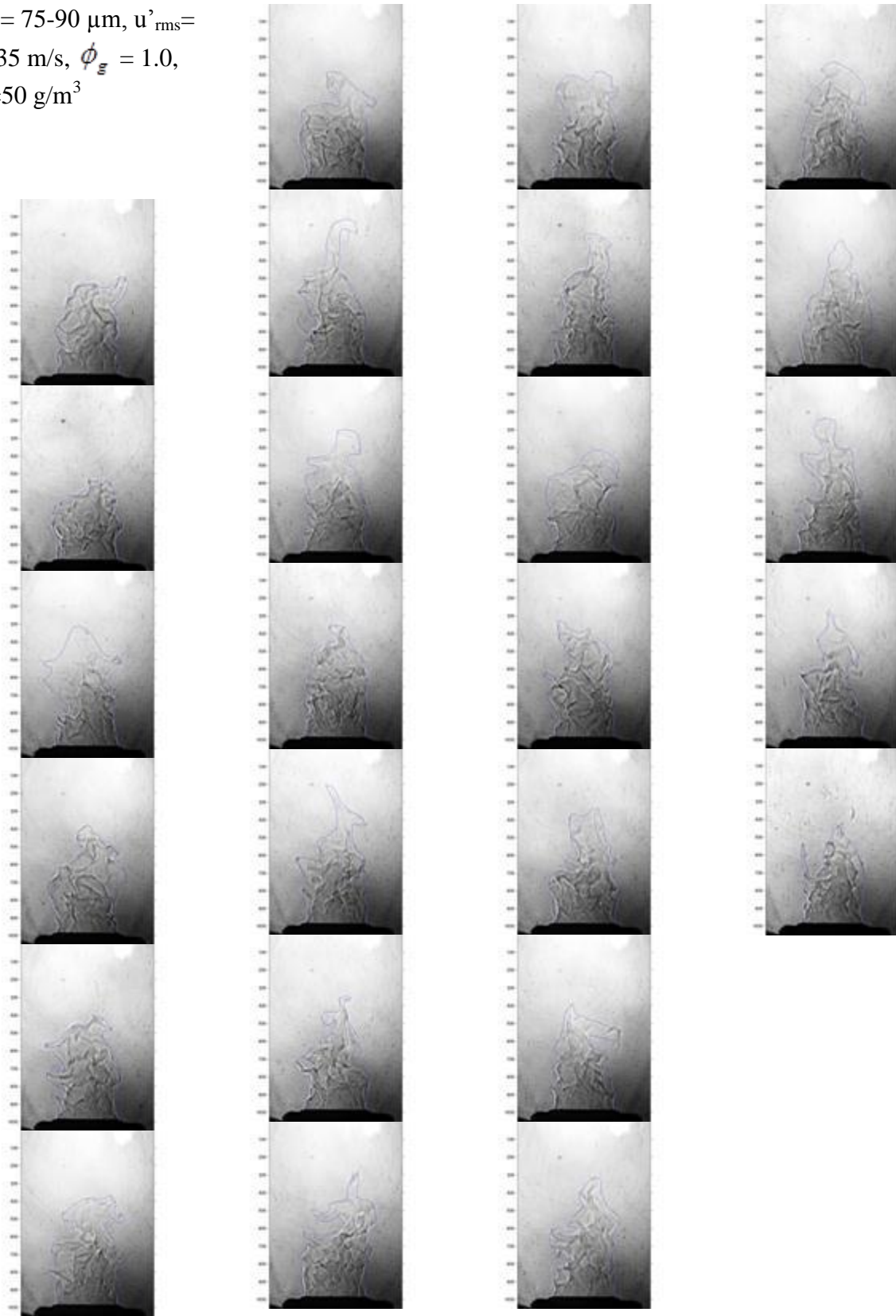
$d_{st} = 75-90 \mu\text{m}$, $u'_{rms} =$
 0.335 m/s , $\phi_g = 0.8$,
 $\lambda_{st} = 75 \text{ g/m}^3$



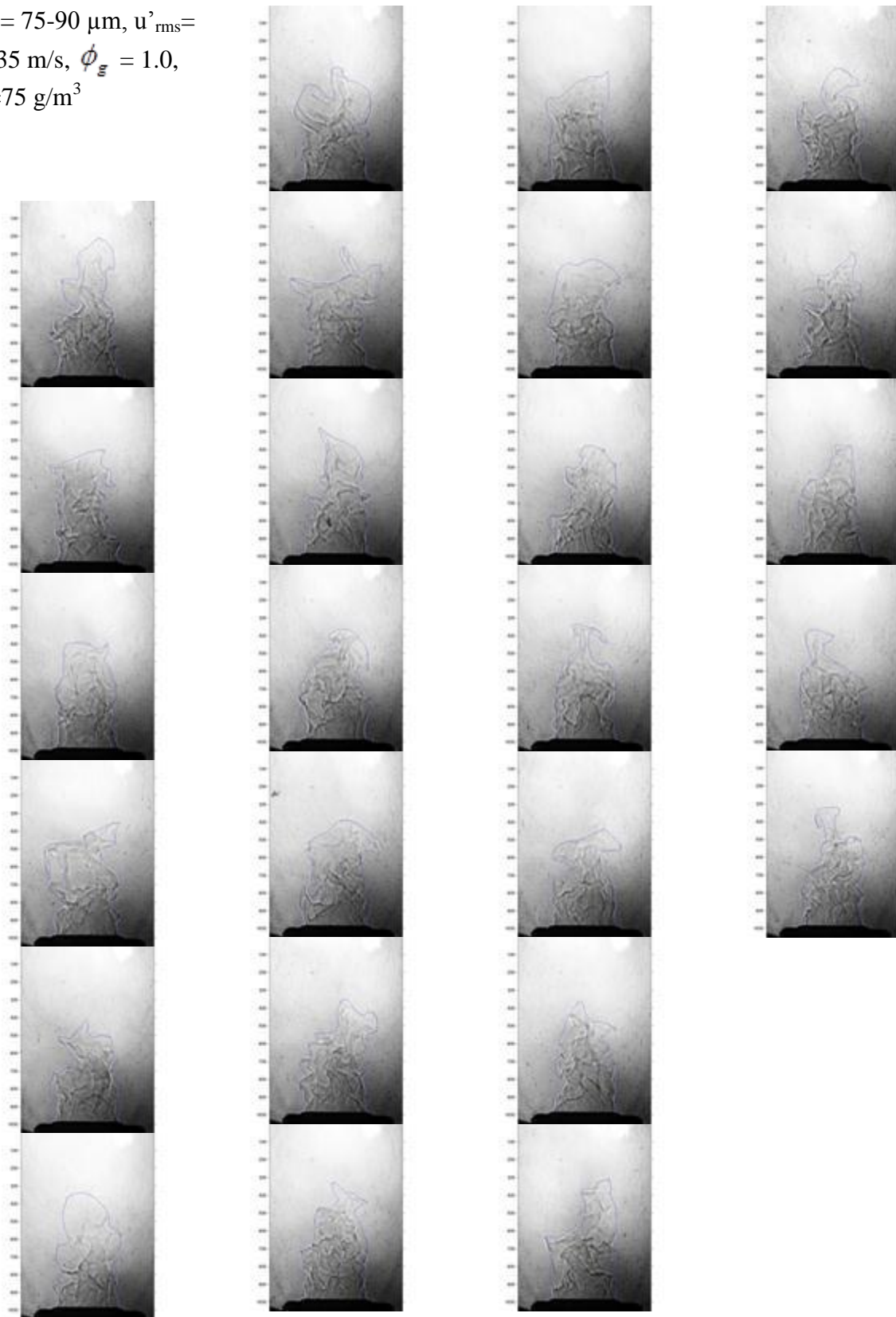
$d_{st} = 75-90 \mu\text{m}$, $u'_{\text{rms}} =$
 0.335 m/s , $\phi_g = 1.0$,
 $\lambda_{st} = 25 \text{ g/m}^3$



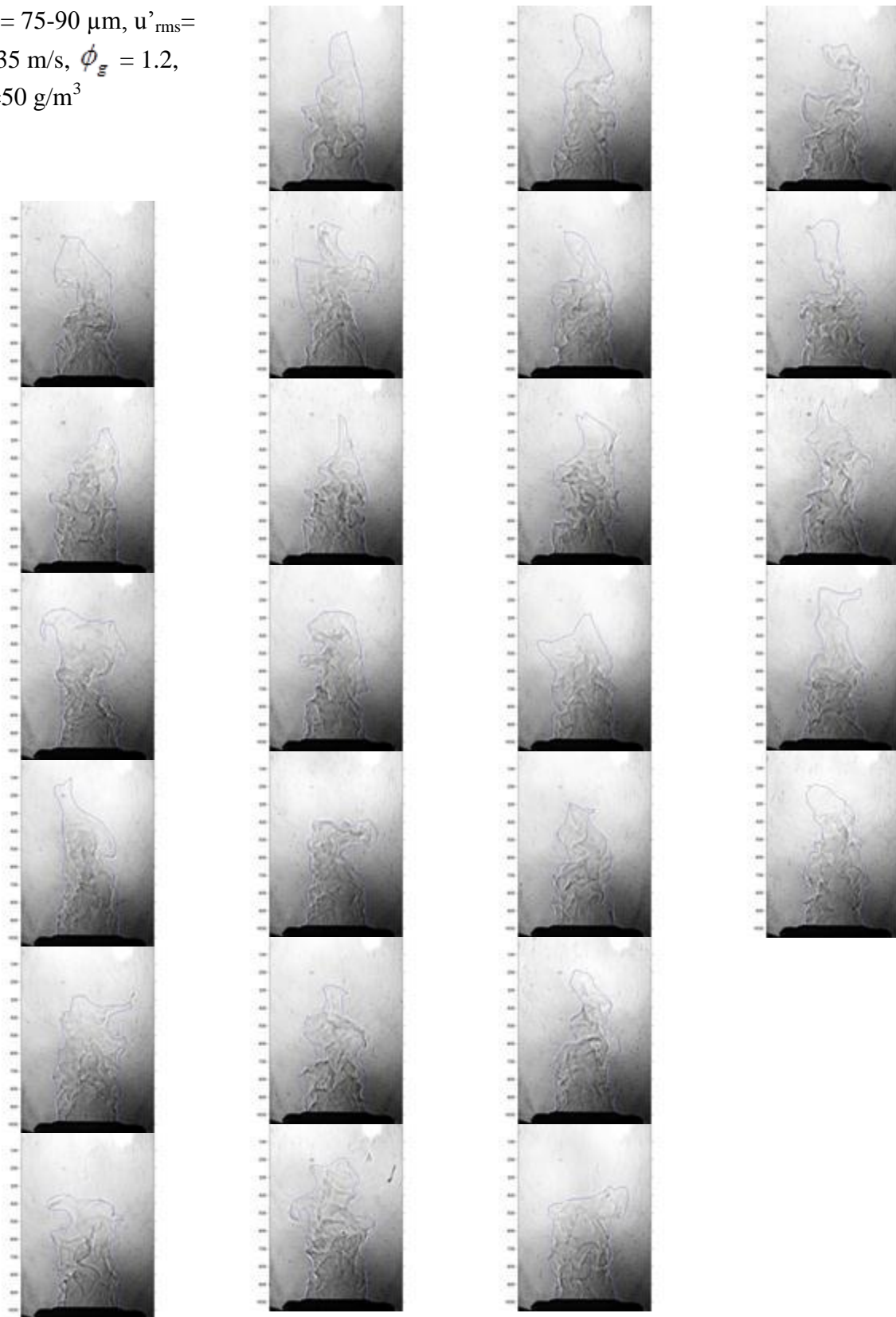
$d_{st} = 75-90 \mu\text{m}$, $u'_{rms} =$
 0.335 m/s , $\phi_g = 1.0$,
 $\lambda_{st} = 50 \text{ g/m}^3$



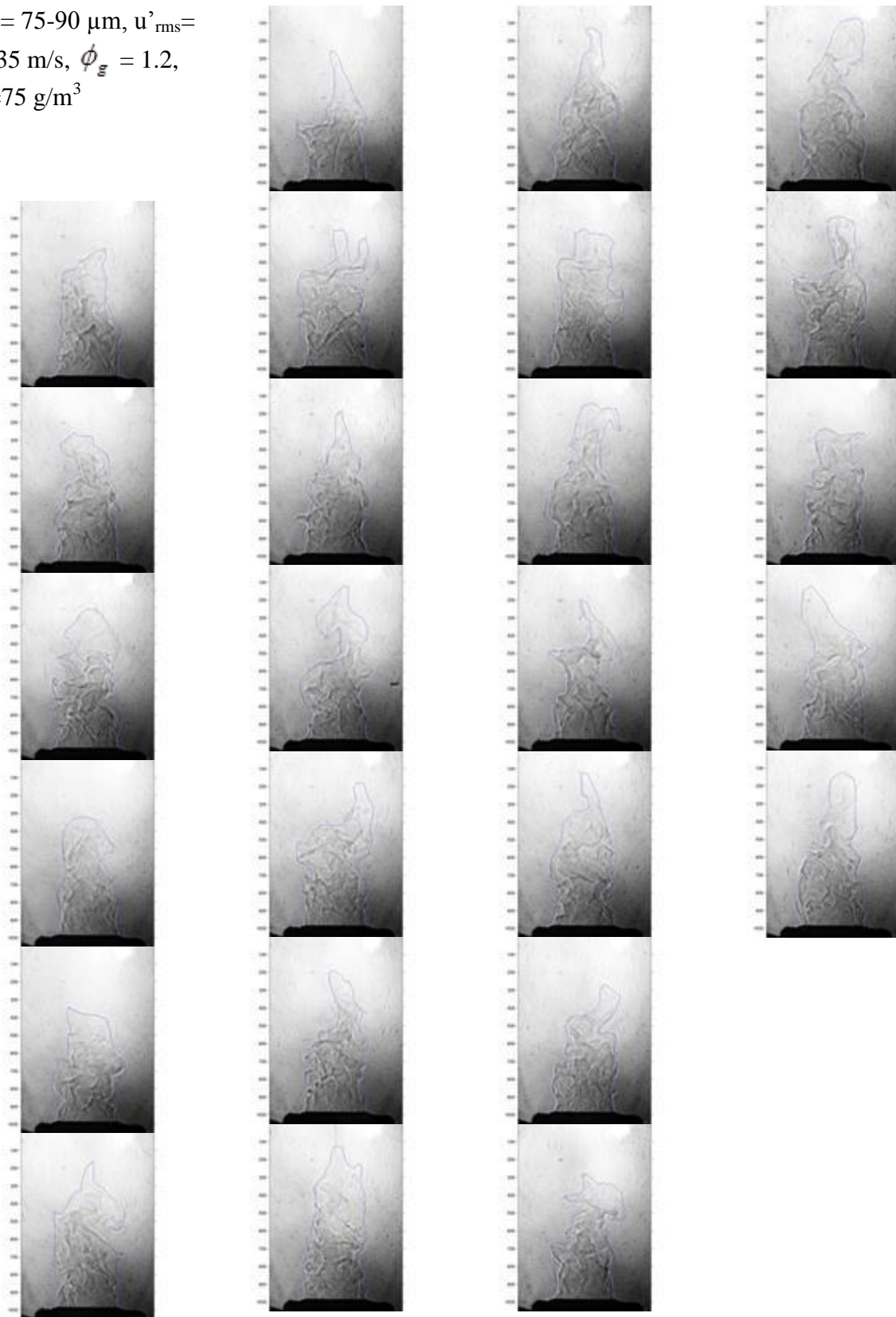
$d_{st} = 75-90 \mu\text{m}$, $u'_{rms} =$
 0.335 m/s , $\phi_g = 1.0$,
 $\lambda_{st} = 75 \text{ g/m}^3$



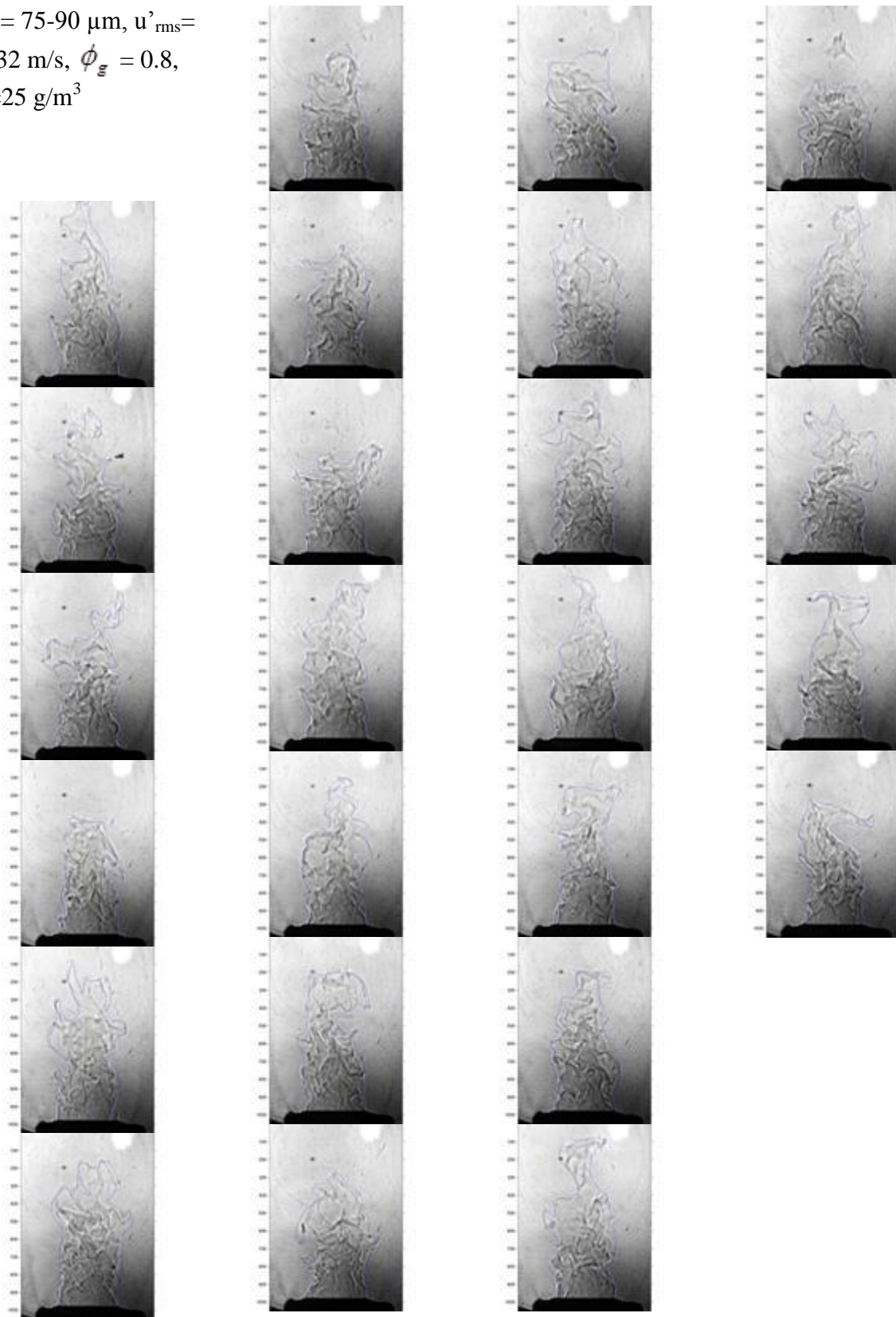
$d_{st} = 75-90 \mu\text{m}$, $u'_{rms} =$
 0.335 m/s , $\phi_g = 1.2$,
 $\lambda_{st} = 50 \text{ g/m}^3$



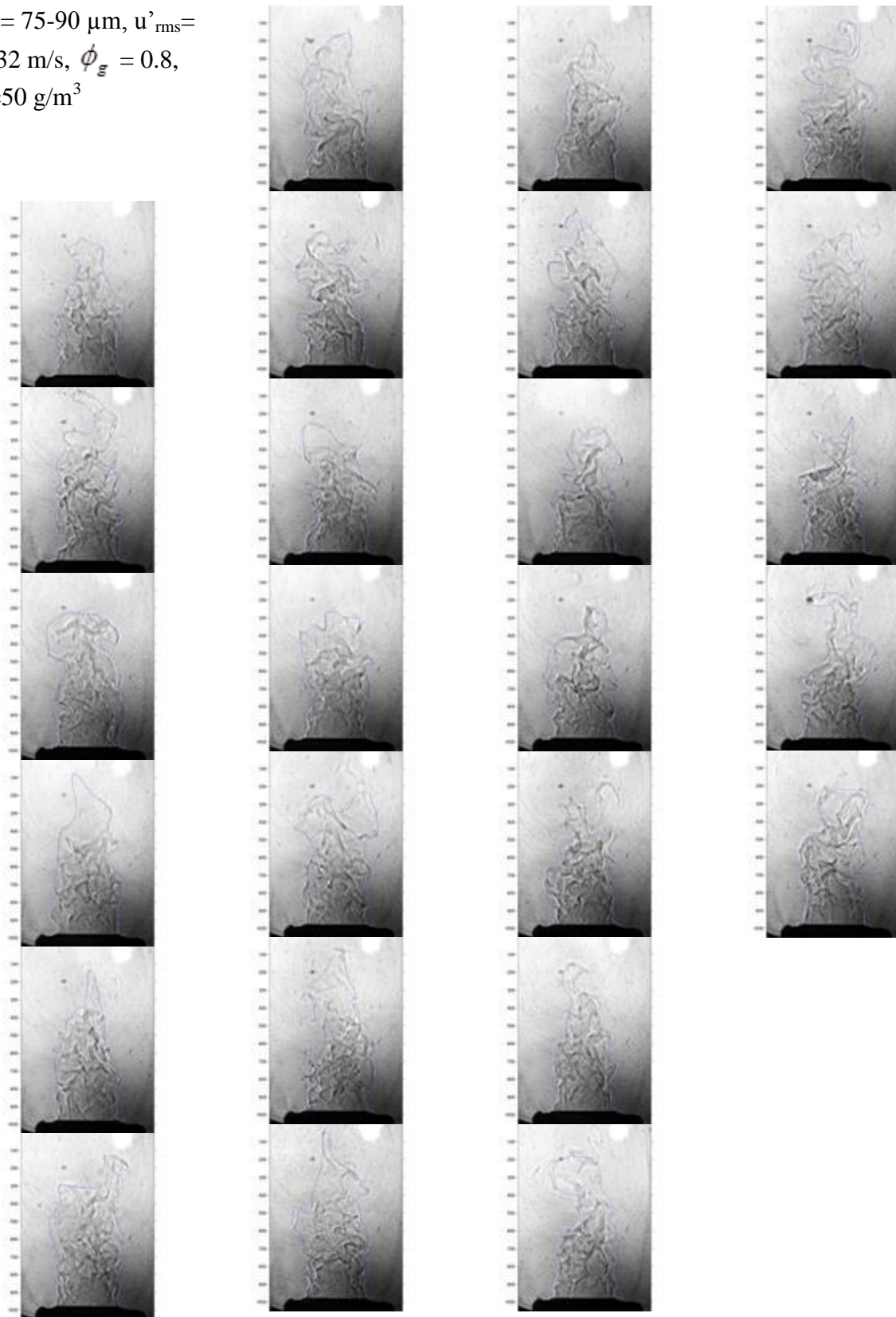
$d_{st} = 75-90 \mu\text{m}$, $u'_{rms} =$
 0.335 m/s , $\phi_g = 1.2$,
 $\lambda_{st} = 75 \text{ g/m}^3$



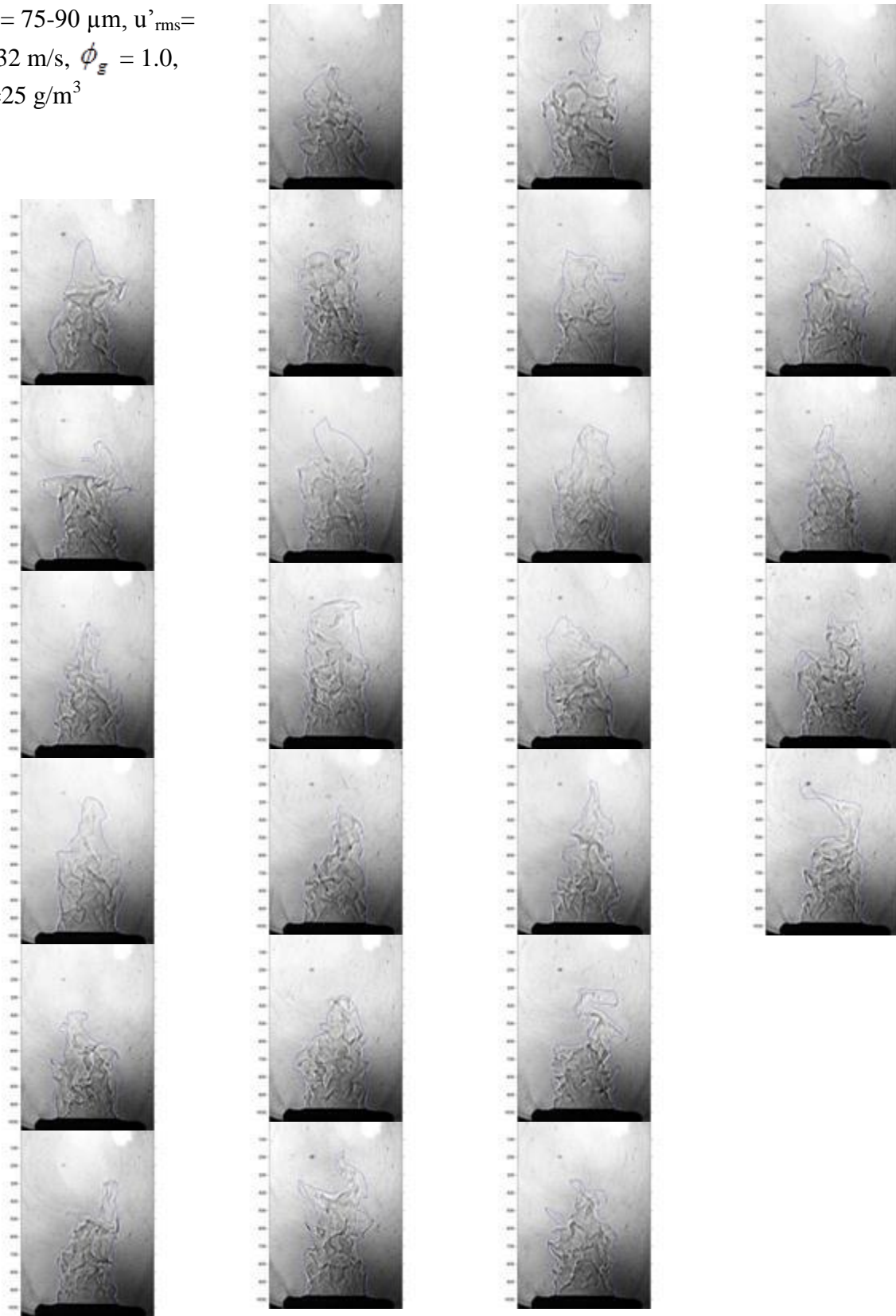
$d_{st} = 75-90 \mu\text{m}$, $u'_{rms} =$
 0.532 m/s , $\phi_g = 0.8$,
 $\lambda_{st} = 25 \text{ g/m}^3$



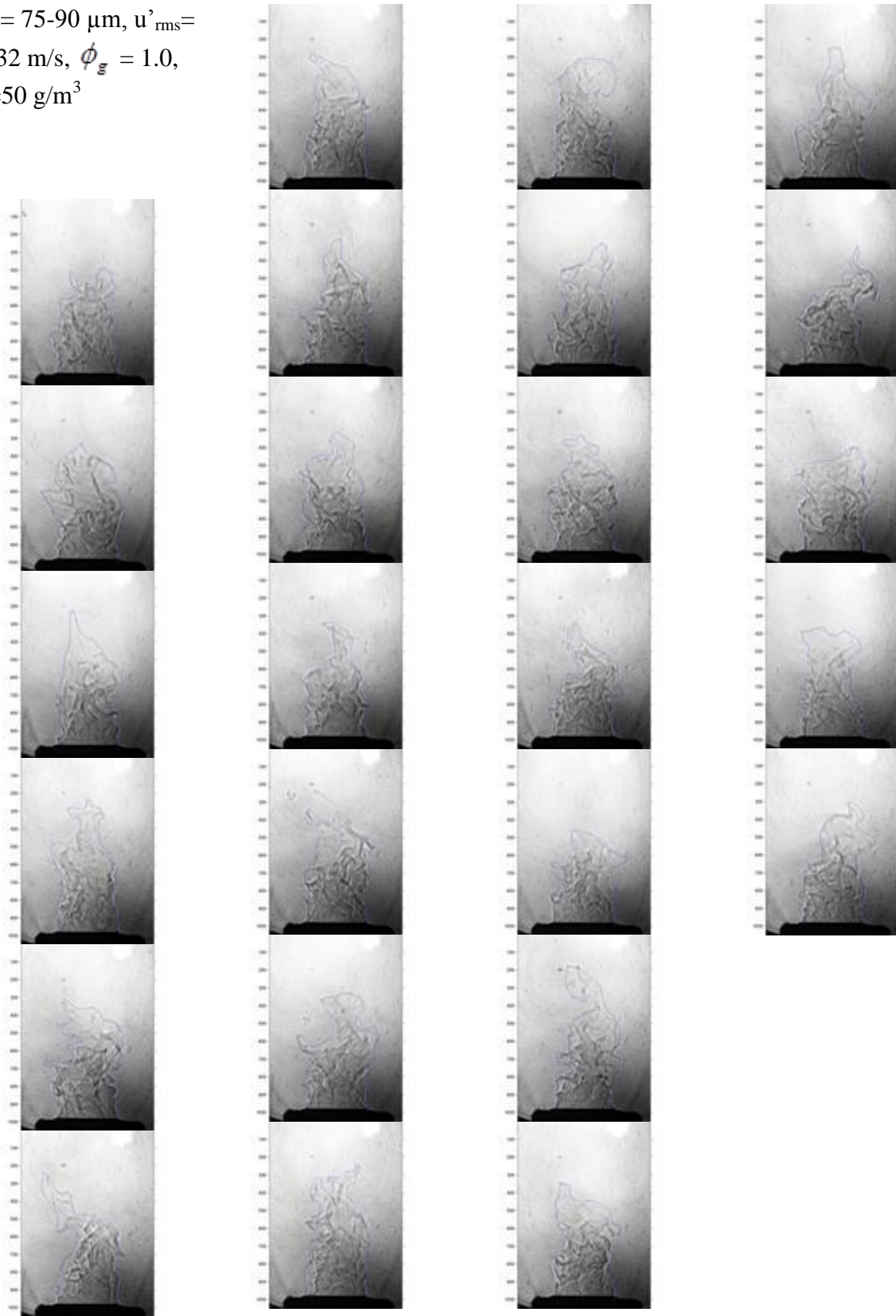
$d_{st} = 75-90 \mu\text{m}$, $u'_{\text{rms}} =$
 0.532 m/s , $\phi_g = 0.8$,
 $\lambda_{st} = 50 \text{ g/m}^3$



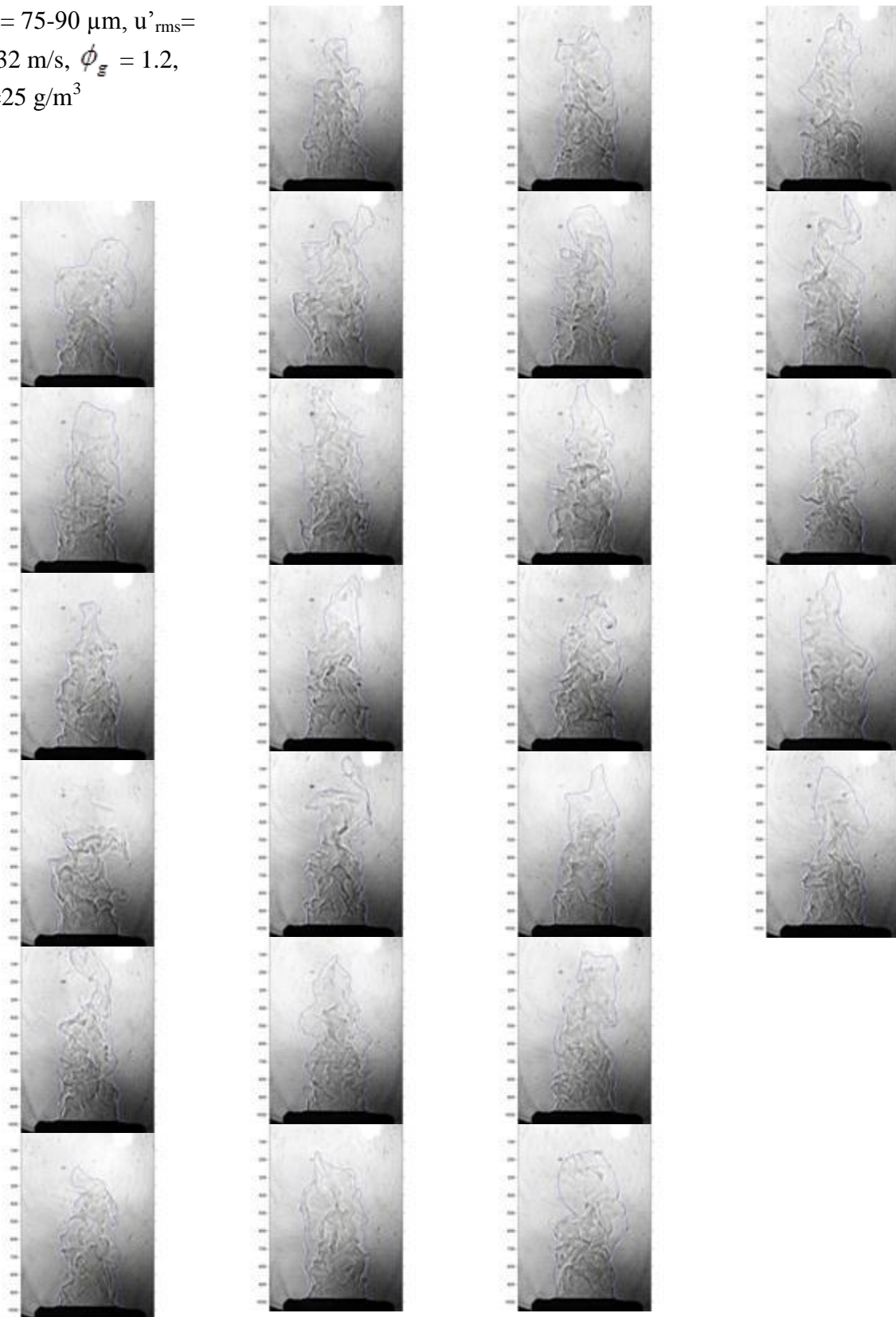
$d_{st} = 75-90 \mu\text{m}$, $u'_{\text{rms}} =$
 0.532 m/s , $\phi_g = 1.0$,
 $\lambda_{st} = 25 \text{ g/m}^3$



$d_{st} = 75-90 \mu\text{m}$, $u'_{rms} =$
 0.532 m/s , $\phi_g = 1.0$,
 $\lambda_{st} = 50 \text{ g/m}^3$



$d_{st} = 75-90 \mu\text{m}$, $u'_{rms} =$
 0.532 m/s , $\phi_g = 1.2$,
 $\lambda_{st} = 25 \text{ g/m}^3$



$d_{st} = 75-90 \mu\text{m}$, $u'_{rms} =$
 0.532 m/s , $\phi_g = 1.2$,
 $\lambda_{st} = 50 \text{ g/m}^3$

